1991

Laser-molecule Interactions And The Effects Of Permanent Dipoles

Anne E. Kondo

LASER-MOLECULE INTERACTIONS

AND THE EFFECTS OF PERMANENT DIPOLES

by

Anne E. Kondo

Department of Chemistry

Submitted in partial fulfilment
of the requirements for the degree of
Doctor of Philosophy

Faculty of Graduate Studies
The University of Western Ontario
London, Ontario
December, 1991.

ISBN 0-315-71962-1

ABSTRACT

The spectral and dynamic effects associated with a non-zero difference, d, between the permanent dipole moments of two molecular states involved in a transition, are investigated for a variety of electromagnetic field-molecule interactions. Both analytical and exact numerical techniques are used to solve the time-dependent Schrödinger equation and to obtain the temporal populations of the molecular states and the associated absorption spectra, for molecular interactions with a Gaussian pulsed, or one or two continuous wave (CW), laser(s).

Analytical rotating wave approximation results are derived for a single CW laser interacting with a two-level $d \neq 0$ molecule with an excited state lifetime, and for a two-level $d \neq 0$ molecule interacting with two CW lasers. A symmetry-adapted Riemann product integral method for exact calculations of pulsed laser-molecule interactions is developed and applied to specific problems. The Floquet technique for the treatment of periodic Hamiltonians is extended to accommodate the interaction of a molecule with two CW lasers.

The one-field RWA results are used to predict and interpret the effects of permanent dipoles on the temporal behaviour of the molecular states for a decaying two-level system interacting with a CW laser, and for a non-decaying two-level system interacting with a pulsed laser. It is shown that the excited state lifetime and the pulse duration can act as internal and external probes, respectively, of the temporal effects of permanent dipoles, relative to the often-studied $d = 0$

problem. The two-field analytical RWA solutions are used to help discuss and predict the effects of permanent dipole moments in two-laser multi-photon transitions. Several examples of multi-photon, two-colour, two-level resonance profiles, calculated in the RWA and by using exact Floquet techniques, are used to demonstrate how particular multi-photon transitions can be optimized, and to help quantify the conditions for the validity of the two-colour RWA. The effects of neighbouring energy levels on the transition of interest, for both probe and pump-probe laser-molecule interactions, are investigated using a series of three- to seven-level model molecular systems.

ACKNOWLEDGEMENTS

I would like to thank Dr. W.J. Meath for his guidance, encouragement, and the many challenging discussions. Thank-you for teaching me the Andor Principle!

To my dear husband Alan, I am grateful for his unfailing sense of humour, and all the "tea and sympathy".

My thanks also to Dr. J.B. Stothers for suggesting the linear giant-dipole molecule used in the numerical examples of Chapter 6; to Drs. A.J. Thakkar and S. Nilar for providing the associated molecular data prior to its publication; and to Anita Elworthy for labelling the many figures.

Finally, I have appreciated the advice of Dr. (hon) R.A. Zimmerman, to "read books, repeat quotations, draw conclusions on the wall" in his 1965 treatise, "Bringing It All Back Home".

TABLE OF CONTENTS

LIST OF TABLES

LIST OF FIGURES

LIST OF FIGURES CONTINUED

CHAPTER 1

INTRODUCTION

The focus of this thesis is the investigation, using both approximate analytical and exact computational techniques, of some of the effects of the diagonal dipole moment matrix elements ("permanent dipoles") of a molecule on laser-molecule interactions. Particular emphasis is placed on molecular transitions induced by the electromagnetic field (EMF) corresponding to a continuous wave, a Gaussian pulsed, or two continuous wave laser(s). A non-zero difference, d, between the permanent dipole moments of two states involved in a transition can lead to substantial differences in the associated resonance profiles (absorption spectra) and the temporal evolution of the molecular states, relative to when $d = 0$. The effects of $d \neq 0$ versus $d = 0$ are investigated as a function of the field parameters, including field strength, frequency, and/or pulse duration, and of the molecular parameters, including the magnitude of d, the excited state decay rate, the transition dipole moments and/or the energy level configuration.

While there has been extensive research on molecule-laser interactions in the absence of permanent dipoles, explicit investigations of the effects of $d \neq 0$ have been confined primarily to the interaction of a molecule, generally a two-level system, with a

continuous wave (CW) electric field [1-4]. The effects of permanent dipoles are of course implicitly contained in exact calculations which include diagonal dipole moment matrix elements [5-11]. Surprisingly, until recently, such studies have apparently generated very few investigations concerned explicitly with the effects of permanent dipole moments.

The two-level system has been fundamental to the understanding of a variety of laser-molecule interactions [12-20], and has been investigated using both exact [5,13,21-24] and analytical techniques [1,2,25,26]. Analytical rotating wave approximation (RWA) solutions, for the temporal population of the molecular states, and for the associated resonances profiles, have long been available for two-level (atomic) systems, where $d = 0$, interacting with a CW laser [18,19]. More recently, RWA solutions to the time-dependent Schrödinger equation for a two-level system, with permanent dipole moments, interacting with a CW laser, have played an important role in the prediction and/or interpretation of the effects of $d \neq 0$ relative to when $d = 0$ [2,3,5,27-30]. These unique effects include multi-photon transitions, forbidden in the RWA when $d = 0$, and the nonlinear nature, as a function of d, the field strength and the frequency, of the $d \neq 0$ molecule-EMF coupling (a measure of the strength of the transition) [2,3]. The latter phenomenon can produce oscillatory fringes in the resonance profiles [2,3,5,13,26], and extremely long periods, which are associated with nodes in the molecule-EMF coupling [3,24], in the time-dependent excited state population; such effects do not occur in the absence of permanent dipole moments. Where quantitatively valid, the RWA analytical solutions are an efficient means of calculating

resonance profiles and the time-dependent molecular state populations associated with laser-molecule interactions. Exact calculations, for which a variety of numerical techniques are available [3,5-9,13-17,21-24,31-33], require much more time and computational effort than the analytical analogues, although the relatively efficient Floquet formalism [3,14-16,23,32,33] can be applied for laser-molecule interactions involving a periodic Hamiltonian. The exact solutions of the time-dependent wave equation, and the associated results for the resonance profiles and time-dependent populations of the molecular states, [illegible]lid under conditions where t[illegible] approximate results are not applicable. Furthermore, the results of exact calculations contain all of the subtle effects of a molecule-field interaction not accounted for in the analytical solutions. For example, the one-photon RWA resonance frequency equals the energy level separation, whereas the exact analogues can have positive or negative Bloch-Siegert shifts [2,3,5,26,28,34], where the resonance frequency is greater or less than the energy level separation when $d \neq 0$, and positive Bloch-Siegert shifts when $d = 0$ [14,35].

Recently, analytical extensions to many-level systems, with diagonal dipole moment matrix elements, have been made using time-dependent perturbation theory [1] and the generalized rotating wave approximation [31]. While the latter is dependent on the energy level configuration, the former is valid only for short times relative to those required to saturate the excited molecular states. Again, these investigations have focused on a many-level system interacting with a continuous wave electric field. To date, only a few complementary exact calculations have been reported: a recent

examination of the interaction of a permanent dipole molecule with a combination of CW and static electric fields considered a three-level molecular system [36], while eight-level manifolds interacting with a CW electric field have been used to explore the effects of diagonal dipole moment matrix elements on infra-red multi-photon vibrational transitions [31].

In general, the combination of approximate analytical and exact solutions to the time-dependent Schrödinger equation is a powerful tool for the prediction and analysis of time-dependent molecule-field interactions and the associated molecular state dynamics and resonance profiles. This combination is applied throughout this thesis, with the application of previously and newly derived RWA analytical solutions and some well established and new exact numerical techniques to the molecule-field interactions of interest.

Chapter 2 contains an extensive discussion, with many references to the literature, of some of the analytical solutions and exact techniques currently available for solving the time-dependent Schrödinger equation in the semi-classical dipole approximation. Many of the equations define notation used throughout this thesis, although a summary of the more frequently employed symbols is given in Table 2.1 at the end of Chapter 2. An outline of the computational techniques which are used, or which are extended and/or modified for use in later chapters, to obtain the many numerical examples in this thesis, is given in Sec. 2.2. These techniques for solving the time-dependent Schrödinger equation include the Riemann product integral method [3,21,37-39], the Taylor series [17b] and power series approaches [17a,23,32], and the powerful Floquet method [3,14-16,32,33]. The

analytical results of time-dependent semi-classical perturbation theory [1], and the rotating wave approximation [2,3], for a permanent dipole molecule interacting with a single linearly polarized continuous wave electric field are reviewed in Sec. 2.3. The consequences of using, and the conditions for the validity of, these approximations are discussed. Many of the spectral consequences of permanent dipole moments, as predicted by these solutions, are discussed in Sec. 2.4. While two-level molecular systems are emphasized, many-level systems are also considered briefly.

The interaction of a CW electric field with a two-level system, including permanent dipoles and a non-zero excited state decay rate, is examined in Chapter 3. Sections 3.1-3.3 contain a detailed derivation and discussion of the rotating wave approximation solutions for this interaction, focusing on the time-dependent molecular state populations. These solutions expand on those available in the literature by considering the combination of the effects due to excited state decay and permanent dipole moments. Here, the time-dependent RWA analytical results, on resonance, are fully exploited to provide as much information as possible about the effects of permanent dipole moments and excited state decay, and the interplay between the two, on the molecule-EMF interaction. This information is used to predict and/or interpret the temporal evolution of a molecule interacting with a CW laser as a function of the decay rate, and to test the validity of the analytical solutions by comparison with exact results. The conditions for the applicability of the RWA in the presence of excited state decay are distinct from those when decay is neglected. When the RWA solutions are no longer quantitatively valid, they retain a

qualitative applicability. Numerical examples for a two-level system, based on a "giant dipole" molecule [28,40], interacting with a CW laser are given and discussed in Sec. 3.4. A quantitative application of the RWA compares the RWA and exact time-dependent excited state populations for the two-level system interacting with a relatively weak electric field, as a function of increasing excited state decay. The RWA solutions are applied qualitatively to the interaction of the two-level system with an intense CW laser, such that the molecule-EMF coupling is close to a node; the interplay between the excited state lifetime and the extremely long "period" of the excited state population is investigated for the one-photon transition. It is shown that excited state decay can act as an internal probe of the dynamic effects of permanent dipole moments.

Ultrashort, intense pulsed lasers, which have recently become experimentally viable [41], provide a mechanism for the external probing of the effects of permanent dipole moments on the temporal evolution of the molecular states due to molecule-EMF interactions. Indeed, the observation of the effects of the non-linear nature of the $d \neq 0$ molecule-EMF coupling will often require the intense electric fields associated with pulsed, rather than purely continuous wave electric fields [24]. A Gaussian pulsed laser can be considered as a continuous wave laser with an amplitude modulator [21,22]. As such, much of the time-dependent molecule-field interaction under the (temporal) centre of a pulse can be interpreted in terms of a CW laser-molecule interaction. Consequently, the RWA results based on a CW laser-molecule interaction can be applied to help interpret pulsed laser-molecule interactions.

Chapter 4 considers the interaction of a Gaussian pulsed laser with a two-level system. The exact calculations are computationally very time consuming because the Hamiltonian associated with a pulsed laser-molecule interaction is not periodic, and therefore the efficient Floquet technique [3,14-16,32,33] cannot be applied. Section 4.1 contains the derivation of an economical half-pulse technique based on the Riemann product integral method [3,21,37-39]. In general, this procedure can be applied for symmetric or anti-symmetric pulses to calculate the time-dependent molecular state populations, over the entire effective duration of the pulse, from the evolution operators calculated over one-half of the pulsed laser-molecule interaction time. In Sec. 4.2, the half-pulse technique is applied in a series of numerical calculations to probe the effects of permanent dipole moments on the time-dependent molecular state populations. The two-level "giant dipole" molecule, used in the examples of Chapter 3, is employed to investigate the interplay between an extremely long $d \neq 0$ period of the excited state population associated with a molecule-EMF coupling node, and the pulse duration, for the one-photon transition. These calculations complement those in Chapter 3, where the excited state decay plays an analogous role to the pulse duration.

Chapters 3 and 4 emphasize the effects of permanent dipoles on the one-photon transition; the effects of $d \neq 0$ versus $d = 0$ are also very apparent when multi-photon transitions are considered [2]. While the effects of permanent dipoles on multi-photon resonance profiles for a two-level molecule interacting with a single CW laser have been well discussed in the literature [2,3,13,26,28,34], the analogous interaction with two CW lasers of different frequencies (colours) is

less well understood. Recently, both perturbative [1b,42] and non-perturbative approaches [43-45] have been used to consider the effects of $d \neq 0$ on two-colour absorption processes, particularly in the special limit where one frequency is extremely small while the other is close to the energy level separation [42-45].

In Chapter 5, the effects of permanent dipole moments on the interaction of two-level systems with two CW lasers of different frequencies are considered. Analytical RWA solutions are derived for a two-level system interacting with two CW lasers in Sec. 5.1. The difficulties and the increased complexities of the two-field problem, relative to the one-field analogue, and the much more restrictive constraints on the applicability of the two-field RWA are discussed in detail. Where applicable, the two-field molecule-EMF coupling, as derived in the RWA, can be used to predict and suggest field parameters that can be used to optimize particular two-colour multi-photon transitions, and/or to enhance the effects of permanent dipoles. Relative to the one-field case, the two-field problem has increased flexibility with respect to the relative sizes of the frequencies, and the choices of field strengths associated with the two CW lasers used to probe the molecule. Modifications of the exact Floquet techniques, used in the one-field analogue, for the two-colour problem are presented in Sec. 5.2, including a cost-efficient method, by appropriate selection of the frequencies, for the computation of the (two-field) temporal evolution of the molecular states and the associated absorption spectra.

In Sec. 5.3, several numerical examples comparing RWA and exact resonance profiles are presented to illustrate the optimization

capabilities of the two-field RWA, and to test the applicability of the RWA results. The interaction of a two-level model system, based on the molecular parameters of typical dipole moment molecules [26,46], with two CW lasers, is investigated as a function of field strengths, the number of photons involved in a transition, and the ratio of the two frequencies.

The investigations of Chapters 3-5 focus on two-level molecular models. The extension to many-level molecular systems is made in Chapter 6. An example of near-nodal molecule-EMF coupling, studied in Chapters 3 and 4 for a two-level system when $d \neq 0$, is examined in a three-level system in Sec. 6.1, as a function of field strength and frequency. In Sec. 6.2, a pump and probe time-dependent investigation of an eight-level model system, based on a second giant dipole molecule, is conducted.

For the pump component of the study in Sec. 6.2, a Gaussian pulsed laser is used to excite the molecule from the ground state, "A", into an excited state, "B". The effects of the neighbouring transitions and neighbouring energy levels on this one-photon transition are minimized by careful selection of the field parameters, for which the one-field RWA acts as a guide. For the probe component of the problem, transitions between excited state "B" and a second excited state "C", where the "B" and "C" have a large difference in permanent dipole moments, are induced using one field, one- or two-photon transitions; the two-field, two-colour analogues are also considered. Where neighbouring transitions strongly perturb the one- or multi-photon transition of interest, slight variations of the energy-level configuration of, or the transition moments to, neighbouring states are

made to further understand the effects of the neighbouring states on the two-level transitions of interest. The RWA expressions for the molecule-EMF coupling for a two-level system interacting with one CW field [2,3,14,18], reviewed in Chapter 2, and with two CW fields, derived in Chapter 5, are used to predict and interpret the temporal evolution of the molecular states for the relevant interaction. Many-level, semi-classical time-dependent perturbation theory [1,47] is also used to help understand the effects of neighbouring energy states.

Finally, a summary of the more important general aspects of this work is given in Chapter 7.

Atomic units [48] are used throughout; a summary of the relevant conversion factors between SI and atomic units is given below [49]:

Atomic Unit	Value in S.I. units
Charge (e)	1.6022×10^{-19} C
Length (a_0)	5.2918×10^{-11} m
Mass (m_e)	9.1095×10^{-31} kg
Angular momentum ($\hbar$)	1.0546×10^{-34} J s
Time	2.4189×10^{-17} s
Circular frequency	4.1341×10^{16} s^{-1}
Energy (hartree)	4.3598×10^{-18} J
Electric dipole moment (ea_0)	8.4784×10^{-30} C m
Electric field strength (ea_0^{-2})	5.1423×10^{11} V m^{-1}

The following equations give the conversions from atomic units (au) to units quoted frequently in experimental applications. Energy, E, and wavenumbers, $\tilde{\nu}$, are related by,

$$\tilde{\nu}(cm^{-1}) = 2.1947x10^{5}E(au), \qquad (1.1)$$

while,

$$E(eV) = 27.212E(au). \qquad (1.2)$$

Field intensity, I, is related to the field strength, $\mathcal{E}^0$, according to,

$$I(Wcm^{-2}) = 3.5095x10^{16}[\mathcal{E}^0(au)]^2. \qquad (1.3)$$

Transition and permanent dipole moments are often given in units of Debye, $1D = 3.336x10^{-30}Cm = 0.39347au$. Also, one picosecond is $1ps = 10^{-12}s \approx 41.341au$ and one femtosecond is $1fs = 10^{-15}s \approx 41.341au$.

CHAPTER 2

BACKGROUND INFORMATION

This chapter contains some background information and reviews the theory relevant to the work presented in later chapters. A general discussion of the Schrödinger equation in Sec 2.1 introduces much of the notation used in this thesis. Many of the symbols are summarized in Table 2.1, given at the end of this chapter. The exact computational techniques used to solve the Schrödinger equation in the semi-classical dipole approximation, for various laser-molecule problems discussed in this thesis, are reviewed in Sec. 2.2. Section 2.3 presents approximate analytical results which are, in many cases, used either to interpret, or to suggest and interpret, the results of exact calculations for laser-molecule interactions. Relevant previous work on the effects of permanent dipoles on the spectral and temporal behaviour associated with molecule-EMF interactions are reviewed for two- and many-level molecular systems in Sec. 2.4.

2.1. GENERAL DISCUSSION OF THE TIME-DEPENDENT SCHRÖDINGER EQUATION.

The Schrödinger wave equation for the time evolution of a system described by the Hamiltonian operator $\hat{H}$ and the wavefunction $\Psi(\underline{r},t)$ is [50-52],

$$\hat{H}\Psi(\underline{r},t) = i\frac{\partial}{\partial t}\Psi(\underline{r},t), \qquad (2.1.1)$$

where $\underline{r}$ is the set of the spatial vectors for all the particles which make up the system, and t is time. The total Hamiltonian (self-adjoint) operator $\hat{H}$ can be expressed as a sum of two operators,

$$\hat{H} = \hat{H}_0 + \hat{V}(\underline{r},t), \qquad (2.1.2)$$

where the time-independent Hamiltonian operator $\hat{H}_0$ applies to the unperturbed system and $\hat{V}(\underline{r},t)$ represents the time-dependent interaction of the unperturbed (molecular) system with an external perturbation.

When a time-dependent perturbation is not present, the wavefunction can be separated into time- and space-dependent terms:

$$\Psi_j(\underline{r},t) = \phi_j(\underline{r})\exp[-iE_j t], \qquad (2.1.3)$$

Here, E_j is the energy of the stationary state $\phi_j(\underline{r})$ and corresponds to an eigenvalue of the unperturbed Hamiltonian operator $\hat{H}_0$,

$$\hat{H}_0\phi_j(\underline{r}) = E_j\phi_j(\underline{r}). \qquad (2.1.4)$$

The stationary state wavefunctions are orthonormal, so,

$$\langle\phi_k(\underline{r})|\phi_j(\underline{r})\rangle = \delta_{jk}, \qquad (2.1.5)$$

where δ_{jk} is the Kronecker delta ($\delta_{jj} = 1$ while $\delta_{jk} = 0$ for $j \neq k$). The Dirac bracket $\langle|\rangle$ is standard notation for integration over all coordinate space [50],

$$\langle\phi_k(\underline{r})|\phi_j(\underline{r})\rangle \equiv \int\phi_k(\underline{r})^*\phi_j(\underline{r})d\underline{r}, \qquad (2.1.6a)$$

where $\phi_k(\underline{r})^*$ is the complex conjugate of $\phi_k(\underline{r})$. For expectation values for an arbitrary property A,

$$\bar{A} = \langle\phi_k(\underline{r})|\hat{A}(\underline{r},t)|\phi_j(\underline{r})\rangle \equiv \int\phi_k(\underline{r})^*\hat{A}(\underline{r},t)\phi_j(\underline{r})d\underline{r}, \qquad (2.1.6b)$$

where $\hat{A}(\underline{r},t)$ is the quantum mechanical operator associated with A.

When a perturbing field is present, the total wavefunction can be expressed as a linear combination of the stationary state basis functions $\phi_j(\underline{r})$ with time-dependent coefficients $a_j(t)$ [50-53]:

$$\Psi(\underline{r},t) = \sum_j a_j(t)\phi_j(\underline{r}). \qquad (2.1.7)$$

The total wave function obeys the normalization condition,

$$\langle\Psi(\underline{r},t)|\Psi(\underline{r},t)\rangle = \sum_j |a_j(t)|^2 = 1. \qquad (2.1.8)$$

Substitution of (2.1.2), (2.1.3), (2.1.4) and (2.1.7) into (2.1.1), yields,

$$\sum_j [E_j a_j(t)\phi_j(\underline{r}) + \hat{V}(\underline{r},t)a_j(t)\phi_j(\underline{r})] = \sum_j i\frac{d}{dt}a_j(t)\phi_j(\underline{r}). \qquad (2.1.9)$$

Multiplying (2.1.9) from the left by $\phi_k(\underline{r})$, integrating over all spatial coordinates, and applying (2.1.6), produces a set of coupled differential equations for the time-dependent coefficients,

$$E_k a_k(t) + \sum a_j(t)\langle\phi_k(\underline{r})|\hat{V}(\underline{r},t)|\phi_j(\underline{r})\rangle = i\frac{d}{dt}a_k(t), \quad k=1,2.. \qquad (2.1.10)$$

This set of equations is exact if j and k cover the complete basis set of stationary state wavefunctions. In practice, only those states which are strongly perturbed by the external field are retained in (2.1.10).

Two of the desired physical quantities that can be obtained from the solutions to the set of coupled differential equations (2.1.10) are the time-dependent populations of the states j [50-52],

$$P_j(t) = |a_j(t)|^2, \qquad (2.1.11)$$

which describe the dynamics of the molecular system as it interacts with the time-dependent perturbation; and the long time-averaged or

steady state populations of the molecular states [50-52],

$$\bar{P}_j = \lim_{\tau\to\infty} \frac{1}{\tau}\int_0^{\tau} P_j(t)dt. \qquad (2.1.12)$$

In the work presented in this thesis, the interactions of molecular systems with three different types of classical time-dependent electric fields $\underline{\mathcal{E}}(t)$ [21,54], are studied: with single continuous wave (CW) electric fields; with two CW fields of different frequencies; and with a Gaussian pulsed electric field. This semiclassical approach (a quantized molecular system interacting with a classical electromagnetic field) is a valid approximation when the number of photons present is large [50].

A monochromatic continuous wave electric field (CW laser) can be expressed as,

$$\underline{\mathcal{E}}(t) = \hat{e}\mathcal{E}^0\cos(\omega t + \delta), \qquad (2.1.13)$$

where $\mathcal{E}^0$ is the field amplitude, ω is the applied frequency, δ is the phase, and $\hat{e}$ is the (linear) polarization unit vector of the field. For two-colour problems in which a molecule interacts with two continuous wave electric fields of different frequencies,

$$\underline{\mathcal{E}}(t) = \sum_{j=1}^{2} \hat{e}_j\mathcal{E}^0_j\cos(\omega_j t + \delta_j), \qquad (2.1.14)$$

with the symbols retaining their definitions from (2.1.13). A Gaussian pulsed electric field can be described as a continuous wave laser with a time-dependent amplitude-modulating envelope $\exp(-t^2/\tau_p^2)$ [19]:

$$\underline{\mathcal{E}}(t) = \hat{e}\mathcal{E}^0\cos(\omega t + \delta)\exp[-t^2/\tau_p^2], \qquad (2.1.15)$$

where τ_p is a measure of the pulse duration. The temporal full width at half maximum of this pulse is related to τ_p by,

$$\Delta t = 2\tau_p\sqrt{\ell n 2}. \qquad (2.1.16)$$

Unlike continuous wave electric fields, pulses are not monochromatic. From the Fourier transform of the envelope [55],

$$\mathcal{F}(\mathcal{E}^0\exp[-t^2/\tau_p{}^2]) = \tfrac{1}{2}\sqrt{\pi}\mathcal{E}^0\tau_p\exp[-\tfrac{1}{4}\omega^2\tau_p^2], \qquad (2.1.17)$$

a Gaussian pulsed electric field has a frequency bandwidth at half maximum about the carrier frequency ω of,

$$\Delta\omega = 4\sqrt{\ell n 2}/\tau_p. \qquad (2.1.18)$$

This bandwidth can lead to the excitation of energy states other than the one(s) on resonance with ω.

The coupling between the molecule and the classical electric field occurs primarily through an electric dipole interaction,

$$\hat{V}(\underline{r},t) = -\hat{\underline{\mu}}\cdot\underline{\mathcal{E}}(t), \qquad (2.1.19)$$

where $\hat{\underline{\mu}}$ is the total electric dipole moment operator of the molecule. To a good approximation, the relatively weaker effects of electric quadrupole and magnetic dipole interactions can be neglected [56], unless differential absorption processes are studied [57-59].

For an N-level molecule, substitution of (2.1.19) into (2.1.10) gives, in matrix form,

$$[\underline{\underline{E}} - \underline{\underline{\mu}}\cdot\underline{\mathcal{E}}(t)]\underline{a}(t) = i\frac{d}{dt}\underline{a}(t). \qquad (2.1.20)$$

$\underline{a}(t)$ is the column vector of the time-dependent coefficients, $\underline{a}(t) = [a_1(t),a_2(t),\ldots a_N(t)]^T$; $\underline{\underline{E}}$ is the $N\times N$ diagonal energy matrix with elements $(\underline{\underline{E}})_{jk} = E_j\delta_{jk}$; and $\underline{\underline{\mu}}$ is the dipole moment matrix with elements $(\underline{\underline{\mu}})_{jk} = \underline{\mu}_{jk} = \langle\phi_j|\hat{\underline{\mu}}|\phi_k\rangle$. The transition dipole moment between stationary states j and k is $\underline{\mu}_{jk} = \underline{\mu}_{kj}$, $j \neq k$, while the permanent

dipole moment of the j-th stationary state is $\underline{\mu}_{jj}$. The time-dependent and long time-averaged state populations, (2.1.11) and (2.1.12), respectively, are independent of the traces of the Hamiltonian matrix in (2.1.20) [1].

Equation (2.1.20) describes the evolution of the system in the Schrödinger representation [60]. A standard transformation of the time-dependent coefficients is,

$$a_j(t) = b_j(t)\exp[-iE_j t], \tag{2.1.21}$$

which, when substituted into (2.1.20), gives the wave equation in an interaction representation [60]:

$$-\sum_j \underline{\mu}_{kj}\cdot\underline{\mathcal{E}}(t)b_j(t)\exp[-iE_{jk}t] = i\frac{d}{dt}b_k(t),\ k=1,2\ldots \tag{2.1.22}$$

where $E_{jk} = E_j - E_k$. The transformation (2.1.21) is unitary since $|a_j(t)|^2 = |b_j(t)|^2$.

Semi-classical theory cannot rigorously account for spontaneous decay processes, or other mechanisms of decay, that result in finite lifetimes of the excited states relative to the ground state. Instead, the full quantization of the electric field and the system, a much more complicated problem, is required to account for these phenomena [50]. However, excited state decay can be incorporated into the semi-classical approach by making the excited state energies complex [19,61,62]. This approach has become one of the common techniques [61-65] for introducing excited state decay into the time-dependent wave equation (2.1.20),

$$[\underline{\underline{E}} - \frac{i}{2}\underline{\underline{\gamma}} - \underline{\underline{\mu}}\cdot\underline{\mathcal{E}}(t)]\underline{a}(t) = i\frac{d}{dt}\underline{a}(t). \tag{2.1.23}$$

$\underline{\underline{\gamma}}$ is a diagonal matrix with $(\underline{\underline{\gamma}})_{jk} = \gamma_j\delta_{jk}$ where γ_j is the decay rate of

the excited state j. The ground state does not decay, so $\gamma_1 = 0$. This introduction of γ_j into the wave equation ensures that the excited state decays exponentially [61] in the absence of an external perturbation. Here,

$$i\frac{d}{dt}\underline{a}(t) = [\underline{\underline{E}} - \frac{i}{2}\underline{\underline{\gamma}}]\underline{a}(t), \tag{2.1.24}$$

so the time-dependent state amplitude becomes,

$$a_j(t) = a_j(0)\exp[-iE_j t - \tfrac{1}{2}\gamma_j t], \tag{2.1.25}$$

which corresponds to a time-dependent excited state population of,

$$P_j(t) = |a_j(0)|^2\exp[-\gamma_j t]. \tag{2.1.26}$$

The decay rates included in (2.1.23) phenomenologically represent all decay mechanisms for the respective excited states. However, with this inclusion of the excited state decay, the system is not conservative and the total wavefunction does not obey the normalization condition (2.1.8). The Hamiltonian matrix, including decay, is not self-adjoint. In cases where the decay is to other states of the molecule, the solutions to (2.1.23) are meaningful only for $t \leq 1/\gamma_j$ [20]; when the radiation leaves the molecular system, the results are meaningful to much longer times.

The solutions to the time-dependent Schrödinger equation depend on the initial conditions of the molecular system. Unless stated otherwise, for the equations and numerical examples in this thesis, the initial conditions are taken to be,

$$a_j(0) = b_j(0) = \delta_{1j}, \tag{2.1.27}$$

i.e. at $t = 0$, the molecule is entirely in the ground state. The initial conditions for the time derivatives of the time-dependent

coefficients are determined from the time-dependent Schrödinger equation in the relevant representation.

2.2. EXACT COMPUTATIONAL TECHNIQUES

This section reviews a number of computational techniques, used later in this thesis, for exactly solving the time-dependent Schrödinger equation in the semi-classical dipole-approximation for an N-level molecule interacting with a perturbing field. The techniques can be applied to the Schrödinger equation in either the Schrödinger, (2.1.20), or interaction, (2.1.22), representation.

The exact solution for the time-dependent Schrödinger equation, (2.1.20), or (2.1.22), can be expressed in terms of the evolution operator, $\underline{\underline{U}}(t,t_0)$ [50,51,63],

$$\underline{a}(t) = \underline{\underline{U}}(t,t_0)\underline{a}(t_0), \tag{2.2.1}$$

where t_0 is the initial time of the laser-molecule interaction. The initial conditions for the solution of (2.2.1) are,

$$\underline{\underline{U}}(t_0,t_0) = \underline{\underline{I}}, \tag{2.2.2}$$

where $\underline{\underline{I}}$ is the NxN identity matrix. The evolution operator satisfies,

$$\frac{d}{dt}\underline{\underline{U}}(t,t_0) = \underline{\underline{C}}(t)\underline{\underline{U}}(t,t_0), \tag{2.2.3}$$

where,

$$\underline{\underline{C}}(t) = -i\underline{\underline{H}}(t). \tag{2.2.4}$$

Over sequential time intervals, the evolution operator has the property [3,21,63],

$$\underline{a}(t'') = \underline{\underline{U}}(t'',t')\underline{a}(t') = \underline{\underline{U}}(t'',t')\underline{\underline{U}}(t',t_0)\underline{a}(t_0),\ t''\geq t'\geq t_0 \tag{2.2.5}$$

which can be continued over as many intervals as desired. Hence, if the interaction time interval of interest, $[t_0,t]$, is subdivided into n subintervals, then the evolution operator over $[t_0,t]$ can be written as,

$$\underline{\underline{U}}(t,t_0) = \underline{\underline{U}}(t,t_{n-1})\underline{\underline{U}}(t_{n-1},t_{n-2})\ldots\underline{\underline{U}}(t_2,t_1)\underline{\underline{U}}(t_1,t_0)$$

$$= \mathbf{T}\prod_{j=1}^{n}\underline{\underline{U}}(t_j,t_{j-1}) \qquad (2.2.6)$$

$\mathbf{T}$ is a time-ordering operator arranging the evolution operators in chronological order from right (t_0) to left (t).

The evaluation of the evolution operator $\underline{\underline{U}}(t,t_0)$ is carried out in the examples of this thesis by one of three techniques: the Riemann product integral (RPI) method [3,21,37-39,66]; a Taylor series expansion [17b,67]; or a matching power series expansion [23,32,67]. The three techniques differ in their approach to calculating the evolution operator over the subintervals. The RPI is reviewed in Sec. 2.2.1, the Taylor series approach is given in Sec. 2.2.2, and the power series method is contained in Sec. 2.2.3. The Floquet formalism for the efficient evaluation of the temporal and spectral properties for periodic systems is reviewed in Sec. 2.2.4.

2.2.1 THE RIEMANN PRODUCT INTEGRAL TECHNIQUE.

The Riemann product integral (RPI) technique relies on n in (2.2.6) being sufficiently large, and hence $\Delta t = t_j - t_{j-1}$ sufficiently small, such that $\underline{\underline{C}}(t)$ is approximately constant over each interval. Its value is $\underline{\underline{C}}(t'_j)$, where t'_j is an arbitrary point in the time interval $t_{j-1} \le t \le t_j$. Integration of (2.2.3) then yields,

$$\underline{\underline{U}}(t_j,t_{j-1}) = \exp[\underline{\underline{C}}(t'_j)\Delta t_j]. \qquad (2.2.7)$$

The value of $\underline{\underline{C}}(t'_j)$ can be determined by applying the mean value theorem [68] to $\underline{\underline{C}}(t)$ over the interval,

$$\underline{\underline{C}}(t'_j) = \frac{1}{\Delta t_j}\underline{\underline{C}}^{(j)} = \frac{1}{\Delta t_j}\int_{t_{j-1}}^{t_j} \underline{\underline{C}}(t)dt. \qquad (2.2.8)$$

Substitution of (2.2.7) and (2.2.8) into (2.2.6) gives,

$$\underline{\underline{U}}(t,t_0) = \mathbf{T}\prod_{j=1}^{n} \exp[\underline{\underline{C}}^{(j)}]. \qquad (2.2.9)$$

For systems with a periodic Hamiltonian, such as the interaction of a molecule with a single continuous wave electric field, it is convenient [21,23,32] to define the variable θ,

$$\theta = \omega t + \delta. \qquad (2.2.10)$$

Equation (2.2.8) becomes,

$$\underline{\underline{C}}(\theta'_j) = \frac{1}{\Delta\theta_j}\underline{\underline{C}}^{(j)} = \frac{1}{\Delta\theta_j}\int_{\theta_{j-1}}^{\theta_j} \underline{\underline{C}}(\theta)d\theta. \qquad (2.2.11)$$

For a single continuous wave electric field, (2.1.13), interacting with an N-level molecule, the matrix elements of $\underline{\underline{C}}(\theta)$ in the Schrödinger representation are,

$$C_{lm} = -\frac{i}{\omega}[E_l\delta_{lm} - \underline{\mu}_{lm}\cdot\hat{e}\mathcal{E}^0\cos(\theta)], \qquad (2.2.12)$$

where $l,m = 1,2,\ldots N$. Equation (2.2.12) produces matrix elements $\underline{\underline{C}}^{(j)}_{lm}$ of the form [21,23,32],

$$C^{(j)}_{lm} = -\frac{i}{\omega}(\theta_j - \theta_{j-1})\left(E_l\delta_{lm} - 2\underline{\mu}_{lm}\cdot\hat{e}\mathcal{E}^0\cos[\tfrac{1}{2}(\theta_j + \theta_{j-1})]\frac{\sin[\frac{1}{2}(\theta_j - \theta_{j-1})]}{(\theta_j - \theta_{j-1})}\right) \qquad (2.2.13)$$

For a Gaussian pulsed electric field, (2.1.15), the evolution operator is most easily evaluated in the interaction representation [21,60]. From (2.1.22), the matrix elements of $\underline{\underline{C}}(t)$ are,

$$C_{lm} = i\underline{\mu}_{lm}\cdot\hat{e}\mathcal{E}^0\exp[iE_{lm}t]\cos(\omega t + \delta)\exp[-t^2/\tau_p^2] \qquad (2.2.14)$$

For a pulse of zero phase, $\delta = 0$, (2.2.8) gives [21],

$$C_{lm}^{(j)} = i\frac{\sqrt{\pi}}{4}\mu_{lm}\cdot\hat{e}\mathcal{E}^0\tau_p\left[\exp[-(E_{lm}+\omega)^2\tau_p^2/4]\left(\mathrm{erf}(Z_j^+) - \mathrm{erf}(Z_{j-1}^+)\right)\right.$$

$$\left. + \exp[-(E_{lm}-\omega)^2\tau_p^2/4]\left(\mathrm{erf}(Z_j^-) - \mathrm{erf}(Z_{j-1}^-)\right)\right], \qquad (2.2.15)$$

where,

$$Z_j^+ = t_j/\tau_p - \frac{i}{2}(E_{lm}+\omega)\tau_p, \qquad (2.2.16a)$$

$$Z_j^- = t_j/\tau_p - \frac{i}{2}(E_{lm}-\omega)\tau_p. \qquad (2.2.16b)$$

Equation (2.2.15) differs from Equation (31) of Thomas and Meath [21] because the initial time t_0 of interaction has been removed. It is shown in Chapter 4 that the dependence of the matrix $\underline{C}^{(j)}$ on the parameter t_0 can be removed without affecting the final solution.

Once the matrix $\underline{C}^{(j)}$ has been calculated, the result must be exponentiated, see (2.2.7). This is most easily accomplished if $\underline{C}^{(j)}$ is diagonalized [21,69],

$$\underline{C}^{(j)} = \underline{P}^{(j)}\,\underline{\Lambda}^{(j)}\,\underline{P}^{(j)-1}, \qquad (2.2.17)$$

where $\underline{P}$ is the unitary matrix of the orthonormalized eigenvectors of $\underline{C}^{(j)}$, and $\underline{\Lambda}$ is the corresponding diagonal eigenvalue matrix. Since $\underline{P}^{(j)}$ is unitary and $\underline{\Lambda}^{(j)}$ is diagonal, the exponentiation of $\underline{C}^{(j)}$ reduces to,

$$\exp[\underline{C}^{(j)}] = \underline{P}^{(j)}\exp[\underline{\Lambda}^{(j)}]\,\underline{P}^{(j)-1}, \qquad (2.2.18)$$

where,

$$\left(\exp[\underline{\Lambda}^{(j)}]\right)_{lm} = \exp[\Lambda_l^{(j)}]\delta_{lm}. \qquad (2.2.19)$$

Thus the general RPI computational procedure for each interval is:

(1). $\underline{C}^{(j)}$ is calculated from (2.2.8).

(2). $\underline{C}^{(j)}$ is diagonalized; the orthogonal eigenvectors which make up the columns of the matrix $\underline{P}$ are normalized and the associated eigenvalues used to construct the diagonal matrix $\underline{\Lambda}^{(j)}$.

(3). $\underline{C}^{(j)}$ is exponentiated using (2.2.18) and (2.2.19).

The evolution operator to time t is calculated by a time-ordered product of the $\exp[\underline{C}^{(j)}]$, (2.2.9).

2.2.2 THE TAYLOR SERIES EXPANSION.

For the jth-time interval, the first order differential equation (2.2.3) is,

$$\frac{d}{dt}\underline{U}(t,t_{j-1}) = \underline{C}(t)\underline{U}(t,t_{j-1}), \qquad t_j \geq t \geq t_{j-1}. \tag{2.2.20}$$

The solution can be expanded in a Taylor series about t_{j-1} [17b,67],

$$\underline{U}(t,t_{j-1}) = \sum_{n=0}^{\infty} \frac{1}{n!}\left[\frac{d^n}{dt^n}\underline{U}(t)\right]_{t=t_{j-1}} (t - t_{j-1})^n, \tag{2.2.21}$$

where,

$$\left[\frac{d^n}{dt^n}\underline{U}(t)\right]_{t=t_{j-1}} = \sum_{m=0}^{n-1} \frac{(n-1)!}{(n-1-m)!m!}\left[\frac{d^{n-1-m}}{dt^{n-1-m}}\underline{C}(t)\right]_{t=t_{j-1}} \times \left[\frac{d^m}{dt^m}\underline{U}(t)\right]_{t=t_{j-1}} \tag{2.2.22}$$

Since $m < n$, the n-th order derivative of $\underline{U}(t)$ is calculated from the known lower order derivatives of $\underline{U}(t)$. The derivatives of $\underline{C}(t)$ can be calculated directly from (2.2.4). Furthermore, by definition,

$$\left[\frac{d^0}{dt^0}\underline{U}(t)\right]_{t=t_{j-1}} = \underline{U}(t_{j-1},t_{j-1}) = \underline{I}, \tag{2.2.23}$$

and,

$$\left[\frac{d^0}{dt^0}\,\underline{\underline{C}}(t)\right]_{t=t_{j-1}} = \underline{\underline{C}}(t_{j-1}). \qquad (2.2.24)$$

Thus, the general Taylor series procedure is:

(1). The total time $[t_0,t]$ is divided into small intervals $\Delta t_j = t_j - t_{j-1}$.

(2). For each interval, $\underline{\underline{C}}(t)$ and its derivatives are computed at the initial time of the interval.

(3). For each interval, the successive derivatives of $\underline{\underline{U}}(t)$ are calculated from (2.2.22) at the initial time of the interval.

(4). The evolution operator over the interval is constructed from (2.2.21).

(5). The time-ordered product (2.2.6) of the evolution operators is used to find $\underline{\underline{U}}(t,t_0)$.

2.2.3. THE MATCHING POWER SERIES METHOD

The matching power series method was used in early work before it was suggested the Taylor series approach was easier to program, and probably more efficient [17]. The power series technique was used only for the interaction of an N-level molecule with a single continuous wave electric field, and is presented below for this type of interaction. However, it can be easily adapted for other interactions.

As in the RPI and the Taylor series approaches, the total time interval is divided into n subintervals. For subintervals of equal duration $\Delta\phi$, the time variable ϕ (2.2.10) can be expressed as,

$$\phi_j = \eta + (j-1)\Delta\phi, \quad j=1,2\ldots n, \quad 0\le\eta\le\Delta\phi \qquad (2.2.25)$$

where j labels the interval in which ϕ falls.

The time-dependent equation (2.2.3), recast in terms of ϕ through (2.2.10) and (2.2.25), on the jth interval is [23,32],

$$\frac{d}{d\eta}\underline{U}^{(j)}(\phi_j,0) = -\frac{i}{\omega}[\underline{E} - \mathcal{E}^0\cos(\eta+[j-1]\Delta\phi)\underline{\mu}]\underline{U}^{(j)}(\phi_j,0)$$

$$= -\frac{i}{\omega}[\underline{E} - \mathcal{E}^0\cos(\eta)\cos([j-1]\Delta\phi)\underline{\mu}$$

$$+ \mathcal{E}^0\sin(\eta)\sin([j-1]\Delta\phi)\underline{\mu}]\underline{U}^{(j)}(\phi_j,0) \qquad (2.2.26)$$

where,

$$\underline{U}^{(j)}(\phi_j,0) = \sum_{n=0}^{\infty} \underline{\mathcal{E}}_n^{(j)}\eta^n, \qquad (2.2.27)$$

and $\underline{\mathcal{E}}_0^{(1)} = \underline{I}$. The expansion coefficient matrices $\underline{\mathcal{E}}_n^{(j)}$ are determined by substitution of (2.2.27) into (2.2.26), and then grouping like powers of η [23,32,67],

$$\omega(n+1)\underline{\mathcal{E}}_{n+1}^{(j)} = -i\underline{E}\,\underline{\mathcal{E}}_n^{(j)} + i\underline{\mu}\mathcal{E}^0\cos[(j-1)\Delta\phi]\sum_{k=0}\frac{(-1)^k}{(2k)!}\underline{\mathcal{E}}_{n-2k}^{(j)}$$

$$- i\underline{\mu}\mathcal{E}^0\sin[(j-1)\Delta\phi]\sum_{k=0}\frac{(-1)^k}{(2k+1)!}\underline{\mathcal{E}}_{n-2k-1}^{(j)}, \qquad (2.2.28)$$

where $(n - 2k) \geq 0$ and $(n - 2k - 1) \geq 0$. At the beginning of each interval, the initial conditions are updated to $\underline{\mathcal{E}}_0^{(j)} = \underline{U}^{(j-1)}(\phi_{j-1})$.

The general procedure for applying the matching power series method is:

(1). For the first ($j = 1$) interval, the expansion coefficients are calculated from (2.2.28), with $\underline{\mathcal{E}}_0^{(1)} = \underline{I}$.

(2). The evolution operator $\underline{U}^{(1)}(\Delta\phi,0)$ is calculated from (2.2.27), for $\eta = \Delta\phi$.

(3). The initial conditions for the second interval are set to $\underline{\mathcal{E}}_0^{(2)} = \underline{U}^{(1)}(\Delta\phi,0)$.

For the jth interval,

(4). The expansion coefficients are calculated from (2.2.28) with

the new set of initial conditions $\underline{\underline{G}}_0^{(j)} = \underline{\underline{U}}^{(j-1)}((j-1)\Delta\theta,0)$.

(5). The evolution operator $\underline{\underline{U}}^{(j)}(j\Delta\theta,0)$ is calculated from (2.2.27), for $\eta = \Delta\theta$.

(6). The initial conditions for the next interval are set to $\underline{\underline{G}}_0^{(j+1)} = \underline{\underline{U}}^{(j)}(j\Delta\theta,0)$.

(7). Steps (4) through (6) are repeated until the evolution operator is calculated over the entire time interval of interest.

2.2.4. PERIODIC HAMILTONIANS AND THE FLOQUET FORMALISM

If the Hamiltonian is periodic and self-adjoint, the time-dependent populations to long times can be calculated from the evolution operators over the first period [3,14,16,32,33,70]. Furthermore, the Floquet technique can be used to efficiently determine the long time- and phase-averaged populations of the molecular states [32]. The Floquet formalism presented here is distinct from the Floquet secular equation approach [16,33].

In what follows, the interaction of a molecule with a single continuous wave electric field is considered, where the Hamiltonian is periodic in the variable θ, (2.2.10), with period 2π. It can be shown that the time-dependent coefficients (2.2.1) can be written as,

$$\underline{a}(\theta+2k\pi) = \underline{\underline{U}}(\theta,0)[\underline{\underline{U}}(2\pi,0)]^k\underline{\underline{U}}^{-1}(\delta,0)\underline{a}(0), \quad k=0,1,2,\ldots \qquad (2.2.29)$$

where $\underline{a}(0)$ is the occupation matrix at $t = 0$, and $0 \leq \theta \leq 2\pi$. Thus, the computation of the evolution operators only over the interval $[0,2\pi]$ provides sufficient information to determine the time-dependent coefficients at any time t.

The matrix $\underline{\underline{U}}(2\pi,0)$ can be efficiently raised to the power k by

first diagonalizing $\underline{\underline{U}}(2\pi,0)$ [32,69]:

$$\underline{\underline{U}}(2\pi,0) = \underline{\underline{S}}\ \exp[i2\pi\underline{\underline{\Delta}}]\ \underline{\underline{S}}^{-1}, \tag{2.2.30}$$

where $\underline{\underline{S}}$ is the unitary matrix of orthonormal eigenvectors of $\underline{\underline{U}}(2\pi,0)$; $\exp[i2\pi\underline{\underline{\Delta}}]$ is a diagonal matrix containing the characteristic exponents, Δ_{jj}, which are related to the eigenvalues λ_j of $\underline{\underline{U}}(2\pi,0)$ through [10,32],

$$\begin{aligned} 2\pi\Delta_{jj} &= \arctan[\mathrm{Im}(\lambda_j)/\mathrm{Re}(\lambda_j)], && \mathrm{Re}(\lambda_j) \geq 0, \\ &= \pi + \arctan[\mathrm{Im}(\lambda_j)/\mathrm{Re}(\lambda_j)], && \mathrm{Re}(\lambda_j) < 0 \end{aligned} \tag{2.2.31}$$

where $\mathrm{Im}(\lambda_j)$ and $\mathrm{Re}(\lambda_j)$ are the imaginary and real components of λ_j, respectively. From (2.2.30), successive multiplication of $\underline{\underline{U}}(2\pi,0)$ yields,

$$\underline{\underline{U}}(2k\pi,0) = [\underline{\underline{U}}(2\pi,0)]^k = \underline{\underline{S}}\exp[i\underline{\underline{\Delta}}2k\pi]\underline{\underline{S}}^{-1}. \tag{2.2.32}$$

Hence, the computation of the time-dependent coefficients to long times reduces to the calculation of,

$$\underline{a}(\theta+2k\pi) = \underline{\underline{U}}(\theta,0)\underline{\underline{S}}\exp[i\underline{\underline{\Delta}}2k\pi]\underline{\underline{S}}^{-1}\underline{\underline{U}}^{-1}(\delta,0)\underline{a}(0). \tag{2.2.33}$$

The temporal results presented above are independent of Floquet's theorem [3,14,32].

The Floquet technique yields an efficient method of calculating the long time- and phase-averaged populations from the properties of $\underline{\underline{U}}(2\pi,0)$. The eigenvectors and characteristic exponents of $\underline{\underline{U}}(2\pi,0)$, see (2.2.30), are used to construct the periodic matrix $\underline{\underline{Z}}(\theta)$,

$$\underline{\underline{Z}}(\theta) = \underline{\underline{U}}(\theta,0)\underline{\underline{S}}\exp[-i\underline{\underline{\Delta}}\theta] = Z(\theta + 2k\pi), \tag{2.2.34}$$

and the phase-dependent column vector $\underline{b}_0(\delta)$,

$$\underline{b}_0(\delta) = \underline{\underline{S}}^{-1}\underline{\underline{U}}^{-1}(\delta,0)\underline{a}(0). \tag{2.2.35}$$

Substitution of (2.2.34) and (2.2.35) into (2.2.33) gives the time-dependent coefficients in Floquet form [32],

$$\underline{a}(\vartheta + 2k\pi) = \underline{\underline{Z}}(\vartheta)\exp[i\underline{\underline{\Delta}}(\vartheta+2k\pi)]\underline{b}_0(\delta). \tag{2.2.36}$$

The time- and phase-dependent population of the state j is $P_j = |a_j(t)|^2$, see (2.1.11), which can be expressed as [32],

$$P_j(\vartheta) = \sum_{p,q} Z_{jp}(\vartheta)\beta_{pq}(\vartheta,\delta)Z^*_{qj}(\vartheta), \tag{2.2.37}$$

where,

$$\underline{\underline{\beta}}(\vartheta,\delta) = \exp[i\underline{\underline{\Delta}}\vartheta]\underline{b}_0(\delta)\underline{b}^{\dagger}_0(\delta)\exp[-i\underline{\underline{\Delta}}\vartheta]. \tag{2.2.38}$$

The diagonal elements of this matrix have the form $|b_{0p}(\delta)|^2$, while the off-diagonal elements have the form $b_{0p}(\delta)b^*_{0q}(\delta)\exp[i(\Delta_p - \Delta_q)\vartheta]$.

The long time-averaged phase-dependent state population is given by [3,32],

$$\begin{aligned}\bar{P}_j(\delta) &= \lim_{t\to\infty}\frac{1}{\tau}\int_0^{\tau} P_j(t)dt \\ &= \sum_p \frac{1}{2\pi}\int_0^{2\pi}|Z_{jp}(\vartheta)b_{0p}(\delta)|^2 d\vartheta,\end{aligned} \tag{2.2.39}$$

where the oscillating off-diagonal terms of $\underline{\underline{\beta}}(\vartheta,\delta)$ average to zero, and the periodicity of $\underline{\underline{Z}}(\vartheta)$ permits the change of the integration limits.

The time-dependent, phase-averaged population of state j is,

$$\bar{P}_j(t) = \frac{1}{2\pi}\int_0^{2\pi} P_j(t)d\delta, \tag{2.2.40}$$

while the long time- and phase-averaged population is given by,

$$\bar{P}_j = \sum_p \frac{1}{4\pi^2}\int_0^{2\pi}\int_0^{2\pi}|Z_{jp}(\omega t + \delta)b_{0p}(\delta)|^2 d\delta d(\omega t). \tag{2.2.41}$$

When the effect of phase is significant, the physically meaningful time-dependent or long-time averaged populations generally correspond to the phase-averaged time-dependent or steady state populations,

(2.2.40) or (2.2.41), respectively [3,32]. Equation (2.2.41), as a function of ω, can often correspond to the physically observed absorption spectrum of the molecule [3,23,71-73].

The procedure for evaluating the temporal and/or long time- and phase-averaged populations for periodic (in 2π) molecule-EMF interactions can be summarized as follows:

(1). The evolution operators in ϕ are calculated over the interval $[0,2\pi]$.

(2). $\underline{U}(2\pi,0)$ is diagonalized; the matrices $\underline{S}$ and $\underline{S}^{-1}$ are constructed from the orthonormalized eigenvectors of $\underline{U}(2\pi,0)$ and the characteristic exponents are calculated from the eigenvalues of $\underline{U}(2\pi,0)$.

(3). Equation (2.2.33) is used to calculate the time-dependent coefficients to long times.

(4). For long time- and phase-averaged results, the periodic matrix $\underline{Z}(\phi)$ is constructed from (2.2.34) and $\underline{b}_0(\delta)$ is constructed from (2.2.35).

(5). The required long time- and/or phase-averaged state population can be calculated from (2.2.39), (2.2.40), or (2.2.41).

2.2.5. GENERAL COMPUTATIONAL CONSIDERATIONS

Of the three methods reviewed in Secs. 2.2.1, 2.2.2 and 2.2.3 for the evaluation of the evolution operators, the RPI is the most computationally efficient and the easiest to apply, since the integral in (2.2.8) is the same for each matrix element, and the elements differ only in the values of E_l (or E_{lk} for the interaction representation) and μ_{lk}. Both the RPI and Taylor series are "interval contained", in

that they calculate explicitly each $\underline{U}(t_j,t_{j-1})$, and apply the time-ordered product (2.2.6) to determine $\underline{U}(t,0)$. The matching power series does not calculate the $\underline{U}(t_j,t_{j-1})$ individually, but directly produces $\underline{U}(t,0)$, because the initial conditions of each interval are updated to the evolution operator of the previous interval. This step makes the matching power series slightly more complicated to apply than the Taylor series approach, which starts afresh with each subinterval.

The determination of the computational parameters needed for convergence can require considerable investigation. The convergence of the RPI method is determined by the number of subintervals into which the time interval of interest is subdivided. However, after a certain point, further subdivision does not lead to increased significant figures [17,31]. The convergence of the Taylor and power series method can be taken to as many significant figures as desired. The size of the subintervals and the number of terms in the Taylor or power series expansion can be balanced to find the most efficient means of calculating the evolution operators [17,23,32]. In general, the conditions for convergence are problem dependent. Hence, a discussion of the computational parameters for the relevant exact calculations is given directly with the examples in this thesis.

The evaluation of the time-dependent and steady state populations of the molecular states for these calculations requires the use of standard computational methods. Diagonalization of matrices was performed by the EISPACK subroutine CG [74]. The complex error functions, present in the Riemann product integral analysis of pulsed laser-molecule interactions via (2.2.15), are evaluated by the IMSL Special Functions Library subroutine CERFZ [75]. For the interaction

of a molecule with a continuous wave electric field, only the evolution operators over the first period, $0 \leq t \leq 2\pi/\omega$, are required for the evaluation of all the relevant populations of the molecular states; integration over this interval to find the long time- and/or phase-average of the temporal state populations was performed using Simpson's Rule [76]. The number of integration points employed is given with each set of examples.

The IMSL Special Functions Library subroutine BSJNS [75] is used to calculate Bessel functions of integer order, which are required in the applications of some of the approximate solutions to the time-dependent Schrödinger equation discussed later in this thesis.

2.3. APPROXIMATE SOLUTIONS TO THE SCHRÖDINGER EQUATION

Exact solutions provide an accurate description of molecule-EMF interactions, but can be difficult to interpret. Approximate, analytical solutions provide a means of analyzing and predicting the effects of changing various molecular and field parameters. The approximate solutions to the time-dependent wave equation, (2.1.20) or (2.1.22), as derived by two standard methods, time-dependent perturbation theory [1,10,47] and the two-level rotating wave approximation [2,12,18,19], will be reviewed here for the interaction of a molecule with a single continuous wave electric field, (2.1.13). In what follows, the transition from the initially fully populated ground state, labelled 1, to a discrete excited state k is considered.

2.3.1. TIME-DEPENDENT PERTURBATION THEORY

Following time-dependent perturbation theory, the time-dependent

coefficients in (2.1.22) are expanded perturbatively,

$$b_j(t) = \sum_{n=0}^{\infty} b_j^{(n)}(t), \tag{2.3.1}$$

where n indicates the order of the perturbation. Substitution of (2.3.1) into (2.1.22) yields a series of coupled differential equations for the $b_j^{(n)}$:

$$\frac{d}{dt}b_j^{(n)} = \frac{i}{2}\mathcal{E}^0 \sum_{p=1}^{\infty} (\underline{\mu}_{jp}\cdot\hat{e})b_p^{(n-1)}\left(\exp[i\delta]\exp[i(E_{jp} + \omega)t]\right.$$

$$\left. + \exp[-i\delta]\exp[i(E_{jp} - \omega)t]\right) \tag{2.3.2}$$

For frequencies tuned to $\omega \approx E_{k1}/n$, these equations can be readily solved [1,10] when only the resonance term is considered, that is, the term with the denominator of the form $(E_{k1} - n\omega)$. This resonance term will be large relative to all the other (non-resonant) terms. The solution for the dominant resonant term in $b_k^{(n)}$, for all n, is [1],

$$b_k^{(n,res)}(t) = (-\tfrac{1}{2}\mathcal{E}^0)^n e^{[-in\delta]}\mathcal{M}^{(n)}\,\frac{e^{[-i(n\omega-E_{k1})t]} - 1}{(n\omega - E_{k1})}, \tag{2.3.3}$$

where, for $n > 1$,

$$\mathcal{M}^{(n)} = \sum_{p_1}\sum_{p_2}\cdots\sum_{p_{n-1}=1}^{\infty} \frac{\underline{\mu}_{kp_1}\cdot\hat{e}\;\underline{\mu}_{p_1p_2}\cdot\hat{e}\;\cdots\underline{\mu}_{p_{n-1}1}\cdot\hat{e}}{[(n-1)\omega-E_{p_1 1}][(n-2)\omega-E_{p_2 1}]\cdots[\omega-E_{p_{n-1}1}]} \tag{2.3.4}$$

and for $n = 1$, $\mathcal{M}^{(1)} = \underline{\mu}_{k1}\cdot\hat{e}$.

From (2.1.11) and (2.3.3), the time-dependent transition probability for the n-photon absorption from the ground to the kth excited state is [1,10],

$$|b_k^{(n,res)}(t)|^2 = 4(\tfrac{1}{2}\mathcal{E}^0)^{2n}|\mathcal{M}^{(n)}|^2\,\frac{\sin^2[(n\omega - E_{k1})t/2]}{(n\omega - E_{k1})^2}. \tag{2.3.5}$$

The resonance approximation for the time-dependent population of the excited state is very useful in interpreting n-photon absorption

effects [1,10]. For example, it predicts that the one-photon transition (n = 1) between states 1 and k depends only on the transition dipole between the two states and on the strength and polarization vector of the applied CW field. For n = 1, the molecule-EMF coupling occurring in (2.3.5) is $\mathcal{M}^{(1)}\mathcal{E}^0 = \underline{\mu}_{k1}\cdot\hat{e}\mathcal{E}^0$. The perturbative result indicates that the effects of permanent dipoles, and neighbouring energy states, on the 1 → k transition occur in higher order photon transitions (n > 1). Some results for the crucial quantity $\mathcal{M}^{(n)}$ occurring in (2.3.5), relevant to this point (see also Sec. 2.4), are given below for n-photon transitions (n = 1,2,3) and for two- and three-level systems [1,10].

For a two-level system (final state k = 2):

$$\mathcal{M}^{(1)} = \underline{\mu}_{21}\cdot\hat{e}, \tag{2.3.6a}$$

$$\mathcal{M}^{(2)} = -\frac{1}{\omega}[(\underline{\mu}_{22} - \underline{\mu}_{11})\cdot\hat{e}]\underline{\mu}_{12}\hat{e}, \tag{2.3.6b}$$

$$\mathcal{M}^{(3)} = \frac{1}{4\omega^2}\left(2[(\underline{\mu}_{22} - \underline{\mu}_{11})\cdot\hat{e}]^2 - (\underline{\mu}_{12}\hat{e})^2\right)\underline{\mu}_{12}\hat{e}, \tag{2.3.6c}$$

and for a three level system,

$$\mathcal{M}^{(1)} = \underline{\mu}_{k1}\cdot\hat{e},\ k = 2,3 \tag{2.3.7a}$$

$$\mathcal{M}^{(2)} = -\frac{1}{\omega}[(\underline{\mu}_{kk}-\underline{\mu}_{11})\cdot\hat{e}]\underline{\mu}_{12}\hat{e} + \frac{1}{(\omega-E_{p1})}[\underline{\mu}_{kp}\cdot\hat{e}][\underline{\mu}_{p1}\hat{e}],\ p\neq 1,k \tag{2.3.7b}$$

$$\begin{aligned}\mathcal{M}^{(3)} = {} & \frac{1}{4\omega^2}\left(2[(\underline{\mu}_{kk} - \underline{\mu}_{11})\cdot\hat{e}]^2 - (\underline{\mu}_{1k}\hat{e})^2\right)\underline{\mu}_{1k}\hat{e} \\ & - \frac{1}{(\omega-E_{p1})\omega}[(\mu_{kk} - \underline{\mu}_{11})\cdot\hat{e}][\underline{\mu}_{kp}\cdot\hat{e}][\underline{\mu}_{p1}\hat{e}] \\ & + \frac{1}{(2\omega-E_{p1})(\omega-E_{p1})}[(\mu_{pp} - \underline{\mu}_{11})\cdot\hat{e}][\underline{\mu}_{kp}\hat{e}][\underline{\mu}_{p1}\hat{e}] \\ & + \frac{1}{2\omega}[\underline{\mu}_{k1}\hat{e}]\left[\frac{-1}{(2\omega-E_{p1})}[\underline{\mu}_{kp}\hat{e}]^2 + \frac{1}{(\omega-E_{p1})}[\underline{\mu}_{1p}\hat{e}]^2\right]\Big),\quad p\neq 1,k.\end{aligned} \tag{2.3.7c}$$

Perturbation theory is valid only for weak perturbations and for short times [47,56]. For strong perturbations, the non-resonant terms in (2.3.2) are no longer negligible. On resonance, $\omega = E_{k1}/n$, and (2.3.5) becomes [1],

$$|b_k^{(n,res)}(t)|^2_{n\omega=\Delta E} = (\tfrac{1}{2}\mathcal{E}^0)^{2n}|\mathcal{M}^{(n)}|^2 t^2, \qquad (2.3.8)$$

which exceeds unity (see (2.1.8)) for $t > (\tfrac{1}{2}\mathcal{E}^0)^{-n}|\mathcal{M}^{(n)}|^{-1}$. The divergence of perturbation theory results at long times can be avoided by using the rotating wave approximation, or, of course, exact techniques.

2.3.2. THE ROTATING WAVE APPROXIMATION

Generalized rotating wave approximation (GRWA) techniques are available for the interaction of many-level molecules with a CW laser [17,31,77-79]. The basic idea is to identify in the time-dependent wave equation, through the use of appropriate transformations, the dominant resonance terms; the other ("counter-rotating") terms are off-resonance, tend to average to zero upon integration of the time-dependent wave equation, and are neglected. The resulting effective Hamiltonian for the problem is independent of time, which enables the corresponding (approximate) time-dependent wave equation to be readily solved without recourse to perturbation theory. However, the nature of the GRWA solution depends on the stationary state energy level configuration of the molecule and on the particular transition being investigated [17,31,77-80]. Furthermore, the GRWA does not generally yield closed-form analytical results for the required transition probabilities. Hence, the direct interpretive and predictive usefulness of the GRWA regarding laser-molecule interactions

is limited.

The precursor to the GRWA for many-level problems is the two-level analogue, the rotating wave approximation (RWA) [2,12,18,19]. The RWA yields closed form analytical expressions for the populations of the molecular states and is one of the most powerful methods available for interpreting and predicting the effects, in two-level molecule-laser interactions, due to changes in the parameters characterizing the molecule and the CW laser [2,3,5,12-18,22,24-30]. The results for the two-level RWA are summarized here for systems with [2] and without [12,14,18,19] permanent dipoles and neglecting excited state decay. A detailed derivation of the two-level RWA with permanent dipoles, and including the effects of excited state decay, is given in Sec. 3.1. The results given below, including the criteria for the validity of the RWA, can be extracted as special cases of the results in Sec. 3.1. The initial conditions for what follows are given by (2.1.27), noting that a two-level system is being considered and transitions from the ground state one to the excited state two are being investigated.

The RWA solution for the time-dependent excited state population is [2],

$$P_2^{(N)}(t) = \frac{|C(N)|^2}{(\Delta E - N\omega)^2 + |C(N)|^2} \sin^2\left(\tfrac{1}{2}\left[(\Delta E - N\omega)^2 + |C(N)|^2\right]^{1/2} t\right) \qquad (2.3.9)$$

where C(N) is the molecule-EMF coupling [2],

$$C(N) = 2N\omega \frac{\underline{\mu}_{12}\cdot\hat{e}}{\underline{d}\cdot\hat{e}} J_N(\underline{d}\cdot\hat{e}\mathcal{E}^0/\omega)\exp[iN\delta], \quad N \geq 1. \qquad (2.3.10)$$

N is the number of photons involved in the transition from the ground state one to the excited state two, $J_N(z)$ is a Bessel function [81] of integer order N and argument z, and $\underline{d}$ is the difference between the permanent moments of the two states,

$$\underline{d} \equiv \underline{\mu}_{22} - \underline{\mu}_{11}. \tag{2.3.11}$$

Unlike perturbation theory, the RWA can be used to long times, and the time-dependent excited state population is a smooth sinusoidal pattern of absorption and emission, with period,

$$T_{RWA} = \frac{2\pi}{[(\Delta E - N\omega)^2 + |C(N)|^2]^{1/2}}. \tag{2.3.12}$$

On resonance, $\omega = \Delta E/N$, the period is,

$$T_{RWA}^{res} = \frac{2\pi}{|C(N)|_{res}}, \tag{2.3.13}$$

where C(N) is evaluated the resonance frequency.

When d = 0, the molecule-EMF coupling (2.3.10) becomes,

$$\lim_{d\to 0} C(N) = \underline{\mu}_{12}\cdot\hat{e}\mathcal{E}^0\delta_{N,1}, \tag{2.3.14}$$

since $\lim_{z\to 0}[2J_N(z)/z] = \delta_{N1}$ [81]. The time-dependent excited state population (2.3.9) reduces to the Rabi result for a two-level atom [12,18,19],

$$P_2^{Rabi}(t) = \frac{|\underline{\mu}_{12}\cdot\hat{e}\mathcal{E}^0|^2}{(\Delta E-\omega)^2 + |\underline{\mu}_{12}\cdot\hat{e}\mathcal{E}^0|^2}\sin^2\left(\tfrac{1}{2}\left[(\Delta E-\omega)^2+|\underline{\mu}_{12}\cdot\hat{e}\mathcal{E}^0|^2\right]^{1/2}t\right), \tag{2.3.15}$$

with a resonance period (the Rabi period),

$$T_{Rabi}^{res} = \frac{2\pi}{|\underline{\mu}_{12}\cdot\hat{e}\mathcal{E}^0|}. \tag{2.3.16}$$

When averaged over long times, see (2.1.12), the excited state population, as a function of the applied field frequencies around resonance, gives the N-photon absorption spectrum of the molecule. In the absence of decay, the time-dependent excited state population for a given frequency reaches a steady state, where the long time-averaged excited state population is generally a non-zero constant. The RWA

steady state population for state two is [12,18,19],

$$\bar{P}_2^{(N)} = \frac{|C(N)|^2}{2[(\Delta E - N\omega)^2 + |C(N)|^2]} . \qquad (2.3.17)$$

If C(N) is approximately constant over the frequency spread of the N-photon resonance profile, then $\bar{P}_2^{(N)}$ as a function of frequency is essentially a Lorentzian curve with a full width at half maximum (FWHM) of [2],

$$FWHM(N) = 2|C(N)|_{res}/N . \qquad (2.3.18)$$

For d = 0, the curve is perfectly Lorentzian,

$$\bar{P}_2^{Rabi} = \frac{|\underline{\mu}_{12}\cdot\hat{e}\mathcal{E}^0|^2}{2[(\Delta E - \omega)^2 + |\underline{\mu}_{12}\cdot\hat{e}\mathcal{E}^0|^2]} , \qquad (2.3.19)$$

with,

$$FWHM(Rabi) = 2|\underline{\mu}_{12}\cdot\hat{e}\mathcal{E}^0| . \qquad (2.3.20)$$

The RWA is a valid approximation if [2,3,26,34],

$$|C(N)| \ll \omega \simeq \Delta E/N, \qquad (2.3.21)$$

and if the spectral peaks are well separated. The constraint (2.3.21) ensures that the counter-rotating terms oscillate many times in the period of the excited state population, and thus average to zero. Another useful parameter in the RWA is the coupling strength, $\beta(N)$,

$$\beta(N) = N|C(N)|/\Delta E. \qquad (2.3.22)$$

Thus, from (2.3.21), when $\beta(N) \ll 1$, the RWA is quantitatively applicable.

In the RWA, the neglected counter-rotating terms account for the differences between the results of exact and RWA calculations. The RWA predicts the time-averaged excited state population goes to zero for

off-resonance frequencies, since from (2.3.17) $\bar{P}_2 \to 0$ as $(\Delta E - N\omega)$ increases. In exact calculations, the background (off-resonance) excited state population is generally larger than that predicted by the RWA. The counter-rotating terms also cause deviations of the exact resonance frequencies, called Bloch-Siegert shifts for $d = 0$ [14,35], from the "ideal" perturbative or RWA predictions $\omega = \Delta E/N$, $N = 1,2,3...$ Finally, the RWA temporal solution predicts smooth oscillations with time between zero and maximum population of the excited state. However, in exact calculations, small oscillations with period $\simeq \pi/\omega$ are superimposed on the larger oscillations of the time-dependent excited state population [21,32]. These small oscillations are also attributable to counter-rotating effects [32].

Depending on how well the conditions for its applicability are met, the RWA provides either a qualitatively or a quantitatively accurate picture of the time-dependent and spectral features of the molecule-laser interaction for a two-level system [2,3,24,26,28,34]. The deviations from the RWA - non-zero backgrounds, Bloch-Siegert shifts, and the oscillations superimposed on the RWA temporal behaviour - can be accounted for only by a more rigorous treatment. However, despite its inability to predict these features, the RWA is a powerful interpretive and predictive tool in the analysis of temporal and spectral results. Indeed, even by distinguishing between resonance and counter-rotating effects, the RWA is invaluable in the analysis of two-colour absorption processes, see Chapters 5 and 6.

The effect of collision decay has been considered for the two-level system in the RWA for $d = 0$; spontaneous decay will be considered in Chapter 3 for $d \neq 0$. Collisions between molecules can

induce emission by the excited state. In this case, the average time $\mathcal{T}$ between molecular collisions is the average lifetime of the excited state. The number of molecules decaying per unit time due to collisions is given by a Poisson distribution [82-84],

$$dn(t) = \frac{1}{\mathcal{T}}\exp[-t/\mathcal{T}]dt. \tag{2.3.23}$$

The average population of the excited state is [82-84],

$$\bar{P}_2^{Rabi,\mathcal{T}} = \frac{1}{\mathcal{T}}\int_0^\infty P_2(t)\exp[-t/\mathcal{T}]dt \tag{2.3.24}$$

$$= \frac{|\underline{\mu}_{12}\cdot\hat{e}\mathcal{E}^0|^2}{2\left((\Delta E-\omega)^2 + \mathcal{T}^{-2} + |\underline{\mu}_{12}\cdot\hat{e}\mathcal{E}^0|^2\right)}\ . \tag{2.3.25}$$

The original Lorentzian absorption spectrum of (2.3.19) is broadened by the collision rate. The effect of permanent dipoles can easily be incorporated by substituting (2.3.17) into (2.3.24) to obtain,

$$\bar{P}_2^{(N,\mathcal{T})} = \frac{|C(N)|^2}{2\left((\Delta E-N\omega)^2 + \mathcal{T}^{-2} + |C(N)|^2\right)}\ . \tag{2.3.26}$$

2.4. THE EFFECTS OF PERMANENT DIPOLES

The spectral and temporal behaviour of both $d = 0$ and $d \neq 0$ molecules interacting with a continuous wave electric field has been explored by a number of techniques: the RWA [2,3,25,26]; time-dependent perturbation theory [1,10]; perturbation theory based on the Floquet secular equation with the RWA solution as the zeroth order problem [34]; and, of course, exact calculations in the semi-classical dipole approximation [2,3,5,13,22-24,26,31,36,87]. The effects of $d \neq 0$, relative to the $d = 0$ analogue, are first discussed for two-level and then for many-level systems. Rotational averaging is discussed in

2.4.1. TWO-LEVEL SYSTEMS

NO DIFFERENCE BETWEEN PERMANENT DIPOLES

Many of the features of one-photon absorption processes can be discussed by using the RWA d = 0 (Rabi) results for the temporal and steady state populations of the excited state, see (2.3.15) and (2.3.19), respectively. The d = 0 molecule-EMF coupling, (2.3.14), is a linear function of field strength and hence the FWHM(Rabi), (2.3.20), of the one-photon Lorentzian absorption spectra increases linearly with increasing $\mathcal{E}^0$. The RWA resonance frequency is $\omega = \Delta E$, independent of $\mathcal{E}^0$, and the resonance maximum in the spectrum is $P_2^{Rabi} = 0.5$. Similarly, from (2.3.16), the period of the resonant temporal behaviour of the excited state varies inversely with increasing field strength.

As the coupling strength $\beta(1,d = 0) \equiv b = \underline{\mu}_{12} \cdot \hat{e}\mathcal{E}^0/\Delta E$ increases to $b \approx 1$ or $b > 1$, the RWA results become progressively more unreliable. The width of the one-photon resonance profile increases with increasing $\mathcal{E}^0$ but is no longer well represented by (2.3.20); additional dynamic backgrounds occur which are not symmetrical with respect to the resonance frequency; and the resonance frequency is (Bloch-Siegert) shifted to high frequency relative to ΔE [14,35].

Clearly, the RWA, with d = 0, will support only one-photon transitions. For d = 0, the discussion of multi-photon two-level transitions is therefore based on perturbative or exact results involving model systems. For N > 1, the resonance maxima are again 0.5, and for large field strengths $\mathcal{E}^0$, the resonance frequencies are shifted to higher frequency than the weak field limit of $\omega = \Delta E/N$. In

general, these Bloch-Siegert shifts are more pronounced, for a given $\mathcal{E}^0$, as the photonicity of the transition increases. The FWHM(N), for a given (N), increase with increasing field strength but decrease with increasing N for fixed $\mathcal{E}^0$. The period of the time-dependent population of the excited state is qualitatively inversely proportional to the FWHM(N).

Time-dependent perturbation theory, Sec. 2.3.1, can be used to predict that, for a two-level system, all odd N-photon transitions are allowed, and all even N-photon transitions are forbidden when d = 0. If N is even and d = 0, it can be shown, from (2.3.4), that $M^{(N)} = 0$ and hence even photon transitions are forbidden. Equation (2.3.6b) gives an explicit example for N = 2, with $d = \mu_{22} - \mu_{11} = 0$. On the other hand, if N is odd, then $M^{(N)} \neq 0$, as illustrated explicitly for N = 3 by (2.3.6c).

NON-ZERO DIFFERENCE BETWEEN PERMANENT DIPOLES

The above discussion for d = 0 essentially holds for atoms where generally the $\mu_{jj} = 0$. The effects due to lasers interacting with molecules can be considerably different, since, for example, often the $\mu_{jj} \neq 0$ and $d \neq 0$. Some of the features of the effects of $d \neq 0$ [2,3,26-30] on laser-molecule interactions, relative to the d = 0 case [14,18,19], can be explained qualitatively by using the molecular RWA results for the time-dependent and steady state populations of the excited state given by (2.3.9) and (2.3.17), respectively.

The effects of $d \neq 0$ on absorption sprectra can be discussed qualitatively for one-photon transitions by comparing the resonance profiles predicted by (2.3.17), N = 1, with the corresponding d = 0

(Rabi) result of (2.3.19). In keeping with the d = 0 spectra, the d ≠ 0 RWA resonance frequency is $\omega = \Delta E$, and the resonance spectral maximum is 0.5. However, the d ≠ 0 molecule-EMF coupling (2.3.10) is not a linear function of $\mathcal{E}^0$ and is not independent of ω, but depends on $2J_1(z)/z$, where $z = \underline{d}\cdot\hat{e}\mathcal{E}^0/\omega$. This function initially decreases from its maximum of one (at d = 0 or $\mathcal{E}^0 = 0$) with increasing z. For larger z, the molecule-EMF coupling, following the trends of the Bessel function $J_1(z)$, is a damped oscillatory function of increasing z and possesses nodes at certain values of z [2,3,85]. Hence, the FWHM(1), (2.3.18), initally decreases with increasing field strength, and then can increase (with successively decreasing magnitude) or decrease with increasing $\mathcal{E}^0$. This oscillating magnitude of the FWHM(1) with respect to increasing $\mathcal{E}^0$ is in direct contrast to the linear behaviour of the d = 0 FWHM(Rabi) as a function of $\mathcal{E}^0$. Furthermore, the d ≠ 0 resonance profile, unlike the d = 0 absorption peak, is not generally symmetric with respect to the applied field frequency ω [2,3,5,26]. If the field strength is such that $J_1(\underline{d}\cdot\hat{e}\mathcal{E}^0/\omega)_{\omega\simeq\Delta E}$ is close to a node, then small changes in ω can shift the Bessel function away from the critical point resulting in large changes in the magnitude of the molecule-EMF coupling. In such cases, the resonance profile can be highly asymmetric, and (2.3.18) does not apply. A second consequence of the frequency dependence of the molecule-EMF coupling is the RWA prediction of oscillatory fringes in the absorption spectra [2,3,5,26]. These fringes are associated with minima and maxima in the off-resonance population which occur because of the oscillatory nature of C(1) with respect to ω. These fringes are not predicted for the d = 0 spectral analogue.

The oscillating nature of the $d \neq 0$ coupling is also reflected in the period of the resonant excited state population (2.3.13). Since the period varies inversely as the FWHM(1), (2.3.18), the trends in the period as a function of $\mathcal{E}^0$ are the inverse of those discussed above for the FWHM(1). Thus, a general effect of $d \neq 0$ is to increase the period of the excited state population, or reduce the width of the resonance, relative to the atomic ($d = 0$) case.

Unlike the $d = 0$ RWA, the $d \neq 0$ RWA predicts multi-photon transitions, both even and odd, are allowed for a two-level system. The RWA resonance frequency is $\omega = \Delta E/N$, with spectral resonance maximum 0.5, for all N. In contrast to the $d \neq 0$ one-photon transition, the molecule-EMF couplings for all multi-photon transitions initially increase, and then decrease, with increasing field strength. For larger field strengths, the coupling is a damped oscillatory function of increasing $\mathcal{E}^0$. The Bessel functions $J_N(z)$, on which the molecule-EMF coupling depends, are generally decreasing functions of (1) increasing argument for fixed order and (2) increasing order for fixed argument [81,85]. These trends are reflected directly in the FWHM(N), and hence, in general, the FWHM(N), for a given field strength, decrease with increasing N; exceptions occur because of the oscillatory nature of the Bessel function. The asymmetry of the resonance profile and the presence of oscillatory fringes, predicted in the $N = 1$ absorption spectrum, are also anticipated for the multi-photon transitions. The periods of the resonance time-dependent populations for multi-photon transitions follow the inverse of the trends observed in the FWHM(N).

The analytical RWA results for the N-photon resonance profiles,

and for the temporal behaviour of the excited state, are very useful in predicting the effects of $d \neq 0$. Although exceptions can occur for small ΔE and $C(N)$ close to a molecule-EMF coupling node [24,34], the molecular RWA is generally qualitatively reliable for $\beta(N) = |C(N)|N/\Delta E \ll 1$. Thus, for example, since $C(1)$ is a decreasing damped oscillatory function of z, with a maximum value of $\mu_{12}\cdot\hat{e}\mathcal{E}^0$ when $d = 0$, the RWA does not necessarily become progressively less reliable with increasing $\mathcal{E}^0$, as it does when $d = 0$. In fact, for a given molecule, the $d \neq 0$ RWA is generally applicable for field strengths far greater than can be used for the analogous $d = 0$ RWA. Nevertheless, the RWA does not predict many important features of the $d \neq 0$ single- and multi-photon exact two-level problem. For example, the shifts in the resonance frequency, relative to the RWA prediction of $\Delta E/N$, can be to either high or low frequency for $d \neq 0$; for $d = 0$ the Bloch-Siegert shift is always to high frequency relative to the weak field limit of $\Delta E/N$ for $N = 1,3...$

2.4.2. MANY LEVEL SYSTEMS.

In many-level systems, two-level results are quantitatively reliable only when a transition involves two levels that are well separated (decoupled) from the neighbouring states. The usefulness of the two-level problem, as an approximation for more realistic atoms and molecules, has been discussed often in the literature [12-20]. Indeed, this problem, in the electric dipole approximation, has long provided a basis for the study of linear and non-linear interactions between electromagnetic radiation and molecules [2,3,5,13,21-26].

One of the most important analytical techniques for predicting and

interpreting certain aspects of N-photon transitions in many level systems is semi-classical time-dependent perturbation theory, Sec. 2.3.1. It is very useful in predicting allowed transitions and time-dependent transition probabilities and rates, for times much less than those associated with high populations in the excited states [1,10,56]. For example, multi-photon transitions with N even are forbidden in two-level atoms (d = 0) but permitted in many-level atoms. This difference may be illustrated by comparing the results of two- and three-level perturbation theory. The two-photon, two-level transition is zero since, from (2.3.6b), $\mathcal{M}^{(2)} = 0$ when d = 0. On the other hand, $\mathcal{M}^{(2)}$ for the three-level problem, (2.3.7b), is non-zero in this limit, due to the presence of an extra term, which depends on $[\underline{\mu}_{kp}\cdot\hat{e}][\underline{\mu}_{pi}\cdot\hat{e}]$ for the $1 \rightarrow k$ transition. Thus, the presence of the third stationary state provides a mechanism for the two-photon transition between the ground and first excited state when d = 0.

2.4.3. ORIENTATIONAL AVERAGING

In general the molecule-EMF configuration influences a laser-molecule interaction, as illustrated explicitly by the results of time-dependent perturbation theory and the RWA. For example, the RWA indicates that for a two level system, an arrangement where $\hat{e}$ and $\underline{\mu}_{12}$ are perpendicular would not result in excitation of state two while one where $\hat{e}$ and $\underline{d}$ are perpendicular would eliminate the effects of the permanent dipoles.

Molecules, unlike atoms, are not isotropic and hence molecular resonance profiles, and the related temporal effects, are dependent on the orientation of the molecule relative to the direction of the

applied electromagnetic field. For example, the direction of the (molecular fixed) $\underline{\mu}_{12}$ and $\underline{d}$ for a two-level molecule depend on their orientation relative to the (space fixed) polarization vector $\hat{e}$. In the examples in this thesis, only fixed molecule-EMF configurations, where the transition and permanent moments are aligned with the direction of polarization of the field(s), are considered.

In many applications, where molecules are freely tumbling in space, the physically meaningful absorption spectra or temporal behaviour of the molecular states correspond to an orientational average over fixed molecule-EMF configuration results [3,13,22,26,36,71,86,87]. For example, the orientationally averaged steady state spectrum is given by [26,71,88],

$$(\bar{P}_j)_{rot} = \frac{1}{8\pi^2}\int_0^{2\pi}\int_0^{\pi}\int_0^{2\pi}\bar{P}_j(\alpha,\beta,\gamma)\sin(\beta)d\alpha d\beta d\gamma, \qquad (2.4.1)$$

where (α,β,γ) are the Euler angles specifying the rotation of the molecule-fixed coordinate axes with respect to the space-fixed coordinate axes [89], and $\bar{P}_j(\alpha,\beta,\gamma)$ is given by (2.1.12) for a given molecule-EMF configuration.

Rotational averaging can diminish the effects of the molecule-laser interaction relative to the fixed molecule-EMF case. Thus, in the orientationally averaged spectrum, the resonance maximum can be less than 0.5, the FWHM(N) can be narrower, and the resonance profile can be more sharply pointed than the fixed-configuration spectrum.

Table 2.1. Definitions of Frequently Used Symbols

The symbols below are defined in Chapter 2 and occur frequently in the following chapters.

$a_j(t)$ - the time-dependent coefficient of the jth stationary state in the Schrödinger representation.

$b_j(t)$ - the time-dependent coefficient of the jth stationary state in the interaction representation.

C(N) - the RWA molecule-EMF coupling for the two-level system interacting with a continuous wave electric field.

$d_{jk} = \mu_{jj} - \mu_{kk}$, the difference between the permanent dipole moments of the jth and kth stationary states; $d \equiv \mu_{22} - \mu_{11}$.

E_j - the energy of the jth stationary state; eigenvalue of the unperturbed Hamiltonian, $\hat{H}_0$.

$E_{jk} = E_j - E_k$

$\Delta E = E_2 - E_1$

$\underline{\underline{E}}$ - the diagonal energy matrix, $(\underline{\underline{E}})_{jk} = E_j \delta_{jk}$.

$\hat{e}_j$ - the unit polarization vector of the jth electric field.

$\underline{\mathcal{E}}(t)$ - the time-dependent electric field.

$\mathcal{E}^0$ - the amplitude of the electric field.

$\hat{H}$ - the total Hamiltonian operator.

$J_n(z)$ - Bessel function of integer order n and argument $z = \underline{d} \cdot \hat{e} \mathcal{E}^0 / \omega$.

$P_j(t)$ - the time-dependent population of the jth stationary state.

$\bar{P}_j(t)$ - the phase-averaged time-dependent population of the jth stationary state.

Table 2.1 Continued.

$\bar{P}_j(\delta)$ - the fixed-phase long time-averaged population of the jth stationary state.

$\bar{P}_j$ - the long time- and phase-averaged population of the jth stationary state.

t - time.

$\underline{\underline{U}}(t_k, t_{k-1})$ - the evolution operator matrix from $t = t_k$ to $t = t_{k-1}$.

γ_j - the spontaneous decay rate of the jth stationary state.

$\underline{\underline{\gamma}}$ - the diagonal decay matrix, $(\underline{\underline{\gamma}})_{jk} = \gamma_j \delta_{jk}$.

δ_{jk} - the Kronecker delta: $\delta_{jj} = 1$; $\delta_{jk} = 0$ for $j \neq k$.

δ - the phase of the applied electric field.

$\hat{\underline{\mu}}$ - the dipole moment operator.

$\underline{\underline{\mu}}$ - the dipole moment matrix; $(\underline{\underline{\mu}})_{jk} \equiv \langle \phi_j | \hat{\underline{\mu}} | \phi_k \rangle$.

$\underline{\mu}_{jk}$, $j \neq k$ - the transition dipole moment between the jth and kth stationary state; $\underline{\mu}_{jk} = (\underline{\underline{\mu}})_{jk}$.

$\underline{\mu}_{jj}$ - the permanent dipole moment of the jth stationary state.

τ_p - the "pulse duration" associated with a Gaussian pulse.

ω - the circular frequency of the applied electric field.

CHAPTER 3

THE TWO-LEVEL ROTATING WAVE APPROXIMATION

INCLUDING EXCITED STATE DECAY

In this chapter, an analytical solution is derived, in the rotating wave approximation (RWA), for the time-dependent and time-averaged excited state populations for a two-level molecule, with permanent dipoles and subject to excited state decay, interacting with a single continuous wave electric field. The detailed derivation of the RWA results is given in Sec. 3.1. The form, and hence the analysis, of the RWA solutions with excited state decay can be simplified by imposing the resonance condition, see Sec. 3.2. The conditions for the applicability of the RWA are also given in Sec. 3.2. In Secs. 3.1 and 3.2, where appropriate, special limits are taken which reduce the results of this chapter to those contained in Chapter 2. The dynamic effects of permanent dipoles and of excited state decay are discussed in Sec. 3.3. Section 3.4 contains numerical examples, which (1) compare the temporal evolution of the excited state obtained from exact calculations with the predictions from the RWA results derived in Sec. 3.1 and (2) investigate the interplay between the effects of excited state decay and the permanent dipoles. Section 3.5 contains some general comments about the work presented in this chapter.

3.1. DERIVATION OF RWA SOLUTIONS WITH EXCITED STATE DECAY AND PERMANENT DIPOLES.

3.1.1. RWA TEMPORAL SOLUTIONS

To begin the derivation of the RWA analytical solution, the time-dependent wave equation (2.1.23) for a two-level system is recast into an interaction representation via the transformation [2,3],

$$a_j = b_j \exp\left[-i[E_j t - \underline{\mu}_{jj}\cdot\int_0^t \underline{\mathcal{E}}(t')dt']\right], \quad j=1,2, \tag{3.1.1}$$

where $j = 1$ is associated with the ground state and $j = 2$ represents the excited state. Equation (3.1.1) is a unitary transformation since $|a_j(t)|^2 = |b_j(t)|^2$.

Using the definitions $\Delta E \equiv E_2 - E_1$ and $\underline{d} \equiv \underline{\mu}_{22} - \underline{\mu}_{11}$, and substituting (3.1.1) into (2.1.23), yields,

$$i\frac{d}{dt}\underline{b}(t) = \begin{bmatrix} 0 & H_{12} \\ H_{21} & -i\gamma_2/2 \end{bmatrix}\underline{b}(t), \tag{3.1.2}$$

where $H_{12} = H_{21}^*$, and,

$$H_{12} = -\underline{\mu}_{12}\cdot\underline{\mathcal{E}}(t)\exp\left[-i\Delta E t + i\underline{d}\cdot\hat{e}\frac{\mathcal{E}^0}{\omega}[\sin(\omega t+\delta)-\sin\delta]\right]. \tag{3.1.3}$$

The following identities are useful [81],

$$\exp[iz\sin\Omega] = \sum_{k=-\infty}^{\infty} J_k(z)\exp[ik\Omega], \tag{3.1.4}$$

and

$$J_k(z) = (z/2k)(J_{k+1}(z) + J_{k-1}(z)), \tag{3.1.5}$$

where $J_k(z)$ is a Bessel function of integer order k and argument z. The off-diagonal Hamiltonian can be written as,

$$H_{12} = -\frac{1}{2}\underline{\mu}_{12}\cdot\hat{e}\mathcal{E}^0\exp[-i\underline{d}\cdot\hat{e}\frac{\mathcal{E}^0}{\omega}\sin\delta]\sum_{k=-\infty}^{\infty}\frac{2k}{z}J_k(z)\exp[ik\delta]\exp[-i(\Delta E-k\omega)t], \tag{3.1.6}$$

where $z \equiv (\underline{d}\cdot\hat{e}\mathcal{E}^0/\omega)$.

The resonances in (3.1.6) occur when $\omega = \Delta E/N$, $N = 1,2,3\ldots$ Thus, the resonance term, $k = N$, has the form $NJ_N(z)\exp[i0t]$. The counter-rotating terms have the form $kJ_k(z)\exp[-(N-k)\omega t]$, $k \neq N$, and therefore tend to average to zero. Hence, the largest contribution to $b_1(t)$ and $b_2(t)$ comes from the resonance term, and all counter-rotating terms are neglected. The conditions for the applicability of the RWA are discussed in detail in Sec. 3.2.3.

With the neglect of the counter-rotating terms, the RWA off-diagonal Hamiltonian becomes,

$$H_{12} = -\frac{1}{2}C(N)\exp[-i\underline{d}\cdot\hat{e}\frac{\mathcal{E}^0}{\omega}\sin\delta]\exp[-i(\Delta E-N\omega)t], \tag{3.1.7}$$

where $C(N)$ is the molecule-EMF coupling for the N-photon transition,

$$C(N) = 2N\omega\frac{\underline{\mu}_{12}\cdot\hat{e}}{\underline{d}\cdot\hat{e}}J_N(z)\exp[iN\delta]. \tag{3.1.8}$$

This coupling is identical to that found in the one-field RWA [2,3], where permanent dipoles have been included but excited state decay has been neglected, see (2.3.10).

Equation (3.1.2) and (3.1.7) can be used to generate the second order differential equations,

$$\frac{d^2}{dt^2}b_1(t) = -i[\Delta E-N\omega-\frac{i}{2}\gamma_2]\frac{d}{dt}b_1(t) - \frac{1}{4}|C(N)|^2b_1(t), \tag{3.1.9a}$$

and,

$$\frac{d^2}{dt^2}b_2(t) = i[\Delta E-N\omega+\frac{i}{2}\gamma_2]\frac{d}{dt}b_2(t) - [\frac{1}{4}|C(N)|^2 - \frac{i}{2}\gamma_2(\Delta E-N\omega)]b_2(t). \tag{3.1.9b}$$

Subject to the initial conditions $b_1(0) = 1$ and $b_2(0) = 0$, and from (3.1.2) and (3.1.7),

$$\frac{d}{dt}b_1\Big|_{t=0} = 0; \qquad \frac{d}{dt}b_2\Big|_{t=0} = -\frac{1}{2}C(N)^{*}\exp\left[i\underline{d}\cdot\hat{e}\frac{\mathcal{E}^0}{\omega}\sin\delta\right], \tag{3.1.10}$$

the equations (3.1.9) are solved by the method of characteristics [90], yielding,

$$b_1(t) = \exp[-\frac{i}{2}(\Delta E - N\omega - \frac{i}{2}\gamma_2)t]\left(\cos[\frac{1}{2}(\Gamma_R + i\Gamma_I)^{1/2}t] + i\,\frac{(\Delta E - N\omega - \frac{i}{2}\gamma_2)}{[\Gamma_R + i\Gamma_I]^{1/2}}\sin[\frac{1}{2}(\Gamma_R + i\Gamma_I)^{1/2}t]\right), \tag{3.1.11}$$

and,

$$b_2(t) = \frac{-C(N)^{*}}{[\Gamma_R + i\Gamma_I]^{1/2}}\exp[i\underline{d}\cdot\hat{e}\frac{\mathcal{E}^0}{\omega}\sin\delta]\sin[\frac{1}{2}(\Gamma_R + i\Gamma_I)^{1/2}t] \times \exp[\frac{i}{2}(\Delta E - N\omega + \frac{i}{2}\gamma_2)t], \tag{3.1.12}$$

where,

$$\Gamma_R \equiv (\Delta E - N\omega)^2 - \frac{1}{4}\gamma_2^2 + |C(N)|^2, \tag{3.1.13a}$$

$$\Gamma_I \equiv -\gamma_2(\Delta E - N\omega). \tag{3.1.13b}$$

The square-root of the complex number $Z_0 = \Gamma_R + i\Gamma_I$ can be found by expressing Z_0 in polar form [91],

$$Z_0 = r_0(\cos(\theta + 2n\pi) + i\sin(\theta + 2n\pi))$$

$$= r_0\exp[i(\theta + 2n\pi)], \qquad n=0,1,2\ldots \tag{3.1.14}$$

where,

$$r_0^2 = \Gamma_R^2 + \Gamma_I^2, \tag{3.1.15a}$$

$$\cos(\theta + 2n\pi) = \Gamma_R/r_0, \tag{3.1.15b}$$

$$\sin(\theta + 2n\pi) = \Gamma_I/r_0. \tag{3.1.15c}$$

These last two equations may be rewritten,

$$\tan(\phi+2n\pi) = \Gamma_I/\Gamma_R, \text{ or} \tag{3.1.16a}$$

$$\phi = \begin{cases} \arctan(\Gamma_I/\Gamma_R), & \Gamma_R \geq 0 \quad (3.1.16b) \\ \pi + \arctan(\Gamma_I/\Gamma_R), & \Gamma_R < 0 \quad (3.1.16c) \end{cases}$$

where the different values of ϕ for positive or negative Γ_R reflect the periodicity of $\tan(\phi)$ over $[-\frac{1}{2}\pi, +\frac{1}{2}\pi]$.

Taking the root of (3.1.14) yields [91],

$$(Z_0)^{1/2} = (r_0)^{1/2}\exp[i\tfrac{1}{2}(\phi+2n\pi)]$$

$$= \pm(r_0)^{1/2}\exp[i\tfrac{1}{2}\phi], \tag{3.1.17}$$

where the last equation follows since the roots will be distinct only for n = 0 and n = 1. Defining the real and imaginary parts of $(Z_0)^{1/2}$ as α and β, respectively, where α and β are real,

$$(Z_0)^{1/2} \equiv \alpha + i\beta = (\Gamma_R + i\Gamma_I)^{1/2}, \tag{3.1.18}$$

and substituting (3.1.13) into (3.1.17) yields,

$$(r_0)^{1/2} = [\Gamma_R^2 + \Gamma_I^2]^{1/4}, \tag{3.1.19a}$$

$$\alpha = \pm[\Gamma_R^2 + \Gamma_I^2]^{1/4}\cos(\phi/2), \tag{3.1.19b}$$

$$\beta = \pm[\Gamma_R^2 + \Gamma_I^2]^{1/4}\sin(\phi/2), \tag{3.1.19c}$$

where ϕ is defined by (3.1.16). It should be emphasized that, from (3.1.17), the positive root of α is paired with the positive root of β, and likewise for the negative roots.

Another quantity of interest is,

$$\alpha^2 + \beta^2 = [\Gamma_R^2 + \Gamma_I^2\ ]^{1/2}$$

$$= \left([(\Delta E-N\omega)^2 - \tfrac{1}{4}\gamma_2^2 + |C(N)|^2]^2 + \gamma_2^2(\Delta E-N\omega)^2\right)^{1/2}. \qquad (3.1.20)$$

From (2.1.11), (3.1.12) and the definitions above, the time-dependent population of the excited state is,

$$P_2^{(N,\gamma)}(t) = |b_2(t)|^2$$

$$= \frac{|C(N)|^2}{(\alpha^2 + \beta^2)}\exp[-\tfrac{1}{2}\gamma_2 t]\sin[\tfrac{1}{2}(\alpha+i\beta)t]\sin[\tfrac{1}{2}(\alpha-i\beta)t]. \qquad (3.1.21)$$

The following relations [92a,b] are used to reduce (3.1.21),

$$\sin(x\pm y) = \sin(x)\sin(y) \pm \cos(x)\cos(y), \qquad (3.1.22a)$$

$$\sin(ix) = i\sinh(x), \qquad (3.1.22b)$$

$$\cos(ix) = \cosh(x), \qquad (3.1.22c)$$

where sinh(x) and cosh(x) are the hyperbolic sine and cosine of x, respectively. The time-dependent excited state population becomes,

$$P_2^{(N,\gamma)}(t) = \frac{|C(N)|^2}{(\alpha^2 + \beta^2)}\exp[-\tfrac{1}{2}\gamma_2 t]$$

$$X\ [\sin^2(\tfrac{1}{2}\alpha t)\cosh^2(\tfrac{1}{2}\beta t) + \sinh^2(\tfrac{1}{2}\beta t)\cos^2(\tfrac{1}{2}\alpha t)]. \qquad (3.1.23)$$

This equation can be further simplified by using the trigonometric identities,

$$2\cos^2(x) = 1 + \cos(2x), \qquad (3.1.24a)$$

$$2\cosh^2(x) = 1 + \cosh(2x), \qquad (3.1.24b)$$

giving,

$$P_2^{(N,\gamma)}(t) = \frac{|C(N)|^2}{2(\alpha^2 + \beta^2)}[\cosh(\beta t)-\cos(\alpha t)]\exp[-\tfrac{1}{2}\gamma_2 t]. \qquad (3.1.25)$$

The choice of positive or negative roots for α and β in (3.1.19) does not affect $P_2^{(N,\gamma)}(t)$ since $\cosh(-\beta t) = \cosh(\beta t)$ and $\cos(-\alpha t) = \cos(\alpha t)$.

In the absence of excited state decay, $\gamma_2 = 0$, and from (3.1.13), $\Gamma_R > 0$ and $\Gamma_I = 0$. From (3.1.16b), $\vartheta = 0$; hence $\beta = 0$, and

$$\alpha = \Gamma_R^{1/2} = [(\Delta E - N\omega)^2 + |C(N)|^2]^{1/2}. \tag{3.1.26}$$

Substituting $\gamma_2 = 0$, $\beta = 0$ and α from (3.1.26) into (3.1.25) yields the RWA result (2.3.9) for the $\gamma_2 = 0$ time-dependent excited state population in the presence of permanent dipoles [2].

The time-dependent population of the ground state can be shown to be,

$$P_1^{(N,\gamma)}(t) = \frac{\exp[-\frac{1}{2}\gamma_2 t]}{(\alpha^2+\beta^2)} \Big| (\alpha+i\beta)\cos[\tfrac{1}{2}(\alpha+i\beta)t] + i(\Delta E - N\omega - \tfrac{i}{2}\gamma_2)\sin[\tfrac{1}{2}(\alpha+i\beta)t] \Big|^2, \tag{3.1.27}$$

or,

$$\begin{aligned} P_1^{(N,\gamma)}(t) = \frac{\exp[-\frac{1}{2}\gamma_2 t]}{(\alpha^2+\beta^2)} \Big(& [\alpha^2+\beta^2][\sinh^2(\tfrac{1}{2}\beta t)+\cos^2(\tfrac{1}{2}\alpha t)] \\ & + [(\Delta E - N\omega)^2 + \tfrac{1}{4}\gamma_2^2][\sinh^2(\tfrac{1}{2}\beta t) + \sin^2(\tfrac{1}{2}\alpha t)] \\ & - [\alpha(\Delta E - N\omega) - \tfrac{1}{2}\beta\gamma_2]\sinh(\beta t) \\ & + [\beta(\Delta E - N\omega) + \tfrac{1}{2}\alpha\gamma_2]\sin(\alpha t) \Big). \end{aligned} \tag{3.1.28}$$

Again, the choice of positive or negative roots for α and β does not affect $P_1^{(N,\gamma)}(t)$ since $\pm x\sin(\pm y) = +x\sin(y)$ and $\pm x\sinh(\pm y) = +x\sinh(y)$.

3.1.2. TIME-AVERAGED RWA SOLUTIONS.

For completeness, the long time-average (2.1.12) of the excited state population is discussed. In the absence of decay, the long-time average of the time-dependent excited state population reaches a steady state, (2.3.17). Once excited state decay has been introduced, the limit $\tau \to \infty$ in (2.1.12) is not taken, and the concept of a "steady

state" becomes more difficult. When decay is significant, it is the time average, over a particular time τ, of the excited state population, as a function of frequency, which constitutes the spectrum. The time τ, which can be regarded as an observation time, must also be short enough that the system has not completely decayed prior to measurement. From (3.1.25), the time average of the time-dependent excited state population, when excited state decay is included, is,

$$\bar{P}_2^{(N,\gamma,\tau)} = \frac{1}{\tau}\int_0^{\tau} P_2^{(N,\gamma)}(t)dt$$

$$= \frac{|C(N)|^2}{2\tau(\alpha^2+\beta^2)}\left(\left[(\beta^2-\tfrac{1}{4}\gamma_2^2)^{-1}\left(\tfrac{1}{2}\gamma_2\cosh(\beta\tau)+\beta\sinh(\beta\tau)\right)\right.\right.$$

$$\left.-(\alpha^2+\tfrac{1}{4}\gamma_2^2)^{-1}\left(\tfrac{1}{2}\gamma_2\cos(\alpha\tau)-\alpha\sin(\alpha\tau)\right)\right]\exp\left[-\tfrac{1}{2}\gamma_2\tau\right]$$

$$\left.-\tfrac{1}{2}\gamma_2\left[(\beta^2-\tfrac{1}{4}\gamma_2^2)^{-1}-(\alpha^2+\tfrac{1}{4}\gamma_2^2)^{-1}\right]\right), \qquad (3.1.29)$$

where the following integral has been used [92c],

$$\int\cos(\alpha t)\exp[-\tfrac{1}{2}\gamma_2 t]dt = \exp[-\tfrac{1}{2}\gamma_2 t](\alpha^2+\tfrac{1}{4}\gamma_2^2)^{-1}\left(\tfrac{1}{2}\gamma_2\cos(\alpha t)-\alpha\sin(\alpha t)\right) \qquad (3.1.30)$$

The hyperbolic cosine equivalent can be found by replacing α with $i\beta$ and using the relations (3.1.22b,c).

3.2. RWA TIME-DEPENDENT POPULATIONS ON RESONANCE

The RWA temporal solutions (3.1.25) and (3.1.28) are much more complicated than their $\gamma_2 \neq 0$ analogues, see for example, (2.3.9). The discussion of the decay solutions can be simplified by studying the time-dependent populations on resonance, $\omega = \Delta E/N$; indeed, the dynamic evolution of a system is often studied on resonance. The RWA

time-dependent populations of the ground and excited states on resonance are given in Sec. 3.2.1. The behaviour of the resonance solutions is discussed in Sec. 3.2.2.

3.2.1. RWA TIME-DEPENDENT SOLUTIONS ON RESONANCE

When $\omega = \Delta E/N$, $\Gamma_I = 0$, and from (3.1.13a) and (3.1.19),

$$\alpha_r = |(|C(N)|^2 - \tfrac{1}{4}\gamma_2^2)|^{1/2}\cos(\theta/2), \tag{3.2.1}$$

$$\beta_r = |(|C(N)|^2 - \tfrac{1}{4}\gamma_2^2)|^{1/2}\sin(\theta/2), \tag{3.2.2}$$

where the subscript "r" designates the resonance condition. The value of θ, from (3.1.16), depends on the relative sizes of $|C(N)|$ and $\frac{1}{2}\gamma_2$, of which there are three possiblities: $|C(N)| > \frac{1}{2}\gamma_2$ (weak decay [w]); $|C(N)| = \frac{1}{2}\gamma_2$ (critical decay [cr]); and $|C(N)| < \frac{1}{2}\gamma_2$ (strong decay [s]) [63]. There are three corresponding resonance values of θ:

$$\theta_w = 0, \qquad |C(N)| > \tfrac{1}{2}\gamma_2 \tag{3.2.3a}$$

$$\theta_{cr} = 0, \qquad |C(N)| = \tfrac{1}{2}\gamma_2 \tag{3.2.3b}$$

$$\theta_s = \pi, \qquad |C(N)| < \tfrac{1}{2}\gamma_2. \tag{3.2.3c}$$

Using these results, and (3.2.1), (3.2.2) and (3.1.16), the resonance time-dependent populations of the excited state (3.1.25), for the three types of decay, are,

for weak decay:

$$P^{(N,\gamma)}_{2,r,w}(t) = \alpha_r^{-2}|C(N)|^2\exp[-\tfrac{1}{2}\gamma_2 t]\sin^2[\tfrac{1}{2}\alpha_r t]; \tag{3.2.4}$$

for critical decay:

$$P^{(N,\gamma)}_{2,r,cr}(t) = \tfrac{1}{16}\gamma_2^2 t^2\exp[-\tfrac{1}{2}\gamma_2 t] = \tfrac{1}{4}|C(N)|^2 t^2\exp[-\tfrac{1}{2}\gamma_2 t]; \tag{3.2.5}$$

for strong decay:

$$P^{(N,\gamma)}_{2,r,s}(t) = \beta_r^{-2}|C(N)|^2\exp[-\tfrac{1}{2}\gamma_2 t]\sinh^2[\tfrac{1}{2}\beta_r t]. \qquad (3.2.6)$$

The time-dependent population of the excited state for critical decay, (3.2.5), can be extracted from either (3.2.4) or (3.2.6) by taking the limit $\alpha_r \to 0$ or $\beta_r \to 0$, respectively, and making use of the standard limits, $\lim_{x\to 0}[\sin(x)/x] = 1$ and $\lim_{x\to 0}[\sinh(x)/x] = 1$ [68].

The corresponding time-dependent resonant populations of the ground state, which can be derived in an analogous method to $P^{(N,\gamma)}_{2,r}(t)$, are,

for weak damping:

$$P^{(N,\gamma)}_{1,r,w}(t) = \alpha_r^{-2}\exp[-\tfrac{1}{2}\gamma_2 t]\left(\tfrac{1}{2}\gamma_2\sin[\tfrac{1}{2}\alpha_r t] + \alpha_r\cos[\tfrac{1}{2}\alpha_r t]\right)^2; \qquad (3.2.7)$$

for critical damping:

$$P^{(N,\gamma)}_{1,r,cr}(t) = \exp[-\tfrac{1}{2}\gamma_2 t]\left(\tfrac{1}{4}\gamma_2 t + 1\right)^2; \qquad (3.2.8)$$

for strong damping:

$$P^{(N,\gamma)}_{1,r,s}(t) = \beta_r^{-2}\exp[-\tfrac{1}{2}\gamma_2 t]\left(\tfrac{1}{2}\gamma_2\sinh[\tfrac{1}{2}\beta_r t] + \beta_r\cosh[\tfrac{1}{2}\beta_r t]\right)^2 \qquad (3.2.9)$$

The strength of decay influences the behavior of the excited and ground state populations. For weak decay, the solutions (3.2.4) and (3.2.7) apply, and the system has sufficient time to oscillate between the ground and excited states before the damping function begins to dominate. At the point of critical decay, any oscillatory nature of the populations, (3.2.5) and (3.2.8), ceases. For strong decay, the transition between the ground and excited states is supressed even further.

3.2.2. RESONANCE BEHAVIOUR OF THE RWA TIME-DEPENDENT POPULATIONS

The simplified resonance solutions can be used for analytical

interpretive and/or predictive purposes. For example, the temporal locations of the maxima and minima of the resonance excited and ground state population can be found from the time-dependent solutions. The RWA can be used to illustrate how the relative sizes of the decay rate and the coupling influence the times at which the maxima and minima occur. These times also provide a means of comparing the results of exact calculations with the RWA predictions. The behaviour of the time-dependent solutions will be analyzed first for weak decay, then for critical decay, and finally for strong decay.

WEAK DECAY

The critical points in the resonance excited and ground state populations can be found from the nodes in their time-derivatives. For weak coupling, the rate of change of the population in state two, from (3.2.4), is,

$$\frac{d}{dt}P^{(N,\gamma)}_{2,r,w}(t) = \alpha_r^{-2}|C(N)|^2\exp[-\tfrac{1}{2}\gamma_2 t]\sin[\tfrac{1}{2}\alpha_r t]$$

$$\times\left(-\tfrac{1}{2}\gamma_2\sin[\tfrac{1}{2}\alpha_r t] + \alpha_r\cos[\tfrac{1}{2}\alpha_r t]\right). \qquad (3.2.10)$$

Equation (3.2.10) is zero when $\sin[\frac{1}{2}\alpha_r t] = 0$ and when $\left(-\frac{1}{2}\gamma_2\sin[\frac{1}{2}\alpha_r t] + \alpha_r\cos[\frac{1}{2}\alpha_r t]\right) = 0$, or,

$$t = 2n\pi/\alpha_r = 2\pi n/[|C(N)|^2 - \tfrac{1}{4}\gamma_2^2]^{1/2}, \qquad n = 0,1,2... \quad (3.2.11)$$

and,

$$t' = 2\alpha_r^{-1}[\arctan(2\alpha_r/\gamma_2) + n\pi], \qquad n = 0,1,2... \quad (3.2.12)$$

At the times given by (3.2.11), the second order time-derivative of $P^{(N,\gamma)}_{2,r,w}(t)$ is positive, so $t = 2n\pi/\alpha_r$, $n = 0,1,2...$ correspond to minima in the time-dependent excited state population. Substitution of

$t = 2n\pi/\alpha_r$ into (3.2.4) yields $P^{(N,\gamma)}_{2,r,w}(2n\pi/\alpha_r) = 0$. Hence, these minima in the excited state population are zero and their temporal locations are perfectly periodic, with period $2\pi/\alpha_r$. Since α_r decreases with increasing (weak) decay, the period of the excited state population increases with increasing (weak) decay.

At t', the second order time-derivative of $P^{(N,\gamma)}_{2,r,w}(t)$ is negative, hence these times correspond to maxima in the time-dependent excited state population. $P^{(N,\gamma)}_{2,r,w}(t)$ can be evaluated at t' by regarding the angle $\eta = \frac{1}{2}\alpha_r t' = \arctan(2\alpha_r/\gamma_2)$ as part of the right-angled triangle (see (3.2.1) with $\theta_w = 0$),

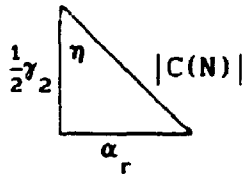

from which the following relations are established:

$$\sin[\tfrac{1}{2}\alpha_r t'] = \alpha_r/|C(N)|, \qquad (3.2.13a)$$

$$\cos[\tfrac{1}{2}\alpha_r t'] = \tfrac{1}{2}\gamma_2/|C(N)|. \qquad (3.2.13b)$$

Substituting (3.2.13a) into (3.2.4), the corresponding excited state population, $P^{(N,\gamma)}_{2,r,w}(t')$, is,

$$\left[P^{(N,\gamma)}_{2,r,w}(t')\right]^{max} = \exp[-\tfrac{1}{2}\gamma_2 t']. \qquad (3.2.14)$$

Thus, the maximum amplitude of the excited state population decreases exponentially with increasing n in (3.2.12). As with the minima, the maxima are separated by $2\pi/\alpha_r$. Hence, the maxima in the excited state population are periodic in time only, and not amplitude.

In the limit that $\gamma_2 \to 0$, $\arctan(2\alpha_r/\gamma_2) = \frac{1}{2}\pi$, and, from (3.2.12), $t' = 2\alpha_r^{-1}(n+\frac{1}{2})\pi$. Hence, for $\gamma_2 = 0$, the time-dependent excited state

population maxima are centred between the minima.

The maxima and minima of the ground state population can be analyzed in a similar manner. The time derivative of $P^{(N,\gamma)}_{1,r,w}$ is,

$$\frac{d}{dt}P^{(N,\gamma)}_{1,r,w}(t) = -|C(N)|^2\alpha_r^{-2}\exp[-\tfrac{1}{2}\gamma_2 t]\sin[\tfrac{1}{2}\alpha_r t]$$

$$X\ (\tfrac{1}{2}\gamma_2\sin[\tfrac{1}{2}\alpha_r t] + \alpha_r\cos[\tfrac{1}{2}\alpha_r t]) \qquad (3.2.15)$$

The zeroes of the rate of change of the ground state population are,

$$t = 2n\pi/\alpha_r \qquad n = 0,1,2... \quad (3.2.16)$$

and,

$$t'' = 2\alpha_r^{-1}[(n+1)\pi - \arctan(2\alpha_r/\gamma_2)]. \qquad n = 0,1,2... \quad (3.2.17)$$

From the second order derivatives, (3.2.16) correspond to maxima in $P^{(N,\gamma)}_{1,r,w}$ while (3.2.17) corresponds to the minima. From the substitution of (3.2.16) into (3.2.7), the maxima in the ground state population decay exponentially with increasing n,

$$\left[P^{(N,\gamma)}_{1,r,w}\right]^{max} = \exp[-n\pi\gamma_2/\alpha_r], \qquad (3.2.18)$$

and coincide temporally with the minima in $P^{(N,\gamma)}_{2,r,w}$, see (3.2.11).

On the other hand, the minima, $P^{(N,\gamma)}_{1,r,w}(t'') = 0$, in the ground state population do not coincide with the maxima in the excited state population. From (3.2.17) and (3.2.12), a maximum of the excited state population and the associated minimum of the ground state population are separated by,

$$(t'' - t') = 2\alpha_r^{-1}[\pi - 2\arctan(2\alpha_r/\gamma_2)]. \qquad (3.2.19)$$

When $\gamma_2 = 0$, (3.2.19) vanishes, and the maxima of $P^{(N)}_{2,r}(t)$ coincide with the associated minima of $P^{(N)}_{1,r}(t)$. As γ_2 increases, $2\alpha_r/\gamma_2$ decreases, and (3.2.19) increases.

On resonance, the sum of the ground and excited state time dependent populations, (3.2.7) and (3.2.4), is,

$$P^{(N,\gamma)}_{tot,r,w}(t) = P^{(N,\gamma)}_{1,r,w}(t) + P^{(N,\gamma)}_{2,r,w}(t)$$

$$= \alpha_r^{-2}\exp[-\tfrac{1}{2}\gamma_2 t]\left[(|C(N)|^2 + \tfrac{1}{4}\gamma_2^2)\sin^2(\tfrac{1}{2}\alpha_r t)\right.$$

$$\left. + \alpha_r^2\cos^2(\tfrac{1}{2}\alpha_r t) + \tfrac{1}{2}\gamma_2\alpha_r\sin\alpha_r t\right]. \qquad (3.2.20)$$

The time derivative of (3.2.20) is,

$$\frac{d}{dt}P^{(N,\gamma)}_{tot,r,w}(t) = -\gamma_2|C(N)|^2\alpha_r^{-2}\sin^2[\tfrac{1}{2}\alpha_r t]\exp[-\tfrac{1}{2}\gamma_2 t],$$

or,

$$\frac{d}{dt}P^{(N,\gamma)}_{tot,r,w}(t) = -\gamma_2 P^{(N,\gamma)}_{2,r,w}(t). \qquad (3.2.21)$$

The rate of decay of the system is zero for $\gamma_2 = 0$; the system is conservative when decay can be neglected. The trends in the rate of change of the total time-dependent population follow the trends of the time-dependent population of the excited state. Hence, the rate of decay of the system is zero when $t = 2n\pi/\alpha_r$, (3.2.11), when the excited state has minimum (zero) population; the magnitude of the rate is largest when $t = t'$, (3.2.12), and $n = 0$, i.e., when the excited state has maximum population. Substitution of (3.2.12) into (3.2.21) gives the fastest rate of decay of the system,

$$\left.\frac{d}{dt}P^{(N,\gamma)}_{tot,r,w}\right|_{t=t'} = -\gamma_2\exp[-(\gamma_2/\alpha_r)\arctan(2\alpha_r/\gamma_2)]. \qquad (3.2.22)$$

This behaviour is consistent with the structure of the model, which decays only from the excited state.

CRITICAL DECAY

A similar analysis can be made of the resonance RWA solutions for

the ground and excited state populations, (3.2.8) and (3.2.5), in the case of critical damping. The rates of change of $P^{(N,\gamma)}_{1,r,cr}(t)$ and $P^{(N,\gamma)}_{2,r,cr}(t)$ are,

$$\frac{d}{dt}P^{(N,\gamma)}_{1,r,cr}(t) = -\tfrac{1}{8}\gamma_2^2 t\exp[-\tfrac{1}{2}\gamma_2 t](\tfrac{1}{4}\gamma_2 t + 1), \qquad (3.2.23)$$

and,

$$\frac{d}{dt}P^{(N,\gamma)}_{2,r,cr}(t) = \tfrac{1}{8}\gamma_2^2 t\exp[-\tfrac{1}{2}\gamma_2 t](-\tfrac{1}{4}\gamma_2 t + 1). \qquad (3.2.24)$$

Thus, $P^{(N,\gamma)}_{1,r,cr}(t)$ does not pass through any maxima or minima for $t > 0$. $P^{(N,\gamma)}_{2,r,cr}(t)$ is zero at $t = 0$, and is a maximum at the other temporal node in (3.2.24),

$$t = 4/\gamma_2. \qquad (3.2.25)$$

The maximum value of $P^{(N,\gamma)}_{2,r,cr}(t)$ is,

$$P^{(N,\gamma)}_{2,r,cr}(4/\gamma_2) = \exp[-2]. \qquad (3.2.26)$$

The rate of decay of $P^{(N,\gamma)}_{1,r,cr}(t) + P^{(N,\gamma)}_{2,r,cr}(t)$ has the same form as (3.2.21), with $P^{(N,\gamma)}_{2,r,w}(t)$ replaced by $P^{(N,\gamma)}_{2,r,cr}(t)$. Hence, from (3.2.26),

$$\left.\frac{d}{dt}P^{(N,\gamma)}_{tot,r,cr}\right|_{t=4/\gamma_2} = -\gamma_2\exp[-2], \qquad (3.2.27)$$

which corresponds to the fastest instantaneous rate of decay of the total system, and coincides with the time of the maximum of the excited state population.

STRONG DECAY

From (3.2.6), the excited state population is zero only when $t = 0$ and $t \to \infty$. The maximum of the excited state population for strong damping occurs when,

$$t' = 2\beta_r^{-1}\text{arctanh}(2\beta_r/\gamma_2), \tag{3.2.28}$$

where $\vartheta = \vartheta_s = \pi$ in (3.2.2). This result can be recast as [93],

$$t' = 2\beta_r^{-1}\text{arcsinh}(\beta_r/|C(N)|). \tag{3.2.29}$$

This time t' corresponds to,

$$\left[P_{2,r,s}^{(N,\gamma)}(t')\right]^{max} = \exp[-\tfrac{1}{2}\gamma_2 t'], \tag{3.2.30}$$

which has the same structure as in the weak damping case, (3.2.14), although t' is different. Since strong damping prohibits oscillations between the ground and excited state, $P_{1,r,s}^{(N,\gamma)}(t)$ is a maximum only at t = 0, where it is unity. The instantaneous rate of the decay of the whole system has the same form as (3.2.21), with $P_{2,r,w}^{(N,\gamma)}(t)$, from (3.2.4), replaced with $P_{2,r,s}^{(N,\gamma)}(t)$, from (3.2.6); as with weak damping, the fastest rate of decay of the whole system for strong damping occurs when the population of the excited state is maximum, namely at t', given by (3.2.29), where,

$$\frac{d}{dt}P_{tot}\Big|_{t=t'} = -\gamma_2\exp[-(\gamma_2/\beta_r)\text{arctanh}(2\beta_r/\gamma_2)]. \tag{3.2.31}$$

3.2.3. CONDITIONS ON THE APPLICABILITY OF THE RWA SOLUTIONS.

The RWA is a resonance approximation, and the criteria for its applicability are partially determined by investigating the resonance solutions. In common with the $\gamma_2 = 0$ analogue, the counter-rotating terms must oscillate rapidly relative to the resonance period of the excited state population, so the counter-rotating terms average to zero over time. However, the size of the decay relative to the magnitude of the molecule-EMF coupling influences this condition.

WEAK DECAY

Only in the case of weak decay does the resonance time-dependent excited state population have an element of periodicity. From (3.2.4), $P^{(N,\gamma)}_{2,r,w}(t)$ is comprised of a periodic term ($\sin^2[\frac{1}{2}\alpha t]$) modified by an exponential decay term ($\exp[-\frac{1}{2}\gamma_2 t]$). The "period" of the excited state population refers to the time required for it to change from minimum to maximum population and back again; the cycle is not truly periodic since the maximum population decreases with each oscillation, see (3.2.14). From (3.2.11), the period of the excited state population is,

$$T^{\gamma}_{RWA}(res) = \frac{2\pi}{\alpha_r} = \frac{2\pi}{[|C(N)|^2 - \frac{1}{4}\gamma_2^2]^{1/2}}. \qquad (3.2.32)$$

The counter-rotating terms, on the other hand, oscillate at frequencies $(N-k)\omega$, $k \neq N$. The longest possible period of the counter-rotating term is $2\pi/\omega$. This and all other counter-rotating terms can be neglected in (3.1.6) if $2\pi/\omega \ll 2\pi/[|C(N)|^2 - \frac{1}{4}\gamma_2^2]^{1/2}$, or,

$$[|C(N)|^2 - \tfrac{1}{4}\gamma_2^2]^{1/2} \ll \omega \qquad (3.2.33)$$

This constraint ensures that the rapidly oscillating counter-rotating terms average to zero over the period of the excited state population. In the limit that $\gamma_2 \to 0$, (3.2.33) reduces to (2.3.21).

CRITICAL AND STRONG DECAY

For weak damping, the period of the excited state - the time for state two to go from minimum to maximum to minimum population - can be compared directly with the period of the counter-rotating terms. The resonant time-dependent excited state populations for critical and

strong damping, (3.2.5) and (3.2.6), respectively, are not periodic. Hence, a rigorous mathematical equivalent to (3.2.33) is not available.

However, for these non-periodic cases, the excited state population does reach a maximum once. This maximum can be treated roughly as a "half-period" analogue to (3.2.32). By similar reasoning as for weak damping, the counter-rotating terms must have a much shorter period than twice the time required to the excited state to reach maximum population.

For critical damping, if twice the time, (3.2.25), required to reach the maximum excited state population is much greater than the period of the counter-rotating terms,

$$4/\gamma_2 = 2/|C(N)| \gg \pi/\omega, \tag{3.2.34}$$

the RWA should be either quantitatively or qualitatively applicable.

Similarly, for strong damping, from (3.2.29), the condition of applicability for the RWA is,

$$2\beta_r^{-1}\text{arcsinh}(\beta_r/|C(N)|) \gg \pi/\omega, \tag{3.2.35}$$

or,

$$[\tfrac{1}{4}\gamma_2^2-|C(N)|^2]^{1/2} \gg |C(N)|\sinh(\tfrac{\pi}{2}[\tfrac{1}{4}\gamma_2^2-|C(N)|^2]^{1/2}/\omega). \tag{3.2.36}$$

3.3. THE DYNAMIC EFFECTS OF PERMANENT DIPOLES

The spectral effects of permanent dipoles in the absence of excited state decay are reviewed in detail in Sec. 2.4. The dynamic effects, which are based on the unique nature of the molecule-EMF coupling when $d \neq 0$ [2,3], are discussed briefly in Sec. 2.4 for

$\gamma_2 = 0$, and in more detail here, for both $\gamma_2 = 0$ and $\gamma_2 \neq 0$.

3.3.1. ZERO EXCITED STATE DECAY

When $d \neq 0$, (2.3.10) predicts the presence of oscillations and nodes in the molecule-EMF coupling as determined by the Bessel function argument $(\underline{d}\cdot\hat{e}\mathcal{E}^0/\omega)$ [2,3,5,25,26,71]. The effects of the permanent dipole moments are most pronounced when the molecule-EMF coupling is close to a node. Even slight changes in the field strength $\mathcal{E}^0$ can result in a change in the molecule-EMF coupling by orders of magnitude.

Since the resonance coupling period (2.3.13) depends inversely on the molecule-EMF coupling, the nodes that are present in the molecule-EMF coupling translate into very long periods of oscillation of the time-dependent population of the excited state [13]. For a given permanent dipole moment molecule, variations in $\mathcal{E}^0$ can be used to establish the field conditions which generate the longest periods of the excited state population. Similar behaviour is not observed when $d = 0$ since the Rabi period, (2.3.16), can only decrease with increasing field strength. Exact numerical calculations [21,23,32] confirm this trend holds for higher-order transitions when $d = 0$. Contrasting (2.3.12) and (2.3.13), the effects of $d \neq 0$ will generally be most significant on resonance when $(\Delta E - N\omega) = 0$.

The field strengths required to generate near-nodal coupling can be large and the RWA solution may not be quantitatively reliable [2,3,26,71]. Large field strengths can generate large Bloch-Siegert shifts, even for an associated weak molecule-EMF coupling [2,3,26,28,34]. These shifts can alter the location of the molecule-EMF coupling node from the RWA predicted value. However, in

these cases, the RWA often remains qualitatively reliable [24], and can still be a powerful tool in interpreting the effects of the permanent dipole moments. Thus, while the RWA predicts the presence of minima in the magnitude of the coupling as a function of $\mathcal{E}^0/\omega$, $\omega \simeq \Delta E/N$, it will often not give accurately the associated values of the parameter $(\underline{d}\cdot\hat{e}\mathcal{E}^0/\omega)$ when $\mathcal{E}^0$ is large.

3.3.2. NON-ZERO EXCITED STATE DECAY.

Excited state decay can strongly affect the evolution of the excited state population. For weak decay, (3.2.32) suggests that the inclusion of excited state decay increases the period of the excited state population relative to when $\gamma_2 = 0$, since $[|C(N)|^2 - \frac{1}{4}\gamma_2^2]^{1/2} < |C(N)|$. The period of the excited state becomes longer as $|C(N)| \to \frac{1}{2}\gamma_2$, that is, as the molecule-EMF coupling approaches the critical decay rate. These trends hold for both $d = 0$ and $d \neq 0$; however, for a given field strength, the nature of the decay for $d = 0$ versus $d \neq 0$ can be very different.

For $d = 0$, as the field strength increases, the molecule-EMF coupling increases. For a given decay rate, then, extremely weak fields imply strong decay, since $|\underline{\mu}_{12}\cdot\hat{e}\mathcal{E}^0| < \frac{1}{2}\gamma_2$. As the field strength (and hence the coupling) increases, the classification of the decay changes from strong to critical to weak. Thus, for increasing field strength, the time-dependent population passes from non-oscillatory to oscillatory behaviour.

For $d \neq 0$, the molecule-EMF coupling oscillates, with decreasing amplitude, with increasing field strength. These oscillations affect the decay classification of the interaction. From (3.2.32), nodal or

near nodal coupling no longer translates into long periods of the excited state time-dependent population when $\gamma_2 \neq 0$. As a coupling node is approached by increasing the field strength, the nature of the decay can change from weak ($|C(N)| > \frac{1}{2}\gamma_2$) to critical ($|C(N)| = \frac{1}{2}\gamma_2$) to strong ($|C(N)| < \frac{1}{2}\gamma_2$) as the molecule-EMF coupling decreases. As the field strength is further increased, $|C(N)|$ moves away from the node, and the classification of the decay can change back from strong to weak. This change in the nature of the evolution of the excited state from oscillatory to non-oscillatory and back again can occur near each node in the coupling, and hence at many different field strengths. This behaviour is in direct contrast to when $d = 0$, where the change from strong to weak decay can only occur at one field strength.

3.4. EXAMPLES OF EXCITED STATE DECAY.

In this section, two sets of time-dependent examples are given which show the effects of excited state decay and permanent dipoles, and which demonstrate the predictive capabilities of the RWA. In the first set, the RWA is quantitatively applicable, while in the second, it remains only qualitatively valid. The first group of calculations concentrates on the effects of excited state decay; weak, critical and strong damping are considered. The results of RWA and exact calculations are compared. The second set of examples contrasts the $d \neq 0$ with the $d = 0$ analogue for the evolution of the excited state population with near nodal molecule-EMF coupling, and examines how excited state decay affects the transition between the states. The qualitative predictions of the RWA are used to help interpret the exact

results.

The two-level molecular system is modeled after the $S_0 \rightarrow S_1$ transition of 1-[p-(N,N-dimethyl-amino)phenyl]-4-(p-nitrophenyl)-1,3-butadiene. This molecule has been used to help investigate the effects of permanent dipoles in single and multi-photon molecular spectra [28,34,40]. In atomic units, the two-level molecule can be described by $\Delta E = 0.0859$, $\mu_{12} = 3.93$, and $d = 11.8$. Since the time-dependent and long time-averaged populations are independent of the traces of the energy and dipole moment matrices [1], μ_{11} and E_1 can be set to zero, with $\mu_{22} = d$ and $E_2 = \Delta E$; these are not equal to the physical values of the molecular parameters. The transition moment μ_{12} and permanent moments μ_{jj} are taken to be aligned with the direction of polarization of the applied electric field. The phase δ of the field is set to zero.

The excited state decay rates employed in the following examples are on the order of $\gamma_2 = 10^{-5}$ to 10^{-2} ($1\text{-}10^3 ps^{-1}$) The associated excited state lifetimes ($1/\gamma_2$) could correspond to molecules adsorbed on a surface [22,94-96]. Longer lifetimes are observed for molecules in solution, or in the gas phase [97,98]. In Sec. 3.4.1, short lifetimes are used in part to illustrate the quantitative agreement between the RWA and exact results on a convenient time scale, with a field strength that is relatively large, but does not violate the RWA conditions of applicability from Sec. 3.2.3. In Sec. 3.4.2, the model calculations are designed in part to illustrate the interplay between the effects of permanent dipoles and excited state decay, relative to a $d = 0$ analogue.

For the exact calculations, the one-photon resonance frequency

must be determined from the exact $\gamma_2 = 0$ steady state spectrum as ω_{res} is not necessarily equal to the RWA ideal resonance, $\omega = \Delta E$. The exact time-averaged phase-dependent ($\delta = 0$) populations were calculated using the RPI and Floquet techniques, see Secs. 2.2.1 and 2.2.4, respectively. Convergence to four significant figures was attained by subdividing the time interval $[0,2\pi/\omega]$ into 200 Riemann intervals; every fourth point was used for (Floquet) temporal integration of the populations, see (2.2.39). The resulting one-photon $\gamma_2 = 0$ resonance frequency is used in the exact time-dependent calculations for all decay rates.

The exact time-dependent calculations at the one-photon resonance frequency were performed using the Taylor series method [17b]. A thirteen term Taylor series expansion over each subinterval of size $\Delta(\omega_{res} t) = \pi/100$ provided numercial convergence to more than four figures. With decay present, the evolution operator is not periodic, so $\underline{U}(2\pi/\omega,0)$ could not be used to find the time-dependent state populations to long times. Hence, the evolution operators were calculated explicitly over the entire time span of interest.

3.4.1. A QUANTITATIVE APPLICATION OF THE RWA

Here, the time-dependent excited state populations are given for the two-level model molecule above, with different excited state decay rates, interacting with a continuous wave electric field of strength $\mathcal{E}^0 = 0.001$ and tuned to the one-photon resonance frequency. The corresponding RWA molecule-EMF coupling, (2.3.10), is $C(1) = 3.9207\text{x}10^{-3}$, and is not close to a coupling node. The excited state decay rates are $\gamma_2 = 0$, $\mathcal{A}$, $10\mathcal{A}$, $100\mathcal{A}$, $\mathcal{B}$, and $500\mathcal{A}$, where

$\mathcal{A} = 2.4189\text{x}10^{-5}$ (10^{12}s^{-1}) and $\mathcal{B} = 2C(1) = 7.8414\text{x}10^{-3}$ $(3.2417\text{x}10^{14}\text{s}^{-1})$. The decay rates $\mathcal{A}$, $10\mathcal{A}$ and $100\mathcal{A}$ are examples of weak decay for this system; $\gamma_2 = \mathcal{B}$ is the point of critical damping; and $\gamma_2 = 500\gamma_2$ is an example of strong damping. The examples will be discussed according to increasing decay rate. The exact one-photon resonance frequency is $\omega_{res} = 1.0001\Delta E$.

WEAK DECAY

The values of α_r, from (3.2.1) and (3.2.3a), for the relevant γ_2 are included in Table 3.1 (page 77), which will be discussed in detail later. In all four cases, $\alpha_r \ll \omega = \Delta E = 0.0859$, so the constraint (3.2.33) is obeyed and the RWA is quantitatively reliable. The RWA resonance time-dependent excited state population is computed from (3.2.4).

The RWA time-dependent excited state populations for weak decay are given for $\gamma_2 = 0$, $\mathcal{A}$, $10\mathcal{A}$, $100\mathcal{A}$, in Fig. 3.1a, b, c and d, respectively, while the exact analogues are given in Fig. 3.1a', b', c' and d', respectively. The time span from $t = 0$ to $t \simeq 8020.2$ was chosen to encompass five full RWA periods of the $\gamma_2 = 0$ excited state population.

The RWA time-dependent excited state populations are perfectly periodic with respect to the temporal displacement of adjacent excited state minima or adjacent excited state maxima. The PWA period as calculated directly from (3.2.11) equals that predicted by the computed time-dependent population (3.2.4). For $\gamma_2 = 0$, $\mathcal{A}$, $10\mathcal{A}$ and $100\mathcal{A}$, the periods are $T^{\gamma}_{RWA} = 1602.6$, 1602.6, 1603.3 and 1684.7, respectively. For each γ_2, the five successive periods in Fig. 3.1 are identified by

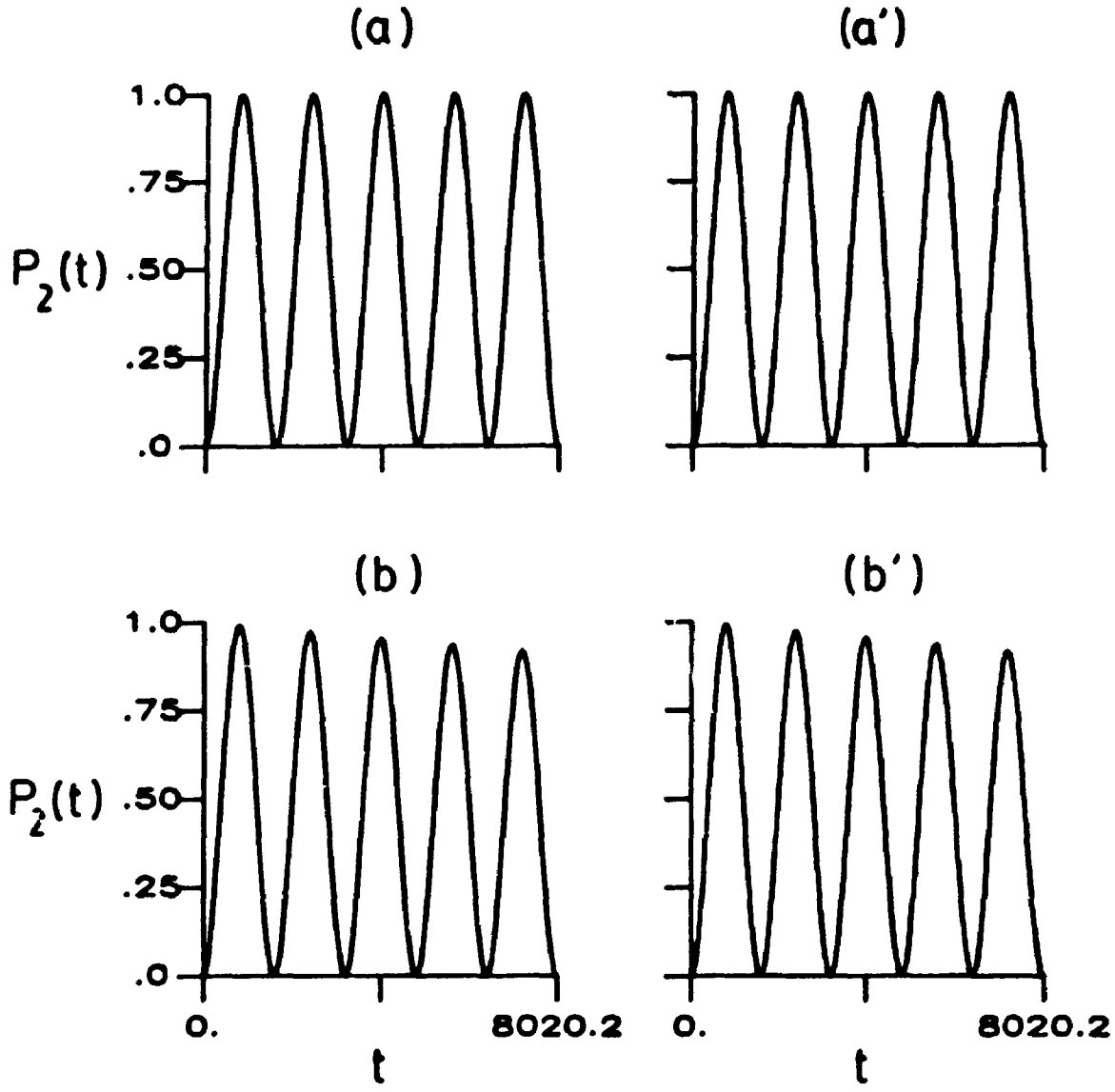

Figure 3.1. The time-dependent excited state population for the one-photon transition, as a function of time and increasing rate of excited state (weak) decay, for a permanent dipole molecule interacting with a single CW laser. Molecular parameters: d = 11.8, μ_{12} = 3.93, ΔE = 0.0859. Field parameters: $\mathcal{E}^0$ = 0.001, $\omega = \Delta E$ (RWA) or $\omega = 1.0001\Delta E$ (exact). Fig. 3.1(a,b,c,d) are the RWA results and Fig. 3.1(a',b',c',d') are the exact results, for $\gamma_2 = (0, \mathcal{A}, 10\mathcal{A}, 100\mathcal{A})$, respectively, where $\mathcal{A} = 2.4189 \times 10^{-5}$.

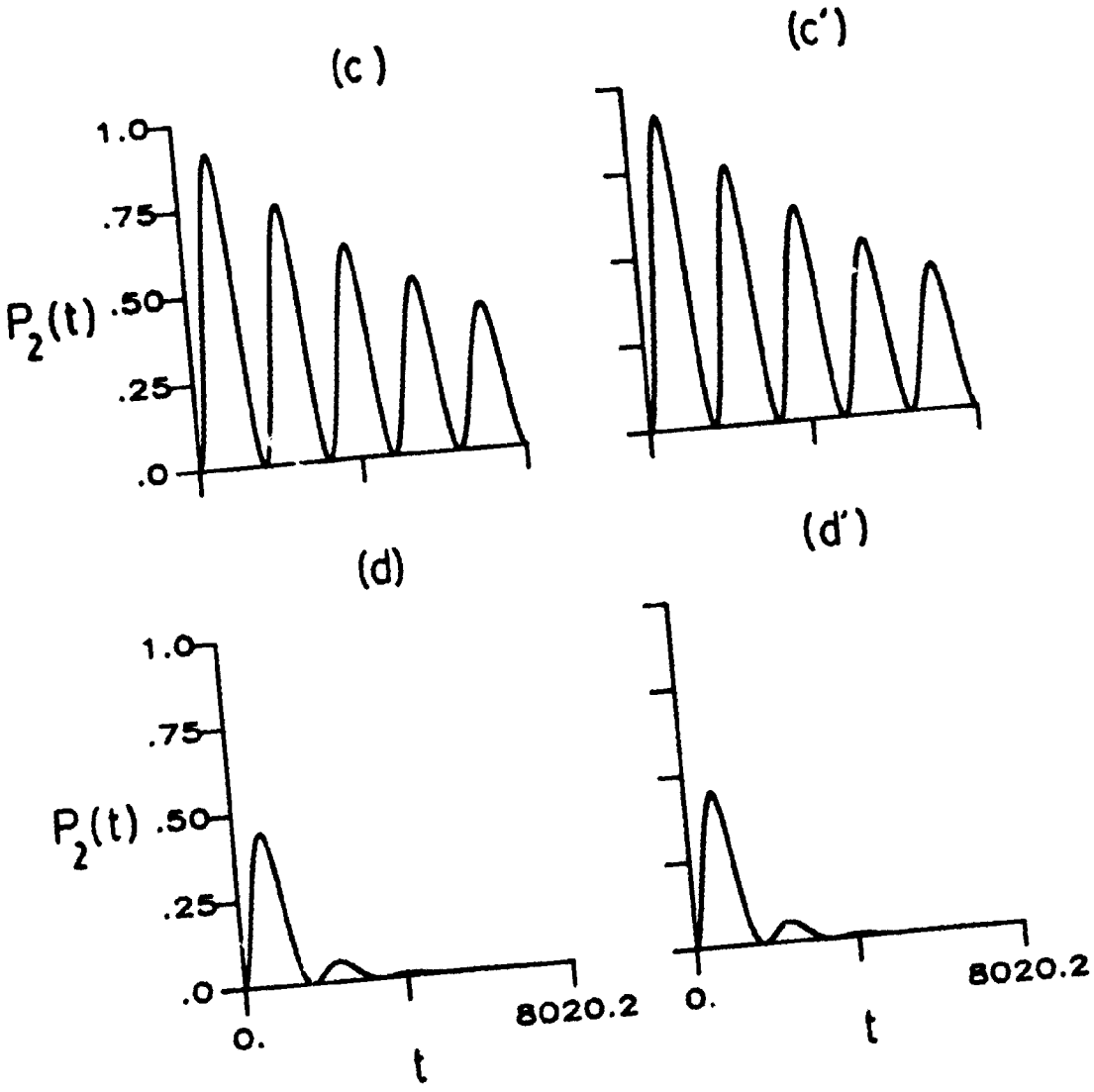

Figure 3.1 continued

$n = 0,1,2,3,4$ according to (3.2.12).

The oscillations between maximum and minimum population are smooth, and for $\gamma_2 \neq 0$, the maximum population decreases with increasing time, and with increasing γ_2. For $\gamma_2 = \Delta$ in Fig. 3.1b, the effects of decay are relatively small over the times considered: the difference in the period relative to the $\gamma_2 = 0$ period is negligible; and it is only after several periods that the decrease in the magnitude of the maximum excited state population is significant. In Fig. 3.1c, where $\gamma_2 = 10\Delta$, the change in the period relative to the $\gamma_2 = 0$ period is still very slight, but the effect of the decay on the excited state population is more pronounced, and is obvious from the first ($n = 0$) period alone. For $\gamma_2 = 100\Delta$ in Fig. 3.1d, there is a large increase in the period of the time-dependent excited state population relative to the period when $\gamma_2 = 0$. The decay is strong enough that only three periods ($n = 0,1,2$) are detectable in Fig. 3.1d, with the other two having P_2^{max} too small to be observed on the scale of the figure. For the RWA results of Fig. 3.1(a-d), the maximum populations of the excited state in each successive period are given in Table 3.1 (page 77), where the times at which the maxima occur, as calculated from (3.2.12), coincide with those computed directly from the time-dependent populations, (3.2.4).

The temporal locations of the maxima initially decrease with increasing γ_2, until $\gamma_2 = 100\Delta$ and for $n = 2, 3, 4$. In general, for sufficiently large n, the times of the maxima of the excited state population in the presence of excited state decay will eventually exceed those found in the absence of decay. From (3.2.12), for $\gamma_2 = 0$, the maxima are located at $t' = 2|C(N)|^{-1}(n + \frac{1}{2})\pi$. These times will be

less than those with $\gamma_2 \neq 0$ when,

$$2|C(N)|^{-1}(n+\tfrac{1}{2})\pi < 2\alpha_r^{-1}(\arctan[2\alpha_r/\gamma_2] + n\pi), \qquad (3.4.1)$$

or,

$$n > (\tfrac{1}{2}\alpha_r - \frac{|C(N)|}{\pi}\arctan[2\alpha_r/\gamma_2])(|C(N)|-\alpha_r)^{-1}. \qquad (3.4.2)$$

For $\gamma_2 = 100\mathcal{A}$, this last equation is satisfied for $n \geq 2$, as observed in Table 3.1.

The exact time-dependent excited state populations for the cases of weak damping are shown in Figs. 3.1a', b', c', and d'. The trends in the time-dependent excited state population, as a function of increasing γ_2, as observed and discussed in the RWA results, are essentially duplicated in the exact calculations.

A number of quantitative comparisons can be made between the exact and RWA results. For ease of comparison, the five cycles from minimum to maximum population and back again in the exact calculation are labelled as in the RWA, n = 0,1,2,3,4. The locations and values of the maxima in the exact excited state population are listed in Table 3.2. Table 3.3 lists the percent difference between the RWA and exact results as given in Tables 3.1 and 3.2. The exact temporal locations and magnitudes of the maxima show excellent numerical agreement with the RWA predictions, with all differences being less than two percent. The largest discrepancies occur in P_2^{max} for $\gamma_2 = 100\mathcal{A}$.

In the RWA and in the exact results, the temporal locations of the minima in the excited state population coincide with those of the maxima of the ground state population. However, as predicted by the RWA, when excited state decay is present, the times of the maxima of the excited state population do not equal the times of the minima of

Table 3.1. The RWA maximum time-dependent excited state population, for the weak decay examples of Fig. 3.1(a-d), with increasing time. The label n represents the cycle number according to (3.2.12). $\alpha_r = [|C(1)|^2 - \frac{1}{4}\gamma_2^2]^{1/2}$ and $C(1) = 3.9207 \times 10^{-3}$.

γ_2	$\alpha_r \times 10^3$		n = 0	n = 1	n = 2	n = 3	n = 4
0	3.9207	t	801.3	2403.8	4006.4	5608.9	7211.5
		P_2	1.00	1.00	1.00	1.00	1.00
Δ	3.9207	t	799.7	2402.2	4004.8	5607.4	7209.9
		P_2	.990	.971	.953	.934	.916
10Δ	3.9189	t	785.9	2389.2	3992.5	5595.8	7199.2
		P_2	.909	.749	.617	.508	.419
100Δ	3.7295	t	674.2	2358.9	4043.6	5728.3	7413.0
		P_2	.442	.0577	.00752	.00098	.00013

Table 3.2. Exact maximum time-dependent excited state population, for the weak decay examples of Fig. 3.1(a'-d'), with increasing time; n represents the cycle number, labelled analogously to the RWA cycles of Table. 3.1.

γ_2		n = 0	n = 1	n = 2	n = 3	n = 4
0	t	802.7	2407.7	4012.9	5604.2	7209.9
	P_2	1.00	1.00	1.00	1.00	1.00
Δ	t	802.7	2407.7	4012.3	5603.5	7209.6
	P_2	.990	.971	.953	.935	.916
10Δ	t	777.1	2385.4	3993.7	5601.3	7208.8
	P_2	.911	.750	.618	.509	.419
100Δ	t	667.7	2349.9	4032.1	5714.3	7431.2
	P_2	.449	.0585	.00762	.00099	.00013

Table 3.3. The percent difference, relative to the exact results, between RWA and exact temporal locations and magnitudes of the maxima of the excited state population, for the weak decay examples of Fig. 3.1. The data is taken from Table 3.1 and Table 3.2.

γ_2		n = 0	n = 1	n = 2	n = 3	n = 4
0	Δt	-.2%	-.2%	-.2%	.09%	.02%
	ΔP_2	0	0	0	0	0
Δ	Δt	-.4%	-.2%	-.2%	.07%	.004%
	ΔP_2	0	0	0	-.1%	0
10Δ	Δt	1.1%	.2%	-.03%	-.1%	-.1%
	ΔP_2	-.2%	-.1%	-.2%	-.2%	0
100Δ	Δt	1.0%	.4%	.3%	.2%	-.2%
	ΔP_2	-1.6%	-1.4%	-1.3%	-1.0%	0

the ground state population. The RWA predictions and exact values for the times of the ground state minima, and the percent difference between the two are given in Table 3.4. The exact and RWA results show excellent numerical agreement, with a maximum percent difference between the two of 0.7%.

The temporal separation between the ground state minimum and the associated excited state maximum population is given in Table 3.5 for the RWA and exact results. For a given n and γ_2, the excited state maximum occurs before the excited state minimum. The temporal separation between the two increases with increasing γ_2. The numerical agreement between the RWA and the exact results is poor for $\gamma_2 = \Delta$, but within 4% for $\gamma_2 = 10\Delta$ and 100Δ.

The RWA predicts that adjacent minima (or adjacent maxima) are separated by $T^{\gamma}_{RWA} = 2\pi/\alpha_r$. However, unlike the RWA results, the exact time-dependent excited state population is not perfectly "periodic" with respect to time. Table 3.6 gives the exact temporal difference between adjacent minima in the excited state population,

$$T_{exact}(n,P_2^{min}) = t[P_2^{min}(n)] - t[P_2^{min}(n-1)], \qquad (3.4.3)$$

where $t[P_2^{min}(-1)] = 0$, and the average "period" over the five cycles. The temporal separation between adjacent maxima in the excited state population is,

$$T_{exact}(n,P_2^{max}) = t[P_2^{max}(n+1)] - t[P_2^{max}(n)]. \qquad (3.4.4)$$

The results are given in Table 3.7, along with the average value of (3.4.4) over the five cycles.

The average values of (3.4.3) and (3.4.4) are within 0.5% of the RWA prediction, (3.2.11). However, from Table 3.6 (3.7), the minima

Table 3.4. RWA and exact times for ground state minima ($P_1^{1,\gamma}(t) = 0$) for the weak decay examples of Fig. 3.1. The percent differences are measured relative to the exact results. For $\gamma_2 = 0$, the temporal location of the ground state minima coincide with that of the excited state maxima, see Tables 3.1 and 3.2. The label n is as in Tables 3.1 and 3.2.

γ_2		n = 0	n = 1	n = 2	n = 3	n = 4
Δ	t_{RWA}	802 9	2405.4	4008.0	5610.5	7213.1
	t_{exact}	803.4	2408.8	4014.2	5604.9	7210.7
	Δ	-.06%	-.1%	-.1%	.1%	.03%
10Δ	t_{RWA}	817.4	2420.7	4024.0	5627.3	7230.7
	t_{exact}	812.2	2417.?	4023.7	5629.4	7235.5
	Δ	.6%	.1%	.01%	-.04%	-.07%
100Δ	t_{RWA}	1010.5	2695.2	4379.9	6064.7	7749.4
	t_{exact}	1017.3	2702.4	4385.7	6069.0	7752.6
	Δ	-.7%	.3%	-.1%	-.07%	-.04%

Table 3.5. The temporal separation between the maxima of the excited state population in Fig. 3.1 and the associated minima of the ground state population, for RWA and exact results. For $\gamma_2 = 0$, the temporal separation is zero for both RWA and exact calculations. The temporal displacement of the ground state minimum from the excited state maximum population in the RWA can be determined by comparing Table 3.4 with Table 3.1 or by direct calculation from (3.2.19). The exact analogue can be found by comparing Table 3.4 with Table 3.2.

		$[t(P_1^{min}) - t(P_2^{max})]_{exact}$					
γ_2	RWA $t''-t'$	n = 0	n = 1	n = 2	n = 3	n = 4	ave
Δ	3.2	0.7	1.1	1.9	1.4	1.1	1.2
10Δ	31.5	35.1	32.5	30.0	28.1	26.7	30.5
100Δ	336.3	349.6	352.5	353.6	354.7	321.4	346.4

Table 3.6. RWA and exact periods for the weak decay examples of Fig. 3.1, as measured between adjacent minima in the excited state population. The average exact period over the 5 cycles is also given.

		$T_{exact}(n, P_2^{min})$					ave
γ_2	T^{γ}_{RWA}	n = 0	n = 1	n = 2	n = 3	n = 4	
0	1602.6	1605.7	1606.1	1587.1	1606.5	1605.7	1602.2
Δ	1602.6	1605.7	1606.1	1587.1	1606.5	1605.7	1602.2
10Δ	1603.3	1606.1	1606.6	1606.0	1588.5	1606.5	1602.7
100Δ	1684.7	1684.0	1684.7	1696.4	1681.8	-	1686.7

Table 3.7. RWA and exact periods for the weak decay examples of Fig. 3.1, as measured between the maxima in the excited state population of the cycles (n+1) and n. The average temporal displacement between the exact maxima over the five cycles is also given.

		$T_{exact}(n, P_2^{max})$				ave
γ_2	T^{γ}_{RWA}	n = 0	n = 1	n = 2	n = 3	
0	1602.6	1605.0	1605.2	1591.3	1605.7	1601.8
Δ	1602.6	1605.0	1604.6	1591.2	1606.1	1601.7
10Δ	1603.3	1608.3	1608.3	1607.6	1607.5	1607.9
100Δ	1684.7	1682.2	1682.2	1682.2	1716.9	1690.9

(maxima) of the excited state populat... in the exact calculations do not occur periodicially, and the deviations from the average can be quite large (see, for example, n = 2 for $\gamma_2 = 0, \mathcal{A}$). These deviations in the exact behaviour from the RWA prediction are directly attributable to the counter-rotating terms that are absent in the RWA.

A second effect of the counter-rotating terms is (just) discernible in Fig. 3.1d'. Relative to Fig. 3.1d, the line in the exact plot of Fig. 3.1d' is slightly thicker, because small oscillations are superimposed on the larger cycles of population change. The magnitude of these oscillations is very small; the deviations of the exact population from the RWA analogue are, on average, ±0.005. The small oscillations are approximately periodic in $2\pi/\omega$. Although not discernible on the scale of Fig. 3.1a', b', and c', these small oscillations are also present for the smaller decay rates. However, if the exact and RWA results for each decay rate are superimposed, the RWA curve passes through the "middle" of the exact curve, "averaging" away the small counter-rotating effects.

CRITICAL DECAY

The decay rate $\gamma_2 = \mathcal{B} = 2|C(1)|$ corresponds to the point of critical decay. The criterion for the applicability of the RWA for critical decay, given by (3.2.34), can be recast,

$$\omega \gg \tfrac{1}{2}\pi|C(N)|. \qquad (3.4.5)$$

Equation (3.4.5) is satisfied since $\omega = 0.0859$, and $\frac{1}{2}\pi|C(1)| = 0.00616$, and the time-dependent population of the excited state on resonance can be calculated from (3.2.5) with relative confidence.

Fig. 3.2a illustrates the RWA result for critical damping,

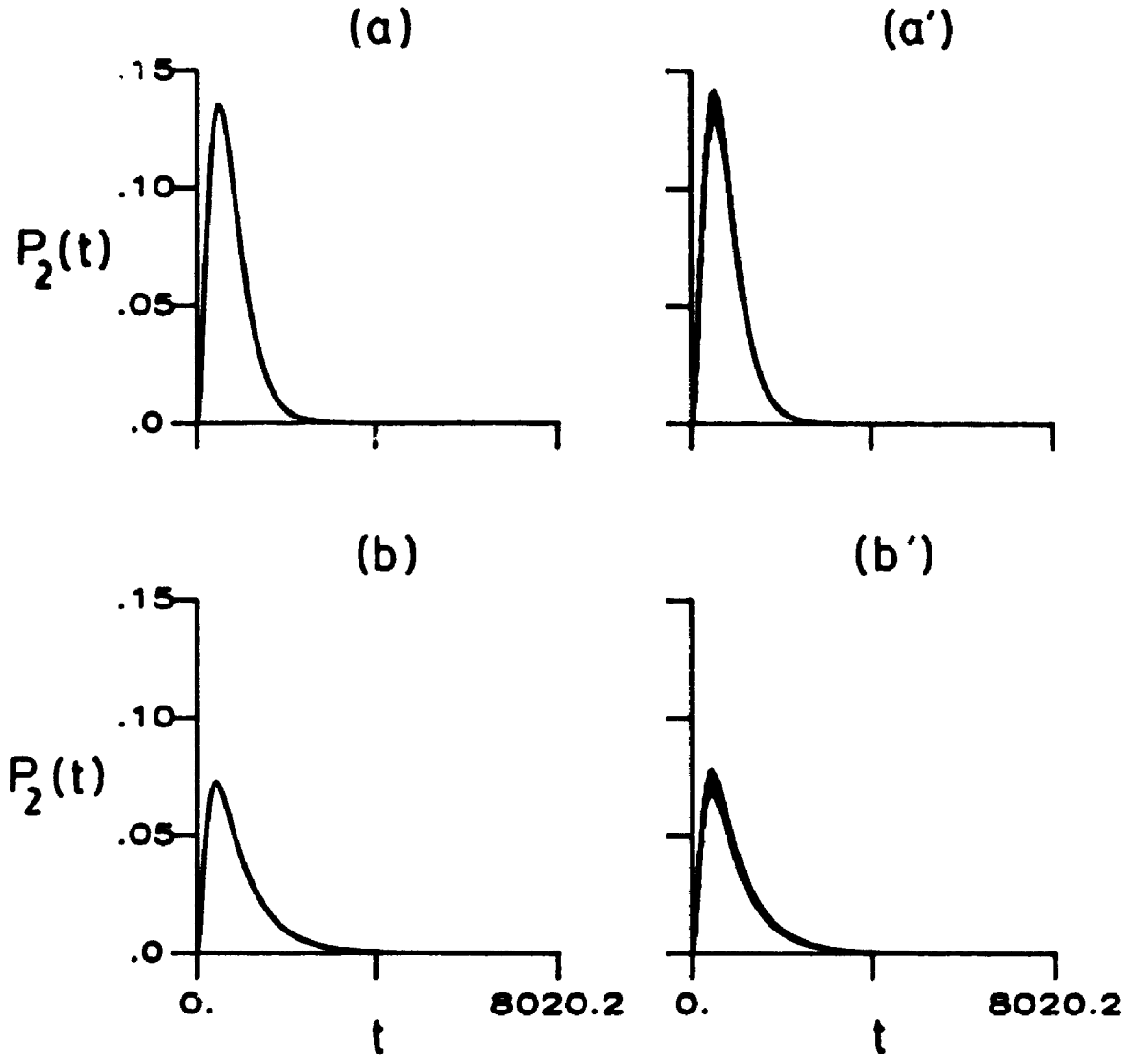

Figure 3.2. The time-dependent excited state population for the one-photon transition, as a function of time, for critical and strong excited state decay, for a permanent dipole molecule interacting with a single CW laser. Molecular and field parameters as in Fig. 3.1. Fig. 3.2(a,b) are the RWA results, and Fig. 3.2(a',b') are the exact results, for $\gamma_2 = (\mathcal{B}, 500\mathcal{A})$, respectively; $\mathcal{B} = 7.8414\times10^{-3}$ and $\mathcal{A} = 2.4189\times10^{-5}$.

$\gamma_2 = 2|C(1)| = 7.8414 \times 10^{-3}$. The time-dependent excited state population exhibits no oscillatory behavior. The population of state two reaches its only maximum of $P_2(t) = 0.135$ when $t = 4/\gamma_2 = 510.1$.

The corresponding exact results for critical damping, shown in Fig. 3.2a', have the same general lineshape as the RWA results. A single maximum of $P_2(t) = 0.142$ occurs when $t = 521.5$. The RWA results agree to 4.9% and 2.1%, respectively. The line representing the exact time-dependent population in Fig. 3.2a' appears much thicker than the RWA analogue in Fig. 3.2a, as a result of the small oscillations that are attributable to the counter-rotating terms in the exact calculation. These oscillations are periodic in $2\pi/\omega$.

STRONG DECAY

The criterion for the applicability of the RWA for strong decay is given by (3.2.36). For $\gamma_2 = 500\Delta$, the left-hand side of (3.2.36) equals 0.004604, while the right-hand side equals 0.00033; hence, the RWA is valid for this decay rate. The time-dependent excited state population on resonance is calculated from (3.2.6); the result is illustrated in Fig. 3.2b. As in case of critical damping, there is no overall sinusoidal behavior, but the decay of the system is more severe than in Fig. 3.2a. Consequently, the maximum of the excited state population is much smaller in Fig. 3.2b. From (3.2.28) and (3.2.30), this maximum occurs when $t = 434.1$, with excited state population $P_2(t) = 0.0724$.

The exact results for strong damping are shown in Fig. 3.2b'. Again, the lineshape mimics the results of the RWA calculation in Fig. 3.2b, but the line representing the time-dependent excited state

population is much thicker due to the $2\pi/\omega$ periodic oscillations, which can be attributed to the counter-rotating terms. The excited state maximum of $P_2(t) = 0.0778$ occurs at $t = 448.4$; the RWA analogues agree to 6.9% and 3.2%, respectively.

In general, the RWA and exact results show excellent quantitative agreement for these examples of weak, critical and strong decay.

3.4.2. A QUALITATIVE APPLICATION OF THE RWA

The interpretive and predictive properties of the RWA can also be applied qualitatively to the interaction of a permanent dipole moment molecule with a CW laser having zero phase and a large field strength, such that the $d \neq 0$ molecule-EMF coupling associated with the one-photon transition when $\gamma_2 = 0$ is close to a node. The following set of examples illustrates the effects of $d \neq 0$ versus $d = 0$ on the one-photon transition, for increasing rates of decay. The molecular parameters are the same as in the examples of Sec. 3.4.1, except the decay rates are 0, $\mathcal{G}$, $10\mathcal{G}$ and $100\mathcal{G}$, where $\mathcal{G} = 4.8378\text{x}10^{-5}$ (2ps^{-1}).

It is emphasized that the RWA cannot quantitatively predict the molecule-EMF couplings for these examples because the condition of applicability (2.3.21) is violated when $d = 0$, and the $d \neq 0$ coupling is very close to a node. However, many of the effects of γ_2 on the behaviour of the resonance time-dependent excited state population as derived in the RWA, in Sec. 3.2, can be applied with an estimate for the exact molecule-EMF couplings. Such an application of the RWA results permits greater insight into the interplay between $\gamma_2 \neq 0$ and $d \neq 0$, versus $d = 0$, for intense CW laser-molecule interactions.

ZERO EXCITED STATE DECAY

For $\gamma_2 = 0$, the field strength which generates a nodal or near-nodal exact $d \neq 0$ molecule-EMF coupling must be found by a series of exact calculations, since for the chosen molecule, the RWA cannot quantitatively predict the locations of this coupling as a function of $(\underline{d}\cdot\hat{e}\mathcal{E}^0/\omega)$, but can only act as a rough guide. As the temporal effects of permanent dipoles are most apparent on resonance, the long time-averaged excited state populations were calculated to find the resonance frequencies for a series of field strengths, based on the predictions of the RWA. The field strength which generates the minimum coupling can be difficult to determine from the FWHM of the resonance profiles because of the intrusive dynamic background [2,5,23,34]. Hence, at the appropriate resonance frequency, the time-dependent excited state population was calculated to determine which field strength corresponds to the longest period of the excited state population.

The results of the exact time-dependent calculations indicate that the one-photon resonance period passes though a local maximum for the model molecule for field strengths $\mathcal{E}^0$ such that $9.10 < d\mathcal{E}^0/\Delta E < 9.30$; the calculations were carried out with increments in the field strength such that $\Delta(d\mathcal{E}^0/\Delta E) \approx 0.10$. When ΔE is replaced by the exact resonance frequency for each case, the coupling minimum in the exact calculations occurs between $10.9 < d\mathcal{E}^0/\omega_{res} < 11.1$; the RWA result predicts a coupling node will occur at $d\mathcal{E}^0/\omega_{res} = d\mathcal{E}^0/\Delta E \approx 10.2$. The field strength $\mathcal{E}^0 \approx 0.0677$, corresponding to $d\mathcal{E}^0/\Delta E = 9.30$, generates a resonance period of $T_{exact} = 6220$ (150.5fs) for $d \neq 0$ and $T_{exact} \approx 21.8$

(0.527fs) for d = 0. This field strength does not produce the maximum d ≠ 0 period, but was chosen to facilitate the corresponding discussion in Chapter 4.

For $\gamma_2 = 0$ and field strength $\mathcal{E}^0 \simeq 0.0677$, the resonance frequency for d ≠ 0 is $\omega_{res} = 0.835\Delta E$; a calculation of the long time-averaged excited state population for d = 0 yields $\omega_{res} = 1.67\Delta E$. These large frequency shifts, relative to the one-photon RWA prediction of $\omega = \Delta E$, are indicative of the non-quantitative applicability of the RWA. The shift of the d ≠ 0 resonance frequency to low frequency relative to ΔE is a unique effect of permanent dipoles, as discussed in Sec. 2.4, see also [2,3,13,21,25,26,34]. The large positive shift for d = 0 is expected for intense field strengths [2,3,23,34,35]. These resonance frequencies are used in all the time-dependent calculations of this section, regardless of the decay rate.

Although the RWA is not quantitatively reliable for this problem, the exact d = 0 and d ≠ 0 periods of the resonance excited state population when $\gamma_2 = 0$ can be used to provide approximations for the exact molecule-EMF couplings by assuming the RWA relationship (2.3.10) holds for the exact values. For d = 0, $T_{exact} \simeq 21.8$ and $C(1)^{d=0}_{exact} = 2\pi/T_{exact} \simeq 0.288$. For d ≠ 0, $T_{exact} = 6220$ and $C(1)^{d\neq0}_{exact} \simeq 0.001010$. Hence, relative to ω_{res}, the d = 0 case corresponds to strong molecule-EMF coupling ($C(1)^{d=0}_{exact} \gg \omega_{res} = 0.143$), while the d ≠ 0 case corresponds to weak coupling ($C(1)^{d\neq0}_{exact} \ll \omega_{res} = 0.0717$).

Figure 3.3 shows the exact time-dependent excited state population for the $\gamma_2 = 0$ molecule interacting with a CW laser with $\mathcal{E}^0 \simeq 0.0677$ and ω fixed at the one-photon resonance frequency; d = 0 in Fig. 3.3a

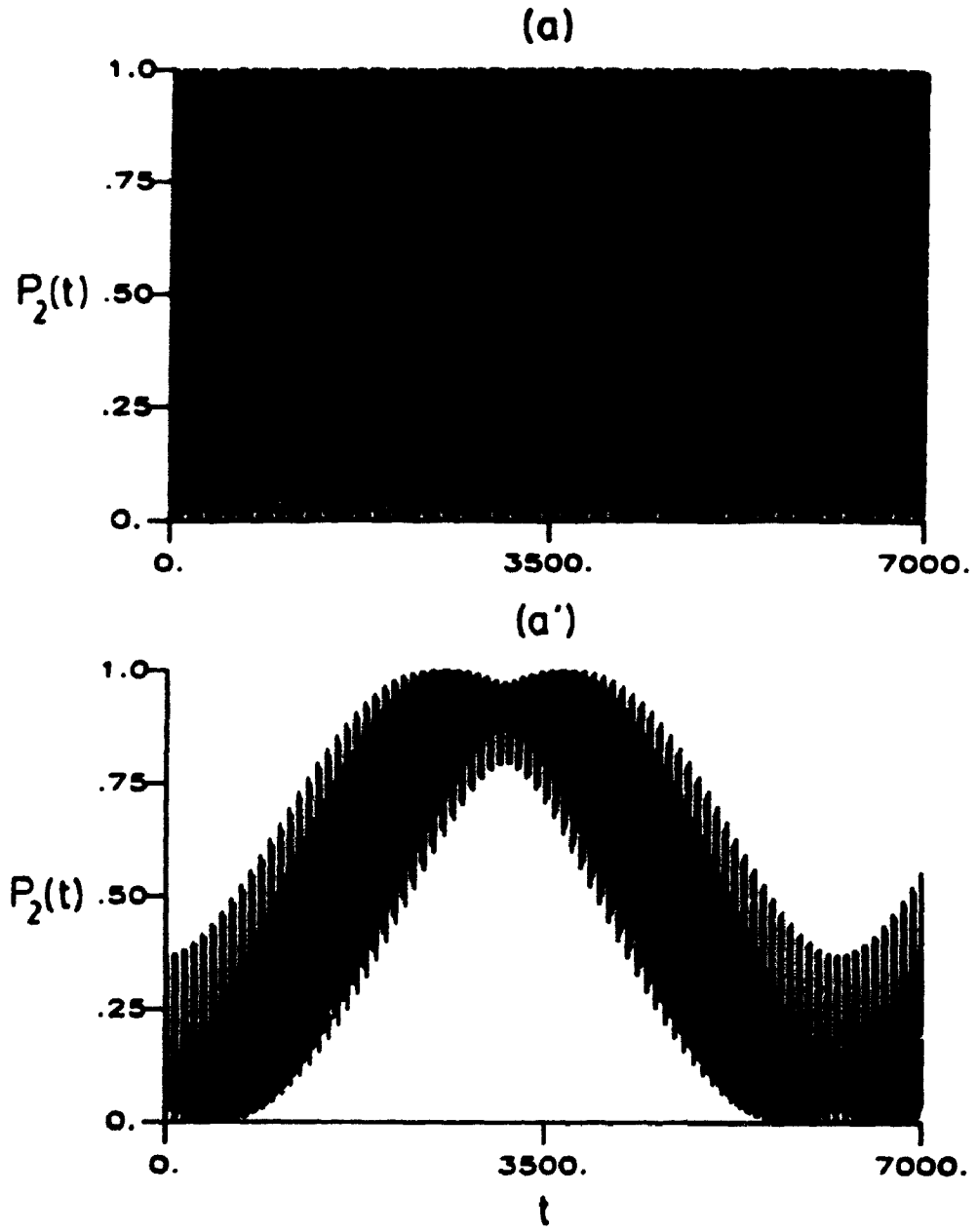

Figure 3.3. The exact time-dependent excited state population for the one-photon transition, as a function of time. for $\gamma_2 = 0$, and $d = 0$ versus $d \neq 0$, for a CW laser-molecule interaction. The molecular parameters are as in Fig. 3.1 and the field parameters are $\mathcal{E}^0 = 0.0677$, $(d\mathcal{E}^0/\Delta E = 9.30)$ and $\delta = 0$. Fig. 3.3(a,b) $d = 0$, $\omega = 1.67\Delta E$; Fig. 3.3(a',b') $d \neq 0$, $\omega = 0.835\Delta E$.

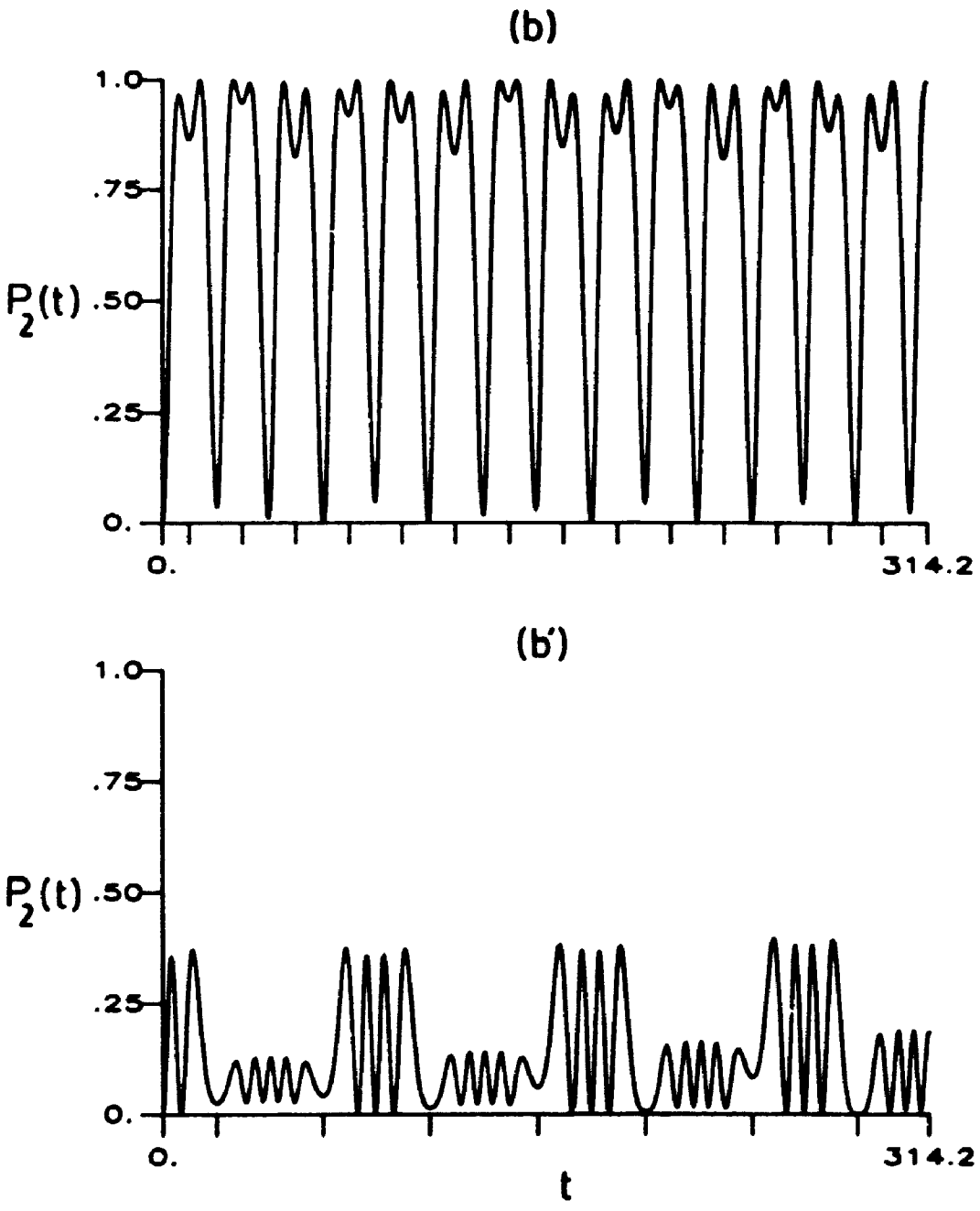

Figure 3.3 continued. Figure 3.3(b,b′) illustrates the results of Fig. 3.3(a,a′) on a shorter expanded time interval.

while $d \neq 0$ in Fig. 3.3a'. The time span of Fig. 3.3a(a') is $0 \leq t \leq 7000.0$ ($\simeq$ 169.3fs), which encompasses at least one full period of the excited state population for $d \neq 0$. Clearly, for $d = 0$, the time-dependent excited state population undergoes very many cycles of stimulated absorption and emission in the time required for one period of the $d \neq 0$ time-dependent excited state population. An expansion of the two patterns for the time interval $0 \leq t \leq 314.2$ ($\simeq$7.60fs) is shown in Fig. 3.3b and 3.3b' for $d = 0$ and $d \neq 0$, respectively. Figures 3.3a and 3.3b versus 3.3a' and 3.3b' contrast nicely the effect of strong versus weak molecule-EMF coupling on the time-dependent evolution of the excited state population for $\gamma_2 = 0$.

When $d = 0$, the molecule-EMF coupling is very large, and the Rabi period, $2\pi/|\mu_{12}\mathcal{E}^0| = 23.6$ (.571fs), is close to the period due to the field frequency, $\pi/\omega = 21.9$ (.530fs). The change of the excited state population is so rapid on the time scale of Fig. 3.3a that the details of the absorption/emission pattern are obscured. From Fig. 3.3b, the time-dependent excited state population increases rapidly from zero to a maximum close or equal to 1.0, decreases slightly before reaching another maximum close or equal to 1.0, and then falls again to (close to) zero. This cycle is repeated many times over the time interval considered, with the relative sizes of the time-dependent population maxima, the magnitude of the slight decrease between them, and the duration of the cycle, changing slightly with each cycle. Although the durations of the cycles vary from $t = 21.0$ to $t = 22.6$ (versus $2\pi/|\mu_{12}\mathcal{E}^0| = 23.6$), and the RWA is not expected to be quantitatively reliable with such intense fields, the individual cycles will be referred to as "Rabi cycles". The value cited for the $d = 0$ period,

$T_{exact} \approx 21.8$, is the average duration of the cycles.

The non-applicability of the RWA is evident in the strong "dip" present in each Rabi cycle, and the fact that $P_2(t)$ is not necessarily zero at the end of each cycle. A study of the numerical data leading to Fig. 3.3(a,b) reveals that the dips between the maxima of each Rabi cycle are perfectly periodic in time, but not magnitude. They occur every $\Delta t = \pi/\omega$, beginning at $t = \frac{1}{2}\pi/\omega$. The tick marks between $t = 0$ and $t = 314.2$ on the abscissa of Fig. 3.3b indicate these π/ω periods. Each Rabi cycle, then, is split by the effect of the field frequency. This effect, which is present even when $\gamma_2 \neq 0$, is not predicted and cannot be explained by the RWA [32].

When $d \neq 0$, the molecule-EMF coupling is much less than the field frequency. From Fig. 3.3a', the general shape of the $d \neq 0$ excited state population over the entire interval $0 \leq t \leq 7000$ is a vastly expanded version of the $d = 0$ Rabi cycle pattern: a transition from $P_2(t = 0) = 0$ to $P_2(t) \approx 1$ is followed by a slight decrease in the excited state population, before it returns to unity, and then decreases to zero. The duration of a $d \neq 0$ cycle is close to 300 times longer than the duration of a $d = 0$ cycle. The overall period of this $d \neq 0$ cycle, $T_{exact} = 6220$ ($\approx$150.5fs), corresponds to the $d \neq 0$, $\gamma_2 = 0$ molecule-EMF coupling period, approximated in the RWA by (2.3.10).

The $d \neq 0$ evolution of the excited state over one period is much more complex than the $d = 0$ Rabi cycle. When $d \neq 0$, the superimposed oscillations, due to the counter-rotating terms, are much more intense and there are many more of them in a single cycle than when $d = 0$. Fig. 3.3b' shows the $d \neq 0$ time-dependent excited state population on an expanded time scale. As when $d = 0$, beginning at $t = \frac{1}{2}\pi/\omega$, every

$\Delta t = \pi/\omega$ there is a local minimum in $P_2(t)$; these are indicated by the tick marks between $t = 0$ and $t = 314.2$. Unlike when $d = 0$, there is a pattern to $P_2(t)$ when $d \neq 0$, which is temporally periodic in $\Delta t = 2\pi/\omega$, beginning at $t = \frac{1}{2}\pi/\omega$. The periodic pattern consists of five low oscillations, followed by four high oscillations in $P_2(t)$. As the overall excited state population increases, this pattern becomes more obscure, and then reappears toward the end of the period as $P_2(t)$ again becomes small. These oscillations cause the excited state population to approach or reach unity many times in the middle of the overall period of the $d \neq 0$ time-dependent excited state population, in contrast to the much shorter $d = 0$ Rabi cycle, during which the excited state population approaches or reaches unity only twice. The $d \neq 0$ time-dependent excited state population reaches unity in two time blocks, centered about $\frac{1}{2}T_{exact}$: $2349 \leq t \leq 2689$ and $3530 \leq t \leq 3870$.

Even though the $d \neq 0$ molecule-EMF coupling is weak, the numerical prediction of the period by the RWA cannot be expected to agree well with the observed overall period; because of the large field strengths employed here, the coupling nodes are shifted from tneir predicted RWA values. However, the qualitative prediction of the RWA for much reduced coupling when $d \neq 0$ accounts for the much longer period than when $d = 0$; the proximity of the exact $d \neq 0$ coupling to a minimum (within $\Delta(\underline{d}\cdot\hat{e}\mathcal{E}^0/\Delta E) = -.20$) explains the magnitude of the difference between the $d \neq 0$ and $d = 0$ periods. Clearly, a much longer time is required for the $d \neq 0$, relative to the $d = 0$, excited state population to reach maximum population.

NON-ZERO EXCITED STATE DECAY

The effect of decay on the exact $d = 0$ and $d \neq 0$ time-dependent excited state populations can be interpreted by qualitative application of the RWA results and discussions of Secs. 3.2 and 3.3. The total population as a function of time, and the rate of change (or "decay") of the total population, are also discussed. Changes in the excited state population are due to stimulated absorption and emission, in addition to spontaneous decay. On the other hand, changes in the total population are more closely related to the effects of spontaneous decay than are either $P_1(t)$ or $P_2(t)$. Consequently, $P_1(t) + P_2(t)$ is a much smoother function of time than its individual components.

$$\gamma_2 = \mathcal{G}$$

According to the RWA, the nature of the excited state decay for the molecule-field interaction can be determined by a comparison of $\frac{1}{2}\gamma_2$ with the molecule-EMF coupling. Applying this idea to the exact molecule-EMF couplings, the decay rate $\gamma_2 = \mathcal{G} = 4.8378\text{x}10^{-3}$ is weak for both $d = 0$ $(C(1)^{d=0}_{exact} \simeq 0.288)$ and $d \neq 0$ $(C(1)^{d\neq0}_{exact} \simeq 0.001010)$. Thus, the RWA predicts that both the $d = 0$ and $d \neq 0$ time-dependent excited state population will oscillate many times between maximum and minimum population when $\gamma_2 = \mathcal{G}$ before the decay of the total population becomes significant. An analogue to the RWA decay period, $2\pi/\alpha_r = 2\pi/[|C(1)|^2 - \frac{1}{4}\gamma_2^2]^{1/2}$, (3.2.11), can also be obtained. When $d = 0$, $\alpha^{d=0}_{r,exact} \simeq 0.288 \simeq |C(1)|^{d=0}_{exact}$, and when $d \neq 0$, $\alpha^{d\neq0}_{r,exact} \simeq 0.0010099 = |C(1)|^{d\neq0}_{exact}$. Hence, the RWA predicts the decay rate $\gamma_2 = \mathcal{G}$ will have no discernible impact on the exact period of the

excited state population, relative to when $\gamma_2 = 0$. The RWA results of Sec. 3.2 are applied only to the nodes, and not the maxima, in the time-dependent excited state population, because the counter-rotating terms disrupt the smooth RWA character of the transitions. For example, it is not possible to identify "the" maximum for a single cycle in Fig. 3.3(a',b).

For $\gamma_2 = \mathcal{G}$, the exact time evolution of the excited state, for $d = 0$ and $d \neq 0$, is shown is Fig. 3.4a and Fig. 3.4a', respectively, for $0 \leq t \leq 7000$ (169.3fs). In the short time interval $0 \leq t \leq 314.2$, the effect of decay is not detectable, and the time-dependent excited state population for $\gamma_2 = \mathcal{G}$ is as for $\gamma_2 = 0$ in Fig. 3.3(b,b').

For $d = 0$, Fig. 3.4a, the exact time-dependent excited state population reaches a maximum of $P_2(t) = 1$ many times, before the effect of decay becomes evident in the decreasing magnitude of the maximum excited state population with increasing time. The temporal locations of the dips between the maxima, and the times of the minima ($P_2(t) \simeq 0$) remain the same as the $\gamma_2 = 0$ analogue. While the RWA does not account for dips between the maxima, it does correctly predict the lack of measurable change in the times of the minima ($P_2(t) \simeq 0$).

For $d \neq 0$, the presence of decay prevents the exact time-dependent excited state population from reaching unity even once; the maximum population is $P_2(t) = 0.95$, which occurs several times from $2261 \leq t \leq 2462$. The general shape of the excited state population loses its symmetry about the central "dip" of the $\gamma_2 = 0$ analogue in Fig. 3.3a', due to the overall decreasing magnitude of the excited state population with increasing time. The duration of the overall cycle $T_{exact} = 6220$ (150.5fs) remains the same as when $\gamma_2 = 0$, as

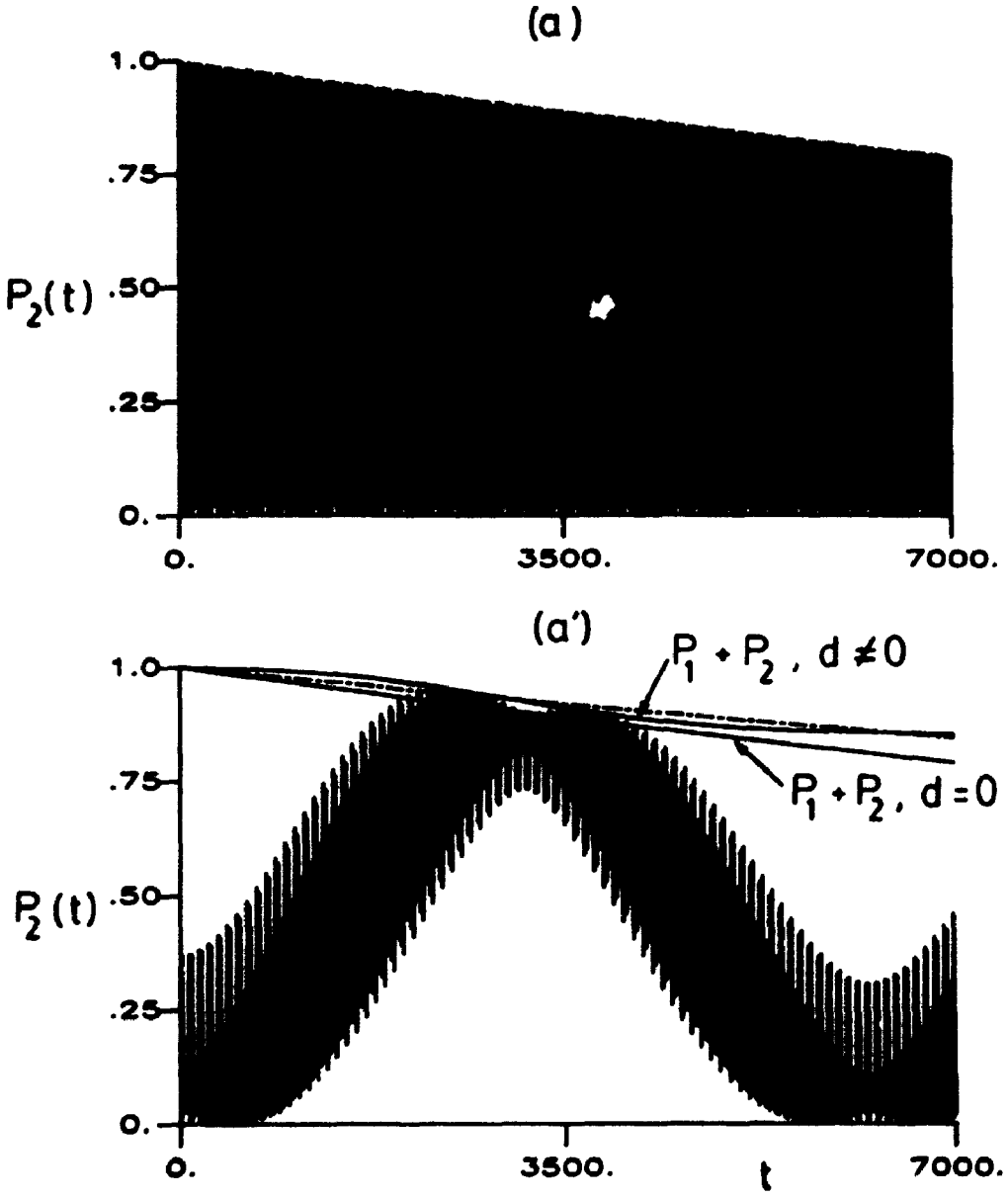

Figure 3.4. The exact time-dependent excited state population for the one-photon transition, as a function of time, for $\gamma_2 = \mathcal{G} = 4.8378 \times 10^{-5}$, and $d = 0$ versus $d \neq 0$, for a CW laser-molecule interaction. Molecular and field parameters as in Fig. 3.3, aside from the value of γ_2. Figure 3.4a $d = 0$, $\omega = 1.67\Delta E$; Fig. 3.4a' $d \neq 0$, $\omega = 0.835\Delta E$. Figure 3.4a' also illustrates the $d = 0$ and $d \neq 0$ total time-dependent populations of the system as a function of time. The dotted in line in Fig. 3.4a' is the function $\exp[-\frac{1}{2}\gamma_2 t]$.

predicted by the RWA.

The exact total population $P_1(t) + P_2(t)$ is given for both $d = 0$ and $d \neq 0$ in Fig. 3.4a'; for $d = 0$, $P_1(t) + P_2(t)$ corresponds to a smooth line passing through the maximum of each Rabi cycle in Fig. 3.4a. From Fig. 3.4a', the $d = 0$ system decays faster than the $d \neq 0$ molecule interacting with the same field. For example, when $t = 3500$, $P_1(t) + P_2(t) = 0.89$ and 0.91 for $d = 0$ and $d \neq 0$, respectively, while when $t = 7000$, the analogous results are 0.79 and 0.85. However, the ratio of the molecule-EMF coupling to the decay rate is much larger when $d = 0$, $|C(1)|^{d=0}_{exact}/\gamma_2 = 5953$, than when $d \neq 0$, $|C(1)|^{d\neq0}_{exact}/\gamma_2 = 21$. Thus, according to the RWA definition of weak decay, the decay is relatively weaker when $d = 0$, than when $d \neq 0$. This apparent dichotomy between the relative strength of the decay compared to the molecule-EMF coupling, and the faster decay of $P_1(t) + P_2(t)$ for $d = 0$ versus $d \neq 0$ is accounted for in the RWA. Equation (3.2.21) predicts the rate of decay of the whole system is a function of γ_2 and $P_2(t)$. Over the duration of Fig. 3.4, the excited state when $d = 0$ is more frequently highly populated than when $d \neq 0$, because $|C(1)|^{d=0}_{exact} \gg |C(1)|^{d\neq0}_{exact}$. Hence, the $d = 0$ total population decays faster than the $d \neq 0$ analogue, although the two systems are interacting with CW fields of identical strength, and have the same γ_2. This trend is also found in the exact results for the larger decay rates $\gamma_2 = 10\mathcal{G}$ and $100\mathcal{G}$.

It is important to distinguish between the phenomenological decay rate γ_2, and the instantaneous rate of decay of the excited state, (3.2.10), or of the total system, (3.2.21). The introduction of γ_2 was designed to ensure that the molecule, in the absence of an external

perturbation, decayed exponentially [61-65]. In the presence of a CW laser, the decay of the excited state is much more complicated. Thus, while the phenomenological decay rate may be classified, according to the RWA, as "weak" relative to the molecule-EMF coupling, the instantaneous rate of decay of the system can be "strong".

The nature of the decay of the exact total population is distinct for $d = 0$ and $d \neq 0$. When $d = 0$, $P_1(t) + P_2(t)$ appears to decay exponentially whereas when $d \neq 0$, $P_1(t) + P_2(t)$ contains an oscillation and its steepest slope occurs just before the central dip in the excited state population. For the larger decay rate, $\gamma_2 = 10\mathcal{G}$, see Fig. 3.5a', these features are much more pronounced; when $d \neq 0$, the damped oscillatory nature of the decay of $P_1(t) + P_2(t)$ is very evident.

For $\gamma_2 = \mathcal{G}$ and $10\mathcal{G}$, this difference in the nature of the decay of $P_1(t) + P_2(t)$ when $d = 0$ versus $d \neq 0$ is also explicable by the RWA result (3.2.21). From (3.2.21), critical or inflection points in $P_1(t) + P_2(t)$ will occur every time $P_2(t)$ is a maximum or minimum: when $d = 0$, this happens very frequently, and hence oscillations in the exact total population are not visible on the scale of Figs. 3.4a' and 3.5a'; on the expanded scale of 3.5b, these oscillations would be just visible. In contrast, when $d \neq 0$, the exact excited state population changes slowly, and the corresponding oscillations in $P_1(t) + P_2(t)$ are clearly evident in Figs.3.4a' and 3.5a'. For example, using $\alpha_{r,\text{exact}}^{d\neq 0}$ for $\gamma_2 = \mathcal{G}$, the RWA result (3.2.21) with (3.2.12) predicts the decay of the total system is largest when $t = t' = 3063$, which is just before the central dip in the excited state population in Fig. 3.4a'. Similarly, the analogous RWA prediction for $\gamma_2 = 10\mathcal{G}$ is $t' = 2710$,

which is also just before the central "dip" in the time-dependent excited state population.

$$\gamma_2 = 10\mathcal{G}$$

According to the RWA, $\gamma_2 = 10\mathcal{G} = 4.8378\text{x}10^{-4}$ can still be classified as weak decay relative to both $C(1)^{d=0}_{exact} \simeq 0.288$ and $C(1)^{d\neq 0}_{exact} \simeq 0.001010$. Thus, the behaviour of the $d = 0$ versus $d \neq 0$ time-dependent excited state populations when $\gamma_2 = 10\mathcal{G}$ will be similar to that for $\gamma_2 = \mathcal{G}$. The ten-fold increase in γ_2 will be evident in the increased severity of the decay of the total system in the same time interval. Furthermore, calculation of the exact analogues to α_r, from (3.2.11), yields $\alpha^{d=0}_{r,exact} \simeq 0.288 \simeq |C(1)|^{d=0}_{exact}$, and $\alpha^{d\neq 0}_{r,exact} \simeq 0.000981$. Therefore, the RWA predicts the $d = 0$ period of the exact time-dependent excited state population will not change when $\gamma_2 = 10\mathcal{G}$ relative to when $\gamma_2 = 0, \mathcal{G}$; when $d \neq 0$, the prediction is the period will increase from $T_{exact} = 6220$ for $\gamma_2 = 0$ and $\mathcal{G}$, to $2\pi/\alpha^{d\neq 0}_{r,exact} \simeq 6406$ for $\gamma_2 = 10\mathcal{G}$.

Figure 3.5a and 3.5a′ illustrate the time-dependent excited state populations for $\gamma_2 = 10\mathcal{G}$ for $d = 0$ and $d \neq 0$, respectively. The total population for both $d = 0$ and $d \neq 0$ are shown in Fig. 3.5a′. The $d = 0$ and $d \neq 0$ excited state populations are repeated Fig. 3.5b and 3.5b′, respectively, but on a shorter expanded time interval. The increased decay rate is reflected in the decreased magnitudes of the maximum excited state population relative to Fig. 3.4.

From Fig. 3.5b, the effect of the increased decay when $d \neq 0$ is evident almost immediately as the maximum excited state population, at the second maximum of the first cycle, is less than 1.0: $P_2(t) = .994$

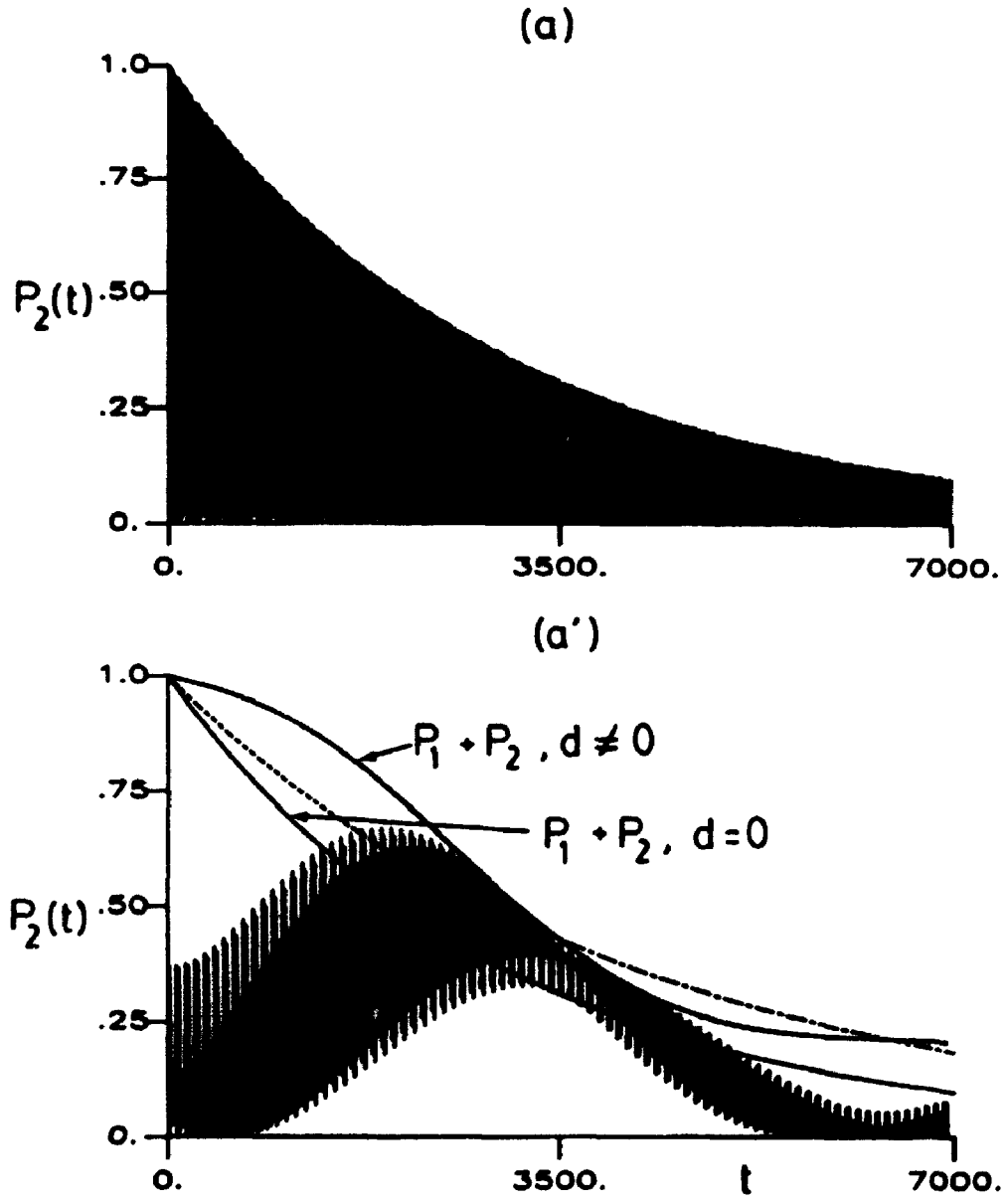

Figure 3.5. The exact time-dependent excited state population for the one-photon transition, as a function of time, for $\gamma_2 = 10\mathcal{G} = 4.8378 \times 10^{-4}$, and d = 0 versus d ≠ 0, for a CW laser-molecule interaction. Molecular and field parameters as in Fig. 3.3, except for γ_2. Fig. 3.5(a,b) d = 0, $\omega = 1.67\Delta E$; Fig. 3.5(a′,b′) d ≠ 0, $\omega = 0835\Delta E$. Figure 3.5a′ also shows the d = 0 and d ≠ 0 total time-dependent populations of the system as a function of time. The dotted in line in Fig. 3.5a′ is the function $\exp[-\frac{1}{2}\gamma_2 t]$.

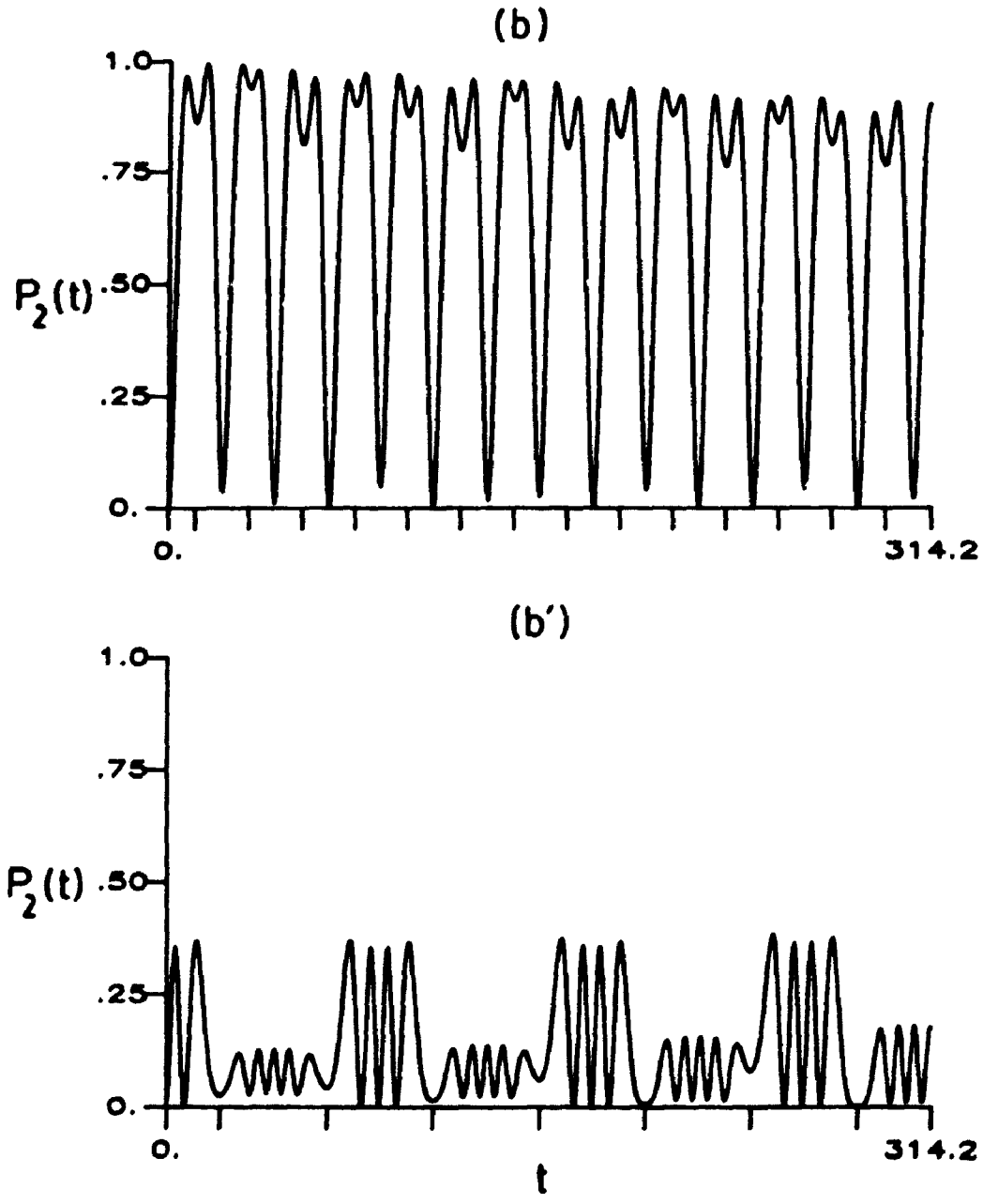

Figure 3.5 continued. Figure 3.5(b,b') illustrates the results of Fig. 3.5(a,a') on a shorter expanded time interval.

at t = 15.5 (.375fs). However, the temporal locations of the dips between the maxima, and of the minima ($P_2(t) \simeq 0$) still coincide with those when $\gamma_2 = 0$. The latter is predicted by the RWA.

For $d \neq 0$ in Fig. 3.5a', the asymmetry of the overall evolution of the time-dependent excited state population increases. The maximum population of the excited state is $P_2(t) = .671$ at t = 1911 (46.24fs). The effect of increasing γ_2, compare Fig. 3.4a' and Fig. 3.5a', is more severe for the greater decay rate, but on the shorter time scale of 3.5b', the decay of the excited state population is not graphically detectable. The overall period increases from $T_{exact} \simeq 6220$ ($\simeq$150.5fs) for $\gamma_2 = 0$ to $T_{exact} \simeq 6351$ ($\simeq$153.6fs) for $\gamma_2 = 10\mathcal{G}$, in agreement to within 1% with the predictions of the RWA.

$$\gamma_2 = 100\mathcal{G}$$

The RWA predicts that the nature of the decay for $\gamma_2 = 100\mathcal{G}$ will be different for the d = 0 and $d \neq 0$ examples presented here. The quantity $\frac{1}{2}\gamma_2 = 50\mathcal{G} = 2.4189\times10^{-3}$ is less than $|C(1)|^{d=0}_{exact} = 0.288$, but greater than $|C(1)|^{d\neq0}_{exact} = 0.001010$. Hence, the RWA classifies $\gamma_2 = 100\mathcal{G}$ as weak decay when d = 0 but as strong decay when $d \neq 0$. The behaviour of the $\gamma_2 = 100\mathcal{G}$, d = 0 time-dependent excited state population should be an "exaggerated" version of the $\gamma_2 = \mathcal{G}$ and $10\mathcal{G}$ analogues. Since $\frac{1}{2}\gamma_2$ is roughly one percent of $|C(1)|^{d=0}_{exact}$, changes in the duration of the Rabi cycles through $\alpha^{d=0}_{r,exact}$ will be very small, on the order of $\Delta t = 10^{-3}$. When $d \neq 0$, the RWA predicts the time-dependent excited state population will not show any oscillatory behaviour. If the transition between minimum and maximum time-dependent excited state population was smooth, the RWA would

predict the maximum excited state population would occur when $t = t' = 1383$, from (3.2.29) with $\beta^{d\neq0}_{r,exact} = [\frac{1}{4}\gamma_2 - |C(1)^{d\neq0}_{exact}|^2]^{1/2}$ $= 0.002198$.

The rate of decay of the whole system for weak decay is given by (3.2.21); the strong decay result has an identical form with $P^{(N,\gamma)}_{2,r,w}(t)$ replaced with $P^{(N,\gamma)}_{2,r,s}(t)$. Thus, for both weak and strong decay, the instantaneous decay rate of the whole system is determined by the product of the phenomenological decay rate γ_2 and the excited state population. When $d = 0$, (3.2.22) predicts the largest rate of decay of the system will be $[dP^{(N,\gamma)}_{tot,r,w}/dt]_{t=t'} = 4.7\times10^{-3}$ $(t' = 10.8)$. The analogous result for the strong damping case when $d \neq 0$ is given by (3.2.31), predicts $[dP^{(N,\gamma)}_{tot,r,s}/dt]_{t=t'} = 1.7\times10^{-4}$ $(t' = 1383)$. Since (3.2.22) and (3.2.31) are based on the times (t') and magnitudes of the maxima in the excited state population in the RWA, and the analogous quantities are not easily identifiable in the exact results, the RWA will likely not be quantitatively valid for these rates. However, for $\gamma_2 = 100\mathcal{G}$, the RWA predicts that the $d = 0$ system, which is classified as weak decay relative to the molecule-EMF coupling, will decay faster than the $d \neq 0$ system, which is classified as strong decay relative to the molecule-EMF coupling. Although tne phenomenological decay rate γ_2 is identical when $d = 0$ and $d \neq 0$, the difference in the maximum instantaneous rate occurs because $[dP^{(N,\gamma)}_{tot,r}/dt]$ is dependent on the magnitude of $P_2(t)$, and the $d = 0$ excited state is more quickly and frequently populated than when $d \neq 0$.

The time-dependent excited state populations are shown for $\gamma_2 = 100\mathcal{G}$ for $d = 0$ in Fig. 3.6a and for $d \neq 0$ in Fig. 3.6a′; Fig. 3.6a′ also contains the $d = 0$ and $d \neq 0$ total populations. The

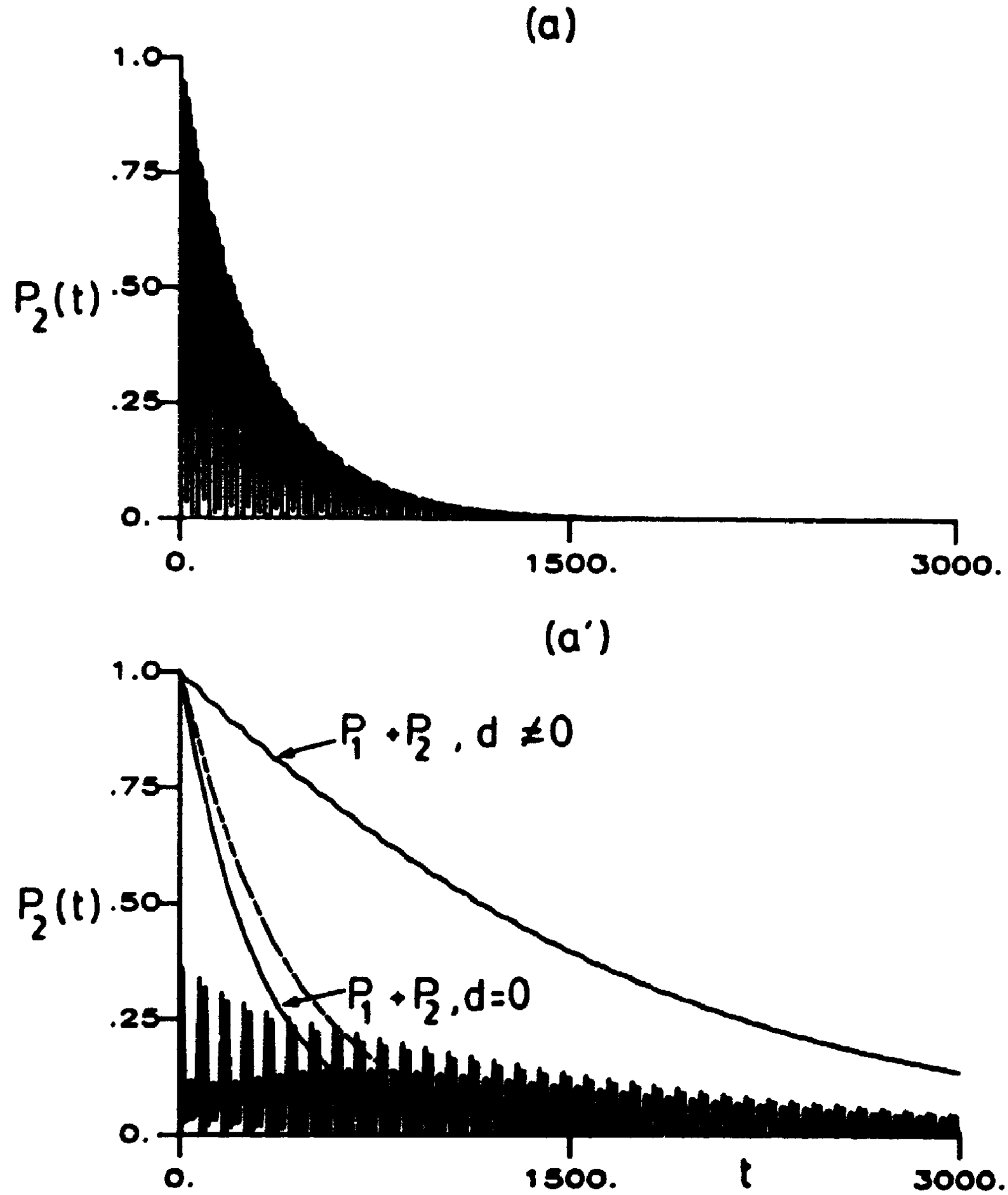

Figure 3.6. The exact time-dependent excited state population for the one-photon transition, as a function of time, for $\gamma_2 = 100\vartheta = 4.8378\text{x}10^{-3}$, and d = 0 versus d ≠ 0, for a CW laser-molecule interaction. Molecular and field parameters as in Fig. 3.3, except for γ_2. Fig. 3.6(a,b) d = 0, $\omega = 1.67\Delta E$; Fig. 3.6(a′,b′) d ≠ 0, $\omega = 0.835\Delta E$. Figure 3.6a′ also illustrates the d = 0 and d ≠ 0 total time-dependent populations of the system as a function of time. The dotted in line in Fig. 3.6a′ is the function $\exp[-\frac{1}{2}\gamma_2 t]$.

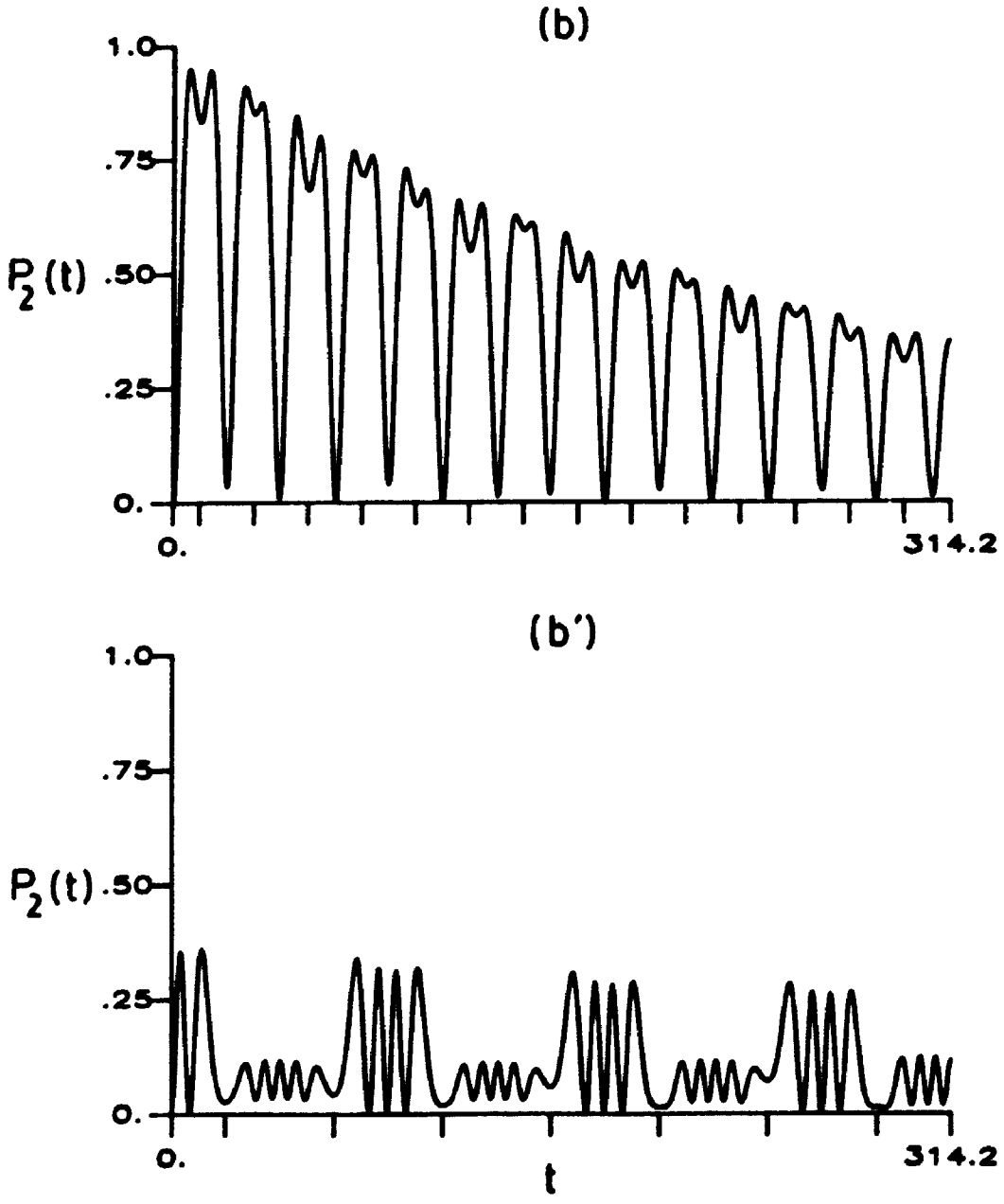

Figure 3.6 continued. Figure 3.6(b,b') illustrates the results of Fig. 3.6(a,a') on a shorter expanded time interval.

time interval has been decreased to $0 \leq t \leq 3000$ (72.57fs), relative to Figs. 3.3-3.5, to account for the increased decay. Fig. 3.6(b,b') repeats Fig. 3.6(a,a'), but on a shorter expanded time interval.

When $d = 0$, the effect of decay on the magnitude of the maxima of the exact population of state two is quite severe, and is evident even in the short time span of Fig. 3.6b. The maximum of the exact excited state population is reached at the first maximum of the first "Rabi" cycle; $P_2(t) = .949$ at $t = 6.7$ ($\simeq$.16fs), but the time-dependent excited state population still oscillates many times between maximum and minimum population, which is indicative of weak decay, before the total population becomes negligible. In agreement with the RWA prediction, the time-dependent behaviour of the excited state population in Fig. 3.6a essentially duplicates that of Figs. 3.4a and 3.5a, except the effect of the decay is more extreme. The RWA explanations for the behaviour of $P_2(t)$, given for the smaller values of γ_2, hold for $\gamma_2 = 100\mathcal{V}$. However, the results with the larger decay rate differ from the $\gamma_2 = 0$, $\mathcal{V}$ and $10\mathcal{V}$ analogues in that the π/ω periodicity of the "dips" between the excited state population maxima is no longer present, and the times of the minima ($P_2(t) \simeq 0$) are shifted slightly from the $\gamma_2 = 0$ values. These shifts in the duration of the Rabi cycle cannot be seen on the scale of Fig. 3.6b, but can been found by a careful study of the numerical data. The shifts are initially equal to the grid size of the calculation, $\Delta t = 0.22$, but increase with increasing time. The RWA predicted a shift in the duration of the Rabi cycle on the order of $\Delta t = 10^{-3}$, but underestimated the (increasing) size of the change.

When $d \neq 0$ and $\gamma_2 = 100\mathcal{V}$, the excited state population decays very

rapidly, which is evident even in the short time span of Fig. 3.6b'. The maximum population of the state two is represented by one of the spikes attributed to the counter-rotating terms, with $P_2(t) = .36$ at $t = 12.26$ ($\simeq .30$fs). Neglecting the "spikes", the maximum excited state population $P_2(t) \simeq .19$ occurs around $t \simeq 900$. Aside from the counter-rotating terms, the excited state population no longer oscillates, and there is no measurable period at this decay rate, indicating strong decay as predicted by the RWA. The RWA prediction for the time ($t = t' = 1383$) of the maximum population is very different from the exact value. Furthermore, from Fig. 3.6a', the decay of the total population when $d \neq 0$ is not a smooth exponentially decreasing function of time, but contains small oscillations which coincide in time with the "spikes" associated with the counter-rotating effects in $P_2(t)$. Hence, Fig. 3.6a' is an excellent example of how strong counter-rotating effects destroy the quantitative applicability of the RWA.

3.5. SOME GENERAL COMMENTS

The analytical RWA solutions derived in Sec. 3.1 for a two-level molecular system with permanent dipoles and a non-zero excited state decay rate, interacting with a CW laser, have played an important role in the investigation of effects due to permanent dipole moments on the resonance temporal behaviour of the excited state as a function of decay rate, as discussed in Secs. 3.2 and 3.3. The impact of the excited state decay was explored in two sets of examples in Sec. 3.4, under conditions where the $d \neq 0$ RWA results of Sec. 3.1 were first quantitatively, and then strictly qualitatively, applicable.

In the decay examples of Sec. 3.4.1, the RWA is quantitatively valid. For weak decay, the total population decays as a damped sine curve, see (3.2.21). From (3.2.20), at $t = 2\pi n/\alpha_r$, $P_1(t) + P_2(t) = \exp[-\frac{1}{2}\gamma_2 t]$, while at $t = t'$ from (3.2.12),

$$P_1(t') + P_2(t') = \frac{|C(N)|^2 + \gamma_2^2}{|C(N)|^2} \exp[-\tfrac{1}{2}\gamma_2 t'] \simeq \exp[-\tfrac{1}{2}\gamma_2 t']$$

On average then, the decay of the total population can be described by the function $\exp[-\frac{1}{2}\gamma_2 t]$ for weak decay, $|C(N)| > \frac{1}{2}\gamma_2$. For critical and strong damping, the total population decays more slowly than the function $\exp[-\frac{1}{2}\gamma_2 t]$, since from (3.2.5) and (3.2.8), and (3.2.6) and (3.2.9), $P_1(t) + P_2(t)$ is greater than $\exp[-\frac{1}{2}\gamma_2 t]$ for all times $t > 0$.

For the examples of Sec. 3.4.2, where the RWA is only qualitatively applicable, the function $\exp[-\frac{1}{2}\gamma_2 t]$ is shown as a dotted curve in Figs. 3.4a', 3.5a', and 3.6a', for $\gamma_2 = \mathcal{G}$, $10\mathcal{G}$ and $100\mathcal{G}$, respectively. When $d = 0$, the total population decays faster than the exponential function in all three cases, i.e. $P_1(t) + P_2(t)$ is less than $\exp[-\frac{1}{2}\gamma_2 t]$. This difference can be attributed to the counter-rotating effects: $P_2(t)$ is a maximum twice in each "Rabi" cycle, and the total population decays faster the larger the excited state population. When $d \neq 0$ and $\gamma_2 = \mathcal{G}$, $10\mathcal{G}$, the oscillation in $P_1(t) + P_2(t)$ results in the total population being initially greater than, and then less than and then greater than, $\exp[-\frac{1}{2}\gamma_2 t]$. This oscillation is the damped sinusoidal behaviour predicted by the RWA for weak decay. For the example of strong decay, $\gamma_2 = 100\mathcal{G}$, the total population is much greater than $\exp[-\frac{1}{2}\gamma_2 t]$, as predicted by the RWA.

Although the RWA could not quantitatively predict the near-nodal molecule-EMF coupling when $d \neq 0$, or the changing duration of the Rabi

cycle when d = 0, for the examples of Sec. 3.4.2, the approximate RWA results of Sec. 3.2 are still applicable given estimates of the exact couplings. The RWA has been applied to qualitatively predict and interpret many of the unique effects of permanent dipoles, relative to d = 0, and of the interplay between the molecule-EMF couplings and the decay rate γ_2. For example, the near-nodal molecule-EMF coupling associated with d ≠ 0 means that for a given phenomenological decay rate, the excited state is more likely to be strongly damped (relative to the molecule-EMF coupling) than the d = 0 analogue. However, because the d ≠ 0 coupling is so small, the system takes longer to populate the excited state, and does so less frequently than when d = 0. Thus, for the same phenomenological decay rate γ_2, the d = 0 total system actually decays faster than when d ≠ 0 for nodal or near-nodal molecule-EMF coupling.

The examples of Sec. 3.4 focused on the one-photon transitions of a molecule with a short-lived excited state. In principle, the effects of d ≠ 0 will persist in molecular systems with much longer excited state lifetimes, relative to those associated with the phenomenological decay rates employed in Sec. 3.4. The point of critical decay for systems with small phenomenological decay rates can be established by generating a small molecule-EMF coupling, which can be accomplished by using weaker field strengths, tuning the frequency to a multi-photon resonance, or using field strengths corresponding to a molecule-EMF coupling node. It is noted that reducing the field strength used in Sec. 3.4.2 by one percent will significantly decrease the molecule-EMF coupling, as discussed in detail in Chapters 4 and 6.

The absorption/emission patterns are very complex when the field

is very strong, for both $d = 0$ and $d \neq 0$. Part of the complexity is due to "beating" effects between the frequency of the counter-rotating terms and the molecule-EMF coupling. These beating effects are discussed in Chapter 4 with respect to the time-dependent phase-averaged excited state populations, since these results, relative to the phase-dependent analogues, tend to be "smoother", and the beating effect is more obvious, see for example, Fig. 4.1a.

There can clearly be an enormous difference between the $d \neq 0$ versus $d = 0$ evolution and decay of the time-dependent excited state population. The oscillatory nature of the decay of the total system associated with the near-nodal $d \neq 0$ molecule-EMF coupling can act as an indicator of the presence of permanent dipoles. Indeed, the results of Figs. 3.3a'-3.6a' would be misinterpreted if it was assumed that $d = 0$. Thus, the examples of Sec. 3.4.2 suggest that the decay can act as an internal probe of the permanent dipoles. For a given γ_2, which can be determined from the decay of the unperturbed molecule after excitation [97,98], the interaction of the molecule with CW lasers of varying field strengths can indicate the presence of molecule-EMF coupling nodes by changes in the temporal evolution of the excited state population, from weak to strong to weakly damped, relative to the molecule-EMF coupling, as discussed in Sec. 3.3.2.

The excited state decay, as used here, acts as an amplitude modulator on the CW laser-molecule interaction. In this sense, excited state decay is similar to a pulsed laser, where the amplitude modulator of the field "chops" the CW laser-molecule interaction [21,22]. The interaction of a permanent dipole molecule with a pulsed laser is investigated in Chapter 4, and the effects of $d \neq 0$, relative to $d = 0$,

are discussed. In contrast to excited state decay, a pulsed laser can be used as an external probe of the effects and presence of permanent dipoles.

CHAPTER 4

PULSED LASER-MOLECULE INTERACTIONS

The observation of the spectral and dynamical effects of permanent dipoles will often require the intense fields associated with pulsed rather than purely continuous wave lasers. In Sec. 4.2, a set of two-level model calculations is used to illustrate how the effects of $d = \mu_{22} - \mu_{11} \neq 0$ on the molecule-EMF coupling, and on the dynamics of the molecular states involved in a transition, can be probed by sampling the time-dependent population of the excited state through the use of ultrashort to short pulses of varying durations. Of particular interest is the marked increase in the period of the one-photon resonance temporal behaviour of the excited state associated with the nodes in the $d \neq 0$ molecule-EMF coupling predicted in the RWA. The RWA is used to explain qualitatively the interaction of the molecule with an intense continuous wave electric field; these ideas are then used to help interpret the Gaussian pulsed laser-molecule interactions.

The Riemann product integral (RPI) technique [3,21,37-39] is used here for the calculations involving the pulsed laser-molecule interactions; the Floquet formalism is not applicable since the time-dependent Hamiltonian is no longer periodic with respect to the carrier frequency of the pulse. However, in Sec. 4.1, symmetry arguments are used to develop a technique which reduces the

computational effort for pulse-molecule interactions for sine or cosine Gaussian pulses.

4.1. COMPUTATIONAL ASPECTS OF PULSED LASER-MOLECULE INTERACTIONS.

4.1.1. THE INITIAL TIME OF INTERACTION

The transformation (2.1.21) of the time-dependent coefficients from the Schrödinger to the interaction representation can be written in matrix form as,

$$\underline{a}(t) = \exp[-i\underline{\underline{E}}t]\underline{b}(t). \tag{4.1.1}$$

The corresponding matrix equation for the time-dependent wave equation, in the interaction representation, is,

$$\frac{d}{dt}\underline{b}(t) = \underline{\underline{C}}(t)\underline{b}(t), \tag{4.1.2}$$

where,

$$\underline{\underline{C}}(t) = i\underline{\mathcal{E}}(t)\cdot\exp[i\underline{\underline{E}}t]\ \underline{\underline{\mu}}\ \exp[-i\underline{\underline{E}}t]. \tag{4.1.3}$$

Equation (2.2.3), which is the time-dependent equation for the evolution operator matrix in terms of $\underline{\underline{C}}(t)$, depends on the parameter t_0, the initial time of the molecule-EMF interaction.

Reference [21] uses a matrix $\underline{\underline{\mathcal{E}}}(t)$, which is related to $\underline{\underline{C}}(t)$, in an interaction representation defined by,

$$\underline{\underline{\mathcal{E}}}(t) = i\underline{\mathcal{E}}(t)\cdot\exp[i\underline{\underline{E}}(t-t_0)]\ \underline{\underline{\mu}}\ \exp[-i\underline{\underline{E}}(t-t_0)]. \tag{4.1.4}$$

The corresponding time-dependent wave equation is given by,

$$\frac{d}{dt}\underline{c}(t) = \underline{\underline{\mathcal{E}}}(t)\underline{c}(t), \tag{4.1.5}$$

with solution,

$$\underline{c}(t) = \underline{\underline{\mathcal{U}}}(t,t_0)\underline{c}(t_0), \tag{4.1.6}$$

where $\underline{\underline{\mathcal{U}}}(t,t_0)$ is defined by substitution of (4.1.6) into (4.1.5).

For computational purposes, and to facilitate the proof of a symmetry theorem below, it is convenient to work with the time-dependent coefficients $\underline{b}(t)$, (4.1.2). These time-dependent coefficients are related to $\underline{c}(t)$ by the unitary transformation,

$$\underline{c}(t) = \exp[-i\underline{\underline{E}}t_0]\underline{b}(t) \tag{4.1.7}$$

In the $\underline{b}$-representation, the solution to $\underline{b}(t)$ is given by,

$$\underline{b}(t) = \underline{\underline{U}}(t,t_0)\underline{b}(t_0), \tag{4.1.8}$$

where $\underline{\underline{U}}(t,t_0)$ satisfies (2.2.3); $\underline{\underline{C}}(t)$ in (4.1.3) and $\underline{\underline{\mathcal{E}}}(t)$ in (4.1.4) are related by,

$$\underline{\underline{C}}(t) = \exp[i\underline{\underline{E}}t_0]\ \underline{\underline{\mathcal{E}}}(t)\ \exp[-i\underline{\underline{E}}t_0]. \tag{4.1.9}$$

The evolution operator matrices $\underline{\underline{U}}$ and $\underline{\underline{\mathcal{U}}}$ are related by,

$$\underline{\underline{\mathcal{U}}}(t,t_0) = \exp[-i\underline{\underline{E}}t_0]\ \underline{\underline{U}}(t,t_0)\ \exp[i\underline{\underline{E}}t_0]. \tag{4.1.10}$$

Of course, physical observables are independent of the unitary transformation (4.1.7); for example, the temporal population of state j is given by,

$$|c_j(t)|^2 = |b_j(t)|^2$$

$$= \sum_k \sum_l U_{jk}(t,t_0)U^*_{jl}(t,t_0)b_k(t_0)b^*_l(t_0). \tag{4.1.11}$$

Working in the $\underline{b}$-representation simplifies the computation of the evolution operator since $\underline{\underline{C}}(t)$, from (4.1.3), is independent of t_0, whereas $\underline{\underline{\mathcal{E}}}(t)$ in (4.1.4) depends on t_0. It is noted that the solution for the time-dependent coefficients retains its dependence on the

initial conditions through $\underline{b}(t_0)$.

4.1.2. THE HALF-PULSE TECHNIQUE

For a Gaussian pulsed electric field, $\underline{\mathcal{E}}(t)$ is given by (2.1.15). Theoretically, the duration of the pulse, i.e. the time of field-molecule interaction, is $-\infty < t < +\infty$. However, for computational purposes, the effective pulse duration can be taken as $-\alpha\tau_p \leq t \leq +\alpha\tau_p$, where α is a constant such that the field envelope $f(t) = \exp[-t^2/\tau_p^2]$ at $t = \pm\alpha\tau_p$ is very small ($<10^{-6}$); the resulting perturbation of the molecule by the field for $|t| > \alpha\tau_p$ is negligible [21]. Hence, in the absence of excited state decay, the steady state population of the jth state corresponds to $\bar{P}_j = P_j(t = +\alpha\tau_p)$.

The numerical evaluation of the evolution operator for molecule-EMF interactions can be carried out by application of the RPI method, see Sec. 2.2.1. For pulsed laser-molecule interactions, the lack of periodicity in $2\pi/\omega$ for the pulse prevents the Floquet technique from being used to evaluate temporal or steady state populations. In principle then, the evolution operators $\underline{\underline{U}}(t_j, t_{j-1})$ must be calculated for each RPI subinterval over the entire effective duration of the laser-molecule interaction, $-\alpha\tau_p \leq t \leq \alpha\tau_p$, where $\alpha = 3.8$ in the examples presented in this chapter. In practice, however, the subinterval evolution operators need be evaluated explicitly over only half the duration of the interaction, $0 \leq t \leq \alpha\tau_p$, say, for a pulse that is symmetric or antisymmetric about $t = 0$. This half-pulse technique is illustrated for the Gaussian pulse defined by (2.1.15).

For convenience, the time interval corresponding to the duration

of the pulsed laser-molecule interaction, $-\alpha\tau_p \leq t \leq +\alpha\tau_p$, is divided into 2m subintervals equally spaced on either side of t = 0. The analogue of (2.2.6), with n = 2m and $t_0 = -\alpha\tau_p$, can be written as,

$$\underline{\underline{U}}(t=+\alpha\tau_p, t_0=-\alpha\tau_p) = \underline{\underline{U}}(t_m=+\alpha\tau_p, t_{m-1})\underline{\underline{U}}(t_{m-1}, t_{m-2})\ldots\underline{\underline{U}}(t_s, t_{s-1})\ldots$$

$$\ldots\underline{\underline{U}}(t_1, 0)\underline{\underline{U}}(0, -t_1)\ldots\underline{\underline{U}}(-t_{s-1}, -t_s)\ldots$$

$$\ldots\underline{\underline{U}}(-t_{m-2}, -t_{m-1})\underline{\underline{U}}(-t_{m-1}, -t_m=-\alpha\tau_p). \qquad (4.1.12)$$

In the RPI method, the relationship between the evolution operator over the interval $[t_{s-1}, t_s]$ and the matrix $\underline{\underline{C}}$ is given by (2.2.7). Substitution of the expression for the Gaussian pulsed electric field, (2.1.15), into (4.1.3), and applying (2.2.8), yields,

$$C_{jk}^{(s)} = i\underline{\mu}_{jk}\cdot\hat{e}\mathcal{E}^0\int_{t_{s-1}}^{t_s}\exp(-t^2/\tau_p^2)\cos(\omega t + \delta)\exp[iE_{jk}t]dt. \qquad (4.1.13)$$

Making use of the trigonometric expansion of $\cos(\omega t + \delta)$ in (4.1.13) results in,

$$C_{jk}^{(s)} = i\underline{\mu}_{jk}\cdot\hat{e}\mathcal{E}^0\cos\delta\int_{t_{s-1}}^{t_s}\exp(-t^2/\tau_p^2)\cos(\omega t)\exp[iE_{jk}t]dt$$

$$- i\underline{\mu}_{jk}\cdot\hat{e}\mathcal{E}^0\sin\delta\int_{t_{s-1}}^{t_s}\exp(-t^2/\tau_p^2)\sin(\omega t)\exp[iE_{jk}t]dt, \qquad (4.1.14)$$

or,

$$C_{jk}^{(s)} = C_{\cos\delta, jk}^{(s)} - C_{\sin\delta, jk}^{(s)}. \qquad (4.1.15)$$

In matrix form, (4.1.15) can be written as,

$$\underline{\underline{C}}^{(s)} = \underline{\underline{C}}_{\cos\delta}^{(s)} - \underline{\underline{C}}_{\sin\delta}^{(s)}. \qquad (4.1.16)$$

Over the interval $[-t_s, -t_{s-1}]$, the analogue to (4.1.14) can be written as,

$$C_{jk}^{(-s)} = i\underline{\mu}_{jk}\cdot\hat{e}\mathcal{E}^0\cos\delta\int_{-t_s}^{-t_{s-1}}\exp(-t^2/\tau_p^2)\cos(\omega t)\exp[iE_{jk}t]dt$$

$$- i\underline{\mu}_{jk}\cdot\hat{e}\mathcal{E}^0\sin\delta\int_{-t_s}^{-t_{s-1}}\exp(-t^2/\tau_p^2)\sin(\omega t)\exp[iE_{jk}t]dt. \qquad (4.1.17)$$

Using the transformation $t \rightarrow -t$ in the right-hand side of (4.1.17), and recalling $\underline{\mu}_{jk} = \underline{\mu}_{kj}$, this last expression becomes,

$$C_{jk}^{(-s)} = i\underline{\mu}_{kj}\cdot\hat{e}\mathcal{E}^0\cos\delta\int_{t_{s-1}}^{t_s}\exp(-t^2/\tau_p^2)\cos(\omega t)\exp[+iE_{kj}t]dt$$

$$+ i\underline{\mu}_{jk}\cdot\hat{e}\mathcal{E}^0\sin\delta\int_{t_{s-1}}^{t_s}\exp(-t^2/\tau_p^2)\sin(\omega t)\exp[-iE_{jk}t]dt. \qquad (4.1.18)$$

Comparison with (4.1.14) and (4.1.15) yields the relationship,

$$C_{jk}^{(-s)} = C_{\cos\delta,kj}^{(s)} - (C_{\sin\delta,jk}^{(s)})^*, \qquad (4.1.19)$$

or,

$$\underline{\underline{C}}^{(-s)} = [\underline{\underline{C}}_{\cos\delta}^{(s)}]^T - [\underline{\underline{C}}_{\sin\delta}^{(s)}]^*, \qquad (4.1.20)$$

where $\underline{\underline{A}}^T$ denotes the transpose of the matrix $\underline{\underline{A}}$. Hence, the matrix $\underline{\underline{C}}^{(-s)}$, in the "negative" half of the pulse duration, can be expressed in terms of the cosδ and sinδ components of $\underline{\underline{C}}^{(s)}$, in the "positive" half of the pulse duration.

From (2.2.7) and (2.2.8), the relationship between the evolution operator over the interval $[t_{s-1}, t_s]$ and $\underline{\underline{C}}^{(s)}$, as expressed in (4.1.16), is,

$$\underline{\underline{U}}(t_s, t_{s-1}) = \exp[\underline{\underline{C}}_{\cos\delta}^{(s)} - \underline{\underline{C}}_{\sin\delta}^{(s)}]. \qquad (4.1.21)$$

For the corresponding interval in the negative half of the pulse, and using (4.1.20),

$$\underline{\underline{U}}(-t_{s-1}, -t_s) = \exp[(\underline{\underline{C}}_{\cos\delta}^{(s)})^T - (\underline{\underline{C}}_{\sin\delta}^{(s)})^*]. \qquad (4.1.22)$$

The $\sin\delta$ and $\cos\delta$ components of $\underline{\underline{C}}^{(-s)}$ transform differently in terms of the corresponding components of $\underline{\underline{C}}^{(s)}$. Hence, to apply the half-pulse technique to the evolution operators, separate evolution operators must be identified for the each component of $\underline{\underline{C}}^{(-s)}$. However, the separation of $\exp[\underline{\underline{A}} + \underline{\underline{B}}] = \exp[\underline{\underline{B}} + \underline{\underline{A}}]$ into $\exp[\underline{\underline{A}}]\exp[\underline{\underline{B}}]$ requires that $\underline{\underline{A}}$ and $\underline{\underline{B}}$ commute [69,99]. In general, the $\sin\delta$ and $\cos\delta$ components of $\underline{\underline{C}}^{(-s)}$ do not commute and individual evolution operators cannot be identified for a Gaussian pulse of arbitrary phase.

However, the half-pulse technique can be applied if one component of $\underline{\underline{C}}^{(s)}$ vanishes. Equivalently, the Gaussian pulse must be symmetric or antisymmetric about $t = 0$; this occurs when the oscillating component of the field is purely cosine ($\delta = 0, \pi$) or sine ($\delta = \frac{1}{2}\pi, \frac{3}{2}\pi$). The remaining details of the half pulse technique are given for a cosine Gaussian pulse, which is involved in the applications of Sec. 4.2.

For $\delta = 0$ or π, from (4.1.21), the evolution operator over the subinterval $[t_{s-1}, t_s]$ can be written,

$$\underline{\underline{U}}^{\cos\delta}(t_s, t_{s-1}) = \exp[\underline{\underline{C}}^{(s)}_{\cos\delta}]. \tag{4.1.23}$$

From (4.1.22), and noting $\exp[\underline{\underline{A}}^T] = (\exp[\underline{\underline{A}}])^T$, the evolution operator over the corresponding negative interval is,

$$\underline{\underline{U}}^{\cos\delta}(-t_{s-1}, -t_s) = \left(\exp[\underline{\underline{C}}^{(s)}_{\cos\delta}]\right)^T = [\underline{\underline{U}}^{\cos\delta}(t_s, t_{s-1})]^T. \tag{4.1.24}$$

Thus the evolution operators need only be evaluated explicitly over half of the pulse duration for $\delta = 0, \pi$.

From (4.1.12), the evolution operator from $t = -\alpha\tau_p$ to any $t_q > 0$ is,

$$\underline{\underline{U}}^{\cos\delta}(t_q>0, t_0=-\alpha\tau_p) = \underline{\underline{U}}^{\cos\delta}(t_q, t_{q-1})\underline{\underline{U}}^{\cos\delta}(t_{q-1}, t_{q-2})\ldots$$

$$\ldots\underline{\underline{U}}^{\cos\delta}(t_1, 0)[\underline{\underline{U}}^{\cos\delta}(t_1, 0)]^T[\underline{\underline{U}}^{\cos\delta}(t_2, t_1)]^T\ldots$$

$$\ldots[\underline{\underline{U}}^{\cos\delta}(t_{m-1}, t_{m-2})]^T[\underline{\underline{U}}^{\cos\delta}(t_m=\alpha\tau_p, t_{m-1})]^T, \qquad (4.1.25)$$

or, from the properties of the transpose,

$$\underline{\underline{U}}^{\cos\delta}(t_q>0, t_0=-\alpha\tau_p) = \underline{\underline{U}}^{\cos\delta}(t_q, t_{q-1})\underline{\underline{U}}^{\cos\delta}(t_{q-1}, t_{q-2})\ldots$$

$$\ldots\underline{\underline{U}}^{\cos\delta}(t_1, 0)\left[\underline{\underline{U}}^{\cos\delta}(t_m=\alpha\tau_p, t_{m-1})\underline{\underline{U}}^{\cos\delta}(t_{m-1}, t_{m-2})\ldots\right.$$

$$\left.\ldots\underline{\underline{U}}^{\cos\delta}(t_2, t_1)\underline{\underline{U}}^{\cos\delta}(t_1, 0)\right]^T$$

$$= \underline{\underline{U}}^{\cos\delta}(t_q, t_{q-1})\ldots\underline{\underline{U}}^{\cos\delta}(t_1, 0)[\underline{\underline{U}}^{\cos\delta}(\alpha\tau_p, 0)]^T. \qquad (4.1.26)$$

For $t_q = \alpha\tau_p$ [100],

$$\underline{\underline{U}}^{\cos\delta}(\alpha\tau_p, -\alpha\tau_p) = \underline{\underline{U}}^{\cos\delta}(\alpha\tau_p, 0)[\underline{\underline{U}}^{\cos\delta}(\alpha\tau_p, 0)]^T, \ \delta = 0, \ \pi. \qquad (4.1.27)$$

A similar procedure can be followed for the sine pulse, where $\delta = \frac{1}{2}\pi$ or $\frac{3}{2}\pi$. The relationship between the evolution operators for the negative and positive halves of the pulse can be shown to be,

$$\underline{\underline{U}}^{\sin\delta}(t_{s-1}, -t_s) = [\underline{\underline{U}}^{\sin\delta}(t_s, t_{s-1})]^*, \qquad \delta = \tfrac{1}{2}\pi, \ \tfrac{3}{2}\pi. \qquad (4.1.28)$$

For sine and cosine pulses, the half-pulse technique cuts the cost of computing the steady state population by approximately a factor of two relative to the full-pulse calculation. Reductions in the computer time required for evaluating the time-dependent populations of the molecular states also apply for all times $t > 0$. This half-pulse technique cannot be applied to pulses of arbitrary phase because $\underline{\underline{C}}^{(s)}_{\cos\delta}$ and $\underline{\underline{C}}^{(s)}_{\sin\delta}$ do not commute.

Section 4.2.2 contains some examples of a $d \neq 0$ versus a $d = 0$

molecule interacting with a $\delta = 0$ Gaussian pulsed electric field.

4.2. EXAMPLES OF INTENSE LASER-MOLECULE INTERACTIONS: $d \neq 0$ VERSUS $d = 0$.

Although derived for CW laser-molecule interactions, the RWA, through its interpretive and predictive properties, can also be applied qualitatively to the interaction of a permanent dipole moment molecule with a pulsed electric field. For example, the long periods associated with nodal and near-nodal molecule-EMF coupling suggest ultrashort pulses can be used to sample the effects of a nonzero d on the time-dependent transition probabilities. The link between the pulse calculations and the RWA results is provided by exact CW calculations. Essentially, the time-dependence of the excited state population for a molecule-pulse interaction is that for the analogous molecule-CW interaction, with the CW laser "cut off" for times beyond the duration of the pulse [21,22].

The two-level molecular system used here is the same as that used in the decay examples of Sec. 3.4.1 and 3.4.2. The transition moment μ_{12} and permanent moments μ_{jj} are again taken to be aligned with the direction of polarization of the applied electric field.

4.2.1. CW LASER-MOLECULE INTERACTIONS

The exact fixed-phase and phase-averaged time-dependent populations of the states of the system, and the corresponding long-time averages, are determined using the Floquet formalism [3,23,32] from the evolution operators over the first period of the time-dependent Hamiltonian, $0 \leq t \leq 2\pi/\omega$. For the CW examples studied

here, the evolution operator can be determined to six to eight figure accuracy over the first period by using sufficiently small time subintervals in the RPI method; further subdivision ($\Delta t < 2\pi/360\omega$) does not appear to yield improved accuracy. For the evaluation of the steady state populations of the molecular states, six figure accuracy in the evolution operator is more than sufficient [23,32]. Calculations of the time-dependent populations of the states require the computation of $[\underline{U}(2\pi,0)]^n$, n = 2,3,4,... [32]. When n is very large, which occurs in these examples, more accuracy in $\underline{U}(2\pi,0)$ is required to counteract rounding errors [17]. Thus, for calculations of the (CW) time-dependent populations, the matching power series method [23,32] was used over the first period to compute the evolution operator to twelve figure accuracy. It was found that division of the first period into 200 subintervals, each with a 13 term power series expansion of $\underline{U}(t_s,t_{s-1})$, was sufficient to obtain the time-dependent transition probabilities to graphical accuracy for large times; phase-averaging was performed using Simpson's Rule [76] with 50 integration points over $[0,2\pi/\omega]$.

As in Sec. 3.4.2, a number of field strengths were tested to find the $\mathcal{E}^0$ which corresponded to a local maximum in the period of the exact phase-averaged time-dependent excited state population at the one-photon resonance frequency for the CW laser-molecule interaction. For the values of $\underline{d}\cdot\hat{e}\mathcal{E}^0/\Delta E$ = 9.10, 9.20, and 9.30, the resonance periods of the exact phase-averaged time-dependent excited state populations are 3.83×10^3 (92.6fs), $\approx2\times10^5$ ($\approx5\times10^3$fs) and 4.74×10^3 (115fs), respectively. (For a CW laser-molecule interaction, it is generally the phase-averaged time-dependent populations which

correspond to physical observables [3,32,71]; in Chapter 3, the effect of phase was neglected). The field strength $\mathcal{E}^0 \simeq 0.0677$, which corresponds to $\underline{d}\cdot\hat{e}\mathcal{E}^0/\Delta E = 9.3$ and was used in the examples of Sec. 3.4.2, is chosen for illustrative purposes so that the analogous $d = 0$ case, where the resonance period is $T_{exact} \simeq 61$ (1.5fs), could be viewed on the same time scale as the $d \neq 0$ calculation.

Figure 4.1 shows the the phase-averaged time-dependent excited state population for the model molecule interacting with a CW laser with $\mathcal{E}^0 \simeq 0.0677$ and ω fixed at the phase-averaged one-photon resonance frequency; $d = 0$ in Figs. 4.1a and 4.1b, while $d \neq 0$ in Figs. 4.1a′ and 4.1b′. The resonance frequency when $d = 0$ is Bloch-Siegert shifted to $\omega = 1.205\Delta E$. In Figs. 4.1a′ and 4.1b′ ($d \neq 0$), the resonance frequency, $\omega = 0.8329\Delta E$, corresponds to a negative Bloch-Siegert shift; again, this negative shift is a characteristic of permanent dipole moment molecules [2,3,13,25,26,34], although positive shifts are also possible [28,34].

In order to discuss and understand the temporal behavior of the excited state population shown in Fig. 4.1, it is important to recognize that there are three frequencies (and related periods) associated with the interaction of a CW laser with a molecule: the field frequency ω; the molecule-EMF coupling $|C(1)|$; and the beat frequency ω_{beat} between these two. These will be discussed with the aid of the RWA. For $d = 0$, the interplay between the Rabi coupling, $C(1) = \mu_{12}\mathcal{E}^0$, and the field frequency has been discussed previously for $|\mu_{12}\mathcal{E}^0| \ll \omega$ [32,101-103]. It is also noted that there are two periods related to ω: the field period, $2\pi/\omega$, and the period due to the field, π/ω.

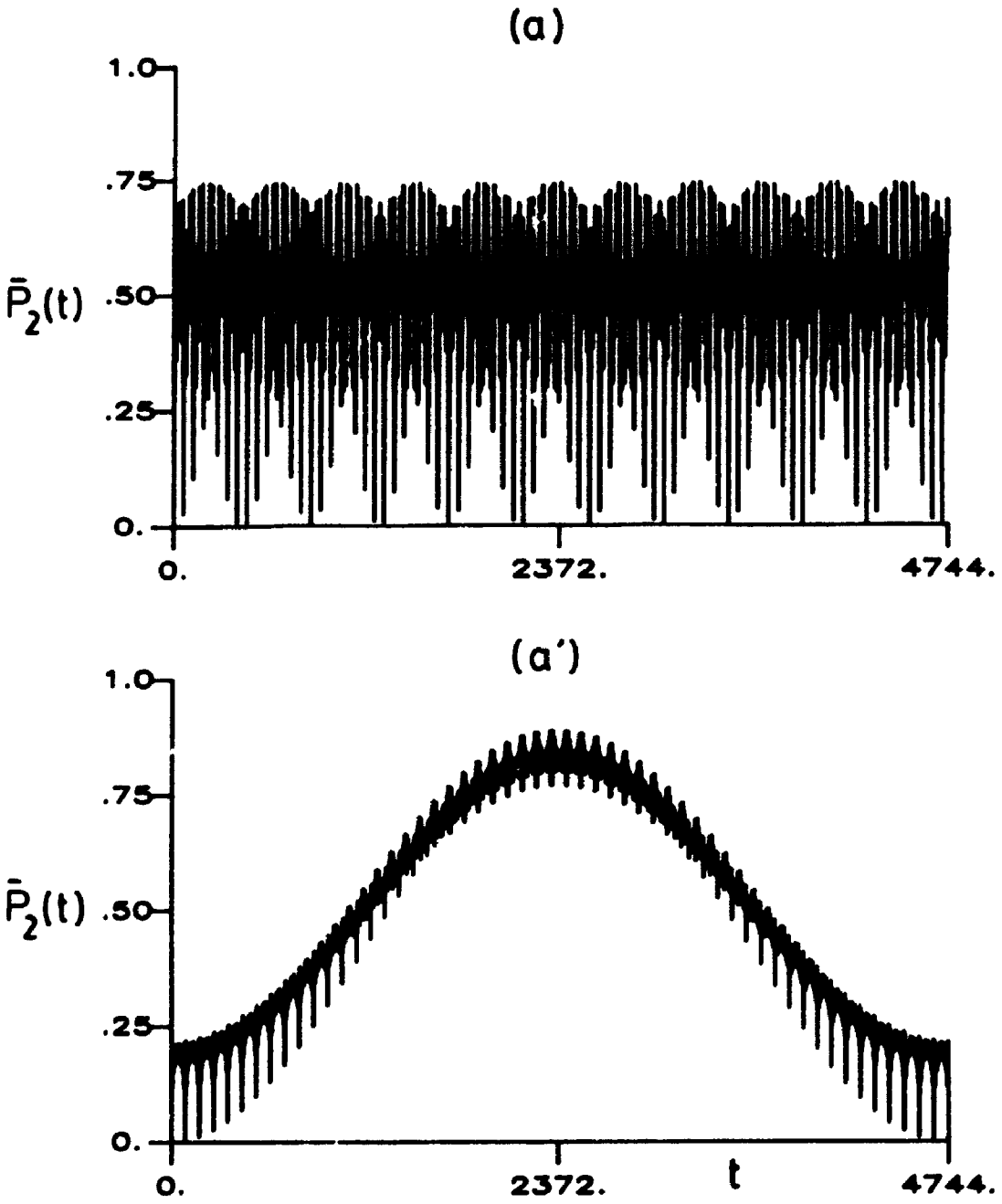

Figure 4.1. One-photon phase-averaged time-dependent excited state population for the model two-level molecule interacting with a continuous wave laser, at the phase-averaged resonance frequency, versus time: $0 \le t \le 4744.0$ (114.7fs) in Fig. 4.1(a,a'); $0 \le t \le 850.0$ (20.56fs) in Fig. 4.1(b,b'). The molecular and field parameters are: $\Delta E = 0.0859$, $d = 11.8$, $\mu_{12} = 3.93$, $d\mathcal{E}^0/\Delta E = 9.30$ ($\mathcal{E}^0 \simeq 0.0677$). Fig. 4.1(a,b) $d = 0$, $\omega = 1.205\Delta E$; Fig. 4.1(a',b') $d \neq 0$, $\omega = 0.8329\Delta E$.

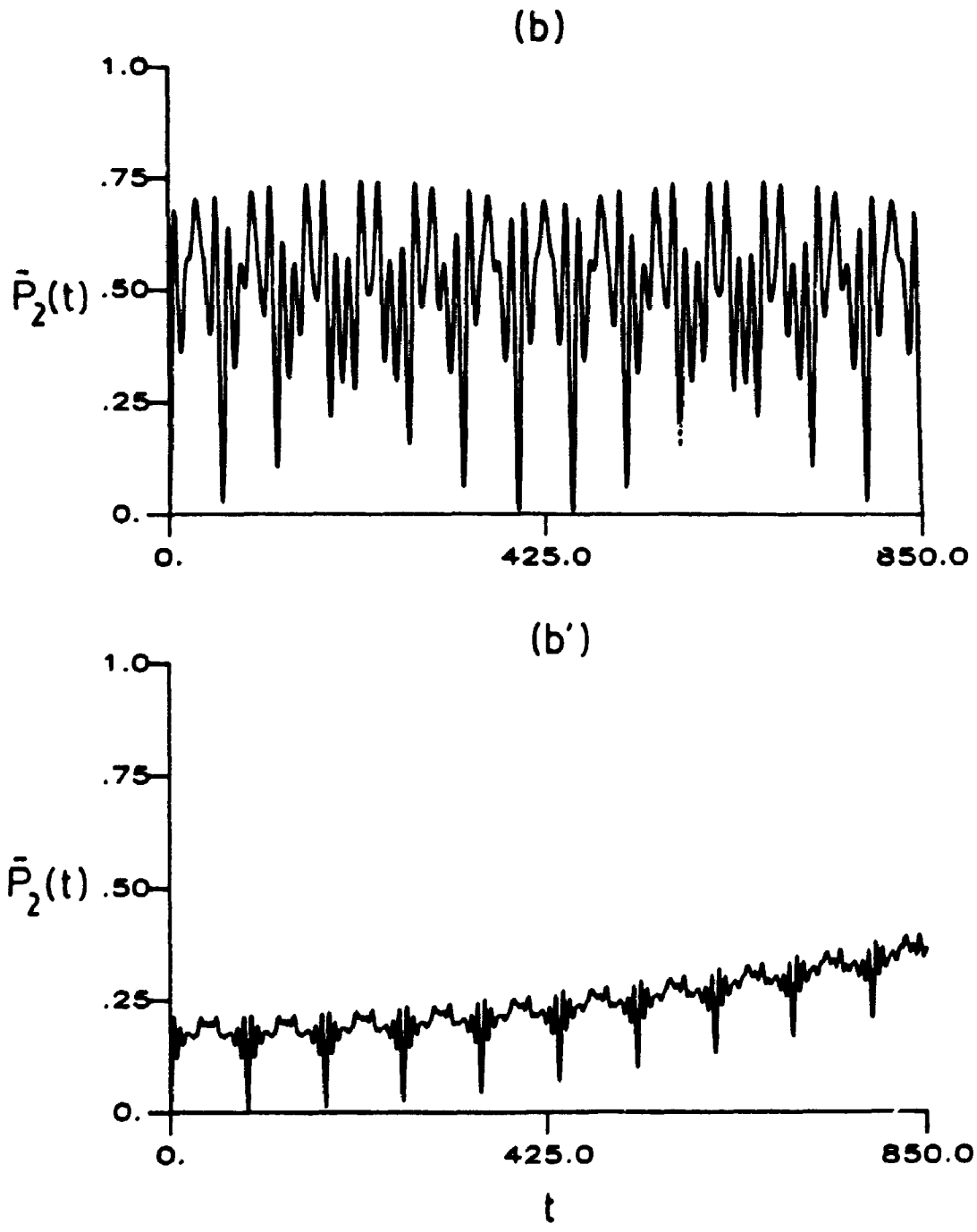

Figure 4.1 continued. Figure 4.1(b,b') illustrates the results of Fig. 4.1(a,a') on a shorter expanded time interval.

The term "period of oscillation" refers to the time required for the excited state to go from zero to maximum population, and back to zero again, with the condition that the absorption/emission pattern over this period then begins to repeat itself. Equation (2.3.9) predicts that at the resonance frequency, the excited state population will undergo smooth oscillations with a period equal to the molecule-EMF coupling period, $2\pi/|C(1)|$. However, as was seen in the examples of Chapter 3, small oscillations with "period" π/ω [32], which are not accounted for in the RWA and which can be attributed to the field frequency and counter-rotating effects, can be superimposed on the large absorption/emission oscillations [32,101-103]. When the counter-rotating effects are significant, the "period of oscillation" can often be better represented by the "beat" period. A beat period is the (minimum) time containing an integer multiple of each of the contributing periods,

$$T_{beat} = m\frac{2\pi}{|C(1)|} = n\frac{\pi}{\omega}. \qquad (4.2.1)$$

T_{beat} represents a common period for both $2\pi/|C(1)|$ and π/ω. From (4.2.1), a beat frequency can be defined as $\omega_{beat} = 2\pi/T_{beat}$, or [104],

$$\omega_{beat} = 2\omega/n = |C(1)|/m, \qquad (4.2.2)$$

where m and n are integers.

The sensitivity of the beat frequency to the ratio between the molecule-EMF coupling and the field frequency is best demonstrated by example. A coupling-to-field frequency ratio such as 4.535 can be resolved into $2m/n = 1814/400$ (i.e. $m = 907$, $n = 400$), whereas a slightly different ratio, say 4.536, corresponds to $2m/n = 1134/250$. The beat frequency in the first case is $\omega/200$, while in the second it

is $\omega/125$; the beat frequency can change significantly for small variations in the molecule-EMF coupling-to-field frequency ratio. Because of the sensitivity of the beat frequency to small changes in the coupling, the beat period determined by (4.2.1) will not be reliable in cases where $|\mathbb{C}(1)| \geq \omega$ since the RWA does not apply rigorously and $|\mathbb{C}(1)|$ is therefore not an accurate representation of the molecule-EMF coupling. The beat period must be determined graphically in the strong coupling case, but this approach is complicated by the fact that the system can appear to be periodic in times much smaller than the beat period. For example, a system with $|\mathbb{C}(1)|/\omega = 4.536$ (beat period = $250\pi/\omega$) can seem to be periodic in $56\pi/\omega$ (since $2m/n = 254/56 \simeq 4.53571$). In cases of strong molecule-EMF coupling, then, the term "beat period" is loosely applied as the time required for the absorption/emission pattern to begin to roughly repeat itself, and this, of course, is not a rigorous definition.

The weak ($|\mathbb{C}(1)| \ll \omega$) versus strong ($|\mathbb{C}(1)| \geq \omega$) molecule-EMF coupling cases (as defined in the RWA, see Sec. 2.3.2) are distinguished by the rate of change of the time-dependent excited state population relative to the field period $2\pi/\omega$. When $|\mathbb{C}(1)| \ll \omega$, the excited state population changes slowly relative to $2\pi/\omega$, but undergoes a full oscillation in $2\pi/|\mathbb{C}(1)|$. The (slight) aperiodicity, due to beating effects, of subsequent full absorptions and emissions is not significant. When $d \neq 0$, and for large field strengths, ω is usually much larger than $|\mathbb{C}(1)|$, because of the general decreasing nature of the Bessel functions in the molecule-EMF coupling as a function of increasing field strength, see Sec. 2.3.2. Hence, the time-dependent excited state population appears to be periodic in $2\pi/|\mathbb{C}(1)|$. When

$|C(1)| \geq \omega$, the excited state population changes rapidly over the field period $2\pi/\omega$, possibly undergoing several aperiodic strong absorption and emission cycles. The oscillations due to the molecule-EMF coupling and the frequency due to the field are both superimposed on an overall oscillation with a period equal to the beat period.

Figures 4.1a and 4.1b versus 4.1a' and 4.1b' contrast the effect of strong versus weak molecule-EMF coupling on the phase-averaged time-dependent evolution of the excited state population. The time interval of Figs. 4.1a and 4.1a' encompasses one molecule-EMF coupling period of the $d \neq 0$ excited state population; from Fig. 4.1a, where $d = 0$, this interval is sufficient time for many strong absorption and emission cycles, which can be divided into roughly five and a half beats. The time scale is expanded in Figs. 4.1b and 4.1b' to show only one beat period of the $d = 0$ excited state population; in this shorter time interval, the population of the $d \neq 0$ excited state population is far from its first maximum.

When $d \approx 0$, the molecule-EMF coupling is very large, and the Rabi period, $2\pi/|\mu_{12}\mathcal{E}^0| \approx 23.6$ (0.571fs), is less than $\pi/\omega \approx 30.4$ (.734fs); the result is the complex dynamics of the excited state population illustrated in Figs. 4.1a and 4.1b. Fig. 4.1b shows the evolution of the excited state over one beat period $28\pi/\omega \approx 850$ (20.6fs); this result for the beat period is not rigorous and represents a minimum beat period. Indeed, from (4.2.2), the ratio $|\mu_{12}\mathcal{E}^0|/\omega \approx 2.57$ is approximately generated by a number of integer ratios: $2m/n = 18/7$, 226/88, 262/102 .... Fig. 4.1b clearly shows that the first ratio listed can be rejected as $t = 7\pi/\omega \approx 212$ (5.14fs) does not correspond to a time where the absorption/emission pattern of $\bar{P}_2(t)$ begins to

repeat itself. On the other hand, in an integer multiple of this time, $t = 28\pi/\omega \simeq 850$ (20.6fs), the absorption/emission pattern does begin to roughly repeat itself, and this time is chosen as the beat period. A numerical study of the excited state population shows that, on average, every $\Delta t \simeq 30.4 = \pi/\omega$ (.734fs), a local minimum or maximum in $P_2(t)$ occurs, beginning at $t = 0$. These critical points correspond to oscillations due to the counter-rotating terms. Oscillations periodic with respect to the Rabi frequency are not apparent in Fig. 4.1b, a reflection of the non-applicability of the RWA and the complexity of the molecule-field interaction. Figs. 4.1a and 4.1b illustrate that the excited state population when $d = 0$ can grow much more quickly than when $d \neq 0$, and can correspond to a time averaged result of 0.5, even when averaged over a short time interval.

When $d \neq 0$, the molecule-EMF coupling and field periods are in reverse order of magnitude than when $d = 0$. In Fig. 4.1a', the emission "spikes" are separated by $\Delta t \simeq 87.8$ (2.12fs), which equals the field period of $2\pi/\omega$; however, a critical point in $P_2(t)$ occurs every π/ω. The overall period $t = 4742$ (114.7fs) corresponds to the molecule-EMF coupling period, approximated in the RWA by (2.3.10). The RWA is not quantitatively applicable for reasons discussed in Sec. 3.4.2, but the qualitative prediction of the RWA for much reduced coupling when $d \neq 0$ accounts for the much longer period than when $d = 0$. The large magnitude of the difference between the two periods is attributable to the closeness of the $d \neq 0$ molecule-EMF coupling to a node. Clearly, a much longer time is required for the $d \neq 0$, relative to the $d \neq 0$, time-averaged transition probability to equal 0.5. From the long resonance period in Fig. 4.1a', the possibility of

monitoring the growth of the excited state population, for $d \neq 0$ versus $d = 0$, with an ultrashort pulse becomes evident.

In the pulsed laser-molecule calculations presented here, the phase is fixed at $\delta = 0$, and it is therefore relevant to consider the effects of phase-averaging on the CW case if the CW and pulsed laser-molecule interactions are to be compared. For weak CW fields, the phase dependence of the time-dependent transition probability is minimal [32,71,105]; the spectra and the temporal populations for the phase-averaged and fixed-phase calculations follow almost identical absorption-emission patterns and the resonance frequencies for the two cases are essentially equal. In such cases, the RWA results, which are phase-independent, are often applicable. For large field strengths, such as the one used in the examples considered here, the fixed-phase and the phase-averaged time-dependent behaviors are very different, especially when $d = 0$ [32,71,105]. The divergence of phase-averaged from fixed-phase results is indicative of the quantitative non-applicability of the RWA.

For direct comparison with the cosine pulsed laser-molecule interactions, the $\delta = 0$ time-dependent excited state populations are required. These results, for $d = 0$ and $d \neq 0$, are given in Sec. 3.4.2. The long-time temporal behaviour of the $\delta = 0$ excited state population is given in Fig. 3.3a and 3.3a', for $d = 0$ and $d \neq 0$, respectively, over $0 \leq t \leq 7000$ (169.3fs); Fig. 3.3b and 3.3b' repeat Fig. 3.3a and 3.3a', respectively, on a shorter, expanded time scale, $0 \leq t \leq 314.2$ (7.60fs), corresponding to the effective duration, $7.6\tau_p$, of the shortest pulse studied here, $\tau_p = 1\text{fs} \approx 41.34$ (see Fig. 4.3). For ease of later comparison of the time-dependent excited state population from

CW versus pulsed laser-molecule interactions, Fig. 3.3b and Fig. 3.3b' are repeated in Fig. 4.2a and 4.2a'.

From Sec. 3.4.2, the $\delta = 0$ time-dependent transition probability for the interaction of the model molecule with a CW laser with $\mathcal{E}^0 \simeq 0.0677$ has a fixed-phase resonance frequency of $\omega = 1.67\Delta E$ for $d = 0$ and $\omega = 0.835\Delta E$ for $d \neq 0$. Recalling that the resonance frequencies in the phase-averaged calculations are $\omega = 1.205\Delta E$ ($d = 0$) and $\omega = 0.8329\Delta E$ ($d \neq 0$), the phase-dependence of the resonance frequency when $d = 0$ emphasizes the non-applicability of the RWA to this case. Conversely, the agreement between the resonance frequency for the phase-averaged and the fixed-phase calculations when $d \neq 0$ is evidence of the weak molecule-EMF coupling due to the presence of permanent dipole moments.

The long-time temporal behavior of the fixed-phase excited state population, shown in Fig. 3.3(a,a'), is distinct from the phase-averaged results of Fig. 4.1(a,a'). For $d = 0$, the excited state population when $\delta = 0$, oscillates between 0.0 and 1.0, while the maximum population of the excited state in the phase-averaged case is less than 0.75, compare Fig. 3.3a and 4.1a, respectively. A study of the $\delta = 0$ time-dependent excited state population to much longer times than shown in Fig. 3.3a indicates the beat period appears to be $492\pi/\omega = 1.08\text{x}10^4$ (261fs). The long time-averaged fixed-phase $d = 0$ excited state population is 0.695; the steady state excited state population can be either less than or greater than 0.5 depending on δ [105]. For $d \neq 0$, a long-time temporal behaviour not unlike that of Fig. 4.1a' occurs for the fixed-phase time-dependent excited state population in Fig. 3.3a', but the $\delta = 0$ overall period, $T_{exact} = 6220$

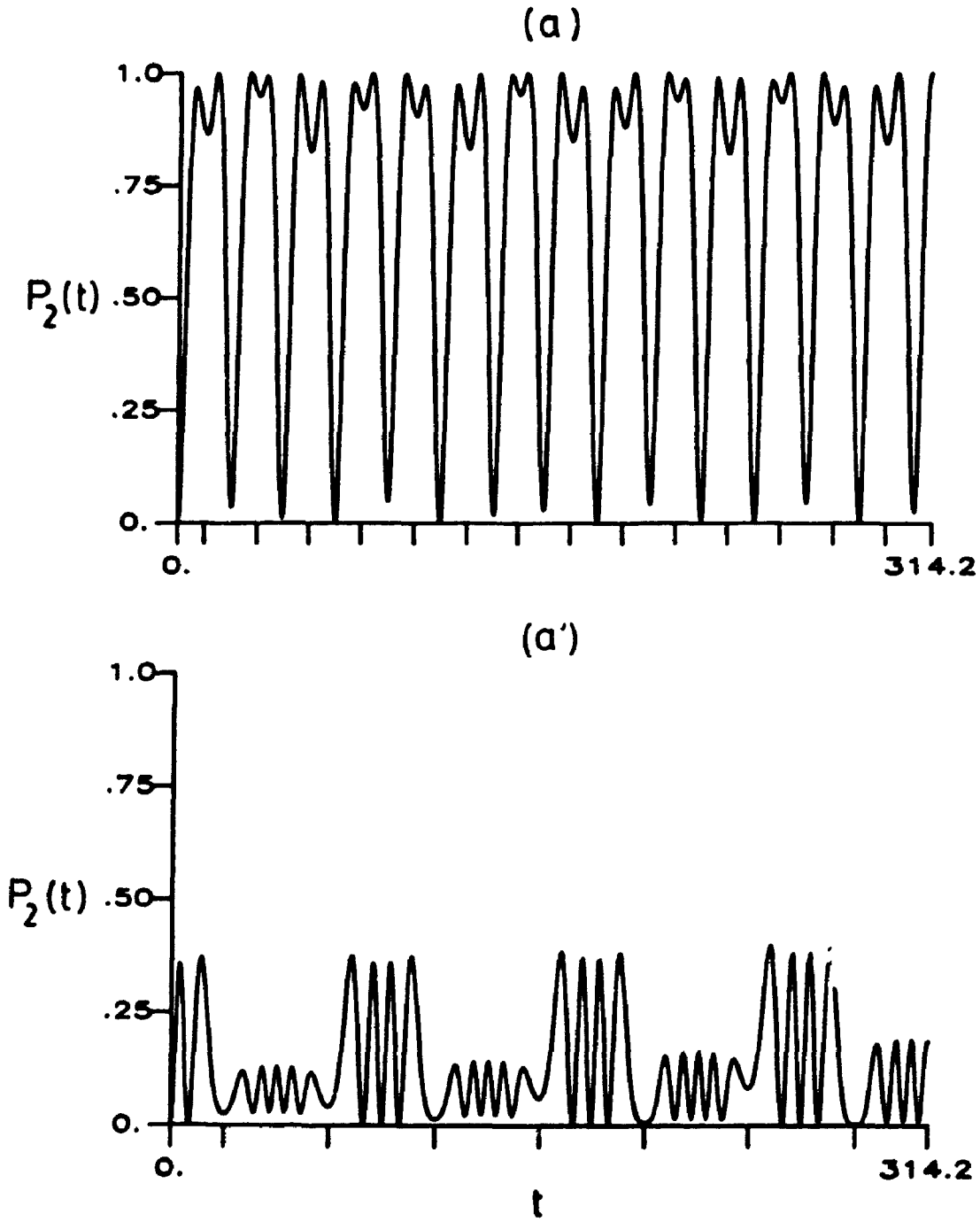

Figure 4.2. Fixed-phase ($\delta = 0$) time-dependent excited state population for the model molecule interacting with a continuous wave laser, at the fixed-phase resonance frequency, versus time, $0 \leq t \leq 314.2$ (7.6fs). The molecular and field parameters are as in Fig. 4.1, except for field frequency. Figure 4.2a, $d = 0$, $\omega = 1.67\Delta E$; Fig. 4.2a', $d \neq 0$, $\omega = 0.835\Delta E$.

(150.5fs), is slightly longer than the phase-averaged analogue, T_{exact} = 4742 (114.7fs); the maximum population of the excited state is 1.0 rather than 0.89; and the superimposed oscillations due to the field period are more intense. The fixed-phase profile also contains a "dip" in the excited state population at the centre of the overall oscillation which is not observed in the phase-averaged results. The $\delta = 0$ long time-averaged excited state population for $d \neq 0$ is $\bar{P}_2(\delta = 0) = 0.517$, showing slight population inversion, while the phase-averaged analogue is $\bar{P}_2 = 0.500$.

When $d = 0$, in the short time span of Fig. 4.2a, the time-dependent excited state has sufficient time to go through 14 cycles of strong absorption and emission, and many of these correspond to full or zero population of the excited state. When $d \neq 0$, the population of the excited state is less than 0.4 for $0 \leq t \leq 314.2$ (7.60fs) (Fig. 4.2a'). This time interval, then, represents only a fraction of the molecule-EMF coupling period. Thus, over the time interval shown in Fig. 4.2, the excited state population for $d = 0$ reaches its maximum many times, while for $d \neq 0$, the population does not have sufficient time to reach maximum population once. This (CW) effect of the small coupling when $d \neq 0$ is also observed when ultrashort pulses interact with the molecular system.

4.2.2. PULSED LASER-MOLECULE INTERACTIONS

For Figs. 4.3 to 4.5, the half-pulse method with the Riemann product integral technique was used to calculate the excited state populations for the interaction of the $d = 0$ and $d \neq 0$ molecule with pulses of increasing duration and a carrier frequency equal to the

respective fixed-phase CW resonance frequency. Using the half-pulse technique, the time-dependent excited state populations were calculated to greater than graphical accuracy using a grid size of $\Delta(t/\tau_p) = 0.001$.

In Fig. 4.3, $\tau_p = 1fs \approx 41.34$. Superposition of Fig. 4.3 on Fig. 4.2 shows that the absorption-emission pattern under the centre of the pulse mimics the CW absorption-emission pattern, although the replication is not perfect. For example, the oscillations are wider in the pulse-molecule interaction. When $d = 0$, Fig. 4.3a, the population of the excited state grows quickly while in the case where $d \neq 0$, Fig. 4.3a', it remains low. This difference can be attributed directly to the long period associated with the small molecule-EMF coupling when $d \neq 0$.

The pulse duration is doubled in Fig. 4.4. More of the absorption/emission pattern of the analogous CW-interaction is revealed, although the reproduction of the CW pattern is clearly not precise. The excited state population when $d \neq 0$ still has insufficient time to reach the maximum of 1.0. In contrast, the excited state population when $d = 0$ oscillates rapidly between 0.0 and 1.0 in the middle of the pulse.

In Fig. 4.5, $\tau_p = 5fs \approx 206.7$, a five-fold increase from its value in Fig. 4.3. When $d = 0$ in Fig. 4.5a, the system undergoes many full CW absorption and emission oscillations during the duration of the pulse. When $d \neq 0$, the excited state finally reaches full population as a function of τ_p, although interestingly, this occurs on the outer edges, rather than at the centre, of the pulse. This unusual behavior can be attributed to the oscillating nature, as a function of field

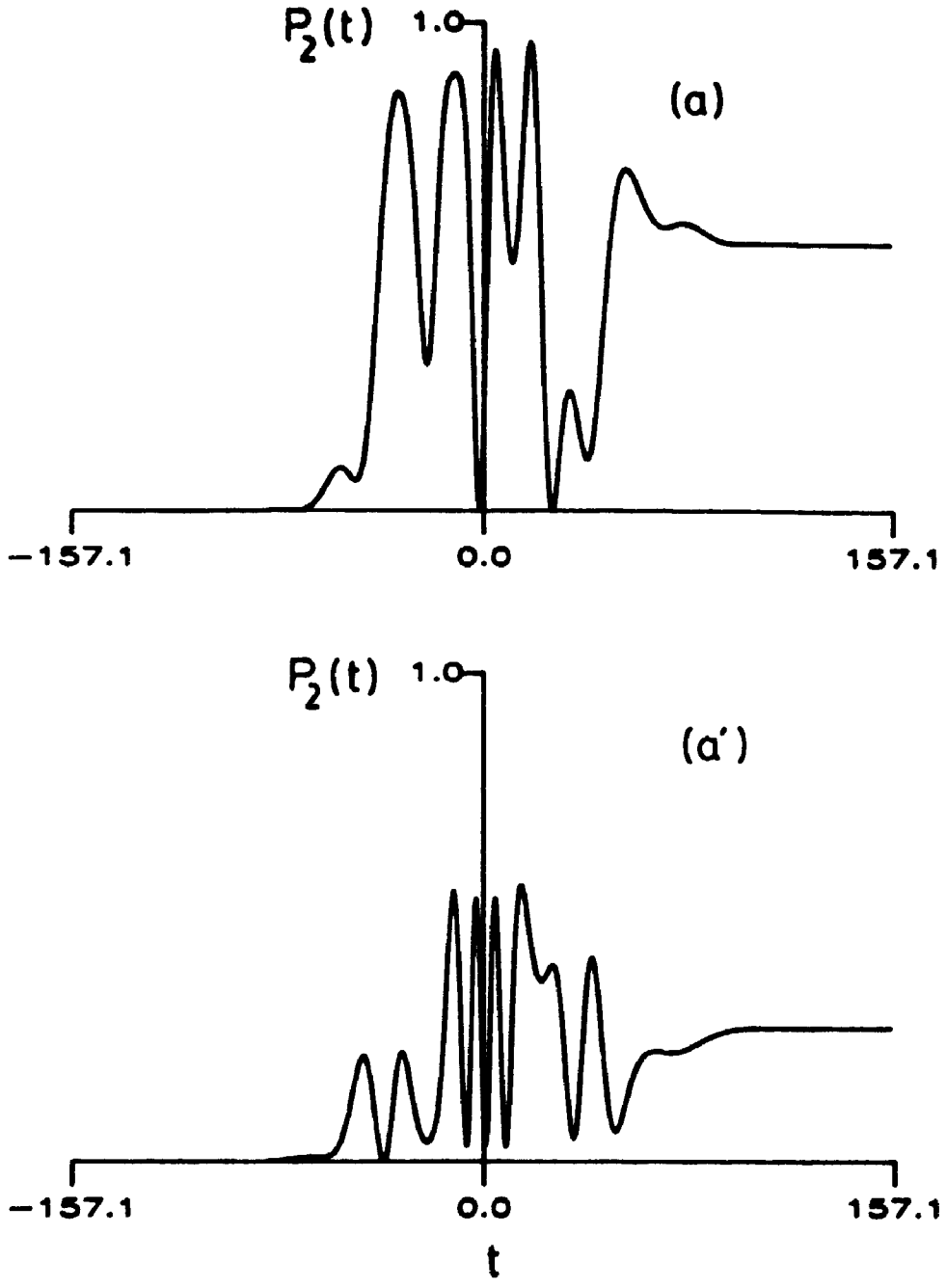

Figure 4.3. Time-dependent excited state population for the model molecule interacting with a pulsed laser, versus time, $|t| \leq 157.1$ (3.80fs). The molecular parameters and field strength are as in Fig. 4.1; pulse phase $\delta = 0$, carrier frequency equals CW($\delta = 0$) resonance frequency, and pulse duration $\tau_p = 1\text{fs} \simeq 41.34$. Figure 4.3a, $d = 0$, $\omega = 1.67\Delta E$; Fig. 4.3a′, $d \neq 0$, $\omega = 0.835\Delta E$.

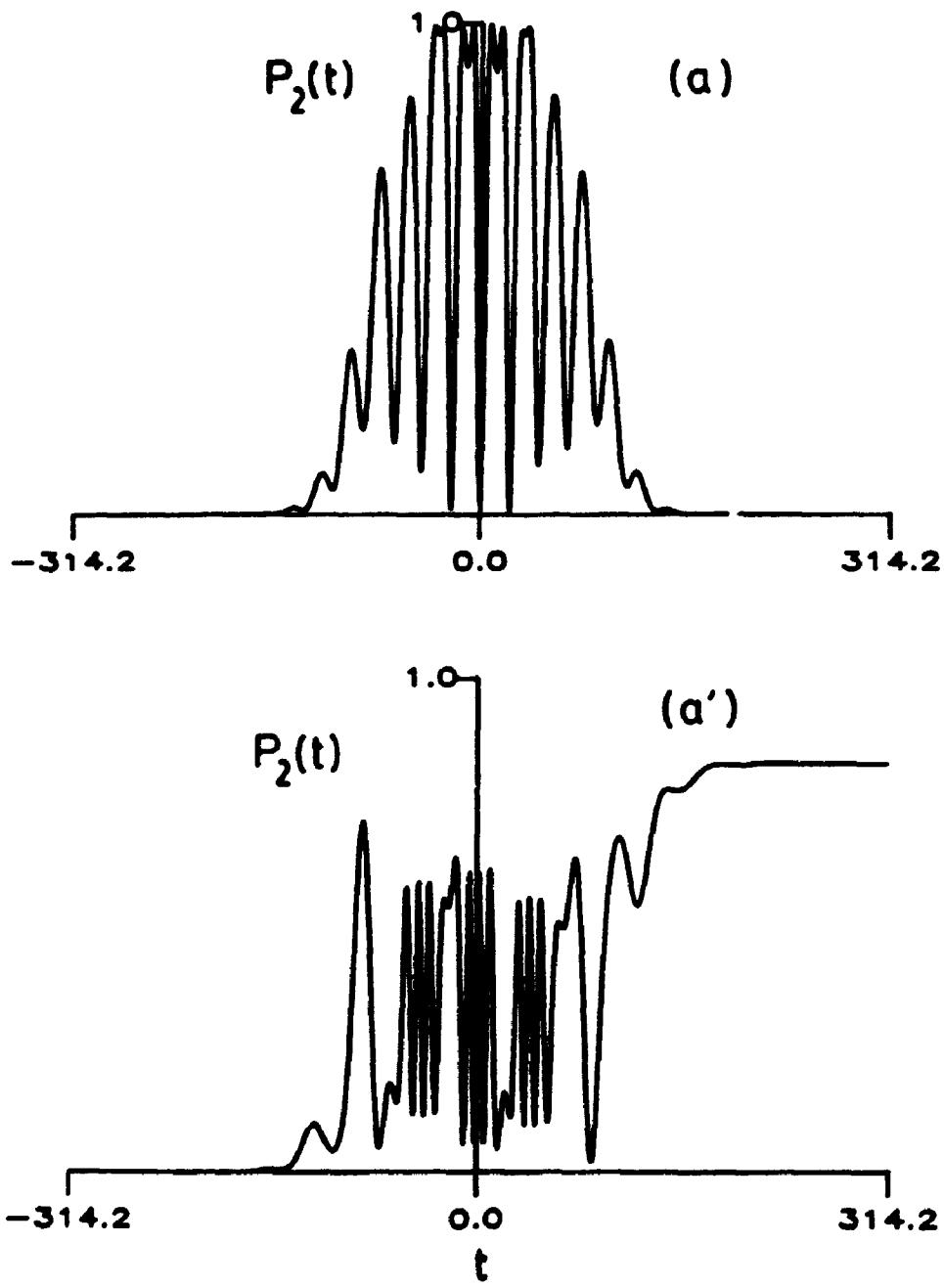

Figure 4.4. Time-dependent excited state population for the model molecule interacting with a pulsed laser, versus time, $|t| \leq 314.2$ (7.60fs). The molecular and field parameters are as in Fig. 4.3, except pulse duration $\tau_p = 2f\pi \approx 81.68$. Figure 4.4a, $d = 0$, $\omega = 1.67\Delta E$; Fig. 4.4a′, $d \neq 0$, $\omega = 0.835\Delta E$.

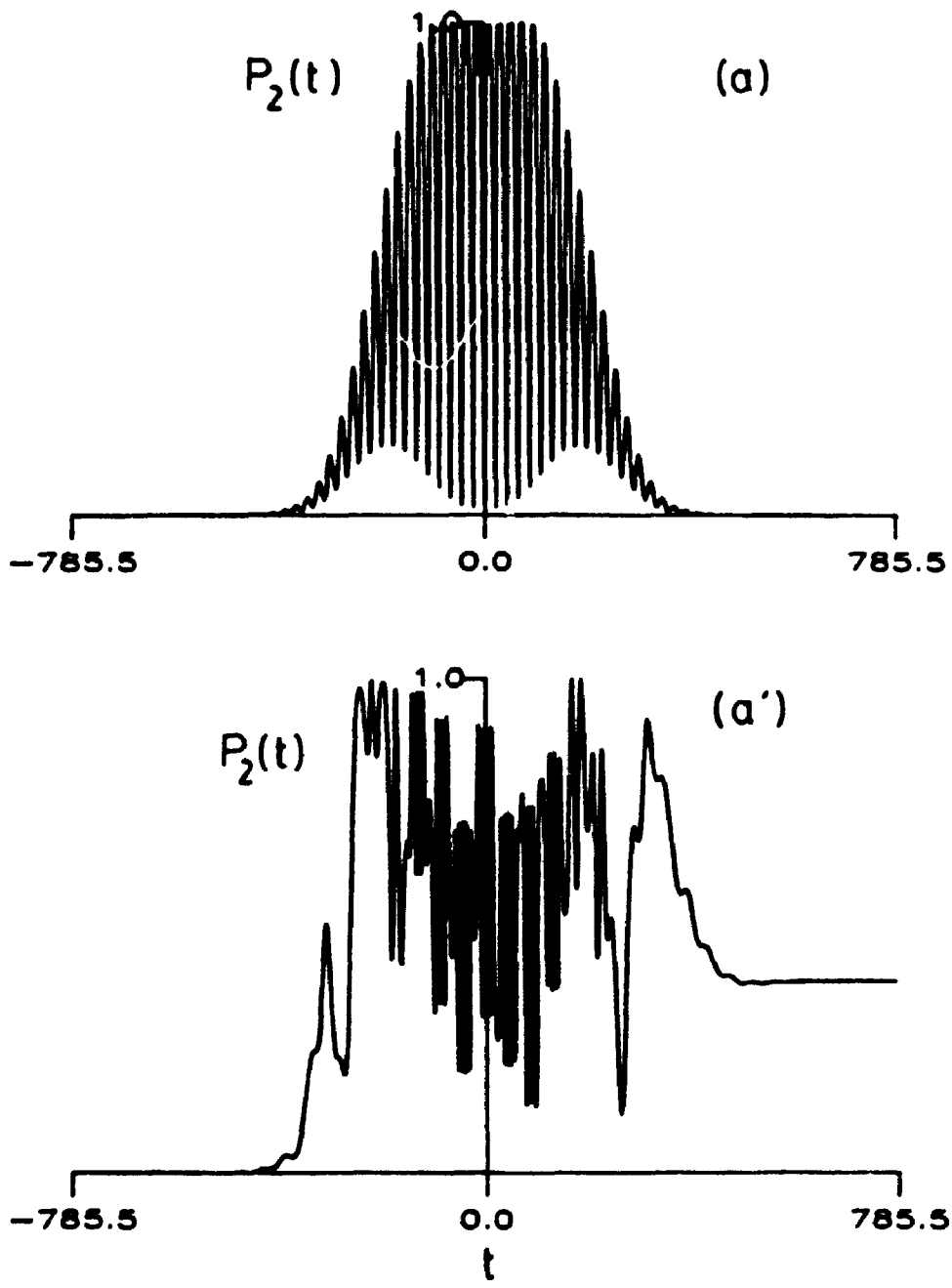

Figure 4.5. Time-dependent excited state population for the model molecule interacting with a pulsed laser versus time, $|t| \leq 785.5$ (19.0fs). The molecular and field parameters are as in Fig. 4.3, except pulse duration $\tau_p = 5fs \approx 2.067x10^2$. Figure 4.5a, $d = 0$, $\omega = 1.67\Delta E$; Fig. 4.5a', $d \neq 0$, $\omega = 0.835\Delta E$.

strength, of the molecule-EMF coupling when d ≠ 0. The envelope of the pulse modifies the effective field strength. Thus while the centre of the pulse may have a field strength which produces near nodal molecule-EMF CW coupling, the smaller field strengths of the wings of the pulse may actually produce greater molecule-EMF coupling.

The absorption/emission patterns under the center of the pulses of Figs. 4.3-4.5 do not precisely mirror the fixed-phase CW spectra of Fig. 4.2. For weaker field strengths, it has been shown [21,22] that a pulse-molecule interaction corresponds to the chopping or cutting off of the analogous CW-molecule interaction, and that as pulse duration increases, more of the temporal behavior associated with the CW-molecule interaction is revealed. However, unlike these previous applications with weaker field strengths and longer pulse durations, for the strong fields investigated here, there are discrepancies between Figs. 4.3 - 4.5 and Fig. 4.2, which can be attributed to a number of causes. Firstly, pulses of very short duration have large bandwidths and hence many frequencies in addition to the carrier frequency may well be inducing transitions. Secondly, the CW resonance frequency depends on the field strength, with large positive or negative Bloch-Siegert shifts occurring for very intense fields. Since the field amplitude is not constant over the duration of the pulse, the resonance frequency will change as a function of time. Thirdly, unlike the earlier work, the field intensity used here is very large. Substantial transitions are occurring under the wings of the pulses. The excited state is likely somewhat populated when the CW pattern begins under the centre of the pulse whereas the initial conditions of all the CW calculations assumed zero population of the excited state.

Finally, when d = 0, the molecule-pulse coupling can only increase (decrease) as the effective field strength $\mathcal{E}^0\exp[-t^2/\tau_p^2]$ increases (decreases). When d ≠ 0, the coupling may in fact decrease (increase) with increasing (decreasing) effective field strength because of the oscillatory nature of the molecule-EMF coupling as a function of field strength. Consequently, transitions under the pulse wings can be stronger than those under the centre of the pulse. This behavior is nicely demonstrated by Fig. 4.5a'.

Comparison of Figs. 4.3 - 4.5 illustrates the dependence of the final value of the excited state population, after the pulsed laser-molecule interaction has eased, on the pulse duration. When d = 0, for all the pulse durations shown, and when d ≠ 0 for τ_p = 5fs, the pulse-molecule interaction induces rapid oscillations in the excited state population between 0.0 and 1.0. In general [21,22], the "steady state" excited state population can take any value between 0.0 and 1.0, depending on how the pulse "chops off" the CW-like interaction under the centre of the pulse. When d ≠ 0, the slow change in the excited state population places limits on its final value. For sufficiently short pulses, as in Figs. 3b and 4b, the steady state value of the excited state population must be less than unity, since there has been insufficient time for the excited state to become fully populated during the pulsed laser-molecule interaction time. The effects of d ≠ 0 on molecule-EMF couplings can therefore be sampled by employing pulses of sufficiently short durations.

4.3. SOME GENERAL COMMENTS

The investigation of the resonance temporal behaviour of the

excited state, as a function of pulse duration, illustrates how ultra-short to short pulses can be used to monitor the effects of $d \neq 0$ on the molecule-EMF coupling and on the dynamics associated with the time evolution of the excited state produced by laser-molecule interactions. The (CW) RWA analytical result for the molecule-EMF coupling plays an important role in predicting and interpreting the effects of $d \neq 0$, versus $d = 0$, on the exact temporal evolution of the excited state in the examples of pulsed laser-molecule interactions in Sec. 4.2. The half-pulse technique, developed in Sec. 4.1, provides a cost-efficient means of calculating the time-dependent excited state populations for pulsed laser-molecule interactions.

The field strength of the examples discussed here does not generate the smallest $d \neq 0$ molecule-EMF coupling. A field strength of $\mathcal{E}^0 = 9.2\Delta E/\underline{d}\cdot\hat{e} \simeq 0.0670$ yields a resonance period of $\simeq 2\times10^5$ ($\simeq$5ps) versus that of 4742 (114.7fs) shown in Fig. 4.1a'. In principle, then, pulses of considerably longer duration than those used in Sec. 4.2.2 could be employed to probe the effects of $d \neq 0$. Furthermore, from the RWA result for the molecule-EMF coupling (2.3.10), minima in the $d \neq 0$ molecule-EMF coupling are expected for arguments $z = \underline{d}\cdot\hat{e}\mathcal{E}^0/\Delta E$ less than 9.2. For example, the RWA predicts the coupling for a one-photon transition will be very small for $z \simeq 3.8$. Exact calculations for the interaction of the two-level model molecule used in the examples of Chapters 3 and 4 with a CW field indicate that the molecule-EMF coupling passes through a node around $z = \underline{d}\cdot\hat{e}\mathcal{E}^0/\Delta E \simeq 2.5$; when ΔE is replaced with the exact resonance frequency, the node occurs around $\underline{d}\cdot\hat{e}\mathcal{E}^0/\omega_r \simeq 3.0$. Thus, minima in the molecule-EMF coupling occur with field strengths more than three times weaker than the one used in the

examples of Sec. 4.2.

The examples of Secs. 3.4.2 and 4.2 exploit the dependence of the RWA $d \neq 0$ molecule-EMF coupling, (2.3.10), for the one-photon transition, on the function $J_1(\underline{d}\cdot\hat{e}\mathcal{E}^0/\omega)$. Consequently, a large field strength was employed to enhance the effects of permanent dipoles. An alternative means of investigating the effects of $d \neq 0$ is to study multi-photon transitions. In Chapter 5, this latter approach is adopted by investigating the interaction of a permanent dipole molecule with two CW electric fields, where a combination of the field frequencies is required to establish an RWA resonance condition. In Chapter 6, the effect of $d \neq 0$ versus $d = 0$ on one- and multi-photon transitions are considered for a set of many-level systems interacting with one or two CW electric fields, where d is the difference in the permanent dipole moments of the two states directly involved in a transition.

CHAPTER 5

TWO-COLOUR SPECTROSCOPY

The closed-form analytical results for the single- and multi-photon temporal transition probabilities and resonance profiles, obtained in the two-level RWA, have played an important interpretive and predictive role with respect to the effects of $d \neq 0$ for the single CW laser problem [2,3,24-27,29-31,34,36,71]. Part of the purpose of this chapter is to derive and illustrate the usefulness of the analogous RWA result for the interaction of a two-level molecule with two CW lasers.

The interaction of a two-level system with two continuous wave lasers has been studied, in the absence of permanent moments, for the cases where both frequencies are tuned close to the energy level separation [106,107]; see also [108]. The effects of $d \neq 0$ on two-colour absorption processes, with particular emphasis on transition rates, have been discussed using both perturbative [1b,42,58a] and non-perturbative approaches [43-45]. The special limit where one frequency is extremely small while the other is close to the energy level separation has been considered [42-45], and, in particular, Band *et al.* [42,44] find the transition rate can be significantly enhanced in such situations.

It is clear from previous work, and what follows, that, as in the

one CW laser problem, the effects of $d \neq 0$ for two-colour absorption processes in two-level systems, relative to the $d = 0$ problem, are pronounced. The presence of permanent dipoles allows a variety of multi-photon resonances to occur, that would otherwise be forbidden. The resonances can be selectively enhanced by the appropriate choice of the parameters characterizing the two CW lasers. The two-colour RWA results given here are very useful in helping to select optimum parameters for this purpose.

Section 5.1 contains the derivation of the RWA results for the time-dependent populations of the molecular states and for the resonance profiles associated with the interaction of a two-level system, with permanent dipoles, with two continuous wave lasers of different frequencies (colours). In the derivation of the two-field RWA, it is found that each term in the interaction Hamiltonian can be designated as either a resonance or a counter-rotating term. Competing resonances can occur when more than one combination of the same set of frequencies of the two applied fields lead to a resonance; this type of effect is not seen in the one-field problem. When one of the possible competing resonances dominates, closed-form analytical solutions for the resonance profiles, and for the time-dependent populations of the molecular states, can be obtained in the dominant-resonance RWA (DR-RWA). When there are at least two significant competing resonances, but the counter-rotating terms are unimportant, numerical calculations for the resonance profiles and temporal populations can be carried out using the Hamiltonian operator for the many-resonance RWA (MR-RWA). Closed-form analytical solutions are generally not available in the MR-RWA. Comparisons of results obtained in the DR-RWA, MR-RWA

and by using the exact Hamiltonian for the two-colour, two-level problem can be used to distinguish between the effects of competing resonances and counter-rotating terms. Section 5.1 also contains a general discussion of the conditions of the applicability of the DR-RWA; these are considerably more complicated than those for the one-colour RWA for a two-level system. The analytical solution of the molecule-EMF coupling, in the DR-RWA, can be used to estimate the field strengths and/or ratio of the applied EMF frequencies that selectively enhance a particular multi-photon, two-colour transition.

Section 5.2 gives a discussion of the Floquet techniques [3,14,33,104,108] used for the MR-RWA and exact calculations, while Sec. 5.3 contains several examples of multi-photon, two-colour, two-level resonance profiles calculated in the DR-RWA, MR-RWA, and by using the exact Hamiltonian. These examples are used to further discuss the validity of the DR-RWA and the MR-RWA as a function of the field parameters, and to illustrate the interpretive and predictive nature of the two-colour RWA results. Section 5.4 contains some general comments.

5.1. TWO-COLOUR RWA RESULTS

Although excited state decay is neglected here, the derivation of the two-colour RWA results parallels that given in Sec. 3.1 for a single continuous wave laser interacting with a molecule with non-zero excited state decay. Section 5.1.1 contains the derivation of the two-colour RWA results, while a discussion of the conditions on the applicability of the RWA results in given in Sec. 5.1.2.

5.1.1. DERIVATION OF TWO-COLOUR RWA SOLUTIONS

For two continuous wave electric fields of different frequencies, the total electric field is given by (2.1.14). Substitution of (2.1.14) into (2.1.20) gives the time-dependent wave equation in the Schrödinger representation. As detailed in Chapter 3, Sec. 3.1, the resonances in the transition probabilities can be located by transforming (2.1.20) into an interaction representation. For a two-level system interacting with two fields, this transformation is defined by,

$$a_j = b_j \exp\left(\frac{i}{2}(-1)^{j+1}[\Delta E t - \underline{d}\cdot\int^t (\underline{\mathcal{E}}_1(t') + \underline{\mathcal{E}}_2(t'))dt']\right). \qquad (5.1.1)$$

The time-dependent coefficients $\underline{b}(t)$ satisfy,

$$i\frac{d}{dt}\underline{b}(t) = \underline{\underline{H}}(t)\underline{b}(t) \qquad (5.1.2)$$

where $H_{11} = H_{22} = 0$, and the off-diagonal elements of the Hamiltonian, which are reduced using the Bessel function identities (3.1.4) and (3.1.5), are given by,

$$H_{12} = H_{21}^{*} = -\sum_{j=-\infty}^{\infty}\sum_{k=-\infty}^{\infty} \exp[-i(\Delta E - k\omega_1 - j\omega_2)t]$$

$$\times J_k(z_1)J_j(z_2)[k\underline{\mu}_{12}\cdot\hat{e}_1\mathcal{E}_1^0/z_1 + j\underline{\mu}_{12}\cdot\hat{e}_2\mathcal{E}_2^0/z_2]$$

$$\times \exp[-i(z_1\sin\delta_1 + z_2\sin\delta_2)]\exp[i(k\delta_1 + j\delta_2)], \qquad (5.1.3)$$

where $z_j = (\underline{d}\cdot\hat{e}_j\mathcal{E}_j^0/\omega_j)$. This result is still exact and does not allow a closed form analytical expression to be derived for $b_j(t)$.

The off-diagonal Hamiltonian contains two kinds of terms: resonance terms, for a given pair of frequencies, have $\Delta E - k\omega_1 - j\omega_2 = 0$; counter-rotating terms, for the same pair of

frequencies, have $\Delta E - k\omega_1 - j\omega_2 \neq 0$. Analogous to the one-field case, see for example, Sec. 3.1 and [2], the rotating wave approximation can be used to eliminate counter-rotating terms in H_{12}. However, in contrast to the one-field case, the two-field off-diagonal Hamiltonian permits more than one multiphoton transition with the same set of applied frequencies, since the resonance condition,

$$\Delta E = N_1\omega_1 + N_2\omega_2, \tag{5.1.4}$$

where N_1 and N_2 are integers, can be satisfied by a number of (N_1,N_2)-combinations, where either N_1 or N_2 can be positive, negative, or one of them zero. Thus, for a given resonance set of frequencies, H_{12} contains not only counter-rotating terms, of the form $\exp[i\eta t]$, $\eta \neq 0$, but also competing resonance terms, of the form $\exp[i0t]$. The counter-rotating terms can be eliminated first by neglecting all terms in the double sum which do not reduce to the form $\exp[i0t]$ on resonance, giving the many-resonance RWA (MR-RWA) off-diagonal Hamiltonian,

$$H_{12} = -\frac{1}{2} \sum_{N_1,N_2} C(N_1,N_2)\exp[-i(\Delta E - N_1\omega_1 - N_2\omega_2)t\ ]$$

$$X\ \exp[-i(z_1\sin\delta_1 + z_2\sin\delta_2 - N_1\delta_1 - N_2\delta_2)]. \tag{5.1.5}$$

The sum is over all sets of integers (N_1,N_2) such that (5.1.4) is obeyed. $C(N_1,N_2)$ is the two-field RWA molecule-EMF coupling for the (N_1,N_2)-photon transition,

$$C(N_1,N_2) = 2J_{N_1}(z_1)J_{N_2}(z_2)\left(N_1\omega_1\left(\frac{\underline{\mu}_{12}\cdot\hat{e}_1}{\underline{d}\cdot\hat{e}_1}\right) + N_2\omega_2\left(\frac{\underline{\mu}_{12}\cdot\hat{e}_2}{\underline{d}\cdot\hat{e}_2}\right)\right). \tag{5.1.6}$$

In the limit that $d \to 0$, $C(N_1,N_2)$ is non-zero only when $(N_1,N_2) = (0,1)$ or $(1,0)$. The resulting molecule-EMF coupling is equal to the Rabi

coupling, (2.3.14); explicitly, $C(0,1)\big|_{d=0} = \underline{\mu}_{12}\cdot\hat{e}_2\mathcal{E}_2^0$ for $\omega_2 \simeq \Delta E$ and $C(1,0)\big|_{d=0} = \underline{\mu}_{12}\cdot\hat{e}_1\mathcal{E}_1^0$ for $\omega_1 \simeq \Delta E$.

Unlike in the one-field analogue [2], the approximation leading to (5.1.5) still does not permit a closed form solution to be obtained for the coefficients $b_j(t)$. When only one resonance term, i.e. one (N_1,N_2) combination, dominates the other resonance terms in (5.1.5), the corresponding Schrödinger equation (5.1.2) can be solved analytically. Following an analogous procedure to that given in Sec. 3.1, the expression for the time-dependent population of excited state 2, subject to the initial conditions $b_1(0) = 1$, $b_2(0) = 0$, is,

$$P_2(t)^{(N_1,N_2)} = |b_2(t)|^2$$
$$= 2\bar{P}_2^{(N_1,N_2)} \sin^2\left(\tfrac{1}{2}[|C(N_1,N_2)|^2 + (\Delta E - N_1\omega_1 - N_2\omega_2)^2]^{1/2}t\right), \tag{5.1.7}$$

where, from (2.1.12), $\bar{P}_2^{(N_1,N_2)}$ is the long time average of $P_2^{(N_1,N_2)}(t)$, and corresponds to the steady state excited state population, given by,

$$\bar{P}_2^{(N_1,N_2)} = \frac{|C(N_1,N_2)|^2}{2\left[(\Delta E - N_1\omega_1 - N_2\omega_2)^2 + |C(N_1,N_2)|^2\right]} . \tag{5.1.8}$$

This equation has the same form as the one-field result, with $N\omega$ and $|C(N)|$ in (2.3.17) replaced with $(N_1\omega_1 + N_2\omega_2)$ and $|C(N_1,N_2)|$, respectively. $\bar{P}_2^{(N_1,N_2)}$, as a function of ω_1 and ω_2, is the (N_1,N_2)-photon absorption spectrum or resonance profile for the two-level system in the dominant-resonance RWA (DR-RWA). In all the examples presented here, the absorption spectra are generated by keeping one frequency constant while varying the other. From (5.1.6), the coupling is a function of frequency; this frequency dependence can lead to asymmetric spectra about the resonance frequency. When

$C(N_1,N_2)$ is approximately constant over a resonance profile, the profile has a full width at half maximum of,

$$FWHM(N_1,N_2) = 2|C(N_1,N_2)|_{res}/N_p, \tag{5.1.9}$$

where ω_p is the frequency being varied and $|C(N_1,N_2)|_{res}$ is evaluated using (5.1.6) at the resonance value of ω_p. From (5.1.7), the resonance period of the time-dependent excited state population is,

$$T^{res}_{RWA}(N_1,N_2) = 2\pi/|C(N_1,N_2)|_{res}. \tag{5.1.10}$$

In what follows, unless stated otherwise, the molecule-EMF couplings will be taken to be at the resonance value for ω_p for fixed ω_q.

5.1.2. CONDITIONS FOR THE APPLICABILITY OF THE TWO COLOUR RWA

The validity of the elimination of counter-rotating terms depends on the molecule-EMF couplings for the transition of interest and on the relationship between the two field frequencies. In the one-field problem without [14,18,19] and with [2,3,25,26,34] permanent dipoles, at the resonance frequency, the counter-rotating terms are all of the form $\exp[ik\omega t]$, $k=\pm1,2,3....$ Thus, the longest possible period of a counter-rotating term is $2\pi/\omega$. A condition of applicability of the RWA in the one-field case is $2\pi/|C(N)| \gg 2\pi/\omega$, see (2.3.21). This constraint ensures that the counter-rotating terms average to zero over the resonance period of the time-dependent excited state population. The analogous two-field rule of thumb for the DR-RWA is similar, except the frequency restriction is determined by integer multiples of the beat frequency [109] between the two field frequencies ω_1 and ω_2.

As in Sec. 4.2.1, the beat frequency can be determined from the beat period, where the latter must contain integer multiples of the

constituent periods [104]. However, the beat frequency between the two applied field frequencies ω_1 and ω_2 is distinct from the beat frequency defined in Chapter 4: the beat frequency here is exact, and is related to the periodicity of the Hamiltonian; the beat frequency in Chapter 4 is an approximation, because the RWA molecule-EMF coupling $|C(N)|$ is not exact, and the beat frequency is related to the periodicity of the time-dependent state populations. The two-field analogue to the beat frequency of Chapter 4 would be an overall beat frequency between the frequencies of the two fields, and, from (5.1.10), the RWA frequency $|C(N_1,N_2)|$.

The two-field Hamiltonian is periodic in $2\pi/\omega_b$ if this period contains an integer multiple m_1 of the period of field one, $2\pi/\omega_1$, and an integer multiple m_2 of the period of field two, $2\pi/\omega_2$. Thus, the beat frequency between the field frequencies can be defined as [104],

$$\omega_b \equiv \omega_1/m_1 = \omega_2/m_2. \qquad (5.1.11)$$

The numbers m_1 and m_2 are the lowest possible integers giving the frequency ratio ω_1/ω_2.

Beating between the two field frequencies can lead to counter-rotating terms of the form $\exp[\pm i\nu t]$ where ν can be less than the smaller of the two frequencies of the applied EMFs. Such terms will have long periods and may not average to zero over the resonance period of the excited state population. The longest period of a counter-rotating term corresponds to the smallest value of ν. From (5.1.3), the counter-rotating terms for the (N_1,N_2)-photon transition oscillate at frequencies,

$$\nu = |\Delta E - k\omega_1 - j\omega_2| = |N_1\omega_1 + N_2\omega_2 - k\omega_1 - j\omega_2|$$

$$= |(N_1 - k)m_1 + (N_2 - j)m_2|(\omega_1/m_1) \neq 0, \qquad (5.1.12)$$

where in the first line ΔE has been replaced with (5.1.4) and ω_2 has been replaced with $m_2\omega_1/m_1$ from (5.1.11). Since $\mathcal{K} = |(N_1 - k)m_1 + (N_2 - j)m_2|$ is an integer, all counter-rotating terms oscillate at an integer multiple of the beat frequency ω_1/m_1. The numbers j and k can take on any integer value from $-\infty < j,k < \infty$, so $\mathcal{K}$ is minimized when $\mathcal{K} = 1$. Thus, the two-field rule arising from the condition that counter-rotating terms must oscillate many times within the period of the excited state population is $2\pi/|C(N_1,N_2)| \gg 2\pi m_1/\omega_1$, or,

$$|C(N_1,N_2)| \ll \omega_1/m_1. \qquad (5.1.13)$$

In comparison with the one-field analogue, given by (2.3.21), the two-field condition, (5.1.13), is the more restrictive of the two since it depends upon the beat frequency, which can be much less than the smaller frequency of the two applied fields.

The magnitudes of the counter-rotating terms are affected by the damped sinusoidal nature of the Bessel functions modifying each term, as a function of increasing argument for a given order, or as a function of increasing order for a given argument. Relative to the dominant resonance term, the magnitude of a counter-rotating term can be reduced by its Bessel function product since Bessel functions are, in general, decreasing functions of increasing order [81,85].

In certain cases, the constraint (5.1.13) for the applicability of the DR-RWA can be relaxed because of the decreasing magnitude of Bessel

functions with increasing order. For example, if the (N_1,N_2) dominant resonance is generated by frequencies ω_1 and ω_2 such that m_2 is large relative to m_1, or both m_2 and m_1 are large (ω_1 and ω_2 are highly incommensurate), the counter-rotating terms of the form $\exp[\pm i\omega_1 t/m_1]$ will be modified by a Bessel function product $J_k(z_1)J_j(z_2)$ where k and/or j are very large. Consequently, these counter-rotating terms will be insignificant. As an illustration, the (2,1) resonance produced by $\omega_2 = 0.999752\Delta E$ and $\omega_1 = 0.000124\Delta E$ has $m_2 = 249938$ and $m_1 = 31$. From (5.1.12), the counter-rotating terms with the minimum frequency $\nu = \omega_1/m_1$ are $J_{-16123}(z_1)J_3(z_2)\exp[i\omega_1 t/31]$ and $J_{16127}(z_1)J_{-1}(z_2)\exp[-i\omega_1 t/31]$, which are negligible due to the large orders of the $J_k(z_1)$ terms. In such cases, the important counter-rotating terms to consider are often those with Bessel functions with orders k and j small relative to N_1 and N_2; these terms oscillate at frequencies $\nu = K\omega_1/m_1$, where $K > 1$, and ν is greater than the beat frequency. The constraint (5.1.13) can therefore be relaxed to $|C(N_1,N_2)| \ll K\omega_1/m_1$. For the example above, the numerically important counter-rotating terms are probably $J_3(z_1)J_1(z_2)\exp[i\omega_1 t]$ and $J_1(z_1)J_1(z_2)\exp[-i\omega_1 t]$, which are associated with the adjacent (3,1)- and (1,1)-photon transitions, respectively. Indeed, when $\omega_2 \gg \omega_1$, the (N_1,N_2) resonance will often be affected only by the counter-rotating terms associated with the adjacent $(N_1\pm1,N_2)$ resonances. Here, the constraint (5.1.13) reduces to $|C(N_1,N_2)| \ll \omega_1$, which is similar in structure to the one-field condition. The discussion above indicates that (5.1.13) represents the strictest constraint, arising from the counter-rotating terms, on the molecule-EMF couplings for which the RWA is valid.

A second condition of applicability of the DR-RWA requires that the width of the spectral peak of interest is much less than the frequency spread to adjacent peaks that are associated with significant resonances. In the one-field RWA, with permanent dipoles [2,3], the N-photon resonance, with FWHM(N) = $2|C(N)|/N$, is separated from the (N+1)-photon resonance, the closest peak, by $\Delta\omega = \Delta E/N(N+1)$. The condition for the validity of the RWA corresponding to the absence of overlap between adjacent resonances is then $2|C(N)| \ll N\omega/(N+1)$ where $\omega \approx \Delta E/N$. In the two-field problem, the derivation of an analogous mathematical condition is complicated by the fact that different combinations of frequencies can lead to a variety of adjacent resonances. Furthermore, the (N_1',N_2')-photon resonance that is adjacent to the (N_1,N_2)-photon resonance as a function of ω_1 is distinct from the (N_1'',N_2'')-photon resonance that is adjacent to the (N_1,N_2)-photon resonance as a function of ω_2. Since variations in either frequency can lead to new resonances, the frequency separations between important neighbouring resonances should be checked with respect to (independent) changes in each frequency. In general, for the DR-RWA to be applicable to the (N_1,N_2)-photon transition, its FWHM must be much less than the frequency spread to the nearest significant resonance transitions. Generally, condition (5.1.13) provides a very useful criterion for the applicability of the DR-RWA.

The applicability of analytical solutions using the DR-RWA is restricted by competing resonant transitions, for a given pair of frequencies, between sets of (N_1,N_2) which obey (5.1.4). The analysis of the counter-rotating terms, see above, assumes there is one dominant resonance coupling per frequency combination. When more than one of

these superimposed resonances is strong, the competing resonances perturb one another and, in general, an analytical solution cannot be found [106]. However, in some cases, the counter-rotating terms can still be eliminated and the MR-RWA can be applied. Since no easily applicable expressions exist for the resonance period or FWHM in these cases, the validity of the MR-RWA must in practice be investigated numerically from (5.1.5), and the results compared with those of exact calculations based on (5.1.3). While there is no computational advantage to using the MR-RWA instead of the exact Hamiltonian, comparisons of the two results (and a DR-RWA result if applicable) can lead to the differentiation between the effects of counter-rotating terms and those of competing resonances, as defined in the context of the RWA (see, for example, some of the discussion related to Figs. 5.3 and 5.4 in Sec 5.3).

In general, many of the higher order transitions (large values of N_1 and/or N_2) can be neglected in (5.1.5) because the greater the number of photons involved, the weaker the coupling. The net number of photons involved in each of the superimposed transitions is given by $|N_1| + |N_2|$ for each resonant set of (N_1,N_2). This trend favouring lower order transitions is a consequence, again, of the overall decreasing nature of the Bessel functions with increasing order. For example, when $m_1 = 2$ and $m_2 = 9$, the coupling $C(1,1) \propto J_1(z_1)J_1(z_2)$ is usually much larger than the competing resonance coupling $C(-8,3) \propto J_{-8}(z_1)J_3(z_2)$. Exceptions can occur, where higher order transitions are stronger than lower order ones due to the oscillating nature of Bessel functions as a function of their arguments. For example, at $z_1 = 7.0$ and $z_2 = 3.1$, $|J_{-8}(z_1)J_3(z_2)| > |J_1(z_1)J_1(z_2)|$,

since $J_1(3.1)$ is past its maximum while $J_3(3.1)$ is increasing in magnitude with respect to increasing argument, and $J_1(7.0)$ is close to a node while $J_8(7.0)$ is not.

The neglect of counter-rotating and competing resonance terms will lead to some differences between the predicted DR-RWA spectra and the exact spectra based on the full Hamiltonian, (5.1.3), in (5.1.2). In the one-field case, counter-rotating terms can cause Bloch-Siegert shifts [2,3,26,28,34], in the value of the resonance frequency from the one-field RWA prediction of $\omega = \Delta E/N$. Counter-rotating terms can also be responsible for a significant non-zero background in resonance profiles for off-resonance frequencies [2,3,26,34].

Bloch-Siegert shifts and non-zero off-resonance backgrounds are also observed in the two-field case. The effects of competing resonances (including the dominant one) on each other can also result in resonance frequency shifts from the DR-RWA prediction. However, a dominant resonance coupling will more strongly perturb a weaker, but still significant, competing resonance than visa versa. These shifts can be to different frequencies for the dominant and the competing resonances so that they become distinct, as is found in the example of Fig. 5.4 in Sec. 5.3. In such cases, the DR-RWA analytical solution may still apply qualitatively for the dominant resonance. The competing resonance can be studied by numerical calculations using the MR-RWA or exact Hamiltonians. If the competing resonance coupling is many orders of magnitude smaller than the dominant resonance coupling, the transition due to the competing resonance may be too narrow to be detected with the frequency increments $\Delta\omega_p$ used to sweep out the profile of the dominant resonance transition. If the frequency shifts

for all transitions are very similar, the smaller competing resonances will be masked by the dominant resonance transition; in such cases the DR-RWA generally applies, as in the examples of Figs. 5.1, 5.2 and 5.5, and to a lesser extent, Fig. 5.4.

Special consideration must be given to cases where one of the resonances in (5.1.5) has either N_1 or N_2 equal to zero. If the dominant resonance has, say, $N_2 = 0$, then for $\omega_1 = \Delta E/N_1$, the DR-RWA resonance profile, given by (5.1.8),as a function of ω_2 is a flat line with $\bar{P}_2^{(N_1,0)} = 0.5$. On the other hand, a frequency sweep with respect to ω_1 yields a DR-RWA resonance profile with $FWHM(N_1,0) = 2|C(N_1,0)|/N_1$, centred at $\omega_1 = \Delta E/N_1$. Assuming that the conditions for the applicability of the DR-RWA are met, the exact and DR-RWA resonance profiles with respect to ω_1 are likely to show good agreement in their FWHMs. However, if the exact resonance profile with respect to ω_1 is Bloch-Siegert shifted from $\omega_1 = \Delta E/N_1$, then $\bar{P}_2(\omega_1 = \Delta E/N_1) \neq 0.5$. The exact resonance profile with respect to ω_2 is still a flat line, but $\bar{P}_2(\omega_2) = \bar{P}_2(\omega_1 = \Delta E/N_1) \neq 0.5$. Thus, the Bloch-Siegert shift has little effect on the shape of the resonance profile as a function of ω_1, but has a profound effect on the resonance profile as a function of ω_2. If a competing ω_2-resonance is significant, it will be superimposed upon the flat line associated with the $(N_1,0)$ resonance. Examples of these effects can be found in the discussion of Figs. 5.3 and 5.4 in Sec. 5.3.

A time-dependent perturbation theory treatment of the two-colour absorption problem indicates that the molecule-EMF coupling for a two-photon $\Delta E = (\omega_1 + \omega_2)$ transition can be written as [1b,42,58a],

$$|C(1,1)|^2_{pert} \propto (\mathcal{E}_1^0\mathcal{E}_2^0)^2\left(\omega_2^{-1}(\underline{\mu}_{12}\cdot\hat{e}_1)(\underline{d}\cdot\hat{e}_2) + \omega_1^{-1}(\underline{\mu}_{12}\cdot\hat{e}_2)(\underline{d}\cdot\hat{e}_1)\right)^2 \tag{5.1.14}$$

This result suggests that the (1,1)-photon transition will be optimized, for given values of $\mathcal{E}_1^0$ and $\mathcal{E}_2^0$, by choosing $\omega_1 = \Delta E - \omega_2$ very small relative to ω_2 [42]; or, alternatively, for a given set of frequencies satisfying $\Delta E = \omega_1 + \omega_2$, by using large field strengths. However, the DR-RWA result (5.1.8), through the analytical expression for the molecule-EMF coupling $C(N_1,N_2)$ given by (5.1.6), shows that criteria based on perturbation theory will often not lead to optimization of a given (N_1,N_2)-photon transition. Indeed, as illustrated below, the optimization conditions are dependent upon maximizing the magnitudes of the dominant Bessel functions in the molecule-EMF coupling (5.1.6) for a given transition, as a function of their arguments $z_j = \underline{d}\cdot\hat{e}_j\mathcal{E}_j^0/\omega_j$. The perturbative result (5.1.14) can be obtained from C(1,1) in (5.1.6) by expanding the Bessel function $J_1(z_j)$ in powers of z_j [81] and retaining only the term proportional to $(\mathcal{E}_1^0\mathcal{E}_2^0)^2$ in the result for $|C(1,1)|^2$.

In general, the validity of analytical solutions using the DR-RWA requires that the counter-rotating terms oscillate rapidly within the period of the time-dependent excited state population (see (5.1.13)), that only one resonance transition is dominant for each set of frequencies, and that the adjacent significant resonances are well separated. As with all approximations, the quantitative and qualitative applicability of the two-field DR-RWA analytical solution must be tested by comparison with the exact results. As pointed out earlier, comparisons with the MR-RWA results for resonance profiles can

also be of interest.

5.2. EXACT COMPUTATIONAL TECHNIQUES FOR TWO CW LASERS-MOLECULE INTERACTIONS.

5.2.1. THE RIEMANN PRODUCT INTEGRAL TECHNIQUE

Section 2.2.4 discusses the Floquet technique as applied to the interaction of an N-level molecule interacting with one CW electric field. This technique can be readily adapted for the interaction of an N-level molecule with two CW electric fields since the total field, and hence the exact and MR-RWA Hamiltonians, are periodic in $2\pi/\omega_b$. The long-time and time-averaged behaviour of the molecular states can be calculated from the evolution operators over this period.

For the examples given here, the evolution operators were calculated over the period $2\pi/\omega_b$ using the Riemann product integral (RPI) method, see Sec. 2.2.1. In general, the number of Riemann intervals used for the temporal integration of the Hamiltonian is $180m_2$, where m_2 is the larger of m_1 and m_2 in the examples. This method of subdivision ensures that the shorter period $2\pi/\omega_2$ was divided into 180 subintervals; the factor of m_2 comes from the m_2 periods of length $2\pi/\omega_2$ contained in the beat period $2\pi/\omega_b = 2\pi m_2/\omega_2$.

For the two-field problem, although the frequencies can be related to each other and the beat frequency by (5.1.11), the phases are not necessarily similarly related Hence, there is no advantage to defining a phase-dependent variable analogous to θ given by (2.2.10). For example, defining a variable $\theta_b = \omega_b t + \delta_b$ results in an electric

field which can be expressed as,

$$\underline{\mathcal{E}}(t) = \sum_{j=1}^{2} \hat{e}_j \cdot \mathcal{E}_j^0 \cos(m_j \vartheta_b + \delta_j - m_j \delta_b),$$

and the effect of phases δ_1 and δ_2 must still be investigated explicitly.

Hence, for the two-field problem, the RPI is applied in terms of time, rather than ϑ. The two-field analogue to (2.2.13) for the exact problem in the Schrödinger representation, is,

$$C_{lm}^{(s)} = -i\Big(E_l \delta_{lm} \Delta t_s - 2 \sum_{j=1}^{2} \frac{1}{\omega_j} \mu_{lm} \cdot \hat{e}_j \mathcal{E}_j^0 \cos[\tfrac{1}{2}\omega_j (t_s + t_{s-1}) + \delta_j] \sin[\tfrac{1}{2}\omega_j \Delta t_s]\Big) \tag{5.2.1}$$

where $\Delta t_s = t_s - t_{s-1} = 2\pi/(180 m_2 \omega_b)$.

Although the MR-RWA Hamiltonian (5.1.5) is given in an interaction representation, it is more convenient to transform the MR-RWA Hamiltonian into a Schrödinger representation, so the exact and MR-RWA Hamiltonian matrices have similar structures. Thus, in the MR-RWA, the RPI is most easily applied if the unitary transformation,

$$b_m(t) = c_m(t) \exp[i(-1)^m \Delta E t/2], \quad m = 1,2 \tag{5.2.2}$$

is applied to (5.1.2) with the non-zero elements of the Hamiltonian matrix in (5.1.2) given by (5.1.5). With this transformation,

$$H_{mm} = \tfrac{1}{2}(-1)^m \Delta E, \qquad m = 1,2 \tag{5.2.3a}$$

and,

$$H_{12} = -\frac{1}{2} \sum_{N_1, N_2} C(N_1, N_2) \exp[i(N_1 \omega_1 + N_2 \omega_2)t] \times \exp[-i(z_1 \sin\delta_1 + z_2 \sin\delta_2 - N_1 \delta_1 - N_2 \delta_2)]. \tag{5.2.3b}$$

Applying (2.2.4) and (2.2.8), over the interval $t_{s-1} \le t \le t_s$, yields,

$$C_{mm}^{(s)} = -\frac{i}{2}(-1)^m \Delta E \Delta t_s, \tag{5.2.4a}$$

and,

$$C_{12}^{(s)} = i \sum_{N_1,N_2} \frac{C(N_1,N_2)}{(N_1\omega_1 + N_2\omega_2)} \sin[\tfrac{1}{2}(N_1\omega_1 + N_2\omega_2)\Delta t_s]$$

$$X \exp[-i(z_1\sin\delta_1 + z_2\sin\delta_2 - N_1\delta_1 - N_2\delta_2)]$$

$$X \exp[\tfrac{i}{2}(N_1\omega_1 + N_2\omega_2)(t_s + t_{s-1})], \tag{5.2.4b}$$

where $C_{21}^{(s)} = -C_{12}^{(s)*}$.

The periodicity of the Hamiltonian in $2\pi/\omega_b$ permits the calculation of the time- and phase-dependent populations from,

$$\underline{b}(t + 2k\pi/\omega_b) = \underline{\underline{U}}(t,0)[\underline{\underline{U}}(2\pi/\omega_b,0)]^k \underline{b}(0), \tag{5.2.5}$$

where $U(2\pi/\omega_b,0)$ is the evolution operator from $t = 0$ to $t = 2\pi/\omega_b$, and k is an integer. Equation (2.2.29), which is expressed in terms of the variable $\vartheta = \omega t + \delta$, and applies to a system periodic in 2π, has a slightly different form from (5.2.5). The term $U^{-1}(\delta,0)\underline{a}(t = 0)$ arises in (2.2.29) because of the transformation from the variable t to ϑ; the form of the initial conditions changes correspondingly since $\underline{a}(\vartheta = \delta) = \underline{a}(t = 0) = \underline{\underline{U}}(\delta,0)\underline{a}(\vartheta = 0)$. In (5.2.5), the effect of phase is built into the evolution operators through the explicit occurrence of δ_1 and δ_2 in the Hamiltonian, see for example, (5.2.3b).

5.2.2. THE FLOQUET FORMALISM AND PHASE-DEPENDENCE

The application of the Floquet formalism of Sec. 2.2.4 uses the periodicity of the two-field Hamiltonian over the beat period, $2\pi/\omega_b$. However, unlike the one-field problem, in the two-field case there is no simple way to isolate the phase-dependent terms such as $\underline{\underline{\beta}}(\vartheta,\delta)$ in

(2.2.37) because an overall "beat" phase cannot be defined. Since it appears that the phase-dependence must be dealt with explicitly, application of the Floquet technique for phase-averaging requires that the evolution operators over $0 \leq t \leq 2\pi/\omega_b$ be recalculated for each set of δ_1 and δ_2.

On the other hand, for fixed-phase calculations, the Floquet method still permits a reduction in the computational effort of the long time-averaged molecular state populations. The procedure is analogous to that presented in Sec. 2.2.4; however, some of the matrices are defined slightly differently when presented in terms of the variable t instead of θ. Only the initial occupation matrix, $\underline{b}(t = 0)$, is independent of the phases of the field; in what follows, the dependence of all other matrices on δ_1 and δ_2 is implied.

Since the Hamiltonian is periodic in $2\pi/\omega_b$, Floquet's theorem allows the construction of the periodic matrix $\underline{\underline{Z}}(t)$ [32,70],

$$\underline{\underline{Z}}(t) = \underline{\underline{U}}(t,0)\underline{\underline{S}}\exp[-i\underline{\underline{\Delta}}\omega_b t] = \underline{\underline{Z}}(t + 2s\pi/\omega_b) \tag{5.2.6}$$

where the matrices $\underline{\underline{S}}$ and $\underline{\underline{\Delta}}$ contain the eigenvectors and characteristic exponents, respectively, of $\underline{\underline{U}}(2\pi/\omega_b,0)$,

$$\underline{\underline{U}}(2\pi/\omega_b,0) = \underline{\underline{S}}\exp[+i2\pi\underline{\underline{\Delta}}]\underline{\underline{S}}^{-1}. \tag{5.2.7}$$

A column vector $\underline{b}_0'$ is defined as,

$$\underline{b}_0' = \underline{\underline{S}}^{-1}\underline{b}(0). \tag{5.2.8}$$

Equations (5.2.6) and (5.2.8) differ from the θ analogues (2.2.34) and (2.2.35), respectively, because the latter set contains a transformation of the initial conditions due to the change to the variable θ.

Substitution of (5.2.6), (5.2.7) and (5.2.8) into (5.2.5) gives the time-dependent coefficients in Floquet form,

$$\underline{b}(t + 2k\pi/\omega_b) = \underline{\underline{Z}}(t)\exp[+i\underline{\underline{\Delta}}(\omega_b t + 2k\pi)]\underline{b}'_0 \qquad (5.2.9)$$

The phase (δ_1,δ_2)- and time-dependent population of the state j is $P_j(t) = |b_j(t)|^2$, or,

$$P_j(t) = \sum_{p,q} Z_{jp}(t)\beta_{pq}(t)Z^*_{qj}(t) \qquad (5.2.10)$$

where,

$$\underline{\underline{\beta}}(t) = \exp[i\underline{\underline{\Delta}}\omega_b t]\underline{b}'_0\underline{b}'^{\dagger}_0\exp[-i\underline{\underline{\Delta}}\omega_b t]. \qquad (5.2.11)$$

From (2.1.12), the long time-average of (5.2.10) gives the steady state phase-dependent population of the jth molecular state,

$$\bar{P}_j(\delta_1,\delta_2) = \sum_p \frac{\omega_b}{2\pi}\int_0^{2\pi/\omega_b}|Z_{jp}(t)b'_{0p}|^2dt \qquad (5.2.12)$$

where the oscillating off-diagonal terms of $\underline{\underline{\beta}}(t)$ average to zero upon integration, and the integration limits change due to the periodicity of $\underline{\underline{Z}}(t)$ in $2\pi/\omega_b$. These changes parallel those used in the derivation of (2.2.39) from (2.2.37). In the numerical examples of Sec. 5.3, the phases are fixed at $\delta_1 = \delta_2 = 0$, and the notation $\bar{P}_j$, in reference to exact results, implies $\bar{P}_j(\delta_1=0,\delta_2=0)$ from (5.2.12).

For the examples presented in Sec. 5.3, the long-time averages of the time-dependent populations were determined from (5.2.12) using Simpson's Rule [76], with the number of integration points being one sixth the number of Riemann points. The steady state populations generally converged to 3 or 4 figures under these conditions. For very sharp transition peaks, the number of Riemann intervals was increased to $456m_2$ to attain the required degree of convergence. For typical frequencies around resonance, the value of the steady state population

produced by the above procedure was tested against that of a more rigorous calculation. Here, before calculating the evolution operators, all the nodes, local maxima and local minima of the beating field were found over the beat period; these points then served as intermediate endpoints in the RPI technique, and were further subdivided to a mesh size of $\Delta t \simeq 0.4$. Having these critical points explicitly included in the calculation ensured that all the "subtle" effects of the beating were accounted for in the solution. However, this latter approach is computationally more time consuming and expensive; the results obtained with both procedures agreed to 3 significant figures for common frequencies for the examples in this paper. Hence the former method of equal-sized integration intervals was used to calculate the exact and the MR-RWA resonance profiles. The exact calculations were used to test the predictions of the MR-RWA and the DR-RWA.

5.2.3. SELECTION OF FREQUENCIES FOR RESONANCE PROFILES

For the one- or two-field case, a resonance profile is determined by calculating a series of points, $(\bar{P}_j, \omega_p)$, where ω_p is the frequency being varied, such that the number of points is sufficiently large, and the frequency separation between the adjacent points is sufficiently small, to give a good representation of the spectral peak. In the one-field problem, the computational effort per point is roughly equal: typically, for each frequency, computing the time-averaged state populations using the Floquet technique requires the calculation of 180 to 200 evolution operators over $0 \leq t \leq 2\pi/\omega$. Thus, in the one-field problem, the selection of frequency values is not critical, and

frequencies can be chosen by (unequal) increments along the frequency width of the resonance profile.

To generate the resonance profile for a two-field problem, where one frequency is fixed and the other is varied, the dependence of the two-field Hamiltonian on the beat frequency renders the choice of the frequency critical. If $180m_2$ evolution operators are calculated over the interval $0 \le t \le 2\pi/\omega_b = 2\pi m_2/\omega_2$, selecting small values of m_2, where possible, will reduce the computational effort. For example, the frequencies $\omega_2 = (10.66\omega_1,\ 10.67\omega_1,\ 10.68\omega_1,\ 10.69\omega_1)$ can be rewritten from (5.1.11) as $\omega_2 = m_2\omega_1/m_1 = (533\omega_1/50,\ 1067\omega_1/100,\ 267\omega_1/25,\ 1069\omega_1/100)$. For these four frequencies, $\sum m_2 = 2936$, and the calculation of the four corresponding steady state populations would require the computation of a total of 180x2936 evolution operators. On the other hand, using the frequencies $\omega_2 = m_2\omega_1/m_1 = (437\omega_1/41,\ 32\omega_1/3,\ 203\omega_1/19,\ 139\omega_1/13) \simeq (10.658\omega_1,\ 10.667\omega_1,\ 10.684\omega_1,\ 10.692\omega_1)$ would generate four points of the resonance profile requiring the computation of a total of only 180x811 evolution operators. Thus, rather than generating the resonance profile by stepwise incrementation of the frequency being varied, careful choices of the frequency can often dramatically reduce the cost of the calculation.

5.3. NUMERICAL EXAMPLES OF TWO-COLOUR SPECTROSCOPY

The molecular parameters in all the following examples are $\Delta E = 0.10$, $\mu_{12} = 3.0$, and $d = 6.5$ [26,44,45]; these are representative of a substituted aromatic with large permanent dipole moments [26,46]. The transition and permanent dipole moments are taken to be aligned

with the direction of polarization $\hat{e}_1 \parallel \hat{e}_2$ of the electric fields. In these calculations, the phases δ_j of the EMFs are taken to be zero.

Choosing $\omega_1 = \Delta E/11.0$ and $\mathcal{E}_2^0 = 5\times10^{-5}$, the optimization in the DR-RWA of the (1,1)-photon transition is considered first. This transition is optimized by fixing $\mathcal{E}_1^0 \approx 2.575\times10^{-3}$ ($z_1 = 1.841184$) which corresponds to the maximum value of $J_1(d\mathcal{E}_1^0/\omega_1)$. The resonance profiles for the (1,1)-photon transition are illustrated in Fig. 5.1 for $\mathcal{E}_1^0 = 5.0\times10^{-5}$, 2.575×10^{-3} and 4.2×10^{-3}. Since only one coupling term dominates in each case, and $|C(1,1)| \leq \omega_1$, the DR-RWA analytical expression (5.1.8) for the resonance profiles can be applied for each $\mathcal{E}_1^0$ for values of ω_2 around $\Delta E - \omega_1$. The corresponding FWHM(1,1), in the DR-RWA, are 5.90×10^{-6}, 1.92×10^{-4} and 1.12×10^{-4}, respectively. It is clear that $\mathcal{E}_1^0 \approx 2.575\times10^{-3}$ maximized the (1,1)-photon transition and, contrary to perturbation theory predictions, increasing $\mathcal{E}_1^0$ beyond the optimal value predicted by the DR-RWA does not increase the molecule-EMF coupling for a fixed ω_1.

The exact (1,1) resonance profiles, evaluated using Floquet/RPI techniques, for the three field strengths are also included in Fig. 5.1. For the weakest field strength, $\mathcal{E}_1^0 = 5.0\times10^{-5}$, the exact and DR-RWA results are graphically indistinguishable on the scale of Fig. 5.1. In agreement with the prediction of the DR-RWA, the smaller of the two remaining field strengths leads to the broadest resonance profile.

For the two stronger field strengths, noticeable differences can arise between the exact and the DR-RWA resonance profiles. The exact FWHM(1,1), namely $\sim2.01\times10^{-4}$ and $\sim1.4\times10^{-4}$ for $\mathcal{E}_1^0 = 2.575\times10^{-3}$ and 4.2×10^{-3}, respectively, are somewhat larger than the corresponding

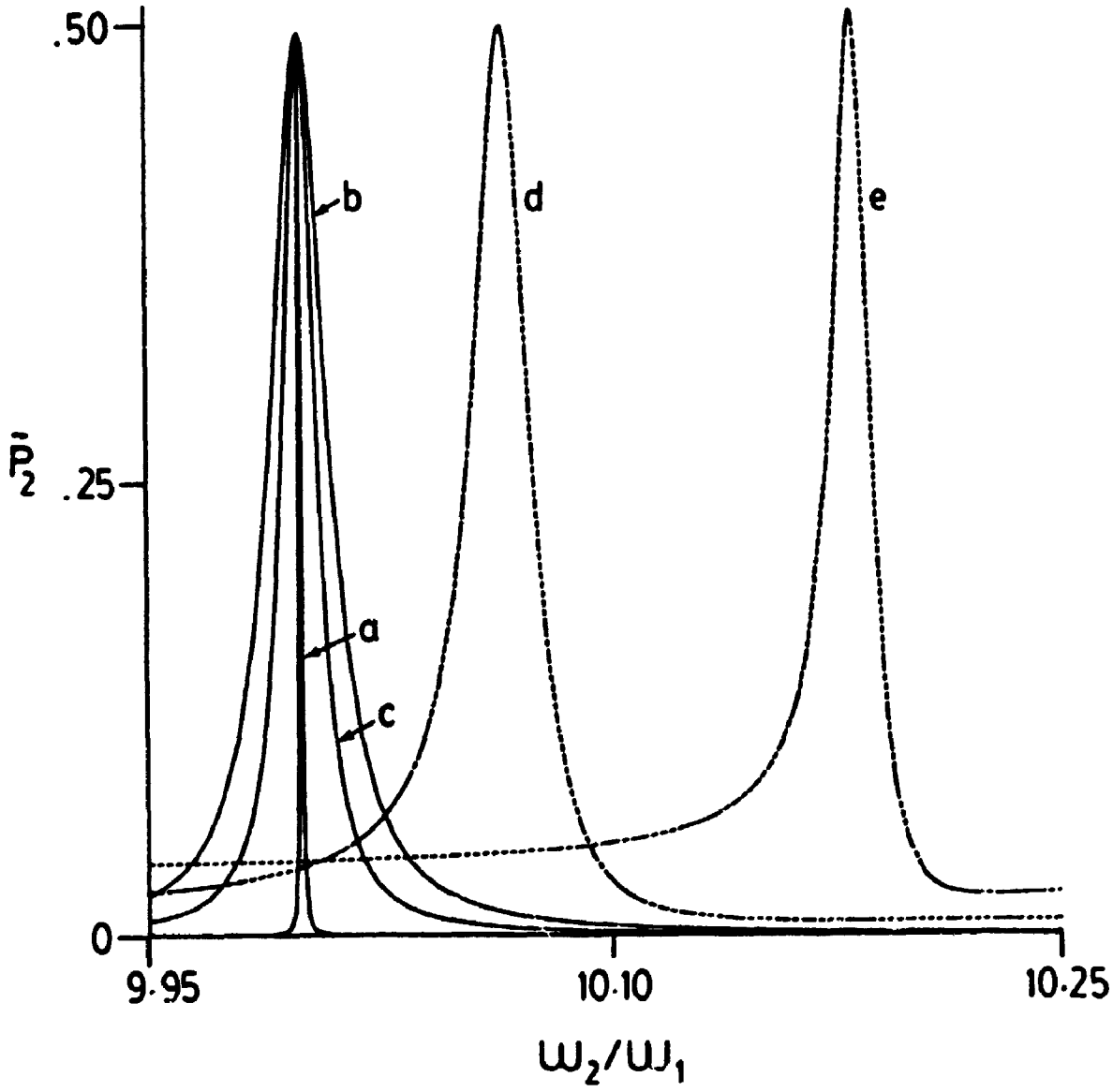

Figure 5.1 The DR-RWA and exact resonance profiles $\bar{P}_2^{(1,1)}$ as a function of ω_2/ω_1 for the model system specified by d = 6.5, μ_{12} = 3.0, ΔE = 0.1, $\omega_1 = \Delta E/11.0$, $\mathcal{E}_2^0 = 5\times10^{-5}$ and $\mathcal{E}_1^0$ changing. DR-RWA results (solid lines): (a) $\mathcal{E}_1^0 = 5\times10^{-5}$, (b) $\mathcal{E}_1^0 \simeq 2.575\times10^{-3}$, (c) $\mathcal{E}_1^0 = 4.2\times10^{-3}$; exact results (dashed lines): (d) $\mathcal{E}_1^0 \simeq 2.575\times10^{-3}$, (e) $\mathcal{E}_1^0 = 4.2\times10^{-3}$. The DR-RWA and exact results for $\mathcal{E}_1^0 = 5\times10^{-5}$ are graphically indistinguishable on the scale of the figure.

DR-RWA results, especially for the larger field strength. Secondly, the exact resonance values of ω_2 are shifted from the DR-RWA result of $(\omega_2/\omega_1)_{res} = 10$; the shift increases with field strength, $(\omega_2/\omega_1)_{res} = 10.067$ and 10.183 for the exact calculations. Finally, as $\mathcal{E}_1^0$ increases, the exact resonance profiles become more asymmetric as a function of ω_2, have larger off-resonance backgrounds, and show "population inversion" [108], i.e. have resonance values of $\bar{P}_2^{(1,1)}$ which can exceed 0.5 ($\bar{P}_2^{(1,1)} = 0.504$ and $\bar{P}_2^{(1,1)} = 0.513$ in the exact calculations). These "high" field effects are due to the increasing influence of counter-rotating terms and (probably) competing resonances as $\mathcal{E}_1^0$ increases. The largest competing resonance coupling for all three field strengths is $|C(11,0)|$, having values 1.4×10^{-28}, 8.7×10^{-10}, and 1.7×10^{-7} for $\mathcal{E}_1^0 = 5.0\times10^{-5}$, 2.575×10^{-3} and 4.2×10^{-3}, respectively.

In the example of Fig. 5.1, for a given $\mathcal{E}_2^0$, ω_1 and ω_2, the (1,1)-photon transition is optimized with respect to $\mathcal{E}_1^0$, by choosing the $\mathcal{E}_1^0$ which maximizes $J_1(z_1)$. However, there are other means of (further) augmenting this multi-photon transition, such as increasing $\mathcal{E}_2^0$. Some caution is required because if both $\mathcal{E}_1^0$ and $\mathcal{E}_2^0$ are set to the values ($\mathcal{E}_1^0 \simeq 0.002575$ and $\mathcal{E}_2^0 \simeq 0.02575$) which optimize $J_1(z_1)$ and $J_1(z_2)$, respectively, the resulting molecule-EMF coupling, $C(1,1) = 0.0313$, violates condition (5.1.13) since $\omega_1 \simeq 0.009091$ and $m_1 = 1$. A field strength of $\mathcal{E}_2^0 = 0.004805$, with $\mathcal{E}_1^0$ maximizing $J_1(z_1)$, produces an enhanced molecule-EMF coupling (with respect to $\mathcal{E}_2^0$) which is equal to ω_1. Another method of enhancing the (1,1)-photon transition is to fix the field strengths, and manipulate the frequencies to increase the molecule-EMF coupling. For example, if the field strengths are fixed at $\mathcal{E}_1^0 = 0.0005$ and $\mathcal{E}_2^0 = 0.00005$, then $J_1(z_1)$

can be increased by changing the frequency of field one from $\omega_1 \simeq 0.009091$ ($m_1 = 1$) to $\omega_1 = 0.00175$ ($m_1 = 7$). $J_1(z_2)$ cannot be maximized for this example; because N_1 and N_2 are fixed, the resonance condition (5.1.4) determines $\omega_2 = 0.09825$ ($m_2 = 393$). The resulting molecule-EMF coupling is $C(1,1) = 8.7\times10^{-5}$ (as opposed to $C(1,1) = 2.51\times10^{-5}$ had ω_1 not been changed from $\omega_1 \simeq 0.009091$). Equation (5.1.13) holds for $C(1,1) = 8.7\times10^{-5}$ since $\omega_1/m_1 = 2.5\times10^{-4}$. The comments above regarding the enhancement of the (1,1)-photon transition may be applied to any (N_1,N_2)-photon transition. Indeed, N_1 and N_2 can also be treated as variables. For example, if $\mathcal{E}_1^0 = 0.0005$, $\mathcal{E}_2^0 = 0.00005$ and $\omega_1 = 0.0009$, then it is more favourable to tune ω_2 to the (2,1) resonance than the (1,1) resonance, since $C(2,1) = 7.42\times10^{-5}$ while $C(1,1) = 4.49\times10^{-5}$. In general, there are several ways to enhance multi-photon transitions between molecular states by careful choices of ω_1, ω_2, $\mathcal{E}_1^0$, $\mathcal{E}_2^0$, N_1 and N_2.

The DR-RWA and exact $(N_1,1)$ resonance profiles, for $N_1 = 2,1,0,-1$, are illustrated in Fig. 5.2 for the field parameters associated with the $\mathcal{E}_1^0 \simeq 2.575\times10^{-3}$ calculation of Fig. 5.1. Again, this value of $\mathcal{E}_1^0$ was chosen to optimize the (1,1)-photon transition for $\omega_1 = \Delta E/11.0$ and $\mathcal{E}_2^0 = 5\times10^{-5}$. In the figure, ω_2 is varied between $8.9\omega_1 \leq \omega_2 \leq 12.1\omega_1$. According to (5.1.4) this range of frequency should contain four major resonance transitions at $\omega_2 = 9.0\omega_1$, $10.0\omega_1$, $11.0\omega_1$ and $12.0\omega_1$, corresponding to the (2,1)-, (1,1)-, (0,1)- and (-1,1)-photon transitions, respectively. Since only one coupling term dominates for each $(N_1,1)$-photon transition, and $|C(N_1,1)| \leq \omega_1$, the DR-RWA analytical expression (5.1.8) for the resonance profiles can be applied for each $(N_1,1)$-photon transition separately for values of ω_2 around

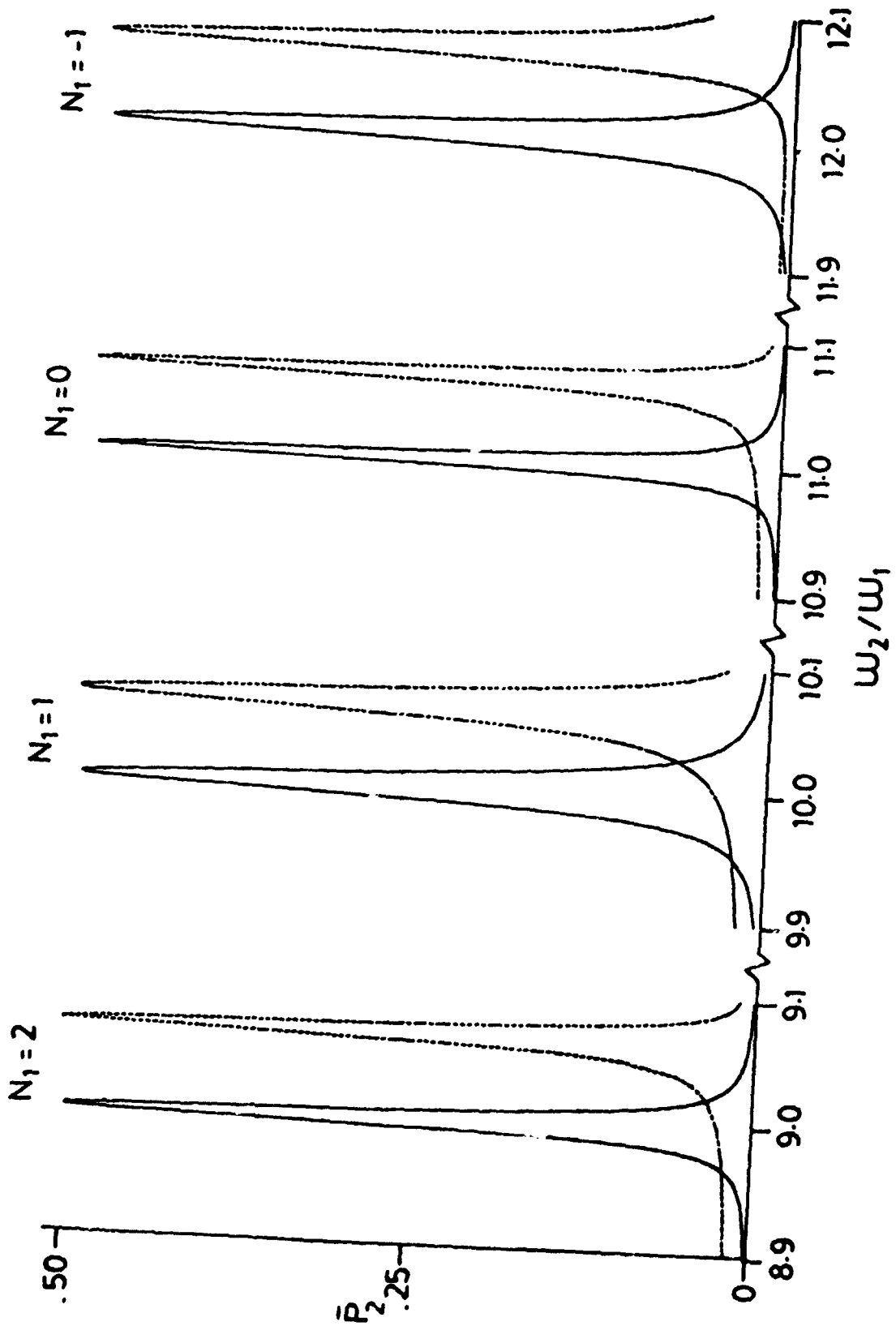
$N_1 = -1$
$N_1 = 0$
$N_1 = 1$
$N_1 = 2$
.50
.25
0
$\bar{P}_2$
8.9
9.0
9.1
9.9
10.0
10.1
10.9
11.0
11.1
11.9
12.0
12.1
ω_2/ω_1

$\Delta E - N_1\omega_1$.

In the DR-RWA resonance profiles of Fig. 5.2, the (1,1) and (-1,1) transitions are strongest, followed by the (2,1) and then the (0,1) transitions; these trends follow those for the relevant molecule-EMF couplings, namely $|C(N_1,1)| = 9.6\text{x}10^{-5}$, $8.0\text{x}10^{-5}$, $5.8\text{x}10^{-5}$ and $4.7\text{x}10^{-5}$ for $N_1 = 1,-1,2,0$, respectively. Since the field strength $\mathcal{E}_1^0$ maximizes $J_1(z_1)$, and $J_1(z_1) = -J_{-1}(z_1)$ [81], this choice of $\mathcal{E}_1^0$ also essentially optimizes the (-1,1) transition. The (1,1) molecule-EMF coupling is slightly larger than the (-1,1) coupling since $J_1(z_2 = d\mathcal{E}_2^0/\omega_2 \ll 1)$ decreases with increasing ω_2 and $\omega_{2,res}^{(1,1)} < \omega_{2,res}^{(-1,1)}$. For $k = 0,2,3\ldots$, $|J_{\pm k}(z_1)| < |J_{\pm 1}(z_1)|$, leading to reduced widths for the $(N_1,1)$, $N_1 = 0,2,3\ldots$, transitions relative to $N_1 = \pm 1$.

Aside from the differences already discussed for the (1,1)-photon transition, with $\mathcal{E}_1^0 = 2.575\text{x}10^{-3}$, of Fig. 5.1, the DR-RWA and exact resonance profiles of Fig. 5.2 agree well. For example, the molecule-EMF couplings evaluated from the FWHM for the exact profiles in Fig. 5.2 by $|C(N_1,1)| = \text{FWHM}/2$ are ~ .1%, 4%, 5% and 1.3% larger than the predictions of the DR-RWA for $N_1 = 2,1,0,-1$ respectively. For all four N_1, the maxima (~ 0.503) in the exact profiles only slightly exceed the DR-RWA result of 0.5 and the Bloch-Siegert shift (to high frequency) is 0.067, relative to $(\omega_2/\omega_1)_{res} = 11 - N_1$. Aside from the asymmetry, as a function of ω_2, in the exact resonance profiles for small values of $\bar{P}_2^{(N_1,1)}$, the DR-RWA and exact profiles are graphically indistinguishable when the resonance frequency of the latter is normalized to the former as a function of N_1.

Figure 5.3 gives an example of when the DR-RWA analytical solution does not apply because of competing resonances. The DR-RWA, MR-RWA and

Figure 5.2 The DR-RWA and exact resonance profiles $\bar{P}_2^{(N_1,1)}$, for $N_1 = 2,1,0,-1$, as a function of ω_2/ω_1 for the two-level model system specified in Fig. 5.1, with $\mathcal{E}_1^0 \simeq 2.575\text{x}10^{-3}$. The solid lines are DR-RWA results while the dashed lines give exact results.

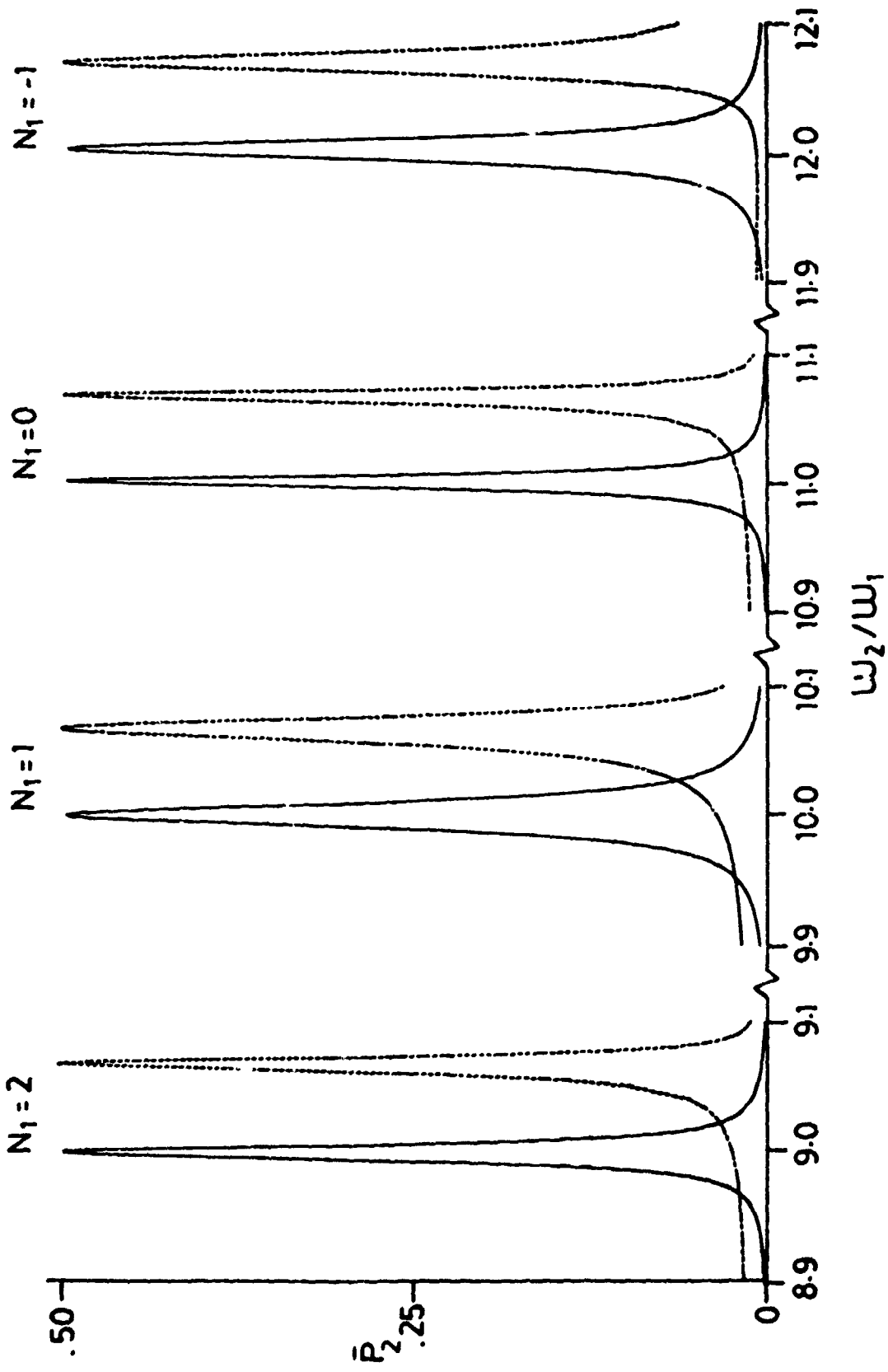
$N_1 = -1$
$N_1 = 0$
$N_1 = 1$
$N_1 = 2$
$\bar{P}_2$
.50
.25
0
8·9
9·0
9·1
9·9
10·0
10·1
10·9
11·0
11·1
11·9
12·0
12·1
ω_2/ω_1

$\Delta E - N_1\omega_1$.

In the DR-RWA resonance profiles of Fig. 5.2, the (1,1) and (-1,1) transitions are strongest, followed by the (2,1) and then the (0,1) transitions; these trends follow those for the relevant molecule-EMF couplings, namely $|C(N_1,1)| = 9.6\text{x}10^{-5}$, $8.0\text{x}10^{-5}$, $5.8\text{x}10^{-5}$ and $4.7\text{x}10^{-5}$ for $N_1 = 1,-1,2,0$, respectively. Since the field strength $\mathcal{E}_1^0$ maximizes $J_1(z_1)$, and $J_1(z_1) = -J_{-1}(z_1)$ [81], this choice of $\mathcal{E}_1^0$ also essentially optimizes the (-1,1) transition. The (1,1) molecule-EMF coupling is slightly larger than the (-1,1) coupling since $J_1(z_2 = d\mathcal{E}_2^0/\omega_2 \ll 1)$ decreases with increasing ω_2 and $\omega_{2,res}^{(1,1)} < \omega_{2,res}^{(-1,1)}$. For $k = 0,2,3\ldots$, $|J_{\pm k}(z_1)| < |J_{\pm 1}(z_1)|$, leading to reduced widths for the $(N_1,1)$, $N_1 = 0,2,3\ldots$, transitions relative to $N_1 = \pm 1$.

Aside from the differences already discussed for the (1,1)-photon transition, with $\mathcal{E}_1^0 = 2.575\text{x}10^{-3}$, of Fig. 5.1, the DR-RWA and exact resonance profiles of Fig. 5.2 agree well. For example, the molecule-EMF couplings evaluated from the FWHM for the exact profiles in Fig. 5.2 by $|C(N_1,1)| = \text{FWHM}/2$ are ~ .1%, 4%, 5% and 1.3% larger than the predictions of the DR-RWA for $N_1 = 2,1,0,-1$ respectively. For all four N_1, the maxima (~ 0.503) in the exact profiles only slightly exceed the DR-RWA result of 0.5 and the Bloch-Siegert shift (to high frequency) is 0.067, relative to $(\omega_2/\omega_1)_{res} = 1 - N_1$. Aside from the asymmetry, as a function of ω_2, in the exact resonance profiles for small values of $\bar{P}_2^{(N_1,1)}$, the DR-RWA and exact profiles are graphically indistinguishable when the resonance frequency of the latter is normalized to the former as a function of N_1.

Figure 5.3 gives an example of when the DR-RWA analytical solution does not apply because of competing resonances. The DR-RWA, MR-RWA and

Figure 5.3 The DR-RWA, MR-RWA and exact resonance profiles as a function of ω_2 for the system $d = 6.5$, $\mu_{12} = 3.0$, $\Delta E = 0.1$, $\mathcal{E}_1^0 = 1.25\times10^{-3}$, $\omega_1 = 0.5\Delta E$, $\mathcal{E}_2^0 = 10^{-6}$. (a) the DR-RWA result based on C(0,1); (b) the MR-RWA result based on C(2,0) and C(0,1); (c) the exact result. The insert at the top of the figure is (b) with the ordinate expanded. The DR-RWA result based on C(2,0) would be a flat line at $\bar{P}_2^{(2,0)} = 0.5$ for all ω_2.

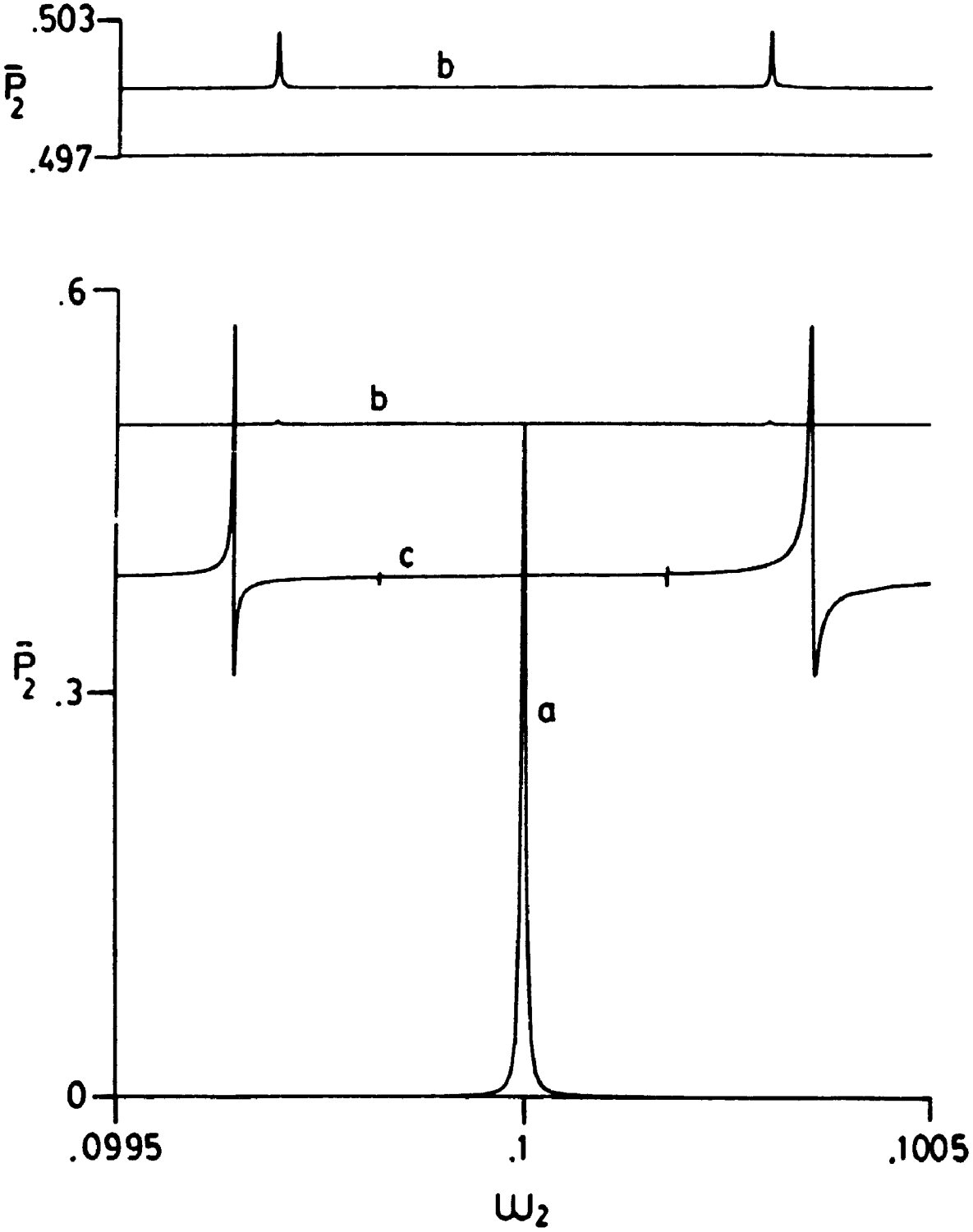
.503
$\bar{P}_2$
.497
b
.6
b
c
$\bar{P}_2$
.3
a
0
.0995
.1
.1005
ω_2

exact resonance profiles are shown in Fig. 5.3 for the field parameters $\omega_1 = \Delta E/2$, $\mathcal{E}_1^0 = 1.25\text{x}10^{-3}$, $\mathcal{E}_2^0 = 10^{-6}$, and ω_2 swept around ΔE. Equation (5.1.5) contains two significant resonance molecule-EMF couplings for the relevant ω_2, namely C(2,0) and C(0,1), and therefore, from (5.1 5), H_{12} can be approximated well by,

$$H_{12} = -\tfrac{1}{2}\left(C(2,0)\exp\left[-i(\Delta E - 2\omega_1)t\right] + C(0,1)\exp\left[-i(\Delta E - \omega_2)t\right]\right) \qquad (5.3.1)$$

where $C(2,0) = 3.04\text{x}10^{-4}$ and $C(0,1) = 2.98\text{x}10^{-6}$. The next largest molecule-EMF coupling is $C(-2,2) = 1.6\text{x}10^{-13}$. The direct application of the DR-RWA, first with C(2,0) only and then with C(0,1) only, leads to two distinct (and incorrect) resonance profiles as a function of ω_2. Equation (5.1.8) based on C(2,0), the larger of the two molecule-EMF couplings, is independent of ω_2, and thus an ω_2-sweep around ΔE gives a DR-RWA resonance profile that is a straight line at $\bar{P}_2^{(2,0)} = 0.5$. Equation (5.1.8) based on C(0,1) gives a sharp spike with $FWHM(0,1) = 5.96\text{x}10^{-6}$ centred around $\omega_2 = \Delta E$.

The MR-RWA numerical solution, determined from (5.3.1) using the same Floquet/RPI techniques as for exact calculations, is also shown in Fig. 5.3. Here, the effect of C(2,0) is seen in the off-resonance background of $\bar{P}_2 = 0.5$. There is no resonance peak at $\omega_2 = \Delta E = 0.1$; instead, there are two small peaks symmetrically displaced about $\omega_2 = \Delta E$, at $\omega_2 \simeq 0.099695$ and $\omega_2 \simeq 0.100304$, both with $\bar{P}_2 \simeq 0.502$. Since only two coupling terms were retained in (5.3.1), these small peaks are likely due to the splitting of the (0,1)-photon transition by the (2,0)-photon transition. The off-resonance background of $\bar{P}_2 = 0.5$ contains two small sharp dips with amplitudes of $\Delta\bar{P}_2 \sim -10^{-5}$, unobservable on the scale of the figure, at $\omega_2 = 0.099848$ and

$\omega_2 = 0.100152$, again symmetrically shifted with respect to ΔE. As (5.3.1) has only two molecule-EMF coupling terms, these dips are not due to another competing resonance, but are a result of further interplay between the (2,0) and (1,0) resonances.

The exact resonance profile in Fig. 5.3 bears little resemblance to the DR-RWA predictions, but exhibits some of the features of the MR-RWA results, although on a much enhanced scale. In the exact calculation, two resonance peaks are observed, symmetrically shifted from $\omega_2 = \Delta E$; each is followed by a excited state population minimum that dips well below the off-resonance background of $\bar{P}_2 \simeq 0.387$. One peak ($\bar{P}_2 \simeq 0.571$) occurs at $\omega_2 \simeq 0.0996433$, followed by a minimum of $\bar{P}_2 \simeq 0.314$ at $\omega_2 \simeq 0.0996448$. The second peak ($\bar{P}_2 \simeq 0.572$) occurs at $\omega_2 \simeq 0.100355$, followed by a minimum of $\bar{P}_2 \simeq 0.314$ at $\omega_2 \simeq 0.100359$. The off-resonance background is also interrupted around $\omega_2 \simeq 0.0998214$ by a small ripple with minimum $\bar{P}_2 = 0.381$ and maximum of $\bar{P}_2 = 0.389$. Around $\omega \simeq 0.100178$, a second ripple occurs with minimum $\bar{P}_2 = 0.380$ and maximum $\bar{P}_2 = 0.394$. The two ripples are symmetrically shifted from $\omega_2 = \Delta E$, but the high frequency ripple has slightly greater amplitude (based on a frequency division of $\Delta\omega_2 = 6\times10^{-7}$ around each ripple).

By comparison with the MR-RWA results, many of the features of the exact calculation can be related to the interaction of the (0,1) and the (2,0) resonances. The strong resonances in the exact calculation at $\omega_2 \simeq 0.0996433$ and $\omega_2 \simeq 0.100355$ are identified as split (0,1)-photon transitions. Although the maxima of the resonances in the exact and the MR-RWA results are very different, the resonance frequencies agree within 0.05%. However, the minima which immediately follow the resonances in the exact calculation do not appear in the

MR-RWA results. Similarly, the ripples in the exact calculation have different structures than the tiny dips seen in the MR-RWA results, but the frequencies associated with the two features agree to within 0.03%. The differences in the frequency shifts between the two methods of calculation may seem pronounced in Fig. 5.3 because of the scale of the ω_2 axis.

The differences in the off-resonance background and the spectral features in the MR-RWA versus the exact results can be attributed primarily to the counter-rotating terms not present in the MR-RWA calculation. The background in the MR-RWA is $\bar{P}_2 = 0.5$ because the (2,0)-photon transition is on resonance at $\omega_1 = \Delta E/2 = 0.05$ for all ω_2 (in the DR-RWA). The background in the exact population is much lower, at $\bar{P}_2 = 0.387$, indicating the (2,0)-photon transition is Bloch-Siegert shifted, an effect of counter-rotating terms, from $\omega_1 = 0.05$. In the MR-RWA, the resonant (2,0)-photon transition likely suppresses the (0,1)-photon transition, allowing little population inversion at the resonance frequencies of the latter. In the exact calculation, the (2,0)-photon transition is slightly off-resonance because of the Bloch-Siegert shift, and the perturbation of the (0,1)-photon transition by the (2,0) resonance is therefore weakened. The result is high population inversion, and other interesting spectral features, at the split (0,1) resonance frequencies.

In the example of Fig. 5.3, the DR-RWA is inapplicable because of two significant competing resonances, where the largest (with $N_2 = 0$) is effectively not a function of the frequency being swept. The MR-RWA correctly predicted the splitting of the (0,1)-photon transition by the (2,0)-photon transition, the associated high and low frequency shifts,

and the high off-resonance background. On the other hand, the MR-RWA does not account for the Bloch-Siegert shift, caused by the counter-rotating terms, of the (2,0)-photon transition in the exact calculation. From Fig. 5.3, this shift clearly has a profound impact on the exact resonance profile.

While Fig. 5.3 illustrates how the strongest molecule-EMF coupling C(2,0) perturbs the weaker (0,1)-photon transition of interest, Fig. 5.4 illustrates how the weaker molecule-EMF coupling C(0,1) perturbs the (2,0) resonance profile. In Fig. 5.4, the DR-RWA result based on C(2,0), the MR-RWA result based on (5.3.1), and the exact resonance profile are shown for the same system as in Fig. 5.3, except that the larger frequency ω_2 is fixed at $\omega_2 = \Delta E$ while ω_1 is varied from $0.048 \leq \omega_1 \leq 0.052$.

By switching the frequency being varied from ω_2 in Fig. 5.3 to ω_1 in Fig. 5.4, one obtains a case where the DR-RWA is applicable. Unlike the example of Fig. 5.3, in Fig. 5.4, the DR-RWA result (5.1.8) with C(2,0) is now a function of the frequency being varied. Furthermore, the resonance profile of interest, corresponding to the (2,0)-photon transition, has a molecule-EMF coupling that is two orders of magnitude larger that the largest competing resonance coupling, C(0,1), while in Fig. 5.3, the resonance profile of interest, the (0,1)-photon transition, is dominated by the competing (2,0) resonance. Hence, the perturbation of the (2,0)-photon transition by the (0,1)-photon transition in Fig. 5.4 will not be as large as the perturbation of the (0,1)-photon transition by the (2,0)-photon transition in Fig. 5.3. This is in agreement with Fig. 5.4, which indicates the competing resonance (0,1) can be neglected as a first approximation, and that the

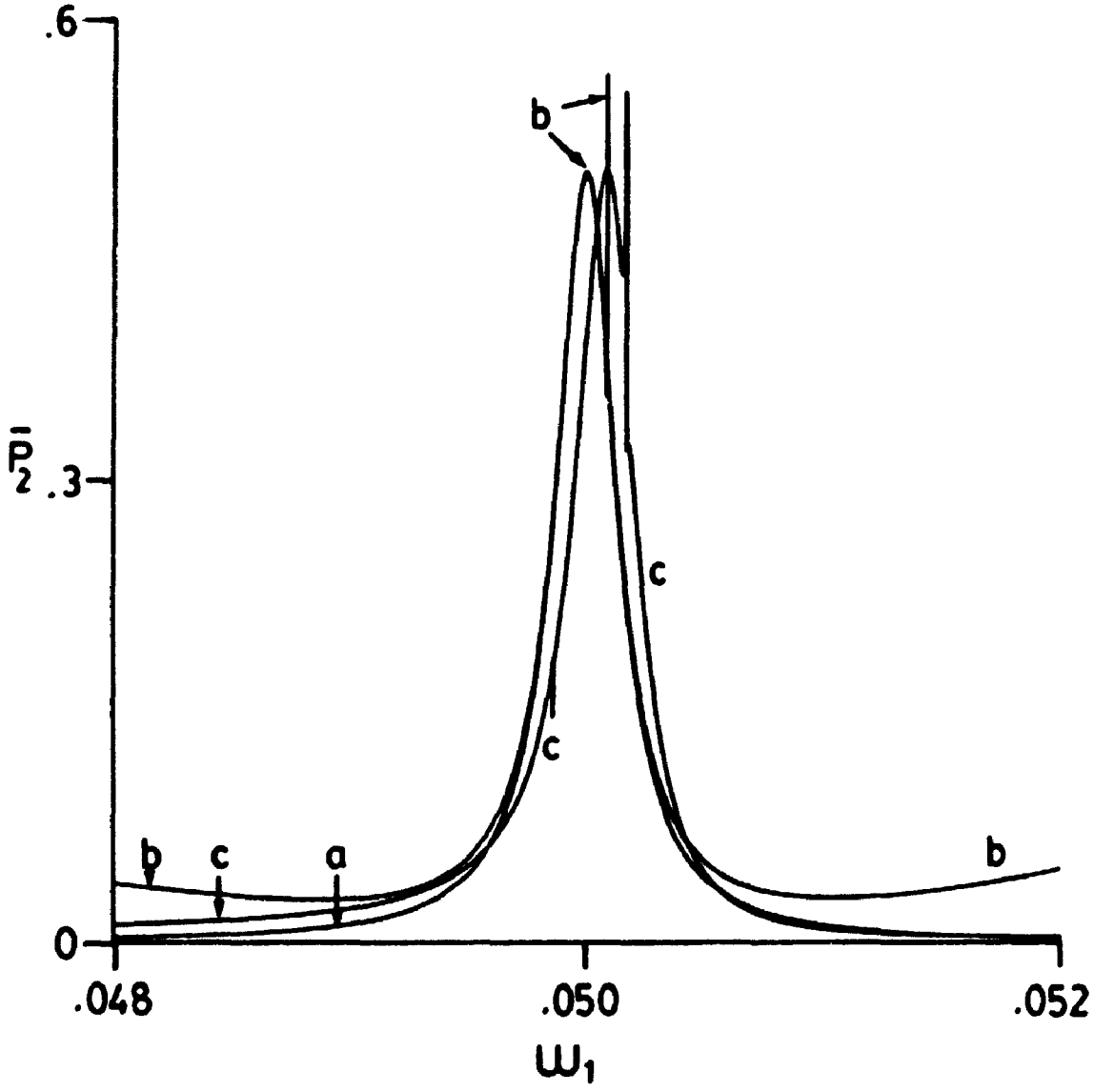

Figure 5.4 The DR-RWA, MR-RWA and exact resonance profiles as a function of ω_1 with $\omega_2 = \Delta E$, all other parameters as in Fig. 5.3. (a) the DR-RWA results based on C(2,0); (b) the MR-RWA results based on C(2,0) and C(0,1); (c) the exact results.

DR-RWA, applied to the (2,0) resonance, yields a reasonable result for the resonance profile. The criterion (5.1.13) is met since $|C(2,0)| = 3.04\times10^{-4}$ is much smaller than $\omega_1 = 0.05$. The DR-RWA result is a single broad Lorentzian curve centred at $\omega_1 = \Delta E = 0.05$ with FWHM $= 6.08\times10^{-4}$.

In Fig. 5.4, the MR-RWA result based on (5.3.1) is a broad peak centred at $\omega_1 = 0.05$ where $\bar{P}_2 = 0.50$, with a second very sharp resonance occurring at $\omega_1 \simeq 0.0500876$ with $\bar{P}_2 \simeq 0.56$. On the low frequency side of the sharp resonance, there is a local minimum of $\bar{P}_2 \simeq 0.35$ ($\omega_1 \simeq 0.0500875$) in the background of $\bar{P}_2 \simeq 0.38$ provided by the broad peak. By comparison with the DR-RWA result, the broad peak is due to the (2,0) resonance. The FWHMs and the heights of the MR-RWA and the DR-RWA resonance profiles are graphically indistinguishable. The two differ off-resonance, where the MR-RWA resonance profile begins to increase as $|\Delta E - 2\omega_1|$ increases, while graphically and from the DR-RWA result, (5.1.8), $\bar{P}_2^{(2,0)} \to 0$ as $|\Delta E - 2\omega_1|$ increases. The narrow transition in the MR-RWA result corresponds to the competing resonance, the (0,1)-photon transition. This transition is highly perturbed by the (2,0)-photon transition, as indicated by the frequency shift and the high population inversion. A FWHM for this narrow peak is not meaningful as it is primarily masked by the (2,0) resonance.

Like the MR-RWA result, the exact calculation for the example of Fig. 5.4 has two overlapping resonances: a broad peak with a maximum of $\bar{P}_2 = 0.501$ is centred at $\omega_1 = 0.0500861$ while a sharp spike with a maximum of $\bar{P}_2 = 0.552$ occurs at $\omega_1 = 0.0501684$. At $\omega_1 = 0.050174$, the sharp transition dips to $\bar{P}_2 = 0.319$, slightly below the background $\bar{P}_2 = 0.323$ provided by the broad peak. In addition, a second dip in

the exact resonance profile from $\bar{P}_2 = 0.180$ to $\bar{P}_2 = 0.146$ occurs at $\omega_1 = 0.0498615$ (a computational grid size of $\Delta\omega_1 \simeq 8\times10^{-7}$ is used around this dip). The broad resonance profile has a FWHM $\simeq 3.0\times10^{-4}$, which agrees very well with the DR-RWA FWHM(2,0) $= 3.04\times10^{-4}$. Again, the FWHM of the narrow resonance transition cannot be determined in the exact calculation due to the overlap of the (2,0)-resonance profile, but by comparison with the MR-RWA results based on (5.3.1), this spike is identified as being due to the (0,1)-photon transition. The resonance frequencies of the broad and narrow transitions are separated by $\Delta\omega_1 = 0.0000823$ in the exact calculation, compared to $\Delta\omega_1 = 0.0000876$ in the MR-RWA result, a difference of 6.4%. As $|\Delta E - 2\omega_1|$ increases, the steady state population of the excited state in the exact calculation follows the trend of the DR-RWA result, not the MR-RWA results, and tends to zero It is noted that at $\omega_1 = 0.05$, $\bar{P}_2 = 0.388$, which corresponds to the background population of the exact calculation from Fig. 5.3.

The dip in the exact resonance profile of Fig. 5.4 at $\omega_1 = 0.0498615$ may correspond to the resonance transition associated with the third strongest competing resonance, (-2,2). Since $C(-2,2) = 1.6\times10^{-13}$, this transition in the exact calculation would be too narrow to be seen with the $\Delta\omega_1$ grid size used. It is unlikely that this dip is an indication of the splitting of the (0,1)-photon transition (as was observed in Fig. 5.3) for three reasons. First, the grid size $\Delta\omega_1 = 8\times10^{-7}$ used around the dip in the exact calculation is fine enough to detect a transition with a FWHM(0,1) $= 5.96\times10^{-6}$. Second, the frequency shifts of the spike and the dip are not symmetric about $\omega_1 = \Delta E/2$ or about $\omega_{1,res}^{(2,0)} = 0.0500861$, while the high and low

frequency shifts of the split (0,1)-photon transition in Fig. 5.3 are symmetric about $\omega_2 = \Delta E$. Finally, no such splitting of the (0,1)-photon transition is observed in the MR-RWA results.

The perturbation of the (0,1)-photon transition of Fig. 5.3 by the (2,0)-photon transition can be substantially decreased by moving ω_1 away from $\Delta E/2$. In Fig. 5.5, the exact and DR-RWA resonance profiles as a function of ω_2 are illustrated for the model molecule interacting with the applied fields with parameters $\omega_1 = 0.045$, $\mathcal{E}_1^0 = 1.25\times10^{-3}$ and $\mathcal{E}_2^0 = 10^{-6}$. The field strengths are as in Figs. 5.3 and 5.4, ω_1 is constant and ω_2 is varied between $0.0999 \leq \omega_2 \leq 0.1003$. For these field parameters, the dominant molecule-EMF coupling in (5.1.5) is $C(0,1) = 2.98\times10^{-6}$, with the largest competing resonance coupling being $C(-20,10) < 10^{-92}$. The conditions of applicability of the DR-RWA are met: only one resonance is significant in (5.1.5), since $|C(0,1)| \gg |C(N_1,N_2)|$, $N_1,N_2 \neq 0,1$; and $|C(0,1)| \ll \omega_1/9$, see (5.1.13).

The DR-RWA resonance profile in Fig. 5.5 is a narrow peak of $FWHM(0,1) = 5.96\times10^{-6}$ centred at $\omega_2 = \Delta E$. The results of the exact calculation show a single resonance peak with a maximum value of $\bar{P}_2 = 0.502$ centred at $\omega_2 = 0.1001805$, and a FWHM $\sim 6\times10^{-6}$. The exact and DR-RWA FWHMs agree within 1%; the Bloch-Siegert shift to high ω_2 of the exact resonance is less than 0.2%. Once the resonance frequency of the exact calculation is normalized to that of the DR-RWA, the exact and DR-RWA resonance profiles are graphically indistinguishable, except for the slight off-resonance background present in the exact calculation.

In the examples of this section, the field strengths of the lasers have been picked to help illustrate the conditions under which the

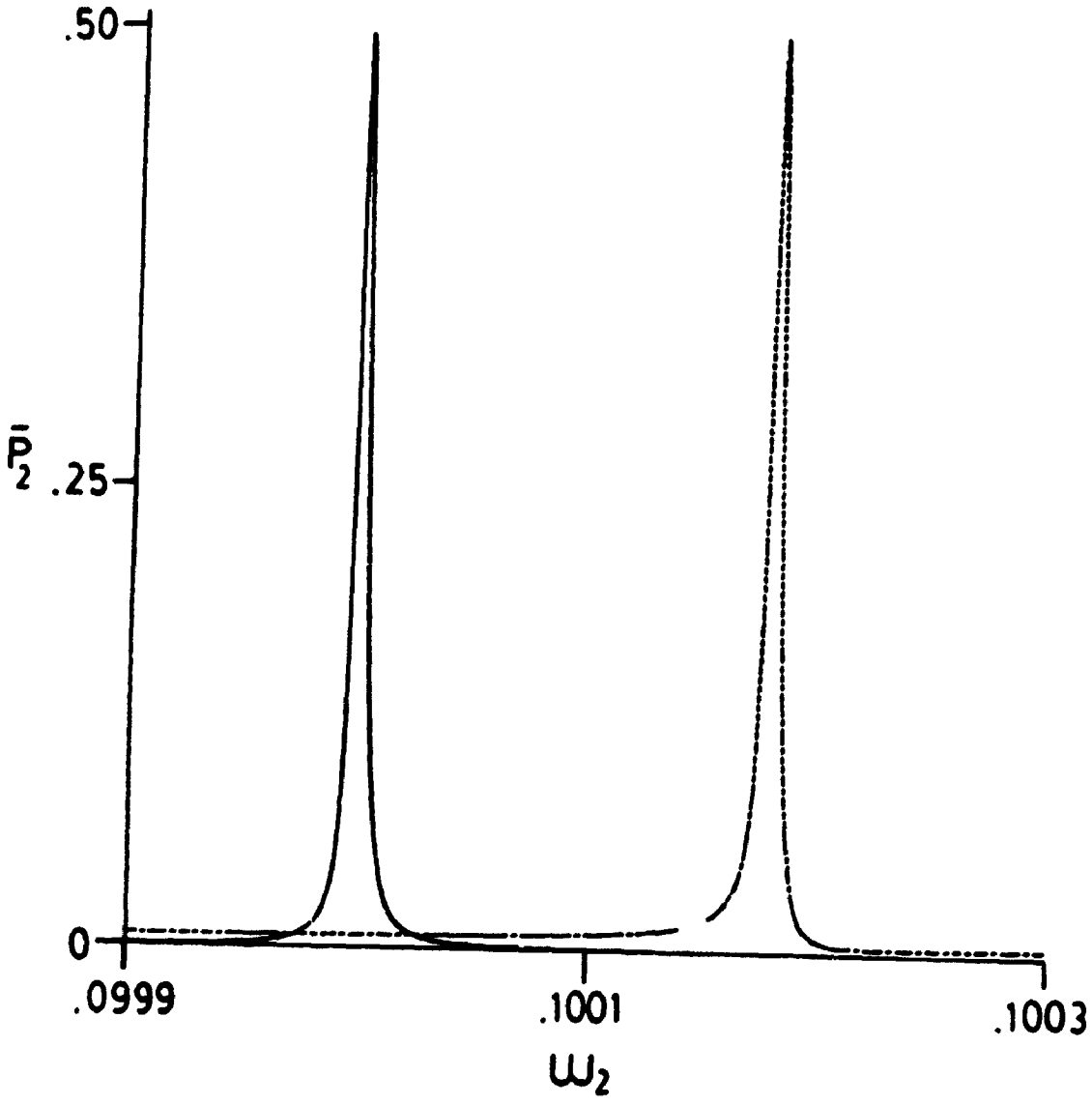

Figure 5.5 The DR-RWA and exact resonance profiles as a function of ω_2 for the system specified in Fig. 5.3, except $\omega_1 = 0.45\Delta E$. The solid line represents results from the DR-RWA analytical solution based on C(0,1) while the dashed line represents the results of the exact calculation.

DR-RWA applies. Generally, the RWA becomes more appropriate as the field strengths decrease.

5.4. SOME GENERAL COMMENTS

In Sec. 5.1, the RWA is applied to the interaction of a two-level system with two CW lasers such that the resonance condition is satisfied by a combination of the field frequencies. The RWA solution for the molecule-EMF coupling, derived in Sec. 5.1.1, is considerably more complicated than the one-field analogue; the conditions of applicability, discussed in Sec. 5.1.2, for the two-field RWA, are correspondingly more restrictive. It is important to recognize that the conditions for the validity of the RWA, for $d = 0$ or $d \neq 0$ and for both one- and two-colour problems, are qualitative; this comment applies to the two-colour problem in particular, due to the wide variety of possible multi-photon transitions that can arise for given values of the laser frequencies. Section 5.2 presents a modification of the exact computational techniques, used in one CW field-molecule interactions, for the treatment of two-field, two-colour analogue. In Sec. 5.3, two-field, two-colour RWA and exact results are compared in order to understand the applicability of the RWA in a more quantitative fashion. Several examples are given of multi-photon, two-colour, two-level resonance profiles, corresponding to one laser frequency fixed and the other one varied, calculated in the DR-RWA, MR-RWA and by using the exact two-level Hamiltonian. The associated discussions help quantify the conditions for the validity of the DR-RWA discussed in Sec. 5.1.2, as a function of the parameters characterizing the applied

CW lasers, and help demonstrate the interpretive and predictive nature of the analytical two-colour RWA results.

For one CW laser, the RWA expression for the N-photon molecule-EMF coupling is given by (2.3.10); the corresponding N-photon resonance profile $\bar{P}_2^N$ is given by (2.3.17). When $d \neq 0$, two-colour spectroscopy is much more flexible than its one laser analogue due to the additional parameters that characterize the two-colour laser-molecule interaction ($\mathcal{E}_1^0$, $\mathcal{E}_2^0$, N_1, N_2, ω_1 and ω_2 subject to $\Delta E = N_1\omega_1 + N_2\omega_2$) versus the one laser-molecule interaction ($\mathcal{E}^0$ and ω subject to $\Delta E = N\omega$). In the two-colour problem, there are many more multi-photon resonances, including those corresponding to one frequency exceeding the energy separation between the molecular states. A wide range of frequencies and frequency combinations, and field strengths and field strength combinations, can be used to tune in a wide variety of multi-photon, two-colour transitions characterized by the values of N_1 and N_2. For both types of spectroscopy, the RWA results for the molecule-EMF coupling can be used to estimate the values of the field parameters that optimize a given multi-photon transition.

The nature of the frequency shifts from the ideal RWA resonance in two-field, two-colour investigations should be of great interest. In the numerical examples of Sec. 5.3, these shifts could be substantial even for relatively weak molecule-EMF couplings. In all cases, the shift was to greater frequency than the RWA prediction, although this is probably not the case in general, given the occurrence of negative Bloch-Siegert shifts when $d \neq 0$ in the one-field analogue [2,3,26,34]. In Fig. 5.2, the $(N_1,1)$-photon spectral peaks were identified for $N_1 = 2,1,0,-1$, in part by the proximity of the exact resonance

frequencies to the RWA predictions, and in part according to the changes in the FWHM(N_1,1) as a function of N_1, or equivalently, of ω_2. Had a large negative shift in the resonance frequency ω_2 (as opposed to a small positive shift) been assumed, these transitions would have been incorrectly identified as corresponding to $N_1 = 1,0,-1,-2$, respectively. The understanding of the resonance frequency shifts in two-colour spectroscopy could be critical for a study of sequential (N_1+n,N_2)-photon transitions, n = 0,1,2..., where the frequency shifts are large ($\simeq\frac{1}{2}\omega_1$) and where the FWHM($N_1$+n,$N_2$) are too similar to distinguish the transitions. Clearly, the photonicity of the transition could be in error by $N_1 \pm 1$.

In Sec. 6.2.3, the effect of neighbouring energy levels and neighbouring transitions on two-field induced transitions between two excited states is investigated. The two-field, two-colour RWA molecule-EMF coupling, (5.1.6), plays a significant role in the interpretation of the time-dependent molecular state populations.

CHAPTER 6

PERMANENT DIPOLE MOMENTS

AND THE EFFECTS OF NEIGHBOURING ENERGY LEVELS

The examples of the previous chapters have focused on isolated two-level systems. This is a valid approximation for a many-level molecule when the external field does not interact strongly with neighbouring energy levels, or when other states do not strongly perturb the two-level molecule-EMF interaction. The energy level which will most strongly perturb a transition between two states is one which has a resonance lying close in energy to the one- or multi-photon resonance transition between the two states of interest. Nearby energy levels to the two states of interest can also cause changes in resonance frequencies relative to the isolated two-level system. Here, the effects of neighbouring states on $j \rightarrow k$ transitions, for $d_{kj} \neq 0$ versus $d_{kj} = 0$, are considered, where $d_{kj} = \mu_{kk} - \mu_{jj}$.

Some of the examples of Chapter 3, and those in Chapter 4, investigate a molecule-EMF coupling node for the one-photon resonance transition in a two-level system. In Sec. 6.1, numerical examples are presented which indicate that the effects of nodal or near nodal coupling persist in a three level system; the changes in the time-dependent and long time-averaged population of state two relative to the two-level analogue are discussed.

Section 6.2 is devoted to a pump and probe temporal investigation of a many-level system. A Gaussian pulsed laser is used to initially excite the molecule from the ground (E_1) to the first excited state (E_2). One or two CW lasers are then used to probe the effects of permanent dipole moments on the $E_2 \rightarrow E_5$ transition for which d_{52} is large. The effects of the neighbouring energy levels (E_3, E_4, E_6, $E_7 \approx 2(E_5 - E_2)$) are investigated by studying "pseudo-molecules", where the energy of state seven is shifted relative to the original seven-level system, or states three and four are removed to produce a five-level system. Even for these many-level systems, the two-level RWA solutions are important for the prediction and interpretation of the results of exact calculations. The $1 \rightarrow 2$ transition due to pulsed laser-molecule interactions in Sec. 6.2.1, and the $2 \rightarrow 5$ transition due to CW laser-molecule interactions in Sec. 6.2.2, can be interpreted in terms of the one-field RWA molecule-EMF coupling. The two-field DR-RWA results from Chapter 5 are relevant in Sec. 6.2.3, where the $2 \rightarrow 5$ transition is probed using two CW lasers of different frequencies. In what follows, the RWA molecule-EMF couplings for the N-photon (or (N_1,N_2)-photon) $j \rightarrow k$ transition are calculated at the ideal resonance frequency, $\omega_{res} = E_{kj}/N$ (or $\omega_{2,res} = [E_{kj} - N_1\omega_1]/N_2$).

6.1 NODAL OR NEAR-NODAL MOLECULE-EMF COUPLING

In Secs. 3.4.2 and 4.2, the effects of a molecule-EMF coupling node were investigated by studying the temporal evolution of the excited state of a two-level system. There are also spectral consequences to a nodal molecule-EMF coupling [2,3,34]. Indeed, resonance profiles can often be used to identify the field parameters

required to generate a resonance molecule-EMF coupling minimum. This technique is illustrated in Sec. 6.1.1 for the two-level system of Secs. 3.4.2 and 4.2, and extended in Sec. 6.1.2 to a three-level system.

6.1.1. TWO-LEVEL RESONANCE PROFILES

The two-level numerical examples in Secs. 3.4.2 and 4.2 were based on the one-photon $S_0 \rightarrow S_1$ transition of 1-[p-(N,N-dimethyl-amino)-phenyl]-4-(p-nitrophenyl)-1,3-butadiene. The molecular parameters of this system are $E_1 = 0.0$, $E_2 = 0.0859$, $(\Delta E = 0.0859)$, $\mu_{11} = 0.0$, $\mu_{22} = 11.8$, $(d_{21} = 11.8)$, and $\mu_{12} = 3.93$ [28,34,40]. It was found that for the two-level system interacting with a CW laser, the period of both the fixed-phase ($\delta = 0$) and phase-averaged exact one-photon resonant time-dependent excited state population was a maximum for a field strength such that $9.10 \leq \underline{d}_{21} \cdot \hat{e}\mathcal{E}^0/E_{21} \leq 9.30$, where $E_{kj} = E_k - E_j$. The field strengths investigated were $\mathcal{E}^0 \approx 0.0677$, 0.0670 and 0.0662, corresponding to $\underline{d}_{21} \cdot \hat{e}\mathcal{E}^0/E_{21} = 9.30$, 9.20 and 9.10, respectively. In keeping with the examples of Secs. 3.4.2 and 4.2.2, the examples here focus on the fixed-phase $\delta = 0$ results, with particular emphasis, initially, on the field strength $\mathcal{E}^0 \approx 0.0677$. The resonance profiles for the two-level system interacting with a $\delta = 0$ CW laser at the three field strengths above are illustrated in Fig. 6.1.

For $\mathcal{E}^0 \approx 0.0677$, the long time-averaged excited state populations, $\bar{P}_2(\delta = 0)$, as a function of ω/E_{21}, are given in Fig. 6.1a and 6.1b for $d_{21} = 0$ and $d_{21} \neq 0$, respectively. When $d_{21} = 0$, the excited state is highly saturated, even for frequencies far from resonance; $\omega_{res} = 1.67E_{21}$ with $\bar{P}_2(\delta = 0) = 0.695$. The time-dependent excited

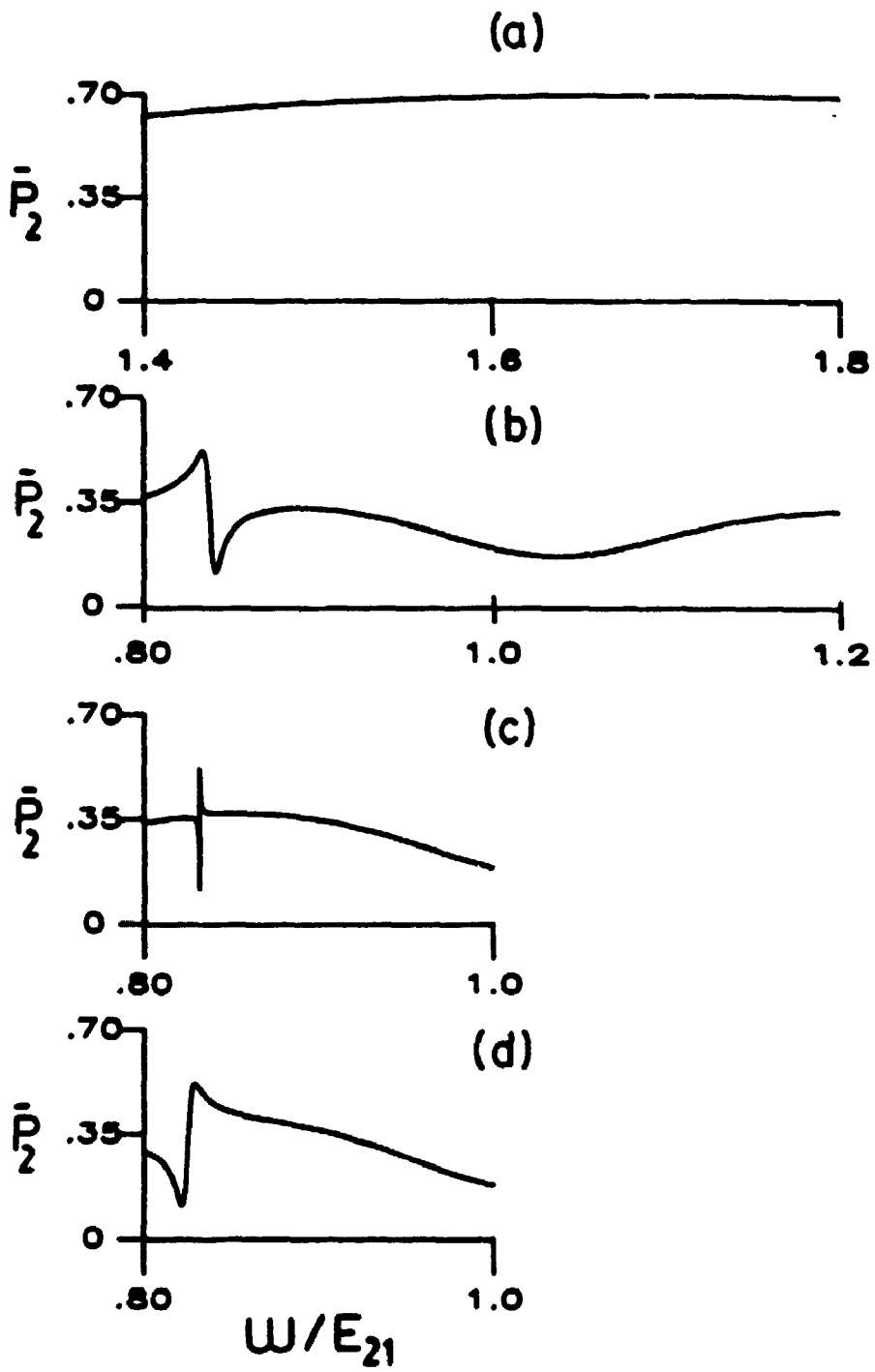

Figure 6.1. The long time-averaged excited state population $\bar{P}_2(\delta = 0)$ as a function of ω/E_{21} for the two-level system of Sec. 3.4.2 interacting with a CW laser of strength $\mathcal{E}^0$: (a) $d_{21} = 0$, $\mathcal{E}^0 \approx 0.0677$; (b) $d_{21} \neq 0$, $\mathcal{E}^0 \approx 0.0677$; (c) $d_{21} \neq 0$, $\mathcal{E}^0 \approx 0.0670$; (d) $d_{21} \neq 0$, $\mathcal{E}^0 \approx 0.0662$.

state population at the resonance frequency is given in Fig. 3.3a. When $d_{21} \neq 0$, the resonance profile is highly asymmetric, with the resonance peak $\bar{P}_2(\delta = 0) = .517$ at $\omega_{res} = 0.835E_{21}$. The associated time-dependent excited state population is given in Fig 3.3a', over one period, $T_{exact} \simeq 6.2\text{x}10^3$. From Fig. 6.1b, the $d_{21} \neq 0$ resonance profile has a high off-resonance background, with a sharp minimum of $\bar{P}_2(\delta = 0) = 0.11$ at $\omega_{min} = 0.842E_{21}$; this dip can be qualitatively explained [2.3,34] by the RWA.

The RWA predicts the $d_{21} \neq 0$ molecule-EMF coupling, (2.3.10), will have nodes at certain values of the parameter $z = \underline{d}_{21} \cdot \hat{e}\mathcal{E}^0/\omega$. If a coupling node is generated, for a given molecule interacting with a CW laser with field strength $\mathcal{E}^0$ at ω_{res}, the resulting resonance profile will be an extremely narrow spike, since the FWHM, (2.3.18), is infinitely small. On the other hand, if the given coupling node is generated with field strength $\mathcal{E}^0$ and an off-resonance frequency (denoted ω_{min}), the resonance profile will contain a "dip" in the off-resonance background population, due to the sharp decrease in the molecule-EMF coupling as it passes through the node at ω_{min}. Since the molecule-EMF coupling is frequency dependent, the greater the separation between the resonance frequency and the frequency associated with the molecule-EMF coupling minimum, the greater the resonance coupling, and correspondingly, the wider the resonance spectral peak.

According to the RWA, for a given molecule-EMF coupling node, $z_{min} = \underline{d}_{21} \cdot \hat{e}\mathcal{E}^0/\omega_{min}$ is a constant; hence, for a fixed d_{21}, ω_{min} will change if $\mathcal{E}^0$ is changed. Conversely, $z_{res} = \underline{d}_{21} \cdot \hat{e}\mathcal{E}^0/\omega_{res}$ is free to vary if $\mathcal{E}^0$ is changed. Furthermore, shifts in ω_{res} due to small changes in $\mathcal{E}^0$ will be small for weak molecule-EMF couplings (see

below). (Although the RWA predicts $\omega_{res} = E_{21}$, the exact values of the resonance frequency are used in the following discussion.) Thus, an on-resonance nodal molecule-EMF coupling can be generated by changing the field strength such that $\omega_{min} \simeq \omega_{res}$. In general, a change in the sign of $\omega_{min} - \omega_{res}$ with a change in field strength from $\mathcal{E}^0$ to $\mathcal{E}^{0'}$ indicates the molecule-EMF coupling has passed through a minimum for a field strength between these two. The sign of $\omega_{min} - \omega_{res}$ indicates whether the field strength should be increased ($\omega_{min} - \omega_{res} < 0$) or decreased ($\omega_{min} - \omega_{res} > 0$). For example, when $\mathcal{E}^0 \simeq 0.0677$, $\omega_{min} = .842E_{21}$ is greater than $\omega_{res} = 0.835E_{21}$; therefore, a slight decrease in the field strength will shift z_{res} closer to z_{min}.

Figures 6.1c and 6.1d show the $d_{21} \neq 0$ fixed-phase ($\delta = 0$) long time-averaged population of state two for $\mathcal{E}^0 \simeq 0.0670$ and 0.0662, respectively; the $d_{21} = 0$ analogues are not given explicitly, but are very similar to Fig. 6.1a, with $\bar{P}_2$ highly saturated across a wide range of frequencies around the associated resonance frequency. When $\mathcal{E}^0 \simeq 0.0670$ and $d_{21} \neq 0$, Fig. 6.1c, the resonance peak is very sharp, with $\bar{P}_2(\delta = 0) = 0.518$ at $\omega_{res} = 0.8322E_{21}$ and $\bar{P}_2(\delta = 0) = 0.11$ at $\omega_{min} = 0.8320E_{21}$. When $\mathcal{E}^0 \simeq 0.0662$ and $d_{21} \neq 0$, Fig. 6.1d, $\bar{P}_2(\delta = 0) = 0.519$ at $\omega_{res} = 0.830E_{21}$, and $\bar{P}_2(\delta = 0) = 0.11$ at $\omega_{min} = 0.822E_{21}$. For these two field strengths, the frequency of the "dip" is at a lower frequency than ω_{res}, in contrast to when $\mathcal{E}^0 \simeq 0.0677$.

The shift in ω_{min} from greater than to less than ω_{res} when the field strength is changed from $\mathcal{E}^0 \simeq 0.0677$ to $\mathcal{E}^0 \simeq 0.0670$ is the RWA spectral indicator of a resonance molecule-EMF coupling node. Thus, the differences in the resonance profiles between Figs. 6.1b and 6.1c

($\mathcal{E}^0 \simeq 0.0677$ and $\mathcal{E}^0 \simeq 0.0670$, respectively) are the result of the changing resonance molecule-EMF coupling as it passes through a node or minimum when $9.20 \leq \underline{d}_{21} \cdot \hat{e}\mathcal{E}^0/E_{21} \leq 9.30$. These limits confirm, and refine, those obtained from the temporal investigations of Chapters 3 and 4, where the lower limit was $\underline{d}_{21} \cdot \hat{e}\mathcal{E}^0/E_{21} = 9.10$. It was recognized in these earlier chapters that $\mathcal{E}^0 \simeq 0.0677$ was not the optimal choice of field strength, and that $\mathcal{E}^0 \simeq 0.0670$ generates a much longer period (the former was chosen so the $d_{21} = 0$ and $d_{21} \neq 0$ phase-averaged time-dependent population of state two could be easily viewed on the same time scale).

Figure 6.1 suggests that the examination of the calculated spectra as a function of field strength is an alternative means to the temporal investigations of Secs. 3.4.2 and 4.2 for finding a fixed-phase molecule-EMF coupling minimum when $d_{21} \neq 0$. This idea is extended next to a three-level system, and also applies to phase-averaged resonance profiles which complement the phase-averaged temporal studies such as those in Sec. 4.2.1.

6.1.2. A THREE-LEVEL MODEL SYSTEM

In the investigations of Secs. 3.4.2 and 4.2, the field strengths employed to generate the molecule-EMF coupling minimum are very large, and possible saturation of neighbouring energy levels is a concern. Here, a third energy level is added to the two-level system, and the molecular system is described, in matrix notation, by the energy and dipole moment matrices,

$$\underline{E} = \begin{bmatrix} 0 & 0 & 0 \\ 0 & 0.0859 & 0 \\ 0 & 0 & 0.1074 \end{bmatrix}, \quad \underline{\mu} = \begin{bmatrix} 0.00 & 3.93 & .9825 \\ 3.93 & 11.8 & 1.965 \\ .9825 & 1.965 & 8.85 \end{bmatrix} \qquad (6.1.1)$$

The molecular parameters of the two-level system are contained in the first two rows and columns of the energy and dipole moment matrices. The energy, transition and permanent dipole moments of the third stationary state correspond to $E_{31} = 1.25E_{21}$, $\mu_{13} = 0.25\mu_{12}$, $\mu_{23} = 0.5\mu_{12}$, and $\mu_{33} = .75(\mu_{22} - \mu_{11})$, and were chosen such that the $1 \rightarrow 2$ transition retains the strongest transition dipole, and the greatest difference in permanent dipoles between the states. The transition and permanent dipole moments are taken to be aligned with the linearly polarized CW field with $\delta = 0$.

The long time-averaged and time-dependent excited state populations are calculated for the three-level system by using the Taylor series and Floquet techniques, see Sec. 2.2. The evolution operators are calculated to 12 figure accuracy with a 13 term Taylor series over an interval size of $\Delta t = 2\pi/180\omega$. The time-dependent excited state populations, calculated from (2.2.33), converge to at least three figures. Numerical integration of the time-dependent populations, using (2.2.39), is performed using Simpson's Rule with 30 integration points, yielding the long time-averaged molecular state populations to greater than graphical accuracy.

Figures 6.2a and 6.2b illustrate, respectively, the $d_{21} = 0$ and $d_{21} \neq 0$ steady state populations $\bar{P}_2(\delta = 0)$ and $\bar{P}_3(\delta = 0)$ as a function of ω/E_{21} for the three level system, when $\mathcal{E}^0 \simeq 0.0677$. When $d_{21} = 0$, state two is highly saturated, and the population of state three is also high, $\bar{P}_3(\delta = 0) \simeq 0.2$, even though the frequency of the CW laser

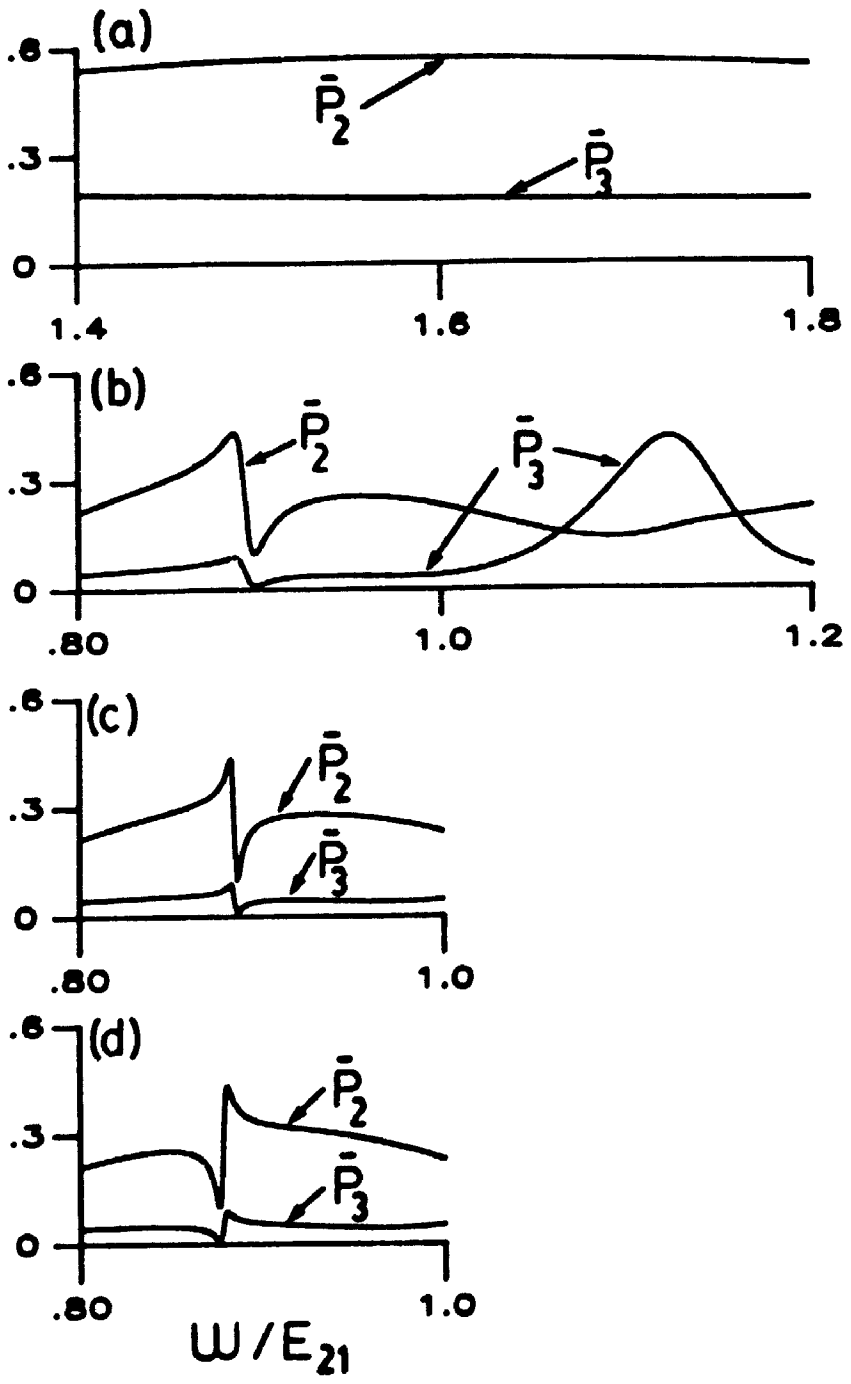

Figure 6.2. The long time-averaged excited state populations $\bar{P}_2(\delta = 0)$ and $\bar{P}_3(\delta = 0)$ as a function of ω/E_{21} for the three-level system, characterized by (6.1.1), interacting with a CW laser of strength $\mathcal{E}^0$: (a) $d_{21} = 0$, $\mathcal{E}^0 \approx 0.0677$; (b) $d_{21} \neq 0$, $\mathcal{E}^0 \approx 0.0677$; (c) $d_{21} \neq 0$, $\mathcal{E}^0 \approx 0.0670$; (d) $d_{21} \neq 0$, $\mathcal{E}^0 \approx 0.0662$.

is not swept near the $d_{21} = 0$ $1 \rightarrow 3$ resonance frequency. For the $1 \rightarrow 2$ transition, $\omega_{res} = 1.58E_{21}$ with $\bar{P}_2(\delta = 0) = 0.569$. Relative to the two-level analogue in Fig. 6.1a, the $1 \rightarrow 2$ resonance frequency has shifted to lower energy, and the maximum steady state population of state two has decreased.

When $d_{21} \neq 0$, Fig. 6.2b, $\bar{P}_2(\delta = 0)$ has a highly asymmetric resonance peak with maximum $\bar{P}_2(\delta = 0) = 0.432$ at $\omega_{res} = 0.8861E_{21}$, a sharp dip in the off-resonance background at $\omega_{min} = 0.898E_{21}$ with $\bar{P}_2(\delta = 0) = 0.10$, and a high off-resonance background. The shape of the resonance profile is very similar to the two-level analogue in Fig. 6.1b. However, for the three-level system, the values of ω_{res}, ω_{min} and the difference between these two frequencies have increased relative to the two-level analogues. For the three-level system, $\omega_{min} - \omega_{res} = 0.012E_{21}$ while for the two-level system, $\omega_{min} - \omega_{res} = 0.007E_{21}$.

In Fig. 6.2b, the steady state population of state three also contains a dip at $\omega_{min} = 0.898E_{21}$, but unlike the $1 \rightarrow 2$ transition, the $1 \rightarrow 3$ resonance peak, centred at $\omega_{res} = 1.124E_{21} = 0.899E_{31}$ with $\bar{P}_3(\delta = 0) = 0.419$, is very symmetric. This symmetry indicates that the molecule-EMF coupling for this transition is approximately constant for frequencies around $\omega_{res} = 1.124E_{21}$.

Although the values of ω_{min} differ for the two- versus three-level systems, the dip in the off-resonance background of $\bar{P}_2(\delta = 0)$ in Fig. 6.2b is interpreted as the consequence of a minimum molecule-EMF coupling. By analogy with the two-level results of Fig. 6.1, it is predicted that a decrease in the field strength from $\mathcal{E}^0 \simeq 0.0677$ for the three-level system will shift ω_{res} and ω_{min} closer together.

In Figs. 6.2c and 6.2d, the $d_{21} \neq 0$ steady state excited state populations are given for the cases where $\mathcal{E}^0 \propto 0.0670$ and 0.0662, respectiveiy. As in the two-level case, the three-level $d_{21} = 0$ resonance profiies for these field strengths are very similar to the one in Fig. 6.2a, when $\mathcal{E}^0 \propto 0.0677$. For $d_{21} \neq 0$ and $\mathcal{E}^0 \propto 0.0670$, $\omega_{res} = 0.8834E_{21}$ with $\bar{P}_2(\delta = 0) = 0.433$ and $\omega_{min} = 0.887E_{21}$ with $\bar{P}_2(\delta = 0) = 0.10$; for $\mathcal{E}^0 \propto 0.0662$, $\omega_{res} = 0.8809E_{21}$ with $\bar{P}_2(\delta = 0) = 0.434$ and $\omega_{min} = 0.877E_{21}$ with $\bar{P}_2(\delta = 0) = 0.10$. As in the two-level case, the decrease in the field strength moves the frequency location of the "dip" to a smaller frequency. However, unlike the two-level analogue, $\omega_{min} - \omega_{res}$ changes sign when the field strength is decreased from $\mathcal{E}^0 \propto 0.0670$ to $\mathcal{E}^0 \propto 0.0662$, rather than when the field strength is decreased from $\mathcal{E}^0 \propto 0.0677$ to $\mathcal{E}^0 \propto 0.0670$. Thus, for the three-level system, the molecule-EMF coupling for the $1 \rightarrow 2$ transition passes through a minimum for $9.10 \leq \underline{d}_{21} \cdot \hat{e}\mathcal{E}^0/E_{21} \leq 9.20$.

In general, when $d_{21} \neq 0$, the population of excited state three is very low for frequencies close to the $1 \rightarrow 2$ resonance. The lack of population in state three, relative to when $d_{21} = 0$, can be attributed to the reduced molecule-EMF coupling due to the presence of permanent dipoles, such that power broadening due to the $1 \rightarrow 2$ and $1 \rightarrow 3$ transitions is not significant for frequencies around ω_{res} for the $1 \rightarrow 2$ transition.

It is clear that the effects of near-nodal molecule-EMF coupling persist in this three-level system. The parameters required to generate the small one-photon $1 \rightarrow 2$ coupling in the three-level system are slightly different from those in the two-level system, with changes occurring in ω_{res} for the $1 \rightarrow 2$ transition, in ω_{min}, and,

significantly, in $\omega_{min} - \omega_{res}$, relative to the two-level system, for a given $\mathcal{E}^0$. The increase (decrease) in the magnitude of $\omega_{min} - \omega_{res}$ when the third energy level is included, has the indirect consequence of increasing (decreasing) the resonance molecule-EMF coupling relative to the two-level analogue. For example, in addition to the discussion for $\mathcal{E}^0 \simeq 0.0677$ already given, when $\mathcal{E}^0 \simeq 0.0670$, for the two-level $d_{21} \neq 0$ system, $\omega_{min} - \omega_{res} = -0.0002E_{21}$ while for the three-level $d_{21} \neq 0$ system, $\omega_{min} - \omega_{res} = +0.004E_{21}$. Comparing Figs. 6.1c and 6.2c, the two-level spectral peak is an extremely sharp spike, whereas the three-level $1 \rightarrow 2$ spectral peak is much broader. Conversely, when $\mathcal{E}^0 \simeq 0.0622$, $\omega_{min} - \omega_{res} = -0.008E_{21}$ for the two-level system while $\omega_{min} - \omega_{res} = -0.004E_{21}$ for the three-level system. Comparing Figs. 6.1d and 6.2d, the two-level spectral peak is slightly broader than the three-level $1 \rightarrow 2$ resonance peak. The impact of the third energy level on the resonance time-dependent excited state populations is investigated next.

The time-dependent excited state populations $P_2(t)$ and $P_3(t)$, as a function of time $0 \leq t \leq 1.16\text{x}10^4$ (281fs), are given in Fig. 6.3a for $\mathcal{E}^0 \simeq 0.0677$ at $\omega_{res} = 0.8861E_{21}$. The time for the population of state two to change from zero to maximum to zero population is $T_{exact} = 4.1\text{x}10^3$ (99fs). Comparing with the temporal behaviour of the two-level analogue, given in Fig. 3.3a', with $T_{exact} = 6.2\text{x}10^3$ (150fs), the time-dependent population of state two for the three-level system has a similar pattern to that in Fig. 3.3a', but a shorter period. However, in keeping with the reduced molecule-EMF coupling when $d_{21} \neq 0$ relative to when $d_{21} = 0$, the period $T_{exact} = 4.1\text{x}10^3$ is still much longer than the three-level $d_{21} = 0$ analogue, where the Rabi period is

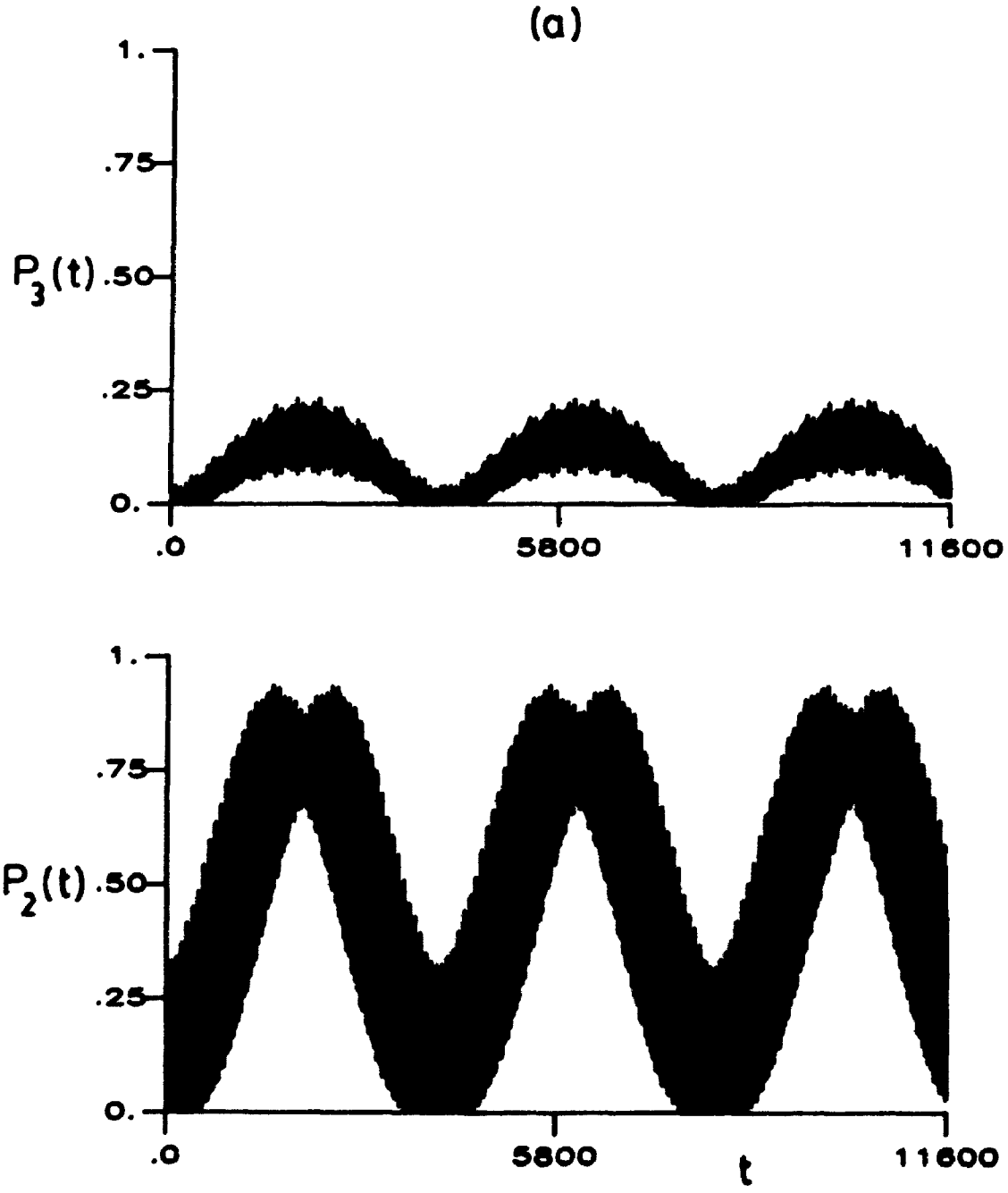

Figure 6.3. The time-dependent excited state populations as a function of time for a three-level molecular system, characterized by equation (6.1), interacting with a continuous wave laser of strength $\mathcal{E}^0$, phase $\delta = 0$, and tuned to the $1 \rightarrow 2$ one-photon resonance frequency, ω_{res}: (a) $\mathcal{E}^0 \approx 0.0677$, $\omega_{res} = 0.8861E_{21}$; (b) $\mathcal{E}^0 \approx 0.0670$, $\omega_{res} = 0.8834E_{21}$. (c) $\mathcal{E}^0 \approx 0.0662$, $\omega_{res} = 0.8809E_{21}$.

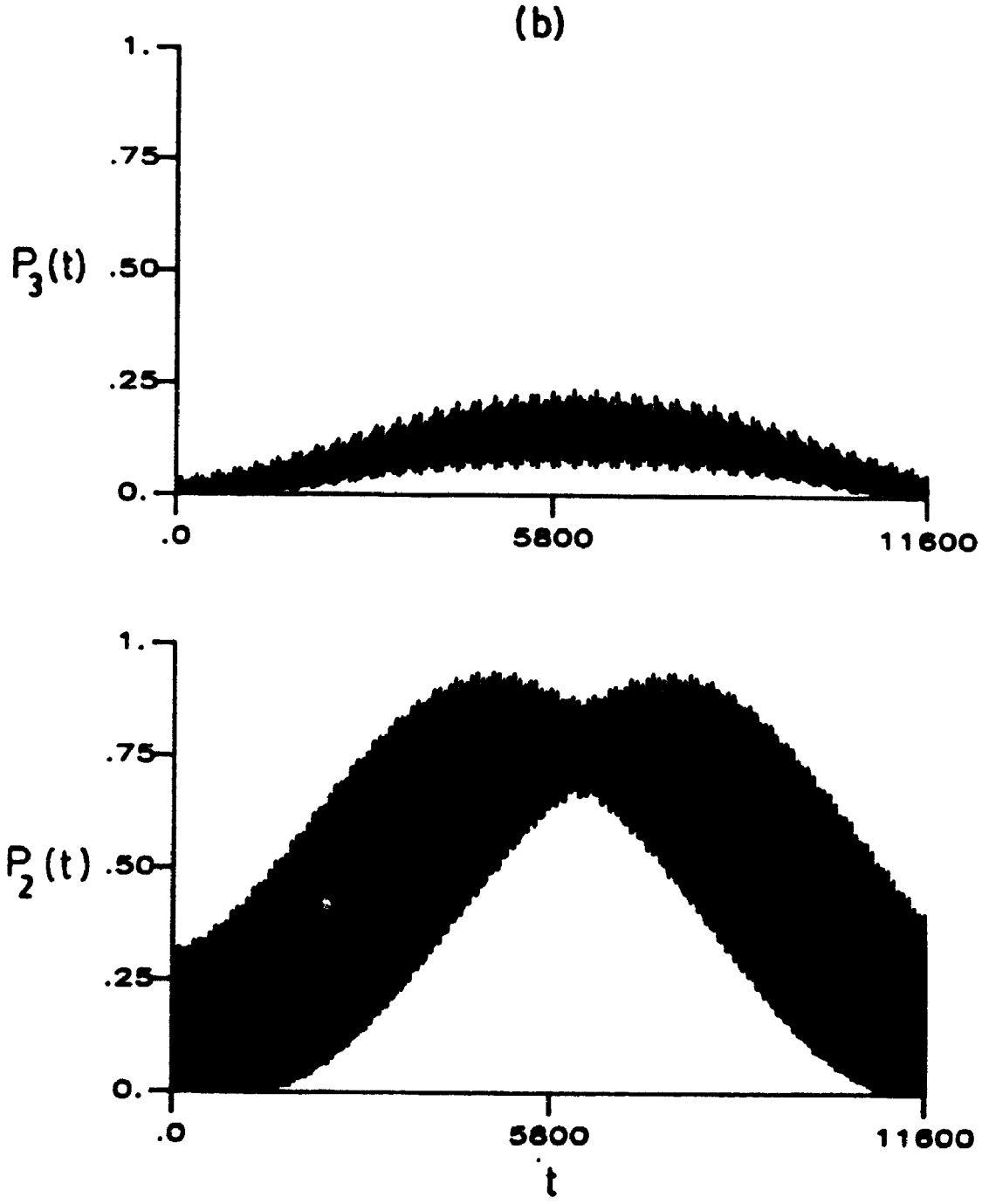

Figure 6.3 continued: Figure 6.3b.

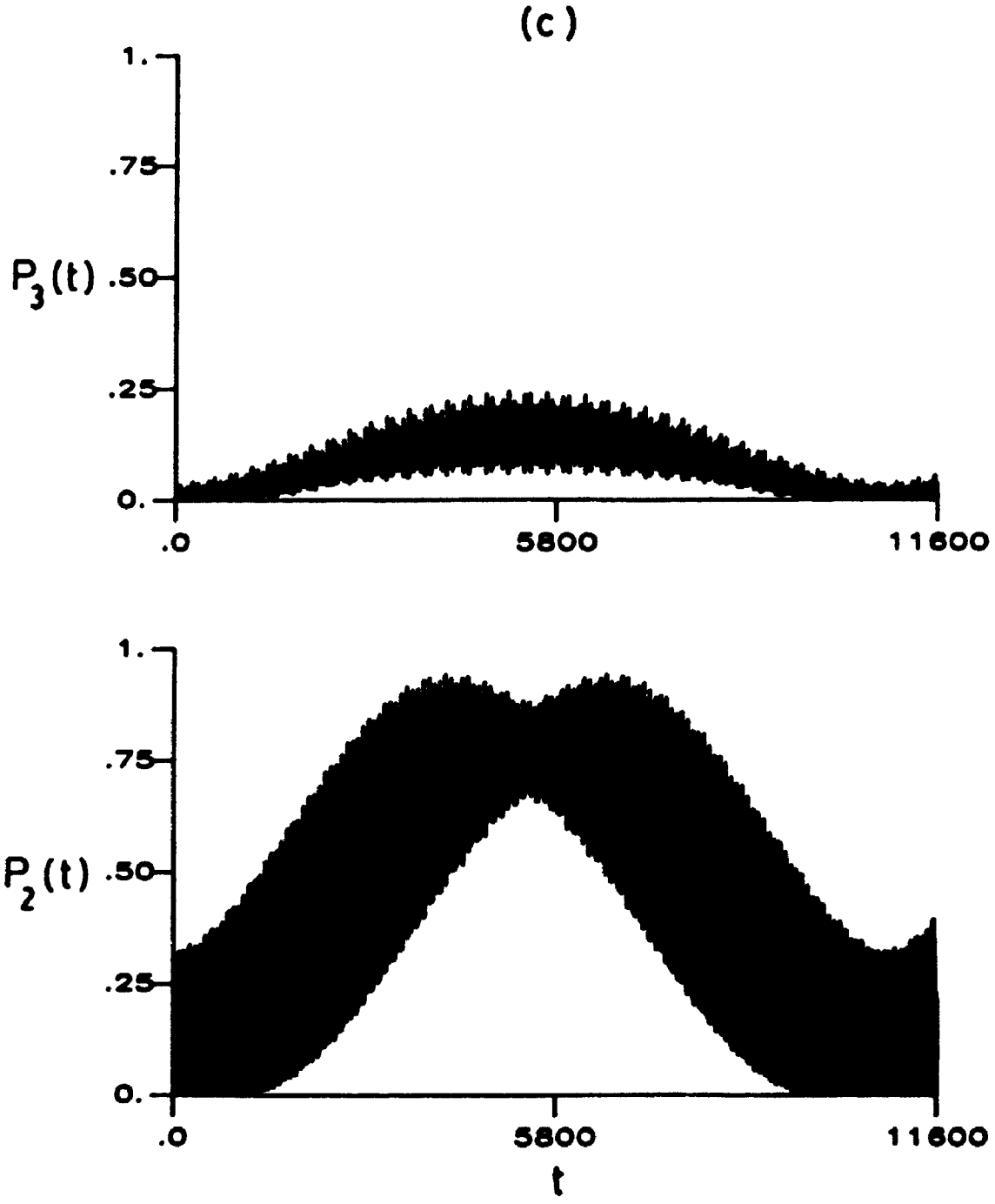

Figure 6.3 continued: Figure 6.3c.

$2\pi/|\underline{\mu}_{12}\cdot\hat{e}\mathcal{E}^0| \simeq 24$ (.6fs).

An extremely long period in the time-dependent excited state population of state two can be found by decreasing the field strength, as suggested by Fig. 6.2. Figures 6.3b and 6.3c show the time-dependent excited state populations when $\mathcal{E}^0 \simeq 0.0670$ and $\mathcal{E}^0 \simeq 0.0662$, respectively. The pattern of the temporal evolution of state two at these field strengths resembles that of Fig. 3.3a', for the two-level system when $\mathcal{E}^0 \simeq 0.0677$, except now the periods are longer than the two-level result, $T_{exact} = 6.2\times10^3$. The period of the three-level time-dependent population of state two is slightly longer when $\mathcal{E}^0 \simeq 0.0670$ than when $\mathcal{E}^0 \simeq 0.0662$: $T_{exact} = 1.2\times10^4$ (290fs) and $T_{exact} = 1.1\times10^4$ (270fs), respectively. From the spectral results of Fig. 6.2, the period could be made even longer by a slight decrease ($\Delta\underline{d}_{21}\cdot\hat{e}\mathcal{E}^0/E_{21} < 0.1$) in the field strength from $\mathcal{E}^0 \simeq 0.0670$ ($\underline{d}_{21}\cdot\hat{e}\mathcal{E}^0/E_{21} = 9.2$).

The resonance profiles of Figs.6.2b-d give examples of the "stealing" of absorption intensity from a level on resonance with a laser by an excited state further off-resonance with respect to the laser frequency. In each case, the frequencies associated with the peak and the dip in $\bar{P}_3$, for $\omega \simeq \omega_{res}(1 \rightarrow 2)$, coincide with those of the $1 \rightarrow 2$ resonance and the associated dip in $\bar{P}_2$. This correlation indicates that state two and three are interacting with the CW laser in a concerted manner, and absorption intensity is being shared between these states through interactions with the ground state and each other. This cooperative behaviour of levels two and three is also seen in the temporal behaviour of these states. For all three field strengths, see Figs. 6.3a-c, the time-dependent population of state three has the same

period as that of state two. Other examples of these types of effects, both temporal and spectral, can be found in the literature [17,36,110].

6.1.3. SOME GENERAL COMMENTS

For the examples given in Sec. 6.1, the spectral and temporal effects of a $d_{21} \neq 0$ molecule-EMF coupling minimum persist when a third neighbouring energy level is considered. The additional energy level, and its energy separation from stationary state two, does affect the value of the resonance frequency for the $1 \rightarrow 2$ one-photon transition relative to the frequency associated with the molecule-EMF coupling minimum. The further the frequency separation between the resonance frequency and the frequency of the coupling minimum, the larger the resonance molecule-EMF coupling. Thus, the resonance frequency shift caused by the presence of a neighbouring energy level can change the period of the $1 \rightarrow 2$ one-photon resonance transition, see for example, Fig. 6.3a versus Fig. 3.3a'. However, appropriate changes in the field strength as outlined above can correct for this effect, by shifting ω_{min} closer to ω_{res}.

In general, the two-level system can be used as a predictive and interpretive model for near nodal molecule-EMF couplings, and to find the approximate field parameters required to generate such couplings. Although the direct quantitative translation of these parameters to the three-level system is not possible for reasons discussed above, only minor adjustments in the field strength appear to be necessary for the three-level example studied here. Like the two-level analogue, the nonlinear behaviour, as a function of $\mathcal{E}^0$ and ω, of the molecule-EMF coupling for the three-level system, can translate minima in the

molecule-EMF coupling to maxima in the periods of the resonance time-dependent state populations.

Changes in other parameters will affect the critical difference between ω_{min} and ω_{res}, when more than two stationary states are considered. For example, in the three-level system of Sec. 6.1.2, the effects of changes in the transition moments μ_{13} and μ_{23}, and the energy separation E_{32} have not been investigated. The difference in the permanent dipole moments between states three and two, and three and one, will also have an impact of the spectral and temporal behaviour associated with the three-level molecule interacting with a CW laser.

6.2. PUMP AND PROBE INVESTIGATIONS OF THE EFFECTS OF PERMANENT DIPOLES IN A MANY-LEVEL MOLECULAR SYSTEM.

The one-field RWA indicates that in the two-level approximation, the molecule-EMF coupling (2.3.10) is a function of the parameter $z = \underline{d}_{21}\cdot\hat{e}\mathcal{E}^0/\omega$, where, on resonance $\omega = E_{21}/N$, and N is the number of photons involved in the transition. From (2.3.10) and the discussions of the previous chapters, the effects of permanent dipoles are enhanced for molecules with large differences in the permanent dipole moments, or small differences in the energies, between the states involved in a transition, or for intense fields [2,3,31,34]. Often, the energy separation between the ground state and the other state(s) of interest can be very large relative to the product $\underline{d}_{kj}\cdot\hat{e}\mathcal{E}^0$. A method of circumventing this large energy gap is to use a pump-probe combination of lasers [111,112]. A "pump" laser is used to generate a highly

populated excited state "B" from the ground state; a second "probe" laser is used to induce transitions between state "B" and a third excited state "C", where the energy gap between "B" and "C" is much smaller than that between "C" or "B" and the ground state.

In this section, a Gaussian pulsed laser is used to "pump" the ground state molecule into the first excited state "B". Immediately following this excitation, one or two CW lasers are tuned to a resonance transition between "B" and another (higher energy) excited state "C". The effects of the permanent dipole moments, neighbouring energy levels, and the differences between one-field, one- and two-photon transitions, and two-field, (0,1)- and (1,1)-photon transitions, between states "B" and "C" are investigated.

An eight-level model molecule is constructed based on the molecule 1-[p-(N,N-dimethyl-amino)-phenyl]-4-(p-nitrophenyl)-butadiyne [113]. The many-level systems which are studied are based on subsets of the eight-level system characterized by the stationary state energies and dipole moment matrix elements [114] given in Table 6.1. Figure 6.4 gives a schematic representation of the energy separations between the stationary states. The transition and permanent dipole moments are taken to be aligned with the direction of polarization of the applied field(s).

The primary transitions of interest are excitation from state 1 to state 2 by a pulsed laser, followed by a probe of the 2 → 5 transition. While a direct probe of the transition 1 → 5 is of course possible, the much smaller energy difference between states two and five render the 2 → 5 transition a more favourable one for investigating the effects of permanent dipoles. States eight and seven will compete for population

Table 6.1. The stationary state energies [114] and dipole moment matrix elements [114] for the eight-level molecular system based on the linear molecule 1-[p-(N,N-dimethyl-amino)-phenyl]-4-(p-nitrophenyl)-butadiyne [113].

E_1	E_2	E_3	E_4	E_5	E_6	E_7	E_8
0.000000	0.139121	0.161480	0.175533	0.203697	0.213477	0.266317	0.280815

$\mu_{jk} = \mu_{kj}$

j = 1	2	3	4	5	6	7	8	k
-4.19953	3.59193	0.11123	1.53366	1.10258	0.11525	-1.09388	-0.03478	1
	-6.55467	-1.07924	-0.38536	-4.62081	1.29951	-1.25418	-0.07814	2
		-5.99205	-0.47189	-2.18021	-0.80311	-0.89247	0.00063	3
			-5.11009	-0.20201	-1.46559	-0.58265	-0.06626	4
				-15.37139	3.44674	4.11064	0.15196	5
					-9.10950	-2.13445	2.17608	6
						-10.92599	1.31415	7
							-7.69679	8

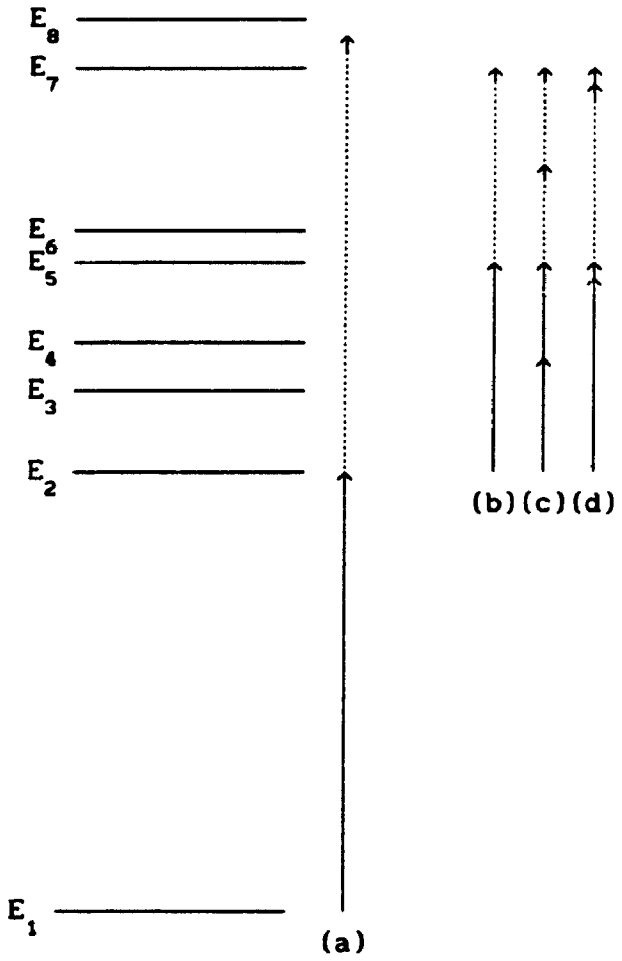

Figure 6.4. Schematic representation of the energy levels of the model molecule in Table 6.1. The solid arrows represent: (a) the 1 → 2 one-photon transition from the pump pulse-molecule interaction; (b) the 2 → 5 one-photon transition from the one CW laser-molecule interaction; (c) the 2 → 5 two-photon transition from the one CW laser-molecule interaction; (d) the 2 → 5 (1,1)-photon transition from the two CW lasers-molecule interaction. The dashed arrows represent some of the possible overlapping resonances.

from states two and five, respectively, since $E_{81} = 0.280815 \simeq 2E_{21} = 0.278242$ and $E_{72} = 0.127196 \simeq 2E_{52} = 0.129152$. In some cases, "pseudo-molecules", which are based on, but slightly different from, the molecule with the parameters given in Table 6.1, are used to investigate the perturbation produced by particular stationary states on the transition of interest.

6.2.1. GENERATION OF A HIGHLY POPULATED EXCITED STATE BY EXCITATION FROM THE GROUND STATE.

In the two-level examples of pulsed laser-molecule interactions in Sec. 4.2, it was shown that the time-dependence of the excited state population for a molecule-pulsed laser interaction is essentially that for the analogous molecule-CW laser interaction, with the CW laser cut off for times longer than the effective pulse duration. The final population of the excited state was determined in large part by the interplay between the pulse duration and the CW-like period of the time-dependent excited state population, where the latter is a function of the strength of the pulsed electric field.

Similarly, for a many-level system, the generation of a highly populated state by a pulsed laser-molecule interaction also requires a balance between a number of factors: the pulse duration τ_p, the pulse strength $\mathcal{E}^0$, and the excited state lifetime $1/\gamma$. The pulse duration must be (1) short enough that the effects of excited state decay do not become a factor before the pump component of the investigation is complete; (2) long enough that the bandwidth of the pulse, (2.1.18), does not result in excitation of neighbouring stationary states; and

(3) long enough to encompass at least half the CW-like period of the resonance time-dependent excited state population. The duration of the CW-like period is a function of field strength, which must be (1) intense enough to fully populate the excited state of interest within the effective pulse duration, and before the effects of excited state decay become significant; and (2) weak enough that power broadening does not result in significant population of the neighbouring states. The delay before, and the duration of, the subsequent probe laser investigation are also factors to be considered with respect to the excited state lifetime.

Here, pulse durations on the order of $\tau_p \simeq 5\text{x}10^3$ (10^2fs) are used; these are sufficiently short such that the effective durations of the pulses, $-4\tau_p < t < +4\tau_p$, are several orders of magnitude smaller than the typical excited state lifetime of a large organic molecule in solution or the gas phase [97,98]. Hence, the effects of excited state decay can be neglected for the pump component of these investigations. On the other hand, the durations are sufficiently long such that, from (2.1.18), the pulse bandwidth, $\Delta\omega < 7\text{x}10^{-4}$, is much smaller than the frequency separation between state two and its closest neighbour, $E_{32} = 0.022359$, and similarly for the two-photon excitation to state eight; excitation of state three and the other states will be minimal.

The field strength is chosen to be on the order of $\mathcal{E}^0 \simeq 10^{-3}$. From (2.3.10), the effect of permanent dipoles on the one-photon $1 \rightarrow 2$ transition will be slight since $z = \underline{d}_{21}\cdot\hat{e}\mathcal{E}^0/E_{21} \simeq 0.0169$, and $2J_1(z)/z \simeq 1$. Consequently, the RWA molecule-EMF coupling for the one-photon $1 \rightarrow 2$ transition, is $C(1) \simeq \mu_{12}\cdot\hat{e}\mathcal{E}^0$. In the absence of strong neighbouring energy level effects, the RWA predicts the Rabi

period will be $2\pi/|\underline{\mu}_{12}\cdot\hat{e}\mathcal{E}^0| \simeq 1.7\text{x}10^3$ ($4\text{x}10^2$fs). Thus, the field strength is sufficiently large and the effective pulse duration is sufficiently long for the latter to incorporate several periods of the time-dependent population of state two.

The molecular system initially studied is a six-level subset of the eight-level system in Table 6.1. Energy levels one through five are retained, as is stationary state eight. The primary transition of interest is the 1 → 2 one-photon transition. States three and four are included to account for one-photon nearby energy level effects. State five is included to establish its initial conditions, ideally zero, for the subsequent probe calculations, since it is the final (probe) state of interest. Finally, state eight has a stationary state energy such that $E_{81} \simeq 2E_{21}$. Since the object of the "pump" is to maximally populate state two, it is important to ensure that the population of state eight, via two-photon or sequential one-photon transitions, remains low. Crude calculations indicate that the additional inclusion of state seven from Table 6.1 has negligible impact on the examples of this section.

The time-dependent excited state populations for this six-level system interacting with a Gaussian pulsed electric field, (2.1.15), of phase $\delta = 0$, carrier frequency $\omega = E_{21}$, field strength $\mathcal{E}^0$ and duration τ_p, is calculated using the half-pulse technique given in Sec. 4.1. The field strengths and durations used are combinations of $\mathcal{E}^0 = 0.001$ or 0.00105 with $\tau_p = 5167.6$ (125fs), 5426.0 (131.25fs) or 4909.3 (118.75fs). A grid size of $\Delta(t/\tau_p) = 0.002$ (2000 Riemann points over the interval $[0,+4\tau_p]$) is sufficiently small to achieve convergence of the time-dependent excited state populations to at least four figures.

Fig. 6.5a shows the time-dependent excited state populations for states two and eight for the six-level system described above interacting with a Gaussian pulsed laser of duration $\tau_p \simeq 5167.6$ (125.00fs) and strength $\mathcal{E}^0 = 0.001$. The populations of states three, four and five are negligible ($P_j(t) < 0.002$, $j = 3, 4, 5$) over the effective duration of the pulse, and zero at $t = +4\tau_p$. The population of state eight remains low, indicating that two-photon and sequential one-photon processes are not a concern; at $t = +4\tau_p$, $P_8(t) = 0.0003$. The time-dependent population of state two goes through five complete cycles from zero to maximum to zero population; its final population after the pulse has effectively vanished is $P_2(t = +4\tau_p) = 0.4446$. The duration of the each cycle is different, but the third cycle under the centre of the pulse, where the effective field strength is essentially $\mathcal{E}^0 = 0.001$, has duration $\Delta t = 0.338\tau_p = 1.75\text{x}10^3$ (42fs), which equals the Rabi period, $2\pi/|\underline{\mu}_{12}\cdot\hat{e}\mathcal{E}^0|$, for the isolated two-level system interacting with a CW laser of strength $\mathcal{E}^0 = 0.001$. The other cycles in $P_2(t)$ are longer; this is not surprising since the effective field strength under the wings of the pulse is less than $\mathcal{E}^0 = 0.001$.

The object of the "pump" pulse-molecule interaction is to produce maximum population of state two. To increase the population of state two from $P_2(t = +4\tau_p) = 0.4446$, different field parameters must be used. In Figs. 6.5b, c,and d, slightly different pulse durations and field strengths are tested. In all three cases, the populations of states three, four and five remain negligible ($P_j(t) < 0.002$, $j = 3, 4, 5$), and are zero at $t = +4\tau_p$.

In Fig. 6.5b, the pulse duration is increased by five percent, τ_p 5426.0 (132.25fs), while the field strength is held fixed,

Figure 6.5. The time-dependent populations of states two and eight of the six-level system, (states E_1, E_2, E_3, E_4, E_5, E_8 from Table 6.1) interacting with a Gaussian pulsed laser of duration τ_p, carrier frequency $\omega = E_{21}$, and strength $\mathcal{E}^0$, as a function of t/τ_p, over the effective duration of the pulse, $[-4\tau_p, +4\tau_p]$. (a) $\tau_p = 5167.6$ (125.00fs), $\mathcal{E}^0 = 0.001$; (b) $\tau_p = 5426.0$ (131.25fs), $\mathcal{E}^0 = 0.001$; (c) $\tau_p = 5167.6$ (125.00fs), $\mathcal{E}^0 = 0.00105$; (d) $\tau_p = 4909.3$ (118.75fs), $\mathcal{E}^0 = 0.001$.

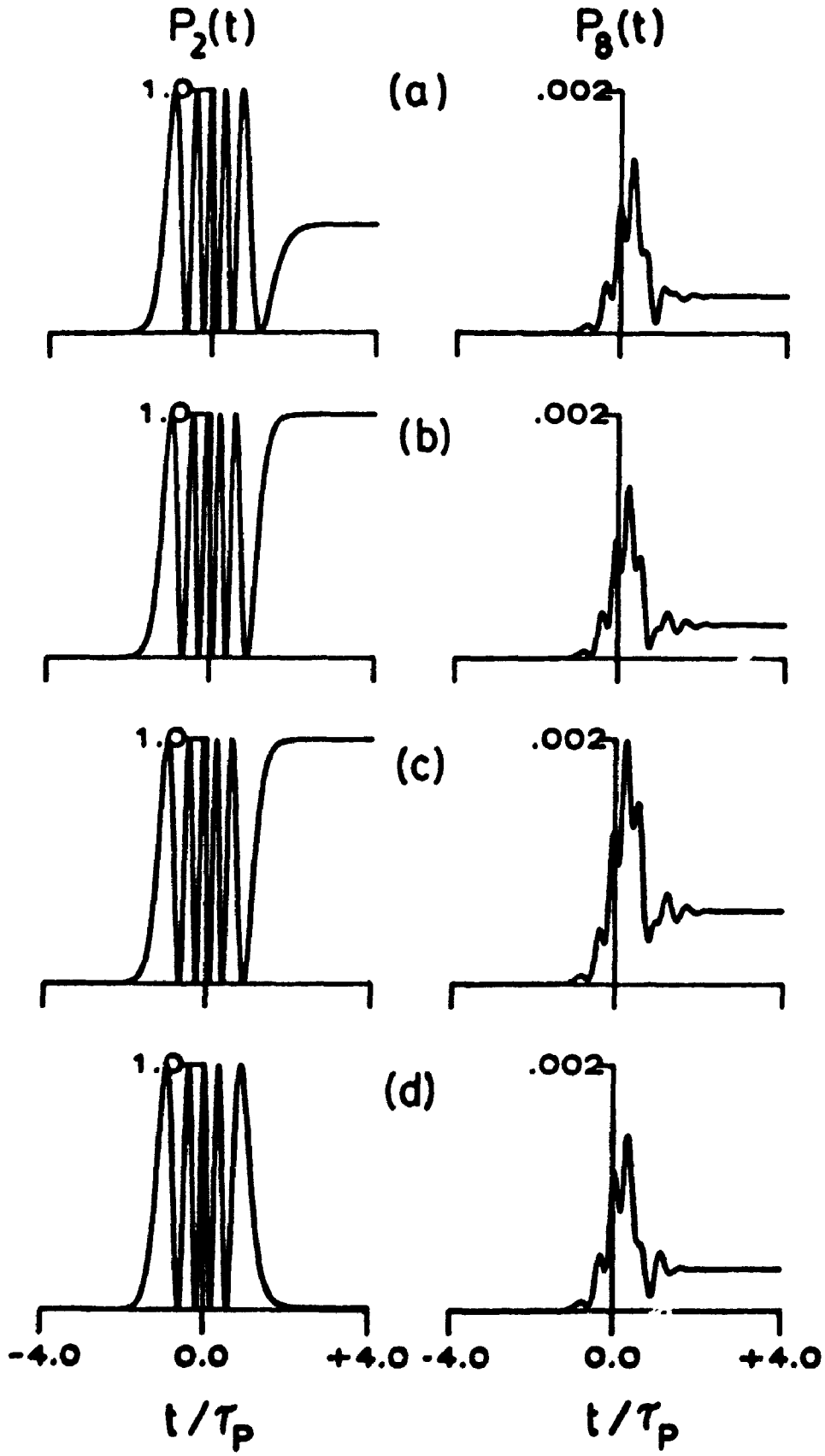
$P_2(t)$
$P_8(t)$
1.0
.002
(a)
(b)
(c)
(d)
-4.0
0.0
+4.0
t/τ_p

$\mathcal{E}^0 = 0.001$, relative to the parameters in Fig. 6.5a. The final population of state two is $P_2(t = +4\tau_p) = 0.9994$, while $P_8(t = +4\tau_p) = 0.0003$.

In Fig. 6.5c, the pulse duration is held fixed, $\tau_p = 5167.6$ (125.00fs), while the field strength is increased by five percent, $\mathcal{E}^0 = 0.00105$, relative to the parameters in Fig. 6.5a. The final population of state two is $P_2(t = +4\tau_p) = 0.9990$, while $P_8(t = +4\tau_p) = 0.0006$.

In Fig. 6.5d, the pulse duration is decreased by five percent, $\tau_p = 4909.3$ (118.75fs), while the field strength is held fixed, $\mathcal{E}^0 = 0.001$, relative to the parameters in Fig. 6.5a. The final population of state two is $P_2(t = +4\tau_p) = 0.0084$, while $P_8(t = +4\tau_p) = 0.0003$.

Of the four cases tested, the optimal field parameters for maximum population of state two are $\tau_p = 5426.0$ (132.25fs) and $\mathcal{E}^0 = 0.001$, Fig. 6.5b. The slightly smaller pulse durations cut off the "CW-like" behaviour of the time-dependent population of state two when $P_2(t)$ is low. Instead of the increase in pulse duration, an increase in field strength by five percent, as in Fig. 6.5c, cuts the time-dependent behaviour of state two when it is high, but leads to slightly greater perturbation of state eight. In general, however, the population of state eight, or states three, four and five, for all four cases is not significant.

A Gaussian pulsed laser of duration $\tau_p = 5426.0$ (132.25fs) and strength $\mathcal{E}^0 = 0.001$ is used to "pump" the model system from the ground state into state two. The final populations of the states at $t = +4\tau_p$ are used to establish the initial conditions for the following "probe"

investigations [115].

6.2.2. A PROBE OF A TRANSITION BETWEEN TWO EXCITED STATES WITH ONE CW LASER.

In this section, the time-dependent evolution of a seven-level system interacting with one CW laser tuned to the one- or two-photon resonance of the $2 \rightarrow 5$ transition is investigated. The primary molecular system is characterized by the parameters of states one through seven given in Table 6.1, and is denoted "molecule $\mathcal{A}$"; some "pseudo-molecules" are also employed:

$$\left.\begin{array}{ll} \text{Molecule } \mathcal{A}\text{:} & \text{states one through seven from Table 6.1} \\ \text{Molecule } \mathcal{B}\text{:} & \text{identical to molecule } \mathcal{A}\text{, except } E_7' = 1.030E_7 \\ \text{Molecule } \mathcal{C}\text{:} & \text{states 1, 2, 5, 6, and 7, from Table 6.1} \\ \text{Molecule } \mathcal{D}\text{:} & \text{identical to molecule } \mathcal{B}\text{, except } \mu_{56} = 0. \end{array}\right\} \quad (6.2.1)$$

Stationary state seven of molecule $\mathcal{A}$ has energy such that $E_{72} = 0.127196 \simeq 2E_{52} = 0.129152$. When multi-photon transitions to state seven are believed to strongly perturb the $2 \rightarrow 5$ transition of interest, the energy of state seven is increased slightly and the time-dependent behaviour of molecule $\mathcal{B}$, where $E_7' = 0.274307$ and $E_{72}' = 0.135186$, is studied. (Increases in E_7 of molecule $\mathcal{A}$ by one percent increments indicate that at least a three percent increase is necessary for the effects of state seven on the relevant one-photon $2 \rightarrow 5$ transition to reduce significantly; the energy of state seven of molecule $\mathcal{B}$ corresponds to a three percent increase relative to E_7 of molecule $\mathcal{A}$.) The effects of states three and four on the $2 \rightarrow 5$ two-photon transition are investigated by comparing the time-dependent

evolution of the states of molecule $\mathcal{A}$ with that of molecule $\mathcal{B}$. The effects of the difference in the permanent dipole moments μ_{55} and μ_{22} are probed by comparing the cases where $\mu_{55} \neq \mu_{22}$ and $\mu_{55} = \mu_{22}$.

The initial conditions ($t' = 4\tau_p \rightarrow 0$) of the probe CW investigation are determined by the populations of states one through five at $t = +4\tau_p$ from the pump pulse-molecule interaction illustrated in Fig. 6.5b, where $P_1(t = +4\tau_p) = 0.0003$ and $P_2(t = +4\tau_p) = 0.9994$ (state eight is neglected), and $P_j(t = +4\tau_p) \simeq 0$, $j = 3\text{-}7$ [115]. The samplings of the probe laser-molecule interactions are taken for times less than $4\text{x}10^4$ (1ps), so the effects of excited state decay can be neglected. For studies to long times, the effects of excited state decay can be incorporated, see Chapter 3. The computation of the long time-averaged molecular state populations in the absence of decay are employed here to find the resonance frequencies.

The field strength in all cases is $\mathcal{E}^0 = 0.001$. This strength is used so that the one-photon RWA molecule-EMF coupling of the isolated $2 \rightarrow 5$ transition in the absence of permanent dipole moments, $C(1) = \underline{\mu}_{25} \cdot \hat{e}\mathcal{E}^0 = 4.621\text{x}10^{-3}$, is less than the smallest energy separation between the nearest stationary state to state two or five; in this case, state six is closest to state five with $E_{65} = 0.00978$. The RWA molecule-EMF couplings for the $\mu_{55} \neq \mu_{22}$ one- and multi-photon $2 \rightarrow 5$ transitions are less than for the $\mu_{55} = \mu_{22}$ one-photon $2 \rightarrow 5$ transition. The phase of the field is fixed at $\delta = 0$.

The resonance frequencies are established by calculating the fixed-phase long time-averaged molecular state populations from (2.2.39). The Taylor series method is used to compute the evolution operators over $[0, 2\pi/\omega]$, using a 13 term Taylor series over the grid

size $\Delta t = \pi/90\omega$. The Floquet technique and Simpson's rule with 30 integration points are employed to find the long-time averages of the time-dependent state populations. The time-dependent populations of the states were found from the evolution operators over $[0,2\pi/\omega]$, calculated as described above, using (2.2.33). These computational parameters provided the steady state and time-dependent populations of the molecular states to much greater than graphical accuracy.

In the two-level RWA, the time-dependent population of the excited state on resonance is a smooth sinusoidal function of time $(\sin^2|C(N)|t/2)$. The ground and excited states behave in a complementary fashion, exhibiting the same time-dependent pattern, except they are $\pi/|C(N)|$ out of phase. On resonance, the long time-averaged population is one half the maximum time-dependent population. At the appropriate $2 \rightarrow 5$ one- or two-photon resonance frequencies, the exact steady state population of state two is $\bar{P}_2 \simeq 0.49$ for all the cases discussed below. The distribution of the remaining population among the other states (relative to $\bar{P}_5 \simeq 0.5$, $\bar{P}_j = 0$, $j = 1, 3, 4, 6,$ and 7) is an indication of how strongly the neighbouring energy levels perturb the $2 \rightarrow 5$ transition. A significant difference between $\bar{P}_5$ and half the maximum of $P_5(t)$ also indicates a deviation from the predictions of two-level RWA.

ONE-PHOTON $2 \rightarrow 5$ TRANSITION

Figure 6.6 illustrates the temporal evolution of the molecular states of molecule $\mathcal{A}$, defined in (6.2.1), interacting with the CW laser tuned very close to the $2 \rightarrow 5$ one-photon resonance frequency, $\omega = 1.026E_{52} \simeq \omega_{res}$, over the time interval $0 \leq t \leq 4.72\text{x}10^3$

Figure 6.6. The time-dependent state populations, over $0 \leq t \leq 4.72 \times 10^3$ (1.141×10^2fs), for molecule $\mathcal{A}$ interacting with a CW laser with $\mathcal{E}^0 = 0.001$, $\delta = 0$ and tuned to the one-photon $2 \rightarrow 5$ resonance, $\omega_{res} \approx 1.026 E_{52}$. Molecule $\mathcal{A}$ is comprised of stationary states one through seven from Table 6.1.

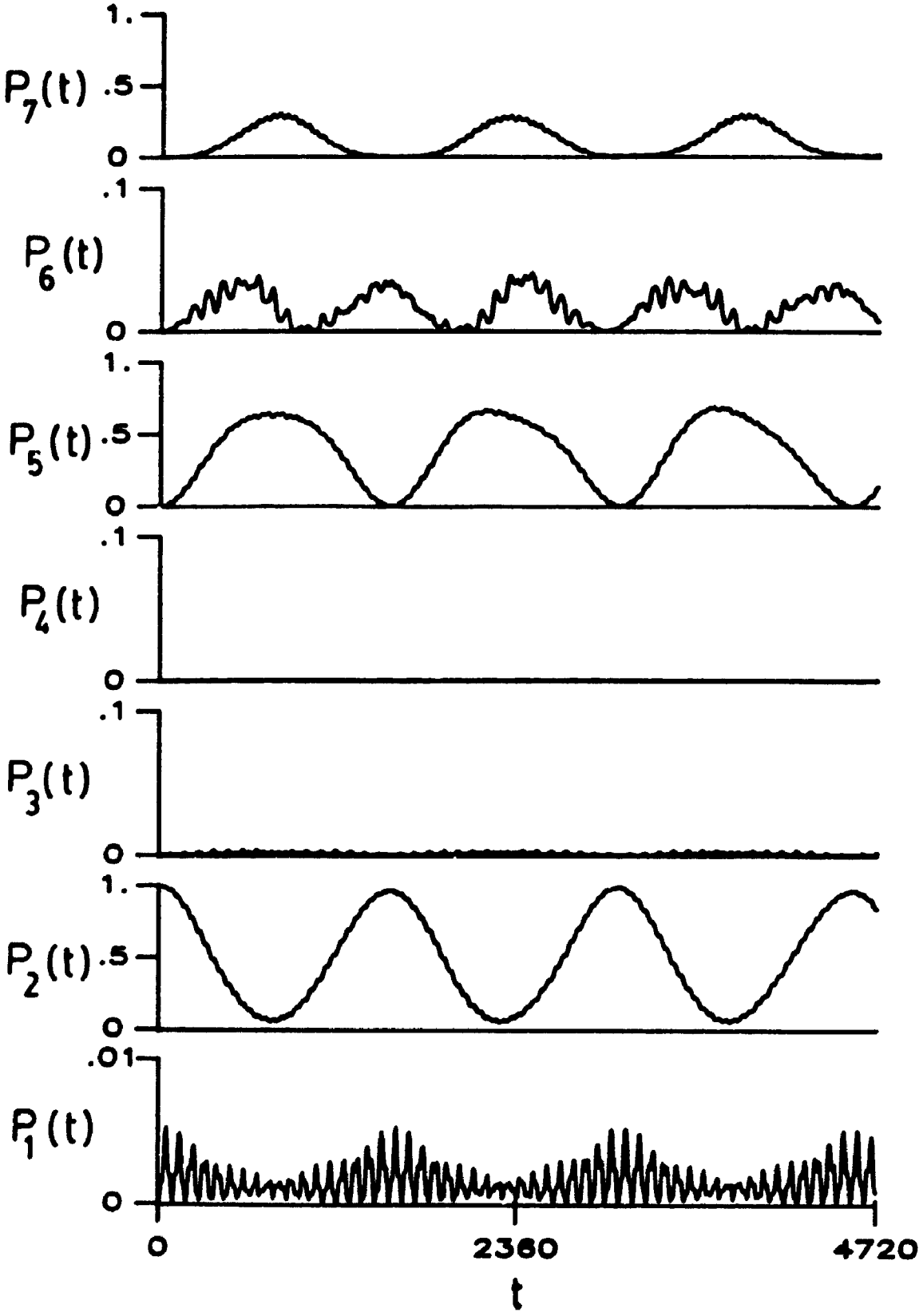

Figure 6.6

(1.14×10^{2}fs). (That the frequency is not exactly on resonance can be deduced from the minima in $P_2(t)$, which are not zero. The true resonance frequency is within $\Delta\omega = \pm 0.001E_{52}$ of the result quoted above.) The period of state five is $T_{exact} = 1.52\times10^{3}$ (3.67×10fs), which is significantly longer than the RWA prediction based on the isolated two-level system characterized by stationary states two and five, $T_{RWA} = 2\pi/C(1) = 1.36\times10^{3}$ (3.29×10fs), where $C(1) = 4.610\times10^{-3}$. The evolution of state five is slightly asymmetric over the periods shown, and its maximum population is only $P_5(t) = 0.643$, not 1.00. The long time-averaged population of state five is $\bar{P}_5 = 0.379$, which is greater than half the maximum of $P_5(t)$ due to the asymmetric and nonsinusoidal behaviour of $P_5(t)$ as a function of time.

A cooperative effect is apparent between states one and two, which share a common period, and similarly for states five and seven. In addition, the time-dependent population of state six is changing in concert with both $P_2(t)$ and $P_5(t)$; the maxima of $P_6(t)$, which are less than $P_6(t) < 0.05$, coincide with those of $P_2(t)$ and $P_5(t)$. Hence, state six is causing slight perturbations of the one-photon $2 \rightarrow 5$ transition. The populations remain below $P_j(t) \ll 0.01$ for $j = 1$, 3, and 4, and these states do not strongly affect the $2 \rightarrow 5$ transition.

The differences in the behaviour of $P_5(t)$ from the two-level RWA prediction can be attributed in large part to stationary state seven. The population of state seven is significant: on average, $\bar{P}_7 = 0.109$. (This steady state population is less than half the maximum of $P_7(t) = 0.299$.) Stationary state seven has a large population relative to the other off-resonance states, and strongly perturbs the $2 \rightarrow 5$ one-photon transition, because the energy of the latter is close to the

$2 \rightarrow 7$ two-photon (or sequential one-photon) resonance, $E_{72} = 0.127196$, and $2E_{52} = 0.129152$.

This interference by state seven can be confirmed by comparison of Fig. 6.6 with Fig. 6.7, which gives the temporal evolution of the states for molecule $\mathcal{B}$, see (6.2.1), interacting with the CW laser at the new $2 \rightarrow 5$ one-photon resonance frequency, $\omega_{res} = 0.985E_{52}$, over the same time span as Fig. 6.6. The shift in the resonance frequency relative to Fig. 6.6 is significant. Had the $2 \rightarrow 5$ one-photon resonance frequency of molecule $\mathcal{A}$ been retained, $P_5(t)$ in Fig. 6.7 would have been far off-resonance: for molecule $\mathcal{B}$, at $\omega_{res}(\mathcal{A}) = 1.026E_{52}$, $\bar{P}_5 = 0.260$ whereas at $\omega_{res}(\mathcal{B}) = 0.985E_{52}$, $\bar{P}_5 = 0.453$. Shifts in ω_{res} due to changes in the energy level configuration (or in the transition or permanent dipole moments) can be on the order of or greater than the half width of the spectral peak of the transition of interest. Since the resonance frequency is dependent upon the molecular parameters, the new resonance frequency is found for the examples in Secs. 6.2.2 and 6.2.3, each time a molecular parameter is changed.

Relative to Fig. 6.6, in Fig. 6.7, the period of $P_5(t)$ has decreased to $1.4\text{x}10^3$ ($3.4\text{x}10$fs), which is more in keeping with the two-level RWA prediction, $T_{RWA} = 1.36\text{x}10^3$, and $P_5(t)$ is much more symmetric over the periods shown. The maximum population has increased to $P_5(t) = 0.910$, which is roughly twice $\bar{P}_5 = 0.453$, while that of state seven has decreased, $\bar{P}_7 = 0.043$. The time-dependent behaviour of states two and five is now very similar, and complementary, which is consistent with an isolated two-level system. In contrast, in Fig. 6.6, the shapes of $P_2(t)$ and $P_5(t)$, as a function of time, are

Figure 6.7. The time-dependent state populations, over $0 \leq t \leq 4.72\text{x}10^{3}$ ($1.141\text{x}10^{2}$fs), for molecule $\mathcal{B}$ interacting with a CW laser as in Fig. 6.6, except tuned to the new one-photon $2 \rightarrow 5$ resonance, $\omega_{res} = 0.985E_{52}$. Molecule $\mathcal{B}$ is identical to molecule $\mathcal{A}$, except state seven in $\mathcal{B}$ has slightly greater energy: $E'_7 = 1.03E_7$, see (6.2.1).

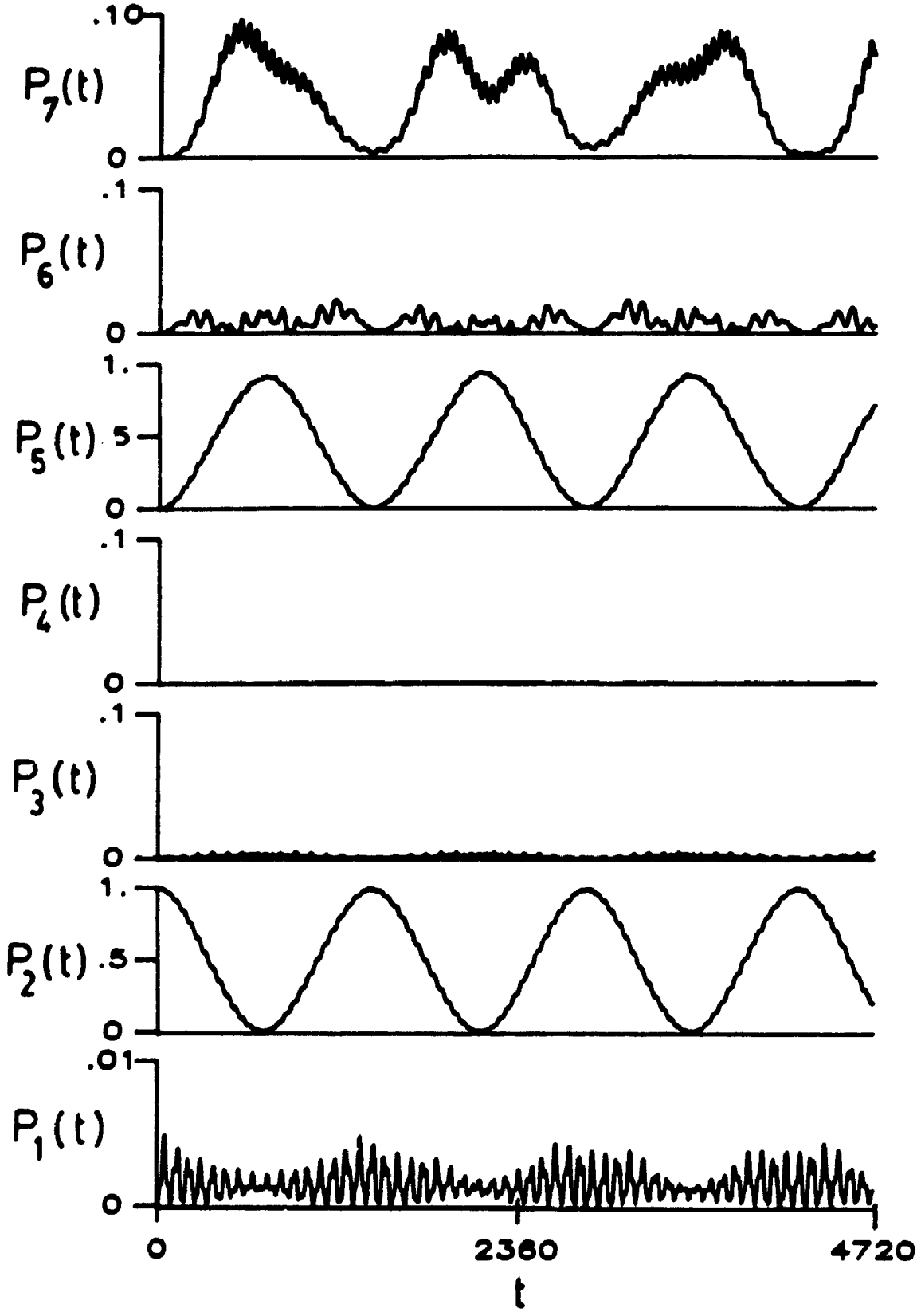

Figure 6.7

very different.

The shift in the energy of state seven has also altered the time-dependent evolution of state six. In Fig. 6.7, $P_6(t)$ is much lower, and does not appear to change in concert with any other state, compared with Fig. 6.6. Since the molecular parameters of state six are identical for Figs 6.6 and 6.7, the perturbation of the one-photon $2 \rightarrow 5$ transition by state six in Fig. 6.6 must involve state seven. Such an indirect perturbation is not unlikely as the transition dipole moments μ_{57}, μ_{67}, and μ_{56} are large, and the related μ_{jj} are significant, relative to many of the other moments in Table 6.1.

The effect of the difference in the permanent dipole moments between states five and two on the one-photon transition is not large. When μ_{55} is set equal to μ_{22}, the resulting resonance frequencies and time-dependent behaviour of the excited states for molecules $\mathcal{A}$ and $\mathcal{B}$ cannot be graphically distinguished from Figs. 6.6 and 6.7, respectively. This result is not surprising, since according to the RWA, for the isolated $2 \rightarrow 5$ transition, $2J_1(z)/z = 0.9977$ for $z = \underline{d}_{52} \cdot \hat{e}\mathcal{E}^0/E_{52} \simeq 0.137$, and hence $C(1) = 4.610 \times 10^{-3}$ when $\mu_{55} \neq \mu_{22}$, while $C(1) = 4.621 \times 10^{-3}$ when $\mu_{55} = \mu_{22}$ ($d_{52} = 0$). The effects of the permanent dipoles are much stronger when multi-photon transitions are considered.

TWO-PHOTON $2 \rightarrow 5$ TRANSITION

The RWA predicts that the two-photon transition for the isolated two-level system composed of stationary states two and five, when $\mu_{55} \neq \mu_{22}$, will have a molecule-EMF coupling of $C(2) = 6.27 \times 10^{-4}$, and the time-dependent population of state five will have period

$T_{RWA} = 1.00 \times 10^4$ $(2.42 \times 10^2 fs)$. When $\mu_{55} = \mu_{22}$, the RWA predicts multi-photon transitions between states two and five are forbidden. To accommodate the longer $\mu_{55} \neq \mu_{22}$ period (relative to the one-photon case), the temporal evolutions of the molecular states are studied over the interval $0 \leq t \leq 3.85 \times 10^4$ $(9.31 \times 10^2 fs)$. Since the $\mu_{55} \neq \mu_{22}$ two-photon coupling is much weaker than the one-photon analogue, the perturbation of the $2 \rightarrow 5$ transition by stationary state seven is not likely to be strong. Transitions to state seven require a four-photon transition, or two sequential two-photon transitions. For weak field strengths such as the one used in these calculations, the higher the number of photons required for a transition, the less probable the transition. Hence the calculations discussed below focus on the model molecules with E_7 as in Table 6.1 (molecules $\mathcal{A}$ and $\mathcal{C}$, see (6.2.1)).

Frequencies close to $\omega \simeq \frac{1}{2}E_{52} = 0.032288$ are off-resonance for the one-photon transitions between states two and three ($E_{32} = 0.022359$), two and four ($E_{42} = 0.036412$), five and four ($E_{54} = 0.028164$), and five and six ($E_{65} = 0.009780$). Hence, stationary states three, four, and six should not strongly perturb or influence the $2 \rightarrow 5$ two-photon transition when $\mu_{55} \neq \mu_{22}$. However, time-dependent perturbation theory, see Sec. 2.3.1, indicates that in the presence of neighbouring energy levels, which act as virtual states, even-photon transitions between two states are permitted even in the absence of permanent dipole moments. Hence, the presence of states three and four can strongly influence the strength of the $2 \rightarrow 5$ two-photon transition when $\mu_{55} = \mu_{22}$. The time-dependent behaviours when $\mu_{55} \neq \mu_{22}$ and $\mu_{55} = \mu_{22}$ are compared for molecules $\mathcal{A}$ and $\mathcal{C}$, from (6.2.1).

Figure 6.8a illustrates the time-dependent populations of all

Figure 6.8. The time-dependent state populations, over $0 \le t \le 3.85 \times 10^4$ $(9.31 \times 10^2 fs)$, for molecule $\mathcal{A}$, see (6.2.1), interacting with a CW laser as in Fig. 6.6, except tuned to new the two-photon $2 \to 5$ resonance frequency: (a) $\mu_{55} \neq \mu_{22}$, $\omega_{res} = 0.5036 E_{52}$; (b) $\mu_{55} = \mu_{22}$, $\omega_{res} = 0.5031 E_{52}$.

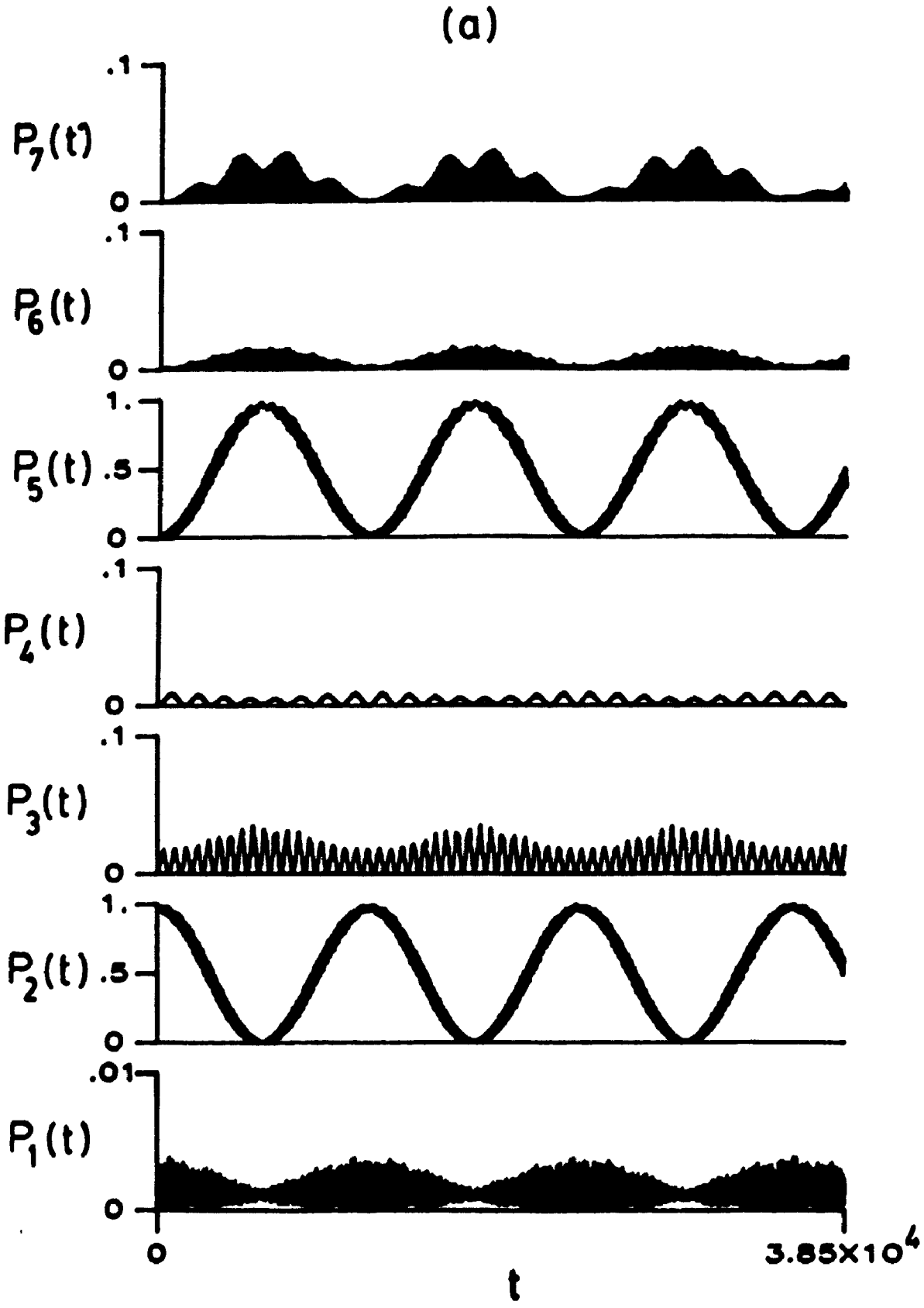

Figure 6.8a

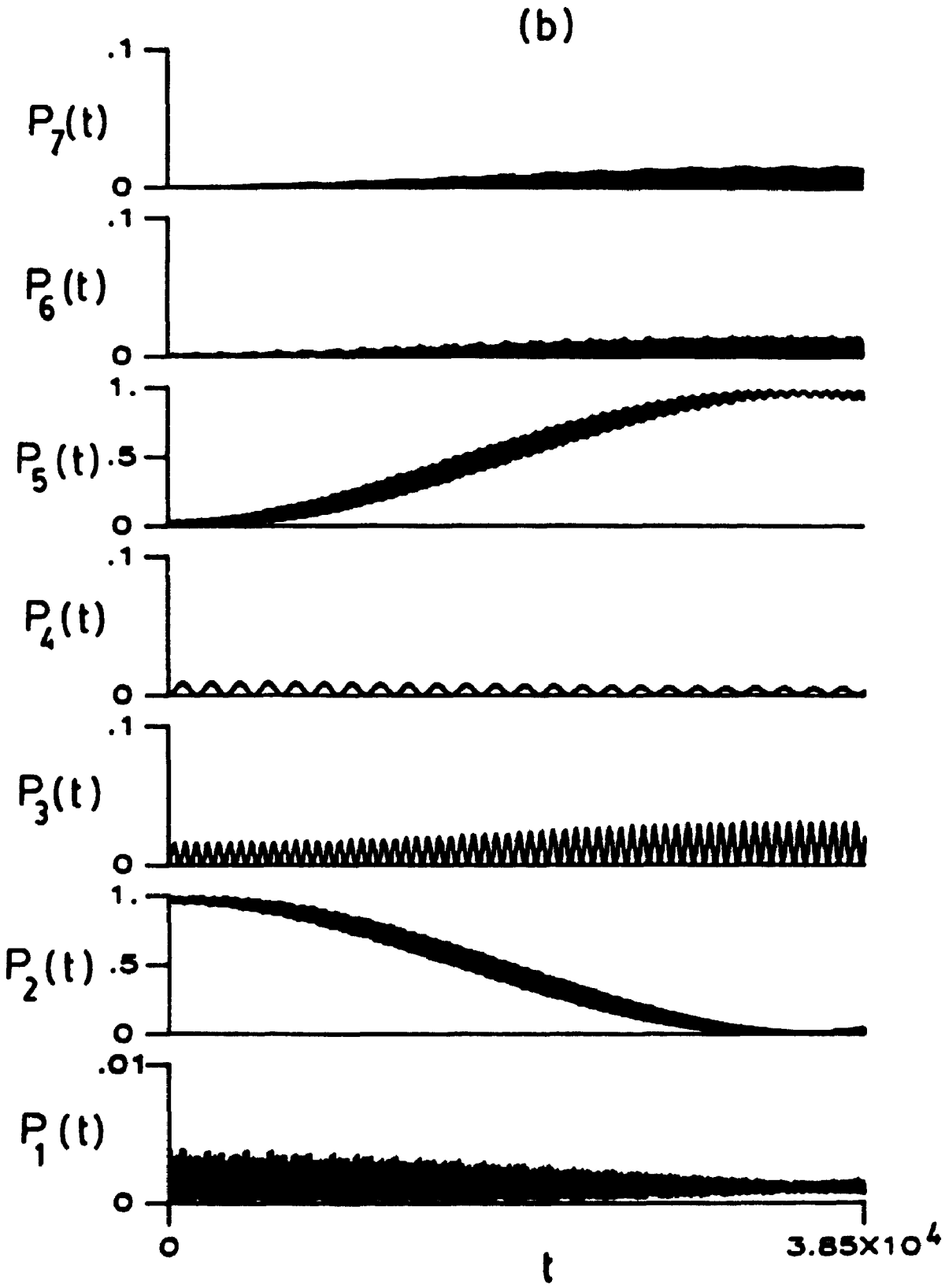

Figure 6.8 continued: Figure 6.8b.

seven states, for molecule $\mathcal{A}$ interacting with the CW laser tuned to the two-photon 2 → 5 resonance frequency, $\omega_{res} = .5036E_{52}$. The populations of all the off-resonance states are below $P_j(t) \leq 0.05$, j = 1, 3, 4, 6, and 7, although $P_3(t)$ and $P_4(t)$ are much greater than for the one-photon analogue, Fig. 6.6. The time-dependent behaviour of states two and five is highly symmetric, and complementary, over each period. To graphical accuracy, the period of $P_5(t)$ is $T_{exact} = 1.2\text{x}10^4$ ($2.9\text{x}10^2$fs), which is longer than the RWA prediction of $T_{RWA} = 1.0\text{x}10^4$. The periods of the cycles of $P_3(t)$, $P_6(t)$ and $P_7(t)$ coincide with that of $P_5(t)$, while the periods of $P_1(t)$ and $P_4(t)$ coincide with that of $P_2(t)$, illustrating a cooperative time-dependent behaviour of this many-level manifold [17,36,110]. For the two-photon 2 → 5 transition, the resonance steady state population of state five is $\bar{P}_5 = 0.484$; its maximum time-dependent population is $P_5(t) = 0.980$. The correlation between $\bar{P}_5$ and one half the maximum of $P_5(t)$ implies a lack of perturbation of the 2 → 5 transition by neighbouring energy levels. As predicted above, the population of state seven is much lower than in the one-photon analogue of Fig. 6.6; for the 2 → 5 two-photon transition, $\bar{P}_7 = 0.007$, and the maximum $P_7(t) = 0.033$.

The difference between the permanent dipoles, $\mu_{55} - \mu_{22}$, has a profound effect on the 2 → 5 two-photon transition. When $\mu_{55} = \mu_{22}$, the 2 → 5 two-photon resonance frequency for molecule $\mathcal{A}$ interacting with the CW laser is $\omega_{res} = 0.5031E_{52}$, with $\bar{P}_5 = 0.488$, and $\bar{P}_j < 0.004$ for j = 1, 3, 4, 6, and 7. (Had the resonance frequency of Fig. 6.8a been retained, the $\mu_{55} = \mu_{22}$ two-photon 2 → 5 transition would have been significantly off-resonance, with the steady state population of state five falling to $\bar{P}_5(\omega = 0.5036E_{52}) = 0.317$.) The temporal

evolution of the molecular states at $\omega_{res} = 0.5031E_{52}$ is given in Fig. 6.8b. In contrast to the case where $\mu_{55} \neq \mu_{22}$, Fig. 6.8a, the temporal evolution of the states is much slower in Fig. 6.8b, where the period of state five is almost double the time interval of the figure. Thus, when $\mu_{55} = \mu_{22}$, the $2 \rightarrow 5$ two-photon molecule-EMF coupling is much weaker than when $\mu_{55} \neq \mu_{22}$. From time-dependent perturbation theory, Sec. 2.3.1, much of the strength of the $2 \rightarrow 5$ two-photon transition when $\mu_{55} = \mu_{22}$ is a result of the presence of states three and/or four, which act as virtual states in the transition.

Figures 6.9a and 6.9b illustrate the time-dependent evolution of molecule $\mathcal{C}$, see (6.2.1), interacting with a CW laser tuned to the associated $2 \rightarrow 5$ two-photon resonance frequency for $\mu_{55} \neq \mu_{22}$ and $\mu_{55} = \mu_{22}$, respectively. In Fig. 6.9a, $\mu_{55} \neq \mu_{22}$, $\omega_{res} = .5029E_{52}$, and the time-dependent population of state five has a period of $T_{exact} = 9.9\text{x}10^{3}$ $(2.4\text{x}10^{2}\text{fs})$. This period is smaller than that $(T_{exact} = 1.2\text{x}10^{4})$ for the seven-level analogue in Fig. 6.8a, and is closer to the two-level RWA prediction of $T_{RWA} = 1.0\text{x}10^{4}$. The long time-averaged population of state five is $\bar{P}_5 = 0.492$, which is close to half the maximum of $P_5(t) = 0.988$; $\bar{P}_j < 0.008$ for $j = 1$, 6 and 7.

When $\mu_{55} = \mu_{22}$ in this five-level system, see Fig. 6.9b, the resonance frequency is $\omega_{res} = 0.5023E_{52}$, the period of $P_5(t)$ is much longer than the time span of the figure, and the populations of all states (except $P_2(t)$) remain very small for $t \leq 3.85\text{x}10^{4}$. Since the steady state populations are $\bar{P}_1 = 0.001$, $\bar{P}_2 = 0.494$, $\bar{P}_5 = 0.497$, $\bar{P}_6 = 0.004$, $\bar{P}_7 = 0.003$, Fig. 6.9b illustrates only a small fraction of the period of $P_5(t)$. The $\mu_{55} = \mu_{22}$ resonance peak has such a narrow FWHM that at the $\mu_{55} \neq \mu_{22}$ resonance frequency, $\omega = 0.5029$,

Figure 6.9. The time-dependent state populations, over $0 \le t \le 3.85\text{x}10^{4}$ ($9.31\text{x}10^{2}$fs), for molecule $\mathcal{C}$ interacting with a CW laser as in Fig. 6.6, except tuned to the new two-photon $2 \rightarrow 5$ resonance: (a) $\mu_{55} \neq \mu_{22}$, $\omega_{res} = 0.5029E_{52}$; (b) $\mu_{55} = \mu_{22}$, $\omega_{res} = 0.5023E_{52}$. Molecule $\mathcal{C}$ is equivalent to molecule $\mathcal{A}$, with states three and four removed, see (6.2.1).

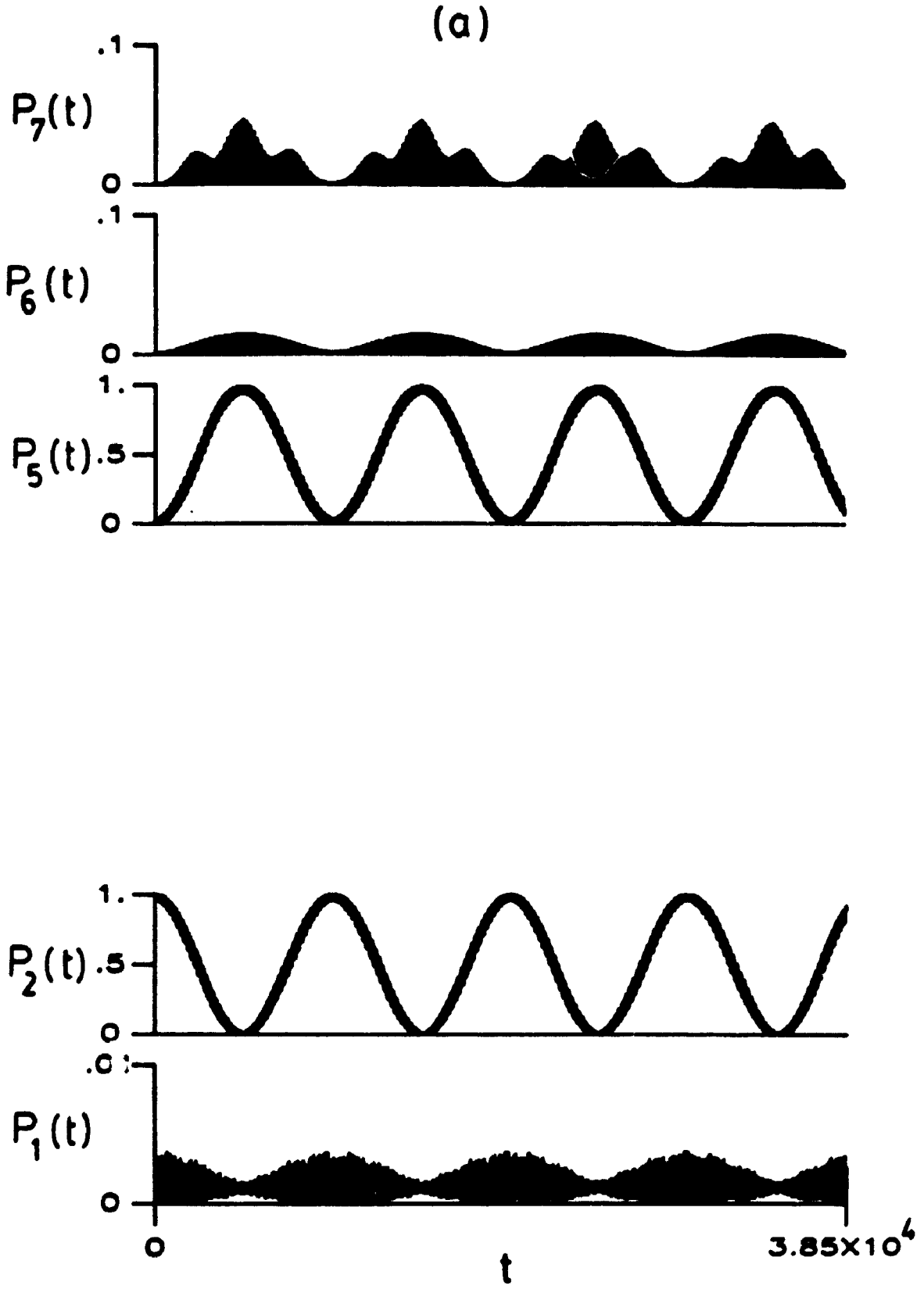

Figure 6.9a.

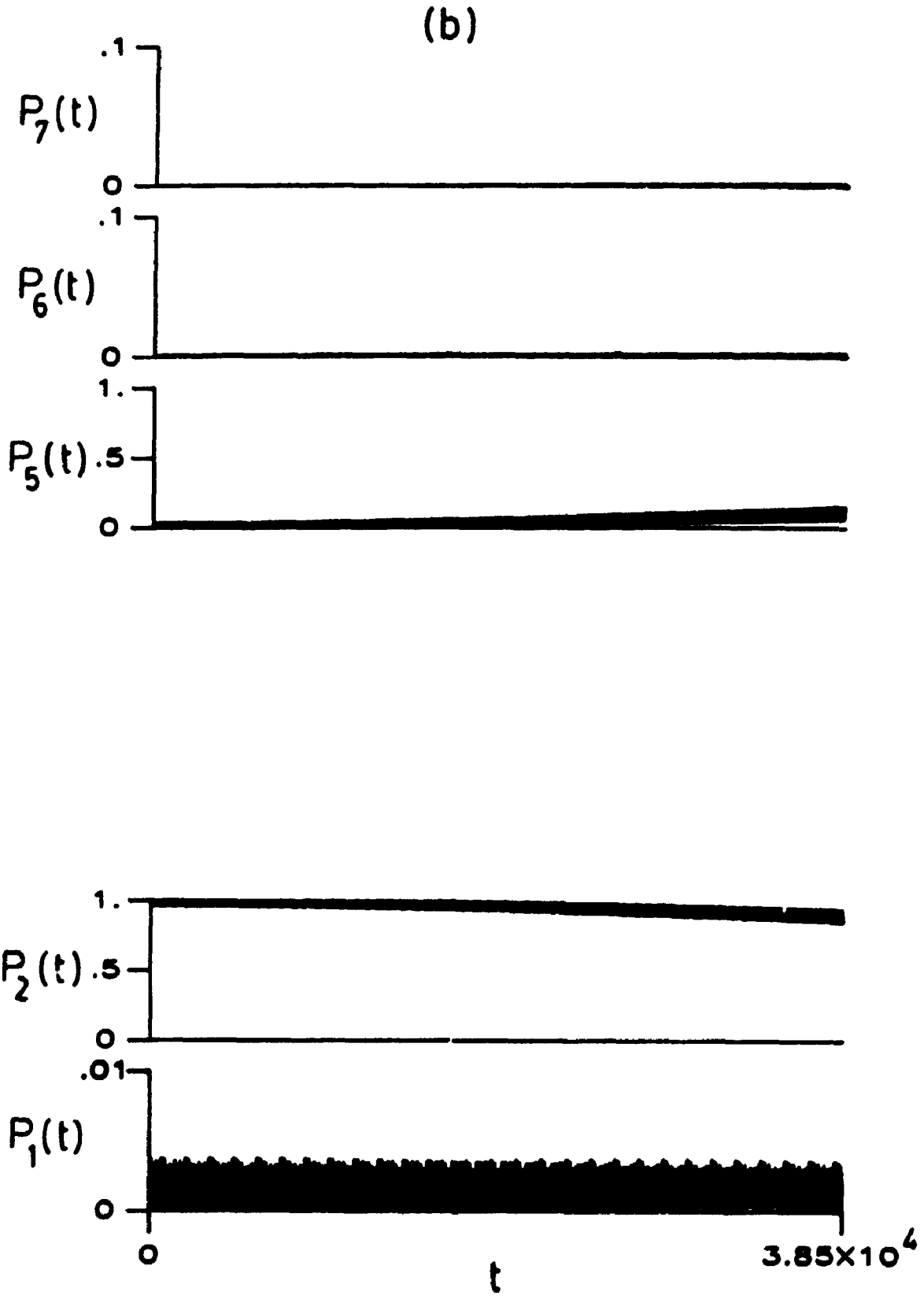

Figure 6.9 continued: Figure 6.9b.

$\bar{P}_2(\mu_{55} = \mu_{22}) = 0.944$ and $\bar{P}_5(\mu_{55} = \mu_{22}) = 0.052$.

Comparing Figs. 6.8b and 6.9b for the $\mu_{55} = \mu_{22}$ seven- and five-level cases, respectively, it is clear that the intermediate states three and/or four play an important role in tne two-photon transition in the absence of a difference in the permanent dipole moments. In Fig. 6.9b, this role has been transferred to states six and/or seven only. Since E_{62} and E_{72} are much greater than $\omega \simeq \frac{1}{2}E_{52}$, while E_{32} and E_{42} are close to $\omega \simeq \frac{1}{2}E_5$, see (2.3.4), the two-photon $2 \rightarrow 5$ resonance transition, when $\mu_{55} = \mu_{22}$ and states three and four are removed, is much weaker than when these states are included in the calculation.

6.2.3. A PROBE OF A TRANSITION BETWEEN TWO EXCITED STATES WITH TWO CW LASERS.

The interaction of the seven-level model molecule $\mathcal{B}$ with two CW lasers is considered. The frequency of field one is set to $\omega_1 = 0.1E_{52} = 0.0064576$, while the frequency of field two is tuned to the (0,1)- or the (1,1)-photon resonance frequency, where, in the two-level, two-field RWA, see Chapter 5, the (N_1,N_2)-photon transition requires energy $N_1\omega_1 + N_2\omega_2$. From (5.1.11), the frequency ω_2 can be expressed as $\omega_2 = m_2\omega_1/m_1$, where m_1 and m_2 are integers; for the (0,1)-photon resonance, $m_2 = 10$ and $m_1 = 1$, whereas $m_2 = 9$ and $m_1 = 1$ for the (1,1)-photon resonance. The field strengths are $\mathcal{E}_1^0 = 0.001$ and $\mathcal{E}_2^0 = 0.0003$, and $\delta_1 = \delta_2 = 0$. The frequency of field one is chosen to be smaller than the energy difference between state five and its closest neighbour, $\omega_1 < E_{65} = 0.00978$, to reduce the effects of competing resonances to neighbouring states, for example, between the

(N_1,N_2)-photon $2 \rightarrow 5$ transition and the $(N_1 + 1,N_2)$-photon $2 \rightarrow 6$ transition, at the same frequencies ω_1 and ω_2. Furthermore, the large difference in magnitude between ω_2 and ω_1 ensures that competing $2 \rightarrow 5$ resonances at the same frequencies are negligible: the strongest competing resonance in the MR-RWA with respect to the $(N_1,1)$-photon $2 \rightarrow 5$ transitions of interest, see (5.1.5), is the (10,0)-photon $2 \rightarrow 5$ transition, with a molecule-EMF coupling, from (5.1.6), of $C(10,0) \simeq 10^{-10} \ll C(N_1,1) \simeq 10^{-3}$, for both $N_1 = 0$ and $N_1 = 1$. In this section, the term "RWA" refers to the "DR-RWA" results of Chapter 5, based on C(0,1) or C(1,1) for $\omega_2 \simeq 10\omega_1$ or $\omega_2 \simeq 9\omega_1$, respectively. The field strength $\mathcal{E}_1^0$ is identical to $\mathcal{E}^0$ used in the one-field studies in Sec. 6.2.2. $\mathcal{E}_2^0$ is chosen so that the two-level, two-field RWA constraint [(5.1.13) with $m_1 = 1$], $C(N_1,N_2) \ll \omega_1$, is not violated by C(0,1) or C(1,1), from (5.1.6), for the isolated $2 \rightarrow 5$ transitions. The frequency ω_1 is sufficiently small and the fields sufficiently weak that the dominant-resonance RWA (DR-RWA) will apply to the (0,1)- and (1,1)-photon $2 \rightarrow 5$ transitions, in the absence of strong neighbouring energy level effects.

Molecule $\mathcal{B}$, which has a higher energy for state seven than molecule $\mathcal{A}$, $E_7' = 1.030E_7$, is used to avoid perturbation of the (0,1)-photon $2 \rightarrow 5$ transition by (0,2)-photon or two sequential (0,1)-photon transitions to state 7, analogous to the perturbations found in the one-field, one-photon case, compare Figs. 6.6 and 6.7. The effects of permanent dipole moments are investigated by comparing the time-dependent populations of the states when $\mu_{55} \neq \mu_{22}$ versus $\mu_{55} = \mu_{22}$. Some pseudo-molecules, based on molecule $\mathcal{B}$ but with certain transition dipole moments set to zero, are used to help interpret

neighbouring energy level effects. The initial conditions [115] for molecule $\mathcal{B}$, and related pseudo-molecules, are as for molecule $\mathcal{A}$ in Sec. 6.2.2.

The resonance frequencies are established from the resonance profiles, evaluated by the Taylor series and Floquet techniques, where the former is described in Sec. 2.2.2 and the latter is adapted for the two-field problem as outlined in Sec. 5.2.2. Since the time-dependent behaviour is of particular interest here, initially only crude calculations of the long time-averaged populations are done to estimate the resonance frequency. A thirteen term Taylor series over a grid size of $\Delta t = \pi/12\omega_2$ [over $2\pi/\omega_b$, where ω_b is the beat frequency defined by (5.1.11)] is used to calculate the evolution operators; every sixth point is used for the numerical integration in (5.2.12) by Simpson's rule. These computational parameters are sufficient to calculate $\bar{P}_5$ to one or two significant figures. Once the resonance frequency is thus estimated, a refined calculation with a grid size of $\Delta t = \pi/60\omega_2$ is done to establish the resonance frequency and associated steady state populations; in these latter calculations, $\bar{P}_5$ converges to more than five figures.

As discussed in Sec. 5.2.3, the careful selection of the frequency ω_2 with respect to its ratio to ω_1, $\omega_2/m_2 = \omega_1/m_1 = \omega_b$, where m_2 and m_1 are integers, can significantly reduce the required computational effort. Thus, the resonance frequencies are not found by smooth incrementation of ω_2, as in the one-field case. However, the resonance frequencies quoted below are accurate within $\Delta\omega_2 = \pm 0.00013$ for Figs. 6.11-6.12, and to within $\Delta\omega_2 = \pm 0.00005$ for Figs. 6.10, and 6.13. The larger error in $\omega_{2,res}$ for Figs. 6.11-6.12 reflects one of the

major difficulties associated with two-field calculations. Because of the dependency of the Floquet calculation on the beat frequency ω_b, and the necessity to express the frequencies ω_1 and ω_2 as integer multiples of ω_b, it can be significantly more complicated and time-consuming to find the two-field resonance frequency, relative to the one-field case. The difficulty is largely determined by the exact resonance values of m_1 and m_2; the computation is facilitated when these turn out to be low integers.

For example, in Fig. 6.10a, the exact resonance frequency is $\omega_{2,res} = 139\omega_1/14$ (relative to the RWA prediction $\omega_2 = 10\omega_1$); the computation of the resonance time-dependent and long time-averaged populations using the Floquet method and/or the Taylor series approach requires the calculation of $m_2 N_T = 139N_T$ evolution operators over $[0,2\pi/\omega_b]$, where the Taylor series grid size is $\Delta t = 2\pi/N_T\omega_2$. Furthermore, confirming $\omega_{2,res}$ to within $\Delta\omega = \pm 0.00004$ only requires checking the frequencies $\omega_2 = 129\omega_1/13$ and $\omega_2 = 149\omega_2/15$. In horrible contrast, in Figs. 6.11-6.12, the resonance frequency is shifted only slightly from $\omega_2 = 9\omega_1$, and $9\omega_1 < \omega_{2,res} < 451\omega_1/50$; computations with $m_2 \geq 451$ are very time consuming, since the evolution operator $U(2\pi/\omega_b,0)$ is computed to time $t = 2\pi/\omega_b = m_2 N_T \Delta t$. Moreover, confirmation of whether or not the resonance frequency is $\omega_{2,res} = 9\omega_1$ to the degree of accuracy of the other figures ($\Delta\omega_2 < \pm 0.00005$) can require lengthy calculations. For example, determining the steady state populations at the frequency $\omega_2 = 3603\omega_1/400 = 9.0075\omega_1$ ($\Delta\omega_2 \simeq 0.000048$ relative to $\omega_2 = 9\omega_1$) using the Floquet formalism of Sec. 5.2.2, would require (in a crude calculation) the computation $N_T m_2 = 24\text{x}3603$ evolution operators over $[0,2\pi/\omega_b]$. In general, the

computational effort needed to find the resonance frequency for two-field calculations, using the Floquet procedure of Sec. 5.2.2, is problem-dependent.

The resonance time-dependent populations are calculated from (5.2.5) using the Taylor series method as discussed above, with the smaller grid size. The evolution operators at $t = 2\pi/\omega_b$ converged to at least twelve figures under these conditions; the related time-dependent populations were obtained to greater than graphical accuracy.

For the (0,1)- and (1,1)-photon 2 → 5 transitions, the two-level, two-field RWA results of Chapter 5 are used to interpret and/or predict the effects of permanent dipole moments, and to discuss the degree of perturbation of the transition of interest, from the RWA predicted behaviour of an isolated two-level system, due to neighbouring energy level effects.

(0,1)-PHOTON 2 → 5 TRANSITION

The two-field RWA resonance condition, (5.1.4), for the (0,1)-photon transition between the isolated two-level system with stationary states two and five, with $\omega_1 = 0.1E_{52}$, is $E_{52} = 0\omega_1 + 1\omega_2$; hence $\omega_2 = E_{52} = 10\omega_1 = 0.064576$. At this frequency combination, the RWA predicts the $\mu_{55} \neq \mu_{22}$ molecule-EMF coupling, (5.1.6), will be $C(0,1) = 8.1\times10^{-4}$. From (5.1.10), the corresponding resonance period of $P_5(t)$ will be $T^{(0,1)}_{RWA} = 7.8\times10^3$ (1.9×10^2fs). On the other hand, when $\mu_{55} = \mu_{22}$, the two-field RWA molecule-EMF coupling for the (0,1)-photon transition reduces to the one-field, one-photon (Rabi) coupling C(1), based on field two, $C(0,1)\big|_{d_{52}=0} = \mu_{25}\cdot\hat{e}_2\mathcal{E}^0_2 = 1.4\times10^{-3}$, see the

discussion immediately following (5.1.6). The associated resonance period of $P_5(t)$ is $T_{RWA}^{(0,1)} = 4.5\times10^3$ $(1.1\times10^2 fs)$. Hence, when $\mu_{55} = \mu_{22}$, the molecule in the two-level RWA "ignores" field one, and the resonance period is much shorter than when $\mu_{55} \neq \mu_{22}$.

The two-field RWA also provides a guide to the effect of neighbouring resonance transitions. As discussed in Sec. 5.1.2, the frequency separations between the transition of interest and important (strong) neighbouring resonances should be checked with respect to independent changes in each frequency, to ensure the spectral peaks are well separated. In a many-level manifold, multi-photon transitions to other states must also be considered. For fixed $\omega_1 = 0.1E_{52}$, the nearest (significant) resonances to the (0,1)-photon $2 \rightarrow 5$ transition with respect to changes in ω_2 are: the (1,1)-photon $2 \rightarrow 6$ transition, at $\omega_2 = 0.067898$; the (0,2)-photon $2 \rightarrow 7$ transition, at $\omega_2 = 0.067593$; and the (2,1)-photon $2 \rightarrow 6$ transition, at $\omega_2 = 0.061441$. These transitions all involve neighbouring states to level five, and not neighbouring multi-photon transitions between states two and five. The nearest $2 \rightarrow 5$ transitions to $\omega_2 = 0.064576$ are the (1,1)-photon and the (-1,1)-photon transitions at $\omega_2 = 0.058118$ and $\omega_2 = 0.071034$, respectively. All the above nearest resonance frequencies fall outside the RWA predicted FWHM $= 1.62\times10^{-3}$, with respect to ω_2, of the (0,1)-photon $2 \rightarrow 5$ transition when $\mu_{55} \neq \mu_{22}$; these comments also hold when $\mu_{55} = \mu_{22}$. Thus the RWA predicts perturbations of the (0,1)-photon $2 \rightarrow 5$ transition due to neighbouring transitions with respect to changes in ω_2 will be slight.

Calculations of the steady state populations as a function of ω_2 with fixed $\omega_1 = 0.1E_{52}$ indicate $\bar{P}_6$ has a spectral peak around

$\omega_2 \simeq 0.0623$, and retains an off-resonance background of $\bar{P}_6 \simeq 0.12$ around $\omega_{2,res}$ for the (0,1)-photon $2 \rightarrow 5$ transition. This peak in $\bar{P}_6$ is probably the (2,1)-photon $2 \rightarrow 6$ transition, given the proximity of $\omega_2 \simeq 0.0623$ to the resonance frequency, $\omega_2 = 0.061441$, predicted by the RWA for th'- transition. Thus, in exact calculations, the (2,1)-photon $2 \rightarrow 6$ transition as a function of ω_2 does indeed perturb the (0,1)-photon $2 \rightarrow 5$ transition.

The resonance profile as a function of changing ω_1 must also be considered. For ω_2 fixed at the (0,1)-photon $2 \rightarrow 5$ RWA resonance frequency, $\omega_2 = E_{52} = 0.064576$, the nearest significant resonances to $\omega_1 = 0.0064576$ with respect to changing ω_1 are: the (2,1)-photon $2 \rightarrow 6$ transition at $\omega_1 = 0.00489$; and the (1,1)-photon $2 \rightarrow 6$ transition at $\omega_1 = 0.00978$. The FWHM of these three transitions as a function of ω_1 are difficult to determine. Since $N_1 = 0$ for the (0,1)-photon $2 \rightarrow 5$ transition, the associated spectral peak does not have a FWHM as a function of ω_1, see (5.1.9) with $N_p = N_1 = 0$. The neighbouring transitions from state two to state six cannot be described in the two-level approximation, since in both cases, $\omega_2 = E_{52}$ and therefore state five cannot be ignored. Indeed, when $\omega_2 = E_{52}$, the (2,1)-photon $2 \rightarrow 6$ transition cannot be distinguished from sequential (0,1)-photon $2 \rightarrow 5$ and (2,0)-photon $5 \rightarrow 6$ transitions, since the resonance frequency for ω_1 is $\omega_1 = E_{65}/2$ for both types of transitions. Similarly, the (1,1)-photon $2 \rightarrow 6$ transition and the sequential (0,1)-photon $2 \rightarrow 5$ and (1,0)-photon $5 \rightarrow 6$ transitions occur at the same RWA resonance frequency $\omega_1 = E_{65}$. The lack of applicability of the RWA in these cases suggests the impact of state six, due to direct of sequential transitions from states two to six, on the (0,1)-photon $2 \rightarrow 5$

transition will probably be significant.

Calculations of the exact resonance profile, as a function of ω_1 with fixed $\omega_2 = E_{52}$, to find the closest resonance to $\omega_1 = 0.1E_{52} = 0.0064576$, indicate a spectral peak in $\bar{P}_6$ occurs when $\omega_1 \simeq 0.0056$, with high populations in both states five and six, $\bar{P}_5 = 0.211$ and $\bar{P}_6 = 0.207$ ($\bar{P}_2 = 0.497$). Given the RWA prediction for the resonance frequency is $\omega_1 = 0.00489$, this peak in $\bar{P}_6$ in the exact resonance profile is identified as the (2,1)-photon $2 \rightarrow 6$ transition, and/or sequential (0,1)-photon $2 \rightarrow 5$, (2,0)-photon $5 \rightarrow 6$ transitions. The proximity of $\omega_1 = 0.1E_{52}$ and $\omega_1 \simeq 0.0056$ suggest perturbations of the (0,1)-photon $2 \rightarrow 5$ transition by either type (direct or sequential) of transition to state six is likely.

Figure 6.10a illustrates the temporal evolution, from exact calculations, of the molecular states for the (0,1)-photon $2 \rightarrow 5$ transition when $\mu_{55} \neq \mu_{22}$. The frequency is tuned to $\omega_2 = 139\omega_1/14 \simeq 0.06411 \simeq \omega_{2,res}$; $\bar{P}_2 = 0.461$, $\bar{P}_5 = 0.374$, $\bar{P}_6 = 0.120$, $\bar{P}_7 = 0.040$ and $\bar{P}_j < 0.003$ for $j = 1, 3, 4$. The temporal evolution of the states has much more structure than the one-field analogue, see Fig. 6.7; the determination of the period of $P_5(t)$ is correspondingly more difficult. On average, $T_{exact} \simeq 9.4\text{x}10^3$ ($2.3\text{x}10^2$fs), which is larger than the RWA prediction based on C(0,1), $T_{RWA}^{(0,1)} = 7.8\text{x}10^3$. As in the one-field case in Fig. 6.7, in Fig. 6.10a, the populations of states three and four are negligible, and the cycles of $P_7(t)$ have roughly the same period as $P_5(t)$, while the cycles of $P_1(t)$ and $P_2(t)$ are also in concert. Unlike in Fig. 6.7, the population in state six in Fig. 6.10a is high, and it changes in a complementary fashion with the "structure" of $P_5(t)$. The most likely explanation of the high

Figure 6.10. The time-dependent state populations, over $0 \leq t \leq 3.85\text{x}10^{4}$ $(9.31\text{x}10^{2}\text{fs})$, for molecule $\mathcal{B}$, see (6.2.1), interacting with two CW lasers with $\mathcal{E}_1^0 = 0.001$, $\omega_1 = 0.1E_{52}$, $\delta_1 = \delta_2 = 0$, $\mathcal{E}_2^0 = 0.0003$ and ω_2 tuned close to the (0,1)-photon $2 \rightarrow 5$ resonance: (a) $\mu_{55} \neq \mu_{22}$, $\omega_2 = 139\omega_1/14 \simeq 0.06411 \simeq \omega_{2,\text{res}}$; (b) $\mu_{55} = \mu_{22}$, $\omega_2 = 79\omega_1/8 \simeq 0.06377 \simeq \omega_{2,\text{res}}$.

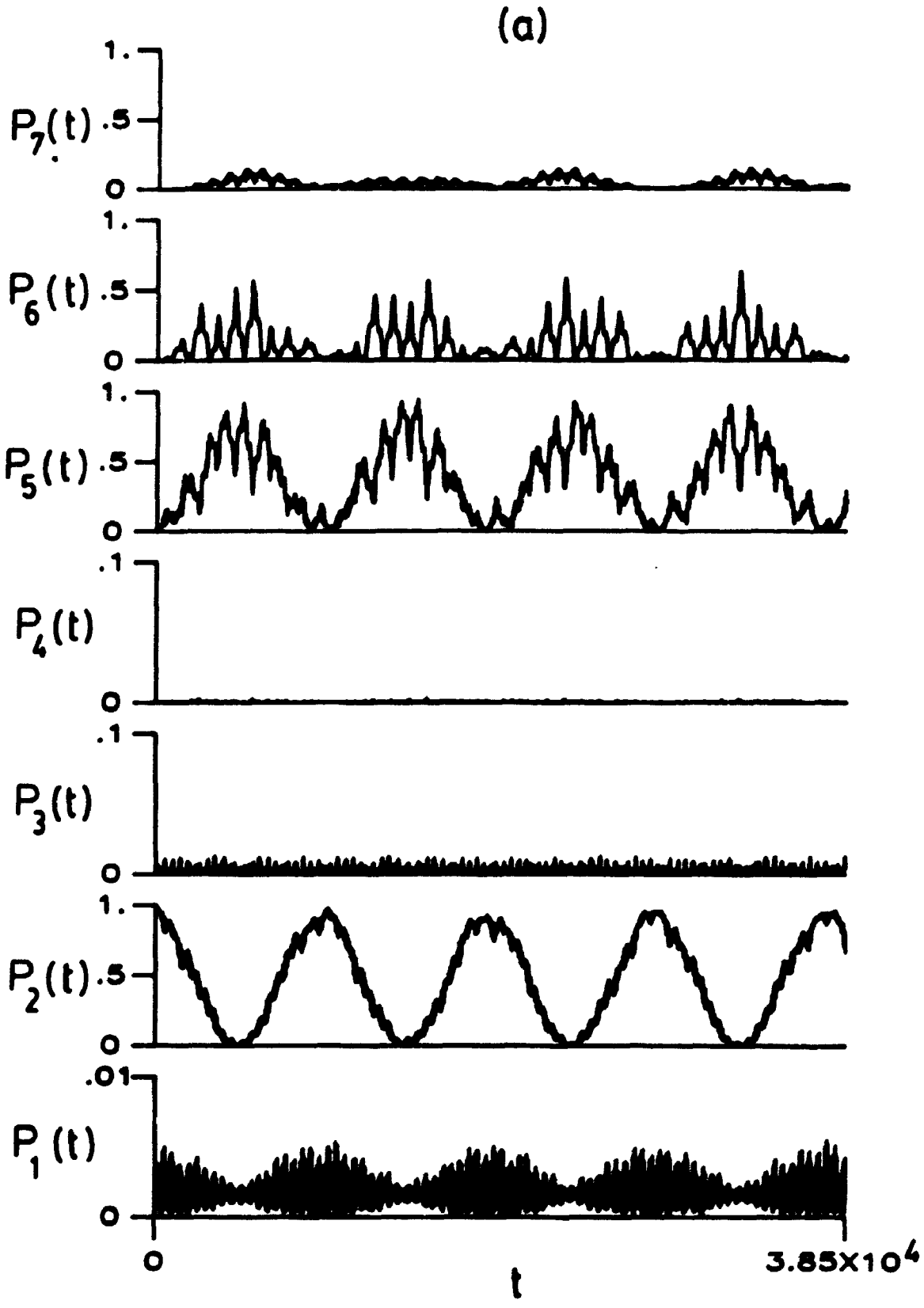
(a)
1.
$P_7(t)$ .5
0
1.
$P_6(t)$ .5
0
1.
$P_5(t)$ .5
0
.1
$P_4(t)$
0
.1
$P_3(t)$
0
1.
$P_2(t)$ .5
0
.01
$P_1(t)$
0
0
t
3.85×10^4

Figure 6.10a

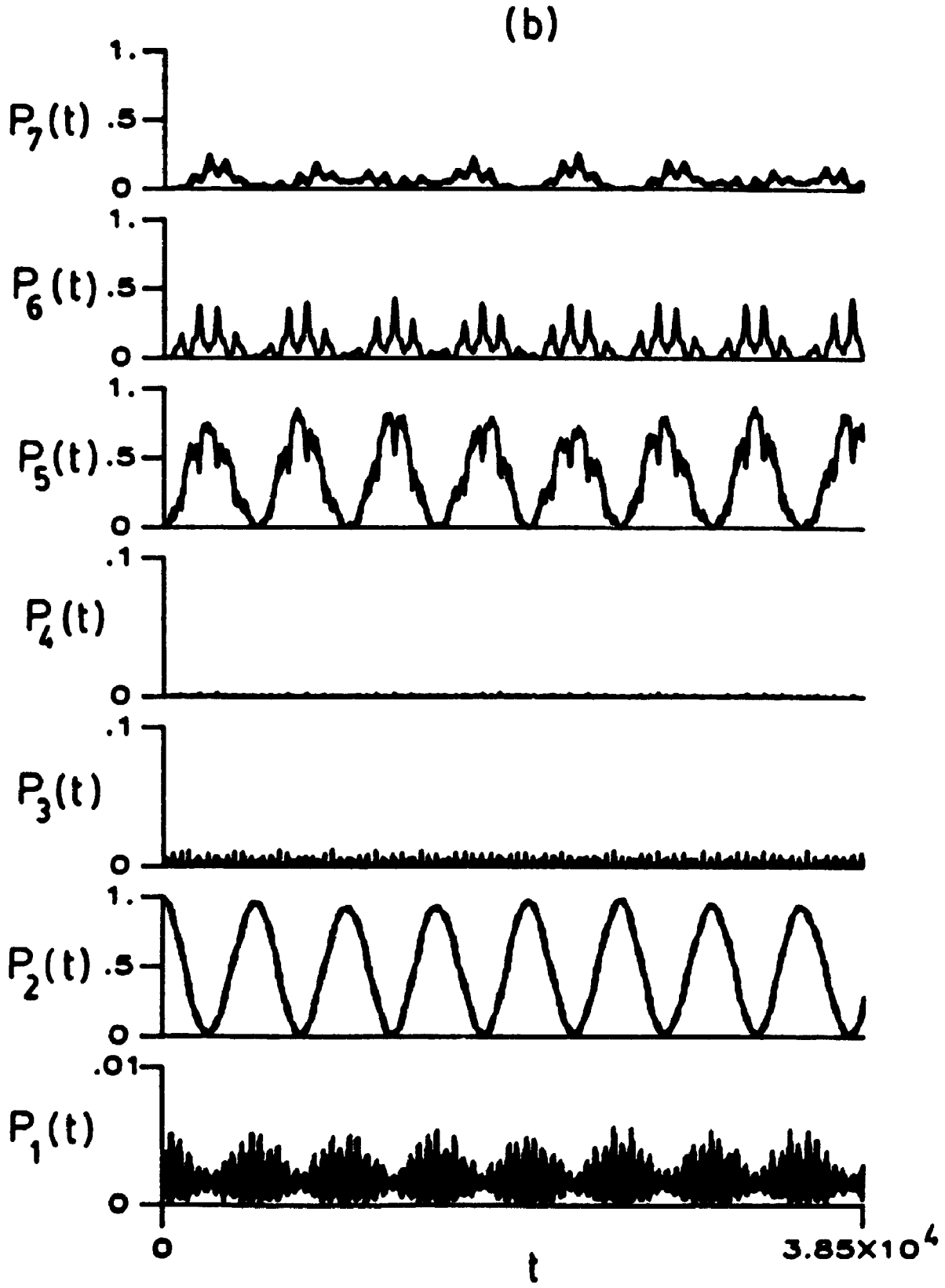

Figure 6.10 continued: Figure 6.10b.

population in state six was discussed in the previous paragraph.

The non-zero difference between the permanent dipole moments of states two and five results in a distinction between the one-field, one-photon $2 \rightarrow 5$ transition (based on field two, since ω_2 is tuned close to E_{52}) and the two-field, (0,1)-photon $2 \rightarrow 5$ transition. According to the RWA, if field one is not present ($\mathcal{E}_1^0 = 0$), the one-field (based on $\mathcal{E}_2^0$) molecule-EMF coupling is $C(1) = 1.4\text{x}10^{-3}$, and the associated period is $T_{RWA} = 4.5\text{x}10^3$; and the effects of the permanent dipole moments are not large, since $z = \underline{d}_{52} \cdot \hat{e}\mathcal{E}_2^0/E_{52} = 0.041$, and $2J_1(z)/z \simeq 0.9998$, see (2.3.10). In contrast, for the two-field problem, the effect of the permanent dipole moments is established through field one, even though the (0,1)-photon $2 \rightarrow 5$ transition has a net absorption of zero ω_1 photons. The two-field (0,1)-photon molecule-EMF coupling, $C(0,1) = 8.1\text{x}10^{-4}$, is much weaker, and the period, $T_{RWA} = 7.8\text{x}10^3$, longer, than the one-field, one-photon analogues. Hence, the one-field, one-photon and two-field, (0,1)-photon transitions are distinct because $\mu_{55} \neq \mu_{22}$.

The effects of permanent dipoles on the (0,1)-photon $2 \rightarrow 5$ transition can be investigated by setting $\mu_{55} = \mu_{22}$. The RWA predicts this transition will be different when $\mu_{55} \neq \mu_{22}$ relative to when $\mu_{55} = \mu_{22}$ since $J_0(z_1) = 0.586$ for $z_1 = \underline{d}_{52} \cdot \hat{e}\mathcal{E}_1^0/\omega_1 \simeq 1.365$, whereas $J_0(z_1) = 1.0$ for $z_1 = 0$; this difference in $J_0(z_1)$ affects the magnitudes of the respective molecule-EMF couplings, see (5.1.6).

The time-dependent populations of the molecular states interacting with the two CW lasers are given in Figure 6.10b for the case where $\mu_{55} = \mu_{22}$. The frequency of field two is tuned to $\omega_2 = 79\omega_1/8 \simeq 0.06377 \simeq \omega_{2,res}$ for the (0,1)-photon $2 \rightarrow 5$ resonance

transition; the long time-averaged state populations are $\bar{P}_2 = 0.483$, $\bar{P}_5 = 0.358$, $\bar{P}_6 = 0.092$, $\bar{P}_7 = 0.061$ and $\bar{P}_j < 0.003$, $j = 1$, 3, and 4. The average populations of states five and six have decreased relative to the $\mu_{55} \neq \mu_{22}$ analogue in Fig. 6.10a, while that of state seven has increased slightly. In keeping with the RWA prediction of $T_{RWA} = 4.5\text{x}10^3$, the period of $P_5(t)$ in Fig. 6.10b is shorter than in Fig. 6.10a where $\mu_{55} \neq \mu_{22}$; here, $T_{exact} = 5.0\text{x}10^3$ ($1.2\text{x}10^2$fs), while in Fig 6.10a, $T_{exact} = 9.4\text{x}10^3$ ($T_{RWA} = 7.8\text{x}10^3$). As in Fig. 6.10a, in Fig. 6.10b, the temporal patterns of states one and six are in concert with those of states two and five, respectively. Although the RWA predicts the $\mu_{55} = \mu_{22}$ molecule-EMF coupling and associated temporal evolution of the state populations are independent of field one, the "structure" of $P_5(t)$ in Fig. 6.10b, although diminished relative to Fig. 6.10a, indicates that the additional field influences the time-dependent behaviour of the molecule. The one-field one-photon transition with $\mathcal{E}^0 = 0.001$, see Fig. 6.7, where the $\mu_{55} \neq \mu_{22}$ and $\mu_{55} = \mu_{22}$ cases are graphically indistinguishable, is much smoother, and state six has little impact on the $2 \rightarrow 5$ transition.

The one-field one-photon $2 \rightarrow 5$ transitions are not distinct when $\mu_{55} \neq \mu_{22}$ and $\mu_{55} = \mu_{22}$ for $\mathcal{E}^0 = 0.001$, see Fig. 6.7 and related discussion. A much stronger field strength would be required to observe the effects of permanent dipole moments with one CW field. On the other hand, by using two CW fields with different field strengths and frequencies, the two-field (0,1)-photon $2 \rightarrow 5$ transitions are very different for $\mu_{55} \neq \mu_{22}$ versus $\mu_{55} = \mu_{22}$, compare Figs. 6.10a and 6.10b. As in the one-field case, the effects of permanent dipole moments in two-field problems can be more pronounced for multi-photon

transitions; the (1,1)-photon 2 → 5 transition is considered next.

(1,1)-PHOTON 2 → 5 TRANSITION

As with the (0,1)-photon transition, the two-field RWA results of Chapter 5 can be used to predict and interpret the spectral and temporal behaviour of the molecular states for the (1,1)-photon 2 → 5 transition. For the isolated two-level system composed of stationary states two and five, the RWA $\mu_{55} \neq \mu_{22}$ molecule-EMF coupling from (5.1.6) is $C(1,1) = 8.2\text{x}10^{-4}$ at the resonance frequency combinati $\omega_1 = 0.1E_{52} = 0.0064576$ and $\omega_2 = 9\omega_1 = 0.9E_{52} = 0.058118$, see (5.1.4). The resonance perio^{d} of $P_5(t)$ from (5.1.10) is $T_{RWA}^{(1,1)} = 7.7\text{x}10^{3}$ ($1.9\text{x}10^{2}$fs). When $\mu_{55} = \mu_{22}$, the RWA forbids multi-photon transitions between states two and five.

It was shown earlier that the (0,1)-photon 2 → 5 transition could not be treated as a completely isolated two-level transition, because transitions to state six, which likely used state five as an intermediate state, strongly perturbed the 2 → 5 transition. For the (1,1)-photon 2 → 5 transition, neighbouring significant resonances which have or contain a frequency combination close to or equal to E_{52} will also use state five as an intermediate state; these neighbouring transitions will perturb the (1,1)-photon 2 → 5 transition.

For fixed $\omega_1 = 0.1E_{52}$, the RWA predicts the closest significant neighbouring transition to the (1,1)-photon 2 → 5 transition at $\omega_2 = 0.058118$ with respect to changes in ω_2 is the (2,1)-photon 2 → 6 transition at $\omega_2 = 0.061441$. This resonance frequency falls outside the RWA FWHM = $1.64\text{x}10^{-3}$ of the (1,1)-photon 2 → 5 transition. Furthermore, $\omega_2 = 0.061411$ is sufficiently far from

$\omega_2 = E_{52} = 0.065476$, so that state five should not strengthen this (2,1)-photon 2 → 6 transition by acting as an intermediate state. This mechanism for the perturbation of the transition of interest is not strong.

For fixed $\omega_2 = 0.9E_{52} = 0.058118$, the closest important resonances to the (1,1)-photon 2 → 5 transition at $\omega_1 = 0.0065476$ with respect to changes in ω_1 are the (2,1)-photon 2 → 5 transition at $\omega_1 = 0.003229$ and the (2,1)-photon 2 → 6 transition at $\omega_1 = 0.008119$. While the former resonance frequency is outside the FWHM = 1.64×10^{-3} of the transition of interest, the latter is very close. Accordingly, direct (2,1)-photon 2 → 6 transitions (as a function of ω_1) will probably perturb the (1,1)-photon 2 → 5 transition. Furthermore, for $\omega_1 = 0.008119$ and $\omega_2 = 0.058118$, the sum of these two frequencies, $\omega_1 + \omega_2 = 0.066237$, is very close to $E_{52} = 0.065476$. Hence, the (2,1)-photon 2 → 6 transition contains a frequency combination which is close to the (1,1)-photon 2 → 5 resonance. Thus, the resonance peak for the sequential (1,1)-photon 2 → 5, (1,0)-photon 5 → 6 transition, will likely overlap, and consequently perturb, the (1,1)-photon 2 → 5 resonance transition.

Figure 6.11 illustrates the $\mu_{55} \neq \mu_{22}$ time-dependent state populations for molecule $\mathcal{B}$ interacting with the two CW fields when ω_2 is tuned close to the (1,1)-photon 2 → 5 resonance frequency, $\omega_2 = 9\omega_1 \simeq 0.05812 \simeq \omega_{2,res}$. The long time-averaged populations are $\bar{P}_2 = 0.310$, $\bar{P}_5 = 0.348$, $\bar{P}_6 = 0.106$, $\bar{P}_7 = 0.150$, and $\bar{P}_j < 0.003$, $j = 1$, 3 and 4. The period of $P_5(t)$ is roughly $T_{exact} \simeq 8.3\times10^3$ (2.0×10^2fs), whereas $T_{RWA}^{(1,1)} = 7.7\times10^3$; the exact period is slightly shorter than that for the (1,0)-photon analogue, for which $T_{exact} = 9.4\times10^3$ and

Figure 6.11. The time-dependent state populations, over $0 \le t \le 3.85\text{x}10^{4}$ $(9.31\text{x}10^{2}\text{fs})$, for molecule $\mathcal{B}$, see (6.2.1), with $\mu_{55} \neq \mu_{22}$, interacting with two CW lasers as given in Fig. 6.10, except ω_2 tuned close to the (1,1)-photon $2 \rightarrow 5$ resonance, $\omega_2 = 9\omega_1 \simeq 0.05812 \simeq \omega_{2,res}$.

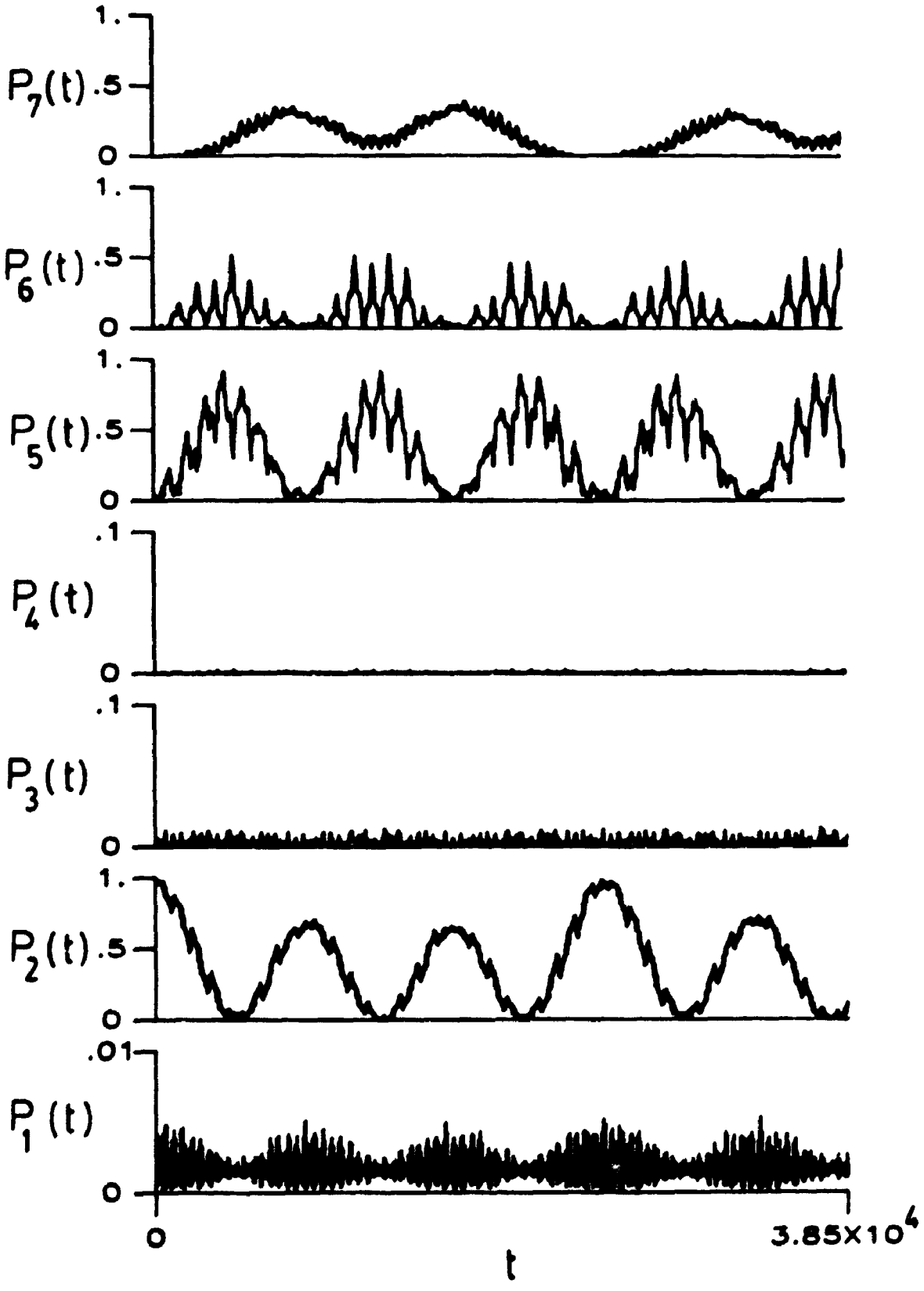
1.
$P_7(t)$ .5
0
1.
$P_6(t)$ .5
0
1.
$P_5(t)$ .5
0
.1
$P_4(t)$
0
.1
$P_3(t)$
0
1.
$P_2(t)$ .5
0
.01
$P_1(t)$
0
0
3.85×10^4
t

Figure 6.11.

$T^{(0,1)}_{RWA} = 7.8\times10^{3}$. The differences between the exact and RWA results can be attributed primarily to the effects of the neighbouring transitions.

The temporal evolution of the state two in Fig. 6.11 is unique from that for the two-field (1,0)-photon and one field two-photon analogues in that the maximum of $P_2(t)$ in some cycles is much less than unity. The lower population in $P_2(t)$ in the first, second and fourth complete cycles in Fig. 6.11 can be traced to state seven, which is no longer changing in concert with states five and six, compare with Fig. 6.10a. Indeed, the similarity between Figs. 6.10a and 6.11 in the time-dependent behaviour of states six and five, versus the differences between the two figures in the time-dependent evolution of states two and seven, suggests that when the frequencies are tuned to the (1,1)-photon $2 \rightarrow 5$ transition, there is a mechanism for population exchange between states two and seven.

The source of the population in state seven can be traced by alternately changing the transition moments of "suspected pathways" to zero. The obvious transition moments to eliminate are μ_{27} and μ_{57}, which represent a direct $(2 \rightarrow 7)$ and the simplest indirect $(2 \rightarrow 5 \rightarrow 7)$ mechanism, respectively, for population to reach state seven from state two. However, the steady state populations at $\omega_2 = 9\omega_1$, when $\mu_{27} = 0$ or $\mu_{57} = 0$, do not change significantly relative to the $\bar{P}_j$ for molecule *B*, see Table 6.2. In contrast, removing the pathway $5 \rightarrow 6$ results in a dramatic drop in the population of states six and seven; thus state six is a critical component of the pathway between states two and seven. Direct transitions between states two and six are not significant, since setting $\mu_{26} = 0$ does not strongly affect the steady state

Table 6.2. The steady state populations when the transition moment $\mu_{jk} = \mu_{kj}$ is set to zero, for molecule $\mathcal{B}$ interacting with two CW lasers, with parameters $\mathcal{E}_1^0 = 0.001$, $\omega_1 = 0.10E_{52}$, $\mathcal{E}_2^0 = 0.0003$ and $\omega_2 = 9\omega_1 = 0.90E_{52}$.

(j,k)	$\bar{P}_1$	$\bar{P}_2$	$\bar{P}_3$	$\bar{P}_4$	$\bar{P}_5$	$\bar{P}_6$	$\bar{P}_7$
-,-	0.002	0.390	0.003	0.0003	0.348	0.106	0.150
2,6	0.002	0.391	0.003	0.0003	0.349	0.105	0.149
2,7	0.002	0.391	0.003	0.0003	0.345	0.105	0.153
5,6	0.002	0.588	0.004	0.0002	0.392	0.001	0.012
5,7	0.002	0.391	0.003	0.0003	0.339	0.107	0.157
6,7	0.002	0.481	0.003	0.0004	0.381	0.127	0.005

populations relative to molecule $\mathcal{B}$. When $\mu_{67} = 0$, the populations in states two, five and six increase, while $\bar{P}_7$ decreases substantially, relative to molecule $\mathcal{B}$. Thus, the perturbation of the $2 \rightarrow 5$ transition in Fig. 6.11 occurs primarily via an indirect pathway from states two to seven: probably $2 \rightarrow 5 \rightarrow 6 \rightarrow 7$. The strength of the $5 \rightarrow 6$ transition is likely a result of the (2,1)-photon $2 \rightarrow 6$ transition (as a function of changing ω_1) containing a frequency combination which is close to E_{52}, as discussed above.

Figure 6.12a illustrates the time-dependent evolution of the states of pseudo-molecule $\mathcal{D}$, which is identical to molecule $\mathcal{B}$ except $\mu_{56} = 0$, interacting with the two CW lasers with the frequency of field two set to the frequency in Fig. 6.11, $\omega_2 = 9\omega_1$. Relative to Fig. 6.11, the temporal evolution of states two and five in Fig. 6.12a are much smoother; the maximum population of state two is now the same in each period; the period of $P_5(t)$ has decreased to $T_{exact} = 7.2\text{x}10^3$ ($1.7\text{x}10^2$fs), compared to the RWA prediction, $T_{RWA}^{(1,1)} = 7.7\text{x}10^3$; and the populations of state six and seven have decreased substantially, see Table 6.2.

In Fig. 6.12a, the frequency ω_2 is slightly off-resonance, since the minima of $P_2(t)$ are not zero. The frequency was changed slightly to try and find the resonance frequency of molecule $\mathcal{D}$. Calculations of the steady state populations indicate that the true resonance occurs for $9\omega_1 < \omega_2 \leq 496\omega_1/55$. At $\omega_2 = 496\omega_1/55 \simeq 0.05824$, the steady state populations are $\bar{P}_2 = 0.509$, $\bar{P}_5 = 0.422$, $\bar{P}_7 = 0.060$, $\bar{P}_j < 0.004$, $j = 1$, 3, 4, and 6; the population of state five has increased from $\bar{P}_5 = 0.392$ at $\omega_2 = 9\omega_1 \simeq 0.05812$.

Figure 6.12b illustrates the temporal evolution of the molecular

Figure 6.12. The time-dependent state populations, over $0 \le t \le 3.85\text{x}10^{4}$ $(9.31\text{x}10^{2}\text{fs})$, for molecule $\mathcal{D}$, see (6.2.1), interacting with two CW lasers as in Fig 6.10, except ω_2: (a) ω_2 tuned as in Fig. 6.11, $\omega_2 = 9\omega_1 = 0.05812$; (b) ω_2 tuned close to the new (1,1)-photon $2 \rightarrow 5$ resonance, $\omega_2 = 496\omega_1/55 \simeq 0.05824 \simeq \omega_{2,res}$. Molecule $\mathcal{D}$ is identical to molecule $\mathcal{B}$, except $\mu_{56} = 0$.

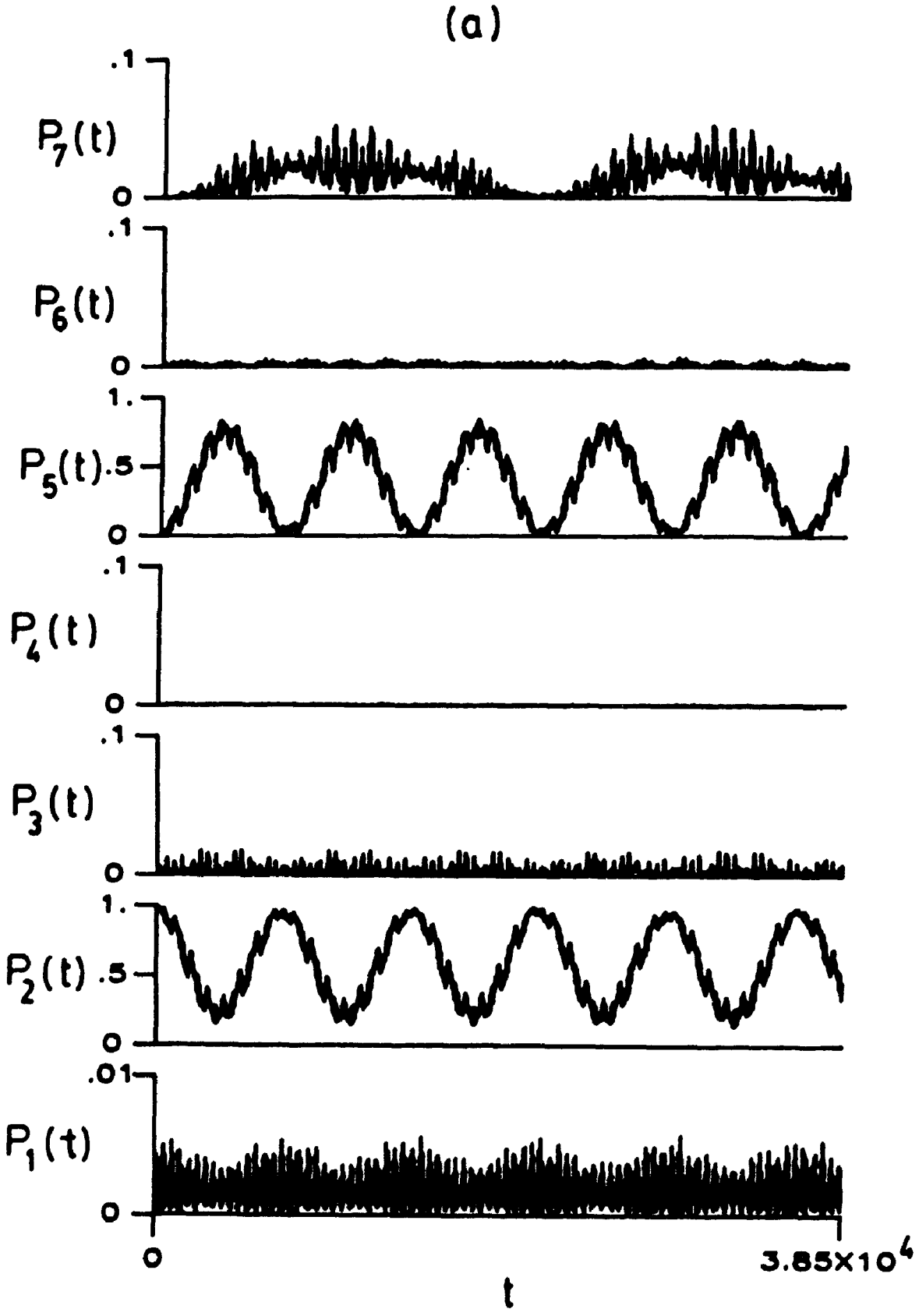
(a)
.1
$P_7(t)$
0
.1
$P_6(t)$
0
1.
$P_5(t)$ .5
0
.1
$P_4(t)$
0
.1
$P_3(t)$
0
1.
$P_2(t)$ .5
0
.01
$P_1(t)$
0
0
3.85×10^4
t

Figure 6.12a.

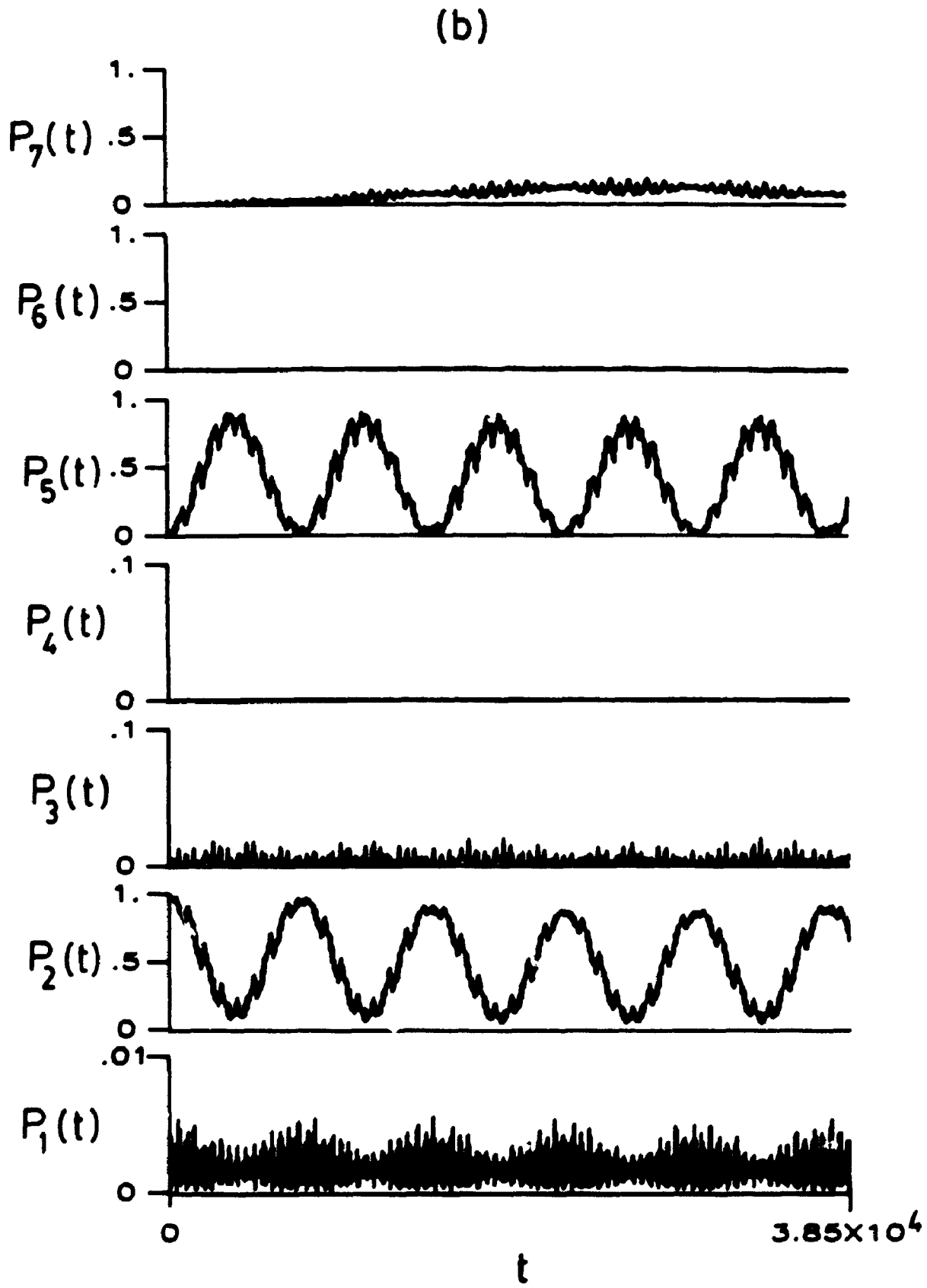

Figure 6.12 continued: Figure 6.12b.

states of molecule $\mathcal{D}$ interacting with the two CW lasers when $\omega_2 = 496\omega_1/55$. The minima of $P_2(t)$ are closer to zero than in Fig. 6.12a, indicating the frequency $\omega_2 = 496\omega_1/55$ is closer to resonance than $\omega_2 = 9\omega_1$. Furthermore, the period of $P_5(t)$ is closer to the RWA prediction for the isolated two-level system; $T_{exact} = 7.5\text{x}10^3$ ($1.8\text{x}10^2$fs) versus $T_{RWA}^{(1,1)} = 7.7\text{x}10^3$. The slightly shorter period in Figs. 6.12a and 6.12b relative to the RWA resonance prediction can be attributed to the off-resonance contribution from $(E_{52} - \omega_1 - \omega_2)$, see for example, (5.1.7). The true resonance frequency, which lies between $9\omega_1 < \omega_2 \leq 496\omega_1/55$, could be found by reducing ω_2 from $496\omega_1/55$ ($m_2 = 496$, $m_1 = 55$), but this would entail very time-consuming calculations with increased m_2 and m_1, see Sec. 5.2.3. Although ω_2 is slightly off-resonance, Fig. 6.12b shows the (1,1)-photon $2 \rightarrow 5$ transition can be largely interpreted as an isolated two-level system when $\mu_{56} = 0$.

The effects of permanent dipole moments on the (1,1)-photon $2 \rightarrow 5$ transition in Fig. 6.11 can be illustrated by setting $\mu_{55} = \mu_{22}$. Figure 6.13 shows the time-dependent populations of the molecular states for molecule $\mathcal{B}$, when $\mu_{55} = \mu_{22}$, at the new (1,1)-photon $2 \rightarrow 5$ resonance frequency, $\omega_2 = 143\omega_1/16 \simeq 0.05771 \simeq \omega_{2,res}$. The corresponding steady state populations are $\bar{P}_2 = 0.488$, $\bar{P}_5 = 0.407$, $\bar{P}_6 = 0.096$, and $\bar{P}_j < 0.003$, $j = 1$, 3, 4, and 7. As in the $\mu_{55} = \mu_{22}$ one-field, two-photon example of Fig. 6 8b, the period of $P_5(t)$ in Fig. 6.13 has substantially increased relative to the $\mu_{55} \neq \mu_{22}$ analogue, and is much longer than the time scale of the figure. The RWA predicts the $\mu_{55} = \mu_{22}$ (1,1)-photon $2 \rightarrow 5$ transition is forbidden. Thus, as in the one-field analogue, the presence of neighbouring energy

Figure 6.13. The time-dependent state populations, over $0 \le t \le 3.85\text{x}10^{4}$ ($9.31\text{x}10^{2}$fs), for molecule $\mathcal{B}$, except $\mu_{55} = \mu_{22}$, see (6.2.1), interacting with two CW lasers as in Fig. 6.10, except ω_2 tuned close to the $\mu_{55} = \mu_{22}$, (1,1)-photon $2 \rightarrow 5$ resonance, $\omega_2 = 143\omega_1/16 \simeq 0.05771 \simeq \omega_{2,res}$.

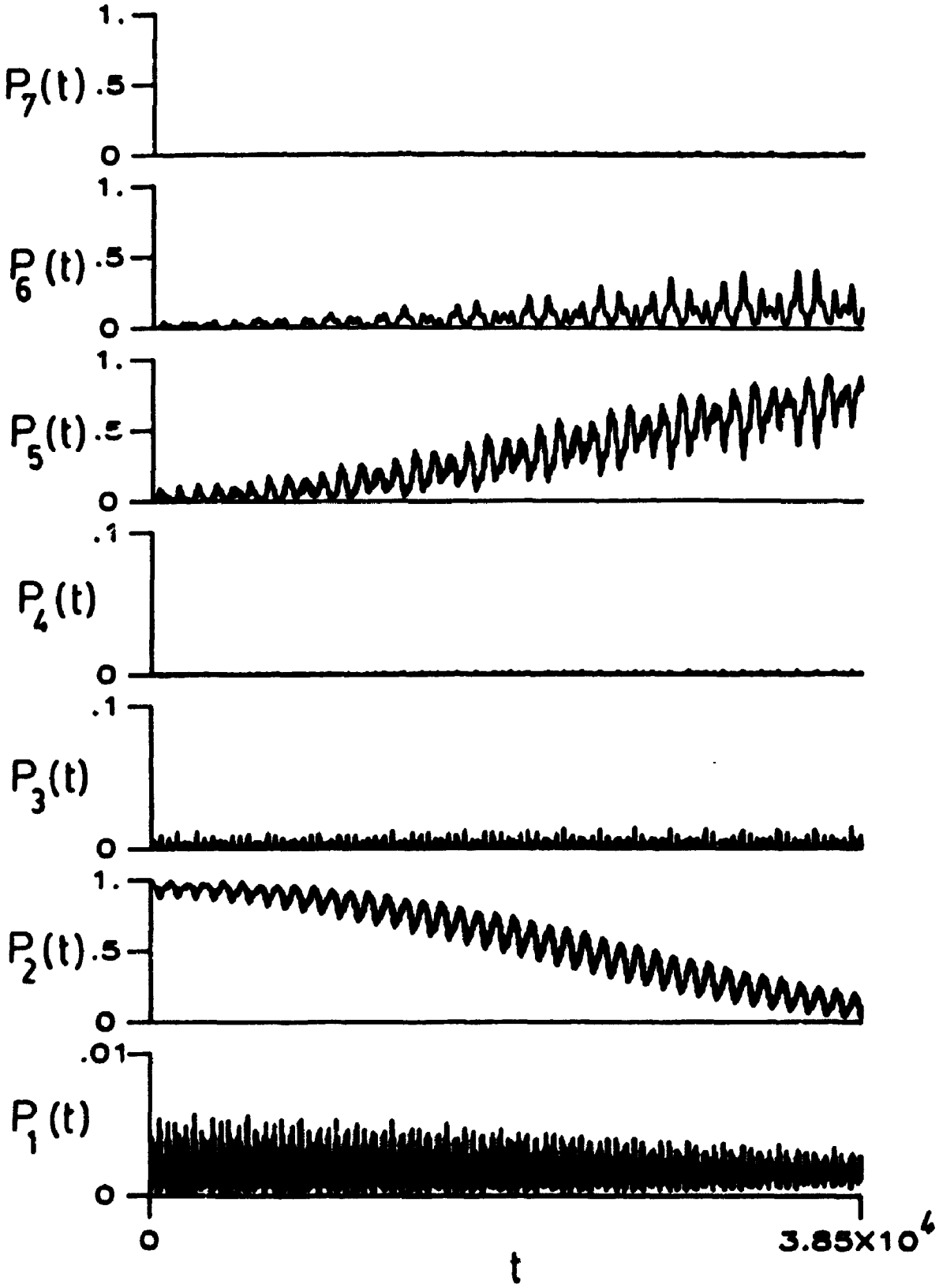

Figure 6.13.

levels, which act as virtual states, provide a weak pathway for the otherwise forbidden transition.

6.2.4. SOME GENERAL COMMENTS

The pump and probe investigations discussed in this section illustrate that the unique multi-photon effects of $d_{kj} \neq 0$, versus $d_{kj} = 0$, on the molecule-EMF coupling for the $j \rightarrow k$ transition and on the associated temporal evolution of the molecular states, persist in many-level systems. In all cases, the RWA solutions based on two-level systems play a critical predictive and/or interpretive role, with respect to the exact results.

In the "pump" component of the investigation, Sec. 6.2.1, where the effects of permanent moments were not significant, the one (CW) field RWA was used to suggest field strengths and pulse durations that would isolate the $1 \rightarrow 2$ transition from neighbouring energy levels, and produce $P_2(t) \simeq 1$ at the end of the effective pulse duration. The possibilities for the field strengths and pulse durations are much wider than the combinations employed in the examples of Sec. 6.2.1 might suggest. For example, the field strength could be weaker and/or the pulse duration shorter so that the CW-like behaviour of $P_2(t)$ is "chopped" by the pulse the first time $P_2(t)$ reaches a maximum near unity. Of course, the pulse duration must be balanced against its bandwidth to minimize excitation of neighbouring energy levels.

The explorations of the effects of permanent dipole moments in the examples of Secs. 6.2.2 and 6.2.3 focus on the permanent dipole moments of the two states directly involved in the transition of interest for the probe investigations. In Sec. 6.2.2, the time-dependent molecular

state populations, when $\mu_{55} \neq \mu_{22}$ relative to when $\mu_{55} = \mu_{22}$, are graphically indistinguishable for the one-photon 2 → 5 transition; for the one-field, two-photon 2 → 5 transitions, the temporal evolution of these excited states is completely different when $\mu_{55} \neq \mu_{22}$ versus $\mu_{55} = \mu_{22}$. The two-field studies, even for a net one-photon transition (the (0,1)-photon 2 → 5 transition), also indicate that substantial differences are found when $\mu_{55} \neq \mu_{22}$ as opposed to $\mu_{55} = \mu_{22}$. For the field strengths employed here, the multi-photon transitions are much weaker when $\mu_{55} = \mu_{22}$, although neighbouring energy levels act as virtual states to provide a pathway for what are RWA (two-level) forbidden transitions.

A comparison of one-field versus two-field interactions with the model molecule also reveals information about the effects of the permanent dipole moments. For example, for the one-field, one-photon 2 → 5 transition in Fig. 6.7, the time-dependent evolution of state five is very smooth, the populations of the nearby states are negligible, and the cases $\mu_{55} \neq \mu_{22}$ versus $\mu_5 = \mu_{22}$ are identical to graphical accuracy. Figure 6.7 does not provide information about whether or not the states involved in the transition have a significant difference in their permanent dipole moments. In contrast, the two-field, (0,1)-photon examples are significantly different when $\mu_{55} \neq \mu_{22}$ versus $\mu_{55} = \mu_{22}$, see Fig. 6.10a and 6.10b, respectively. Relative to the conditions of Fig. 6.7, the frequency of the field with $\mathcal{E}_1^0$ has been reduced to $\omega_1 = 0.1E_{52} = 0.0064576$, and a second, weaker field added.

In Sec. 6.2.2, the one-field, two-photon 2 → 5 transitions are very distinct when $\mu_{55} \neq \mu_{22}$ versus $\mu_{55} = \mu_{22}$, see Figs. 6.8a and 6.8b,

respectively. Furthermore, $P_5(t)$ is much smoother and the effects of the neighbouring transitions much less, than in the two-field (1,1)-analogues in Figs. 6.11 and 6.13. These difficulties with neighbouring transitions are a consequence of two factors: one, the energy level configuration; and two, the choice of the frequency ω_1 in the two-field investigations.

The one-field, two-photon 2 → 5 transition is "clean" because the stationary state energies of states three and four are sufficiently different from $\omega \simeq E_{52}/2$. Had either state had energy close to the two-photon resonance frequency, that state would have strongly perturbed the 2 → 5 transition.

In the two-field, (1,1)-photon 2 → 5 transition, (and also in the (0,1)-photon 2 → 5 transition), the effects of stationary state six become important, primarily due to the size of ω_1: since $E_{65}/2 < \omega_1 < E_{65}$, ω_1 lies between the resonance frequencies for two potentially strong transitions, the (2,0)-photon and the (1,0)-photon 5 → 6 transitions. A smaller ω_1 would avoid many of the neighbouring transition effects due to state six, by making such transitions require the absorption of many more ω_1 photons; at the field strengths used here, these multi-photon 5 → 6 transitions would become more improbable. It is emphasized that the calculations of Secs. 6.2.2 and 6.2.3 are prototype calculations. The field strengths and frequency ratios of the the two-field calculations in Sec. 6.2.3 were chosen in part with time and economic considerations in mind. For exact calculations using the Floquet technique of Sec. 5.2, the smaller ω_1, the more costly and time-consuming the calculations.

The two-field problem has twice the parameters of the one-field

case; this increased flexibility has advantages and disadvantages. The increased flexibility in the choice of the frequency ratios with respect to the energy separation (fixed at $\omega = E_{jk}/N$ in the N-photon one-field case) allows particular transitions to be tuned in, or optimized. On the other hand, many more neighbouring resonances must be taken into consideration.

Ideally, one-field and two-field, one- and multi-photon, probe investigations can be used in a complementary fashion to determine the molecular parameters of an unknown system. One-field, one- versus multi-photon transitions can be used to determine whether the initial and final states have a significant difference in permanent moments. Two-field investigations can be used to confirm such a difference exists, and is not a consequence of virtual states lying close to the one-field multi-photon resonance frequency. Tuning of the smaller frequency in the two-field examples could provide a mechanism for reducing such effects of neighbouring transitions.

Although the effects of the permanent dipole moments of neighbouring states have not been considered explicitly here, these μ_{jj} likely have a significant impact on the strength of a neighbouring transition. For example, for the (0,1)- and (1,1)-photon $2 \rightarrow 5$ transitions, shown in Figs. 6.10a and 6.11 when $\mu_{66} \neq \mu_{55}$, the "stealing" by state six is likely partially due to the overlap with the (2,0)-photon $5 \rightarrow 6$ transition If $\mu_{66} = \mu_{55}$, it is probable this "stealing" would be much weaker since the (2,0)-photon $5 \rightarrow 6$ transition is forbidden in the RWA when $\mu_{55} = \mu_{66}$.

CHAPTER 7

SUMMARY AND CONCLUSIONS

The emphasis of this work has been to present a detailed analysis of some of the time-dependent and spectral effects of permanent dipole moments on a variety of laser-molecule interactions, using previously or newly derived analytical RWA solutions and exact numerical techniques. The major contributions to this area of research include: a study of the interplay between the temporal effects of permanent dipole moments and excited state decay on the time-dependent evolution of the molecular states, using the new RWA analytical solutions of Sec. 3.1 and/or the results of exact calculations (Chapter 3); the consideration of interactions between pulsed lasers and permanent dipole molecules, employing a newly derived half-pulse computational technique (Chapter 4); the derivation of the two-field, two-colour RWA solutions for the $d = \mu_{22} - \mu_{11} \neq 0$ molecule-EMF coupling and the associated time-dependent and long time-averaged excited state populations (Chapter 5); and the presentation of exact two-field computational procedures, and related calculations, illustrating, among other points, the unique optimization capabilities associated wit two-colour spectroscopy when $d \neq 0$ (Chapter 5). The exact calculations presented in Chapter 6 are apparently among the first to investigate explicitly the effects of permanent dipole moments for the interaction

of many-level molecular systems with electromagnetic fields; in Chapter 6, electric fields corresponding to both one CW and two CW lasers are considered.

In Sec. 3.1-3.3, analytical solutions in the rotating wave approximation (RWA) are derived and discussed for the time-dependent molecular state populations of a two-level system, with a non-zero excited state decay rate and permanent dipole moments, interacting with a CW laser. On resonance, the RWA expressions for the time-dependent populations of the states, and the corresponding total time-dependent population of the molecular system, provide an analytical tool for investigating the interplay between the excited state decay rate and the molecule-EMF coupling, and a means of interpreting analogous exact results, as illustrated in Sec. 3.4.

As derived in Sec. 3.2, the criteria for the quantitative applicability of these RWA solutions are dependent on the magnitude of the phenomenological excited state decay rate, γ_2, relative to that of the molecule-EMF coupling. These criteria are strictly qualitative guidelines, especially in the cases of critical and strong damping. In general, the weaker the molecule-EMF coupling, the more reliable the predictions of the RWA, as was found when $\gamma_2 = 0$ [2,3,14,26,71,34]. The numerical examples of Sec. 3.4.1 illustrate a quantitatively reliable application of the RWA when $\gamma_2 \neq 0$ and $d \neq 0$. When $d \neq 0$, some difficulty with the predictive capabilities of the RWA can be encountered with particularly sensitive quantities, such as the values of the parameter $d\mathcal{E}^0/\Delta E$ corresponding to the molecule-EMF coupling nodes. It is worth emphasizing that the RWA is still qualitatively applicable for strong molecule-EMF couplings [2,3,26,34,71].

The model calculations reported in Sec. 3.4.2, based on the $S_0 \rightarrow S_1$ one-photon transition for a "giant dipole" molecule, illustrate nicely some interesting effects of permanent dipole moments on intense CW laser-molecule interactions, both when $\gamma_2 = 0$ and $\gamma_2 \neq 0$. These effects are all related to the oscillations and the overall reduction in the magnitude of the molecule-EMF coupling with increasing field strength when $d \neq 0$ and include shifts in CW resonance frequencies to low frequency [2,3,34], relative to the weak field limit $\omega = \Delta E$ (the Bloch-Siegert shift is always to high frequency when $d = 0$ [14,35]), and marked enhancements, for intense laser fields, in the CW period of the resonance temporal behaviour of the excited state when $d \neq 0$, relative to the very short period associated with $d = 0$.

The unique non-linear nature of the $d \neq 0$ molecule-EMF coupling as a function of field strength, and the possibility of changes in the nature of the decay from weak to strong to weak again with increasing field strength (as the $d \neq 0$ molecule-EMF coupling passes through a node) indicates that the excited state decay rate can act as an internal probe of the effects of the permanent dipoles. Analogous changes in the nature of the decay are not found when $d = 0$. This non-linear nature of the $d \neq 0$ molecule-EMF coupling is also investigated in Chapter 4 using pulsed-laser molecule interactions.

Section 4.1 demonstrates how the symmetry of a pulsed electromagnetic field, about the centre of the pulse, can be used in conjunction with the Riemann product integral method to significantly reduce the computational time required to evaluate the time-dependent populations of molecular states, and their steady-state values, arising from pulsed laser-molecule interactions. This half-pulse technique is

used in the calculations reported in Sec. 4.2 for the two-level giant dipole molecule, employed also in the examples of Sec. 3.4, interacting with a Gaussian pulse. The Gaussian pulsed electric field can be considered as a CW field with an amplitude modulator. Intense CW laser-molecule interactions are also considered in Chapter 4, to help interpret the pulsed laser-molecule interactions, and a detailed analysis is given of the very different phase and beating effects in the CW results for the exact temporal behaviour of the population of the excited state for $d \neq 0$ versus $d = 0$. The close relationship between CW laser-molecule and pulsed laser-molecule interactions is illustrated. For example, for CW laser-molecule interactions, the period of the resonance temporal behaviour of the excited state for $d \neq 0$ can be enhanced to a marked extent by choosing the laser field strength to be that characteristic of the nodes in RWA expression for the molecule-EMF coupling. This extremely long period of the time-dependent excited state population can be probed using pulses of ultrashort to short duration. The $d \neq 0$ RWA results [2,3] are clearly useful for interpreting these pulsed-laser molecule interactions.

Chapters 3 and 4 contain examples that illustrate the use of CW and pulsed lasers to investigate the effects of permanent dipole moments on one-photon transitions. The spectral and dynamical effects of $d \neq 0$ associated with multi-photon transitions are considerably different than in the one-photon case [2,3,13,26,34,71]. For example, in the two-level problem, two-photon transitions occur only if $d \neq 0$. Furthermore, the molecule-EMF coupling initially increases with increasing $d > 0$ for fixed field strength, $\mathcal{E}^0$, or with increasing $\mathcal{E}^0$ for fixed d [2,81]. In contrast, for one-photon transitions, the

molecule-EMF coupling initially decreases from the d = 0 limit with increasing d for fixed $\mathcal{E}^0$, or with increasing $\mathcal{E}^0$ for fixed d. It would be worthwhile investigating the effects of excited state decay on multi-photon transitions, since, in principle, these effects can be more pronounced than for one-photon transitions, due to the general trend of decreasing molecule-EMF couplings with increasing photonicity of the transition. A study of nature of the decay of the excited state as a function of photonicity would provide a distinction between transitions where $d \neq 0$ versus $d = 0$. Pulsed lasers of varying durations can be used to probe the combined effects of $d \neq 0$, $\gamma_2 \neq 0$ and photonicity in laser induced transitions for permanent dipole molecules. Also of interest is the effects of pulse duration and/or excited state decay on the value of the resonance frequency; in the examples of Chapters 3 and 4, such effects were not considered. In Chapter 5, multi-photon transitions are considered for two-level systems interacting with two CW lasers, while in Chapter 6, multi-photon transitions are considered for many-level systems interacting with one or two CW laser(s).

Previously derived analytical RWA results for the temporal populations of the molecular states, and for the associated resonance profiles, for the single- and multi-photon interaction of a two-level system, both for d = 0 [14,18,19] and $d \neq 0$ [2,3,25,26,34], with a single CW laser play a fundamental role in the understanding and/or prediction of the effects of permanent dipole moments in laser-molecule interactions. In Chapter 5, the analogous solutions, in the RWA, for a two-level system interacting with two CW lasers are derived. These new results will also play an important role in the interpretation and

prediction of the effects of $d \neq 0$, versus $d = 0$, for two-colour absorption processes.

The two-field, two-colour RWA is considerably more complicated than the one-field analogue. For the interaction of a single CW laser with a two-level molecule, there is only one resonance associated with each resonance frequency, while for the two-colour case, there can be several significant competing resonances, with the same RWA resonance frequencies. Consequently, in the two-colour problem, there are two levels of rotating wave approximations. When one of many possible competing resonances dominates, the dominant-resonance RWA (DR-RWA) can be used to obtain closed-form analytical results for the multi-photon time-dependent populations of the molecular states and the associated resonance profiles. When there are two or more significant competing resonances, but counter-rotating effects are not important, the many-resonance RWA (MR-RWA) applies. However, in this case, closed-form solutions for the dynamics and resonance profiles are not generally available.

From Sec. 5.1, the conditions for the validity of the RWA for $d \neq 0$ for the two-colour, two-level problem, are much more restrictive than for the interaction of a two-level molecule with one CW laser. In general, the resonance condition, $\Delta E = N_1\omega_1 + N_2\omega_2$, for given frequencies ω_1 and ω_2 of the two CW lasers, can be satisfied by many possible combinations of N_1 and N_2. The DR-RWA can apply when one combination dominates, i.e. when one of the $C(N_1,N_2)$, associated with the given resonance condition, is significantly larger than all the other competing molecule-EMF couplings. For the DR-RWA to be fully applicable in these situations, the resonance of interes must also be

well separated from adjacent significant resonances, and the relevant molecule-EMF coupling must be much less than the beat frequency, see condition (5.1.13), associated with the two CW lasers. In some cases, the constraint (5.1.13) is unnecessarily strict, and can be relaxed, as discussed in Sec. 5.1.2.

A discussion of the two-colour adaptation of the Floquet technique, and a cost-efficient method, by careful selection of the frequency combinations, for the calculation of the exact or MR-RWA time-dependent molecular state populations and the associated resonance profiles, is given in Sec. 5.2. In contrast to one-field calculations, the two-field problem can require significantly more computational effort, depending on the ratio of the two frequencies of the applied electromagnetic fields. The frequencies ω_1 and ω_2 can always be related to each other through a ratio of integers, see (5.1.11). Large integers, which cause the corresponding exact or MR-RWA calculation, using the two-field Floquet technique, to be very time-consuming, can often be avoided by employing slightly different frequencies. For special cases where the integers are almost, but not quite, reducible to a set of much smaller integers, it could be worthwhile pursuing approximate computational techniques for the treatment of almost-periodic systems.

Section 5.3 contains many examples which compare the results for the resonance profiles obtained in the DR-RWA, the MR-RWA, and by exact calculations. These results can be used to help distinguish between the effects of competing resonances versus those of counter-rotating terms that are omitted in both RWA treatments. The examples of Sec. 5.3 also illustrate, for example: that shifts from the DR-RWA

predictions for the resonance position of competing resonances can be caused by the interaction between competing resonances as well as by counter-rotating terms neglected in the RWA; that there are strong versus weak effects due to competing resonance and counter-rotating terms; and that the analytical DR-RWA expression for the molecule-EMF coupling can be used to optimize a particular (N_1,N_2) resonance. It is important to emphasize that the parameters leading to the optimization of a two-colour transition in the RWA may not be realistic, even for a two-level molecule, unless the DR-RWA is quantitatively applicable to the trans'tion of interest.

Both the DR-RWA and the MR-RWA results, and in particular the former, have very useful interpretive and predictive possibilities in which the analytic expression of the molecule-EMF coupling, $C(N_1,N_2)$, given by (5.1.6), plays an important role. Several examples of the optimization/enhancement of multi-photon, two-colour resonances are discussed in Sec. 5.3; clearly, many other possibilities exist. For a given molecule, the analytical expression for the molecule-EMF coupling is proportional to $J_{N_1}(d\cdot\hat{e}_1\mathcal{E}_1^0/\omega_1)J_{N_2}(d\cdot\hat{e}_2\mathcal{E}_2^0/\omega_2)$. To optimize a certain (N_1,N_2)-photon transition, within the RWA, the product of the Bessel functions should be maximized with respect to the parameters $\mathcal{E}_1^0$, $\mathcal{E}_2^0$, ω_1 and ω_2, subject to the resonance condition (5.1.4). In general, N_1 and N_2 can also be considered as variables because of the oscillating nature of Bessel functions as a function of both argument and order: higher order (in N_1 and N_2) multi-photon transitions are not necessarily less probable than lower order multi-photon transitions. Thus, for example, when the field strengths are fixed, N_1, N_2 and the frequencies can be varied, subject to the resonance condition, to

obtain an optimum multi-photon transition.

The unique effects of $d \neq 0$ for molecular interactions with CW lasers are not limited to plane-polarized electromagnetic fields. Interesting effects of permanent dipoles (and quadrupoles) in circular and elliptical dichroism have been discussed in the literature [58,59]. A preliminary RWA investigation has been carried out for circularly (elliptically) polarized light, which can be regarded as two CW fields with the same frequency, the same (different) field strengths, and different polarizations [59].

The usefulness of the two-level system, and its RWA solution for the interaction of a molecule with one CW laser, in the understanding and/or the prediction of the effects of laser-molecule interactions has been well discussed in the literature [3,12-20]. It is clear that the two-level system has its limitations; two-level calculations should be regarded as models unless it is confirmed in explicit applications that the effects of neighbouring energy levels are not significant. This is particularly important for pulsed lasers of short duration since the bandwidths associated with the carrier frequencies can be large, and for interactions with two-colour CW lasers, where many possible combinations of the two frequencies can induce transitions other than the one of interest. The effects of $d_{kj} = \mu_{kk} - \mu_{jj} \neq 0$, relative to when $d_{kj} = 0$, on $j \rightarrow k$ transitions are investigated in Chapter 6 for some many-level systems interacting with one or two CW lasers.

It is shown in Sec. 6.1 that the spectral and temporal effects of a $d \neq 0$ molecule-EMF coupling node persist in a three-level system. In this thesis, two techniques have been used to find the field parameters which generate a molecule-EMF coupling node in exact calculations for a

given molecular system. In Chapters 3 and 4, the temporal evolution of the excited state on resonance is studied as a function of field strength. The molecule-EMF coupling node corresponds to the field strength which produces the longest period of the time-dependent excited state population; a minimum of three calculations is required to establish this field strength. In Sec. 6.1, the resonance profiles are investigated as a function of field strength. The field strength associated with the molecule-EMF coupling node is between those which shift the frequency associated with a dip in the resonance profile from greater to less than the resonance frequency (a minimum of two calculations). The calculation of the exact resonance profiles is also less time-consuming, and hence seems to be a more efficient method of finding the field parameters which generate such a coupling node. The two-level RWA was not quantitatively applicable in either the two- or three-level investigations, but was fundamental to both in the interpretation of the effects of $d \neq 0$ versus $d = 0$. As pointed out in Sec. 6.1, the effects of varying the molecular parameters, such as the energy level configuration, bear further investigation.

Section 6.2 presents a pump and probe investigation of an eight-level molecular system, based on another giant-dipole molecule [113,114]. The pump pulse is used to generate a highly populated excited state, j, which is close in energy to, and has a very different permanent dipole moment than, a second excited state, k. The effects of the difference in permanent moments between these states is investigated for one- and two-photon $j \rightarrow k$ transitions induced by one CW laser, and (0,1)- and (1,1)-photon $j \rightarrow k$ transitions induced by two CW lasers of different colours. It is clear the effects of $d_{kj} \neq 0$,

relative to $d_{kj} = 0$, are important in the strength of the $j \rightarrow k$ transition, and even on the strength of perturbations of this transition by neighbouring transitions, particularly in the two-field studies. When the nature of the temporal evolution of the molecular states j and k differs greatly from the RWA prediction, a number of techniques are presented for investigating the source of the perturbation. For example, slight changes in the energy level configuration, or the zeroing of certain transition moments, can significantly reduce perturbations of the transition of interest. Such studies can be used to suggest alternate field parameters to circumvent the perturbation by neighbouring transitions. One- and multi-photon transitions induced by one CW laser can be used in conjunction with the two-field analogues to probe the effects of permanent dipole moments on laser-molecule interactions.

For a molecule interacting with a weak CW electromagnetic field, the effect of phase, or the initial time of interaction [10,14,32,108], is small [32,71]. Indeed, the one-field RWA solutions for the time-dependent and long time-averaged molecular state populations are independent of the phase of the field. Similarly, the analogous two-field, two-colour DR-RWA solutions are independent of the phases of the fields, suggesting that for weak molecule-EMF couplings, where the DR-RWA is applicable, the effect of the phases in exact calculations will be minimal. For one CW laser-molecule-interactions, the effect of phase on strong molecule-EMF interactions can be very pronounced [32,105]; see, for example, the comparison of phase-averaged and fixed-phase time-dependent excited state populations for $d \neq 0$ (weak coupling) versus $d = 0$ (strong coupling), in Chapter 4. The effect of

relative to $d_{kj} = 0$, are important in the strength of the $j \rightarrow k$ transition, and even on the strength of perturbations of this transition by neighbouring transitions, particularly in the two-field studies. When the nature of the temporal evolution of the molecular states j and k differs greatly from the RWA prediction, a number of techniques are presented for investigating the source of the perturbation. For example, slight changes in the energy level configuration, or the zeroing of certain transition moments, can significantly reduce perturbations of the transition of interest. Such studies can be used to suggest alternate field parameters to circumvent the perturbation by neighbouring transitions. One- and multi-photon transitions induced by one CW laser can be used in conjunction with the two-field analogues to probe the effects of permanent dipole moments on laser-molecule interactions.

For a molecule interacting with a weak CW electromagnetic field, the effect of phase, or the initial time of interaction [10,14,32,108], is small [32,71]. Indeed, the one-field RWA solutions for the time-dependent and long time-averaged molecular state populations are independent of the phase of the field. Similarly, the analogous two-field, two-colour DR-RWA solutions are independent of the phases of the fields, suggesting that for weak molecule-EMF couplings, where the DR-RWA is applicable, the effect of the phases in exact calculations will be minimal. For one CW laser-molecule-interactions, the effect of phase on strong molecule-EMF interactions can be very pronounced [32,105]; see, for example, the comparison of phase-averaged and fixed-phase time-dependent excited state populations for $d \neq 0$ (weak coupling) versus $d = 0$ (strong coupling), in Chapter 4. The effect of

the phases in two-field, two-colour CW lasers-molecule interactions will be different from the one-colour analogue, because the phases of the fields, unlike the quantities $\omega_1 t$ and $\omega_2 t$, do not change in a commensurate fashion, see Sec. 5.2. Where competing resonances are significant, the MR-RWA Hamiltonian applies; in such a case, the time-dependent and long time-averaged populations are probably not phase independent.

Scharf and Band [42] discuss several possible experimental applications of two-colour, two-photon transitions in the limit that one frequency is very small. They also point out the generality of two-colour absorption processes with respect to the various regions of the electromagnetic spectrum.

In principle, two-colour multi-photon transitions may be applied, often with significant enhancement in transition probabilities and certainly more flexibility, to experimental situations where one-colour multi-photon processes are important. While the examples of Chapter 5 focused on the two-colour steady state resonance profiles, the RWA two-colour time-dependent transition probability, (5.1.7), can be used to help investigate the dynamics of the time evolution of the molecular states associated with two-colour absorption processes. In such investigations, the analytical expression for the two-colour molecule-EMF coupling, (5.1.6), will again play an important role in the selection of the parameters of the problem which will optimize the relevant transitions as a function of time. Two-colour pulsed, as well as continuous wave, laser-molecule interactions should be important in such investigations.

The non-linear nature of the one-colour $d \neq 0$ molecule-EMF

coupling (2.3.10), has been applied to molecular beam electric resonance (MBER) studies on symmetric top molecules [30], with investigations of the field strength required to optimize the intensity of one-colour multiphoton time-dependent transition probabilities at a fixed time [30]. The analytical RWA expression for the one-colour multi-photon molecule-EMF coupling, (2.3.10), is useful in these investigations. This type of one-colour experiment should lend itself to adaptation to a two-colour analogue. Similar comments apply to the pump-probe investigations of highly excited states of Li, Na and H by Gallagher *et al.* [29], and Jensen and Susskind [27]. Here, the (near) degeneracy of highly excited states of different ℓ values gives rise to large "permanent" dipoles which are probed by a one-colour microwave laser. The analysis of the experimental data in these cases often presumes the isolation of the two-level transition of interest. Theoretical investigations of the effects of neighbouring transitions and energy levels, as illustrated in Chapter 6 and particularly in two-colour investigations, help determine a qualitative set of criteria for the validity of this assumption.

REFERENCES

[1] (a) Meath, W.J., and Power, E.A., 1984, Molec. Phys., 51, 585; (b) 1984, J. Phys. B., 17, 763.

[2] Kmetic, M.A., and Meath, W.J., 1985, Phys. Lett., 108A, 340.

[3] Meath, W.J., Thuraisingham, R.A., and Kmetic, M.A., 1989, Adv. Chem. Phys., 73, 307.

[4] Dick, B., and Hohlneicher, G., 1982, J. Chem. Phys. 76, 5755.

[5] Thomas, G.F., and Meath, W.J., 1982, Molec. Phys., 46, 743; 1983, *Ibid.*, 48, 649(E).

[6] Ho, T-S., Chu, S-I., 1983, J. Chem. Phys., 79, 4708.

[7] Chu, S-I., Tietz, J.V., and Datta, K.K., 1982, J. Chem. Phys., 77, 2968.

[8] Leasure, S.C., Milfeld, K.F., and Wyatt, R.E., 1981, J. Chem. Phys., 74, 6197.

[9] Leasure, S.C., and Wyatt, R.E., 1980, Opt. Eng., 19, 46; 1979, Chem. Phys. Lett., 61, 625.

[10] Pantell, R.H., and Puthoff, H.E., 1969, "Fundamentals of Quantum Electronics", (Wiley), §5.2.

[11] Shimoda, K., and Shimizu, T., 1972, "Progress in Quantum Electronics", Vol. 2, edited by J. Sanders and S. Stenholm, (Pergamon Press) Part 2, §2.3.

[12] Allen, L., and Eberly, J.H., 1975, "Optical Resonance and Two-Level Atoms", Wiley.

[13] Meath, W.J., and Thuraisingham, R.A., 1988, "Atomic and Molecular Processes With Short Intense Laser Pulses", edited by A.D. Bandrauk (Plenum), p. 453.

[14] Shirley, J.H., 1965, Phys. Rev. B, 138, 979.

[15] (a) Salzman, W.R., 1974, Phys. Rev. A, 10, 461; 1977, *Ibid.*, 16, 1552; (b) Burrows, M.D., and Salzman, W.R., 1977, *Ibid.*, 15, 1636.

[16] Dion, D.R., and Hirschfelder, J.O., 1976, Adv. Chem. Phys., 35, 265.

[17] (a) Nakai, S., Yamashita, A.B., and Meath, W.J., 1990, Molec. Phys., 71, 1333; (b) Nakai, S., and Meath, W.J., 1991, Chem. Phys., 154, 349.

[18] Rabi, I.I., 1937, Phys. Rev., 51, 652.

[19] Sargent III, M., Scully, O., and Lamb, W.E., 1974, "Laser Physics", (Addison-Wesley), Chap. 2.

[20] Delone, N.B., and Krainov, V.P., 1985, "Atoms in Strong Light Fields, Vol. 28 of Springer Series in Chemical Physics", edited by V.I. Goldanskii, R. Gomer, F.P. Schäfer, and J.P. Toennies (Springer-Verlag).

[21] Thomas, G.F., and Meath, W.J., 1983, J. Phys. B., 16. 951.

[22] Meath, W.J., Thuraisingham, R.A., and Mahanty, J., 1991, Surface Sci., 244, 285.

[23] Moloney, J.V., and Meath, W.J., 1978, Molec. Phys., 35, 1163.

[24] Kondo, A.E., and Meath, W.J., 1991, Molec. Phys., 74, 113.

[25] Thomas, G.F., 1986, Phys. Rev. A, 33, 1033.

[26] Kmetic, M.A., Thuraisingham, R.A., and Meath, W.J., 1986, Phys. Rev. A, 33, 1688.

[27] Jensen, R.V., and Susskind, S.M., 1987, "Photon and Continuum States of Atoms and Molecules", Vol. 16 of Springer Proceedings in Physics, edited by N.K. Rahman, G. Guidotti, and M. Allegrini (Springer-Verlag), p. 13.

[28] Hattori, T., and Kobayashi, T., 1987, Phys. Rev. A, 35, 2733.

[29] Gallagher, T.F., Mahon, C.R., Pillet, P., Fu, P., and Newman, J.B., 1989. Phys. Rev. A, 39, 4545.

[30] Meerts, W.L., Ozier, I., and Hougen, J.T., 1989, J. Chem. Phys., 90, 4681; Martinache, L., Ozier, I., and Bauder, A., 1990, J. Chem. Phys., 92, 7128.

[31] Nakai, S., and Meath, W.J., 1991, J. Chem. Phys., in press.

[32] (a) Moloney, J.V., and Meath, W.J., 1976, Molec. Phys., 31, 1537; (b) 1975, *Ibid.*, 30, 171.

[33] Chu, S-I., 1985, Adv. At. Mol. Phys., 21, 197.

[34] Kmetic, M.A., and Meath, W.J., 1990, Phys. Rev. A, 41, 1556.

[35] Bloch, F., and Siegert, A., 1940, Phys. Rev., 57, 522.

[36] Thuraisingham, R.A., and Meath, W.J., 1988, Chem. Phys., 125, 129.

[37] Dollard, J.D., and Friedman, C.N., 1977, J. Math. Phys., 18, 1598; 1978, J. Funct. Anal., 28, 309.

[38] Walker, R.B., and Preston, R.K., 1977, J. Chem. Phys., 67, 2017.

[39] Dougherty Jr., E.P., Augustin, S.D., and Rabitz, H., 1981, J. Chem. Phys., 74, 1175.

[40] Terauchi, M., and Kobayashi, T., 1987, Chem. Phys. Lett., 137, 319.

[41] New, G.C.H., 1983, Rep. Prog. Phys., 46, 877; Shank, C.V., 1986, "Methods of Laser Spectroscopy", edited by Y. Prior, A. Ben-Reunen, and H. Rosenbluh, (Plenum), 51.

[42] Scharf, B.E., and Band, Y.B., 1988, Phys. Lett., 144, 165.

[43] Craig, D.P., and Thirunamachandran, T., 1988, Chem. Phys. Lett., 148, 97.

[44] Band, Y.B., Bavli, R., and Heller, D.F., 1989, Chem. Phys. Lett., 156, 405.

[45] Bavli, R. Heller, D.F., Band, Y.B., Phys. 1990, Rev. A, 41, 3960.

[46] Liptay, W., 1974, "Excited States", Vol. 1, edited by E.C. Lim, (Academic Press), p198.

[47] Dalgarno, A., 1966, "Perturbation Theory and Its Applications in Quantum Mechanics", (Wiley).

[48] Bethe, H.A., and Salpeter, E.E., 1957, "Quantum Mechanics of One- and Two-Electron Atoms", (Academic Press), p3.

[49] Cohen, E.R., and Taylor, B.N., 1973, J. Phys. Chem. Ref. Data, 2, 663.

[50] Messiah, A., 1961, "Quantum Mechanics", Vols. One and Two, (Wiley).

[51] Landau, L.D., Lifshitz, E.M., 1977, "Quantum Mechanics", (Pergamon Press).

[52] Schiff, L.I., 1955, "Quantum Mechanics", (McGraw-Hill).

[53] Dirac, P.A.M., 1927, Proc. Roy. Soc., A114, 243 and 710.

[54] Pauling, L. and Wilson Jr., E.B., 1935, "Introduction to Quantum Mechanics With Applications to Chemistry", (McGraw-Hill).

[55] Kovach, L.D., 1984, "Boundary Value Problems", (Addison-Wesley), p.207.

[56] Atkins, P.W., 1983, "Molecular Quantum Mechanics", (Oxford University Press) p214.

[57] Michel, J., and Thulstrup, E.W., 1986, "Spectroscopy with Polarized Light", (VCH).

[58] Meath, W.J., and Power, E.A., 1987, J. Phys. B., 20, 1945; 1989, J. Mod. Optics., 36, 207.

[59] Meath, W.J., and Kondo, A.E., 1991, J. Molec. Structure (Theochem), 232, 23.

[60] Merzbacher, E., 1961, "Quantum Mechanics", (Wiley).

[61] Weisskopf, V., and Wigner, E., 1930, Z. Physik,63, 54; an English translation is available in Hindmarsh, W.F., 1967, "Atomic Spectra", (Pergamon Press) pp 304-327.

[62] Mollow, B.R. 1975, Phys. Rev. A, 12, 1919.

[63] Cohen-Tannoudji, C., Diu, B., and Laloë, F., 1977, "Quantum Mechanics", (Wiley).

[64] Quack, M., 1978, J. Chem. Phys., 69, 1282.

[65] Drabe, K.E., Kammandeur, J., 1988, "Excited States", Vol. 7, edited by E.C. Lim and K.K. Innes, (Academic Press) 107.

[66] Hirschfelder, J.O., and Pyzalski, R.W., 1985, Phys. Rev. Lett., 55, 1244.

[67] Gerald, C.F., and Wheatley, P.O., 1984, "Applied Numerical Analysis", 3rd ed., (Addison-Wesley), Appendix A.

[68] Edwards Jr., C.H., and Penney, D.E. 1982, "Calculus and Analyical Geometry", (Prentice-Hall).

[69] Anton, H., 1981, "Elementary Linear Algebra", (Wiley), p268.

[70] Erugin, N.P., 1966, "Linear Systems of Ordinary Differential Equations with Applications to Periodic Coefficients", (Academic Press).

[71] Thuraisingham, R.A., and Meath, W.J., 1985, Molec. Phys., 56, 193.

[72] Loudon, R., 1973, "Quantum Theory of Light", (Clarendon) pp90-100.

[73] Oliver, G., 1971, Lett. Nuovo. Cimento, 2, 1075; 1977, Phys. Rev. A, 15, 2424.

[74] Eigenvalue Systems Package (EISPACK)", 1972, second edition, (Argonne National Laboratory).

[75] IMSL Special Functions Library, 1982, Edition nine, (IMSL Inc.).

[76] Margenau, H., and Murphy, G.M., 1956, "The Mathematics of Physics and Chemistry", second edition, (D. Van Nostrand).

[77] Clary, D.C., 1983, J. Phys. Chem., 87, 735.

[78] Quack, M. and Sutcliffe, E., 1985, J. Chem. Phys., 83, 3805.

[79] Whaley, K.B. and Light., J.C., 1984, Phys. Rev. A, 29, 1188.

[80] Shirley, J.H., 1963, J. Appl. Phys. 34, 783.

[81] F.W.J. Olver, 1970, "Handbook of Mathematical Functions", edited by M. Abramowitz and I. Stegun (USA National Bureau of Standards) Chapter 9.

[82] Steinfeld, J.I., 1985, "Molecules and Radiation", (MIT Press).

[83] Breene, R.G., 1961, "The Shift and Shape of Spectral Lines", (Pergamon Press).

[84] Javin, A., 1957, Phys. Rev., 107, 1579.

[85] Watson, G.N., 1958, "A Treatise on the Theory of Bessel Functions", (Cambridge University Press).

[86] Power, E.A., and Thirunamachandron, T., 1974, J. Chem. Phys., 60, 3695; Andrews, D.L., and Thirunamachandron, T., 1977, J. Chem. Phys., 67, 5026.

[87] Thuraisingham, R.A., and Meath., W.J., 1988, Surface Sci., 199, 199.

[88] Yamaoka. K., and Charney, E., 1972, J. Am. Chem. Soc., 94, 8693; Liptay, W., and Czekalla, J., 1961, Z. Electrochem., 65, 721.

[89] Rose, M.E., 1957, "Elementary Theory of Angular Momentum", (Wiley).

[90] Ross, S.L., 1980, "Introduction to Ordinary Differential Equations", third edition (Wiley).

[91] Churchill, R.V., and Brown, J.W., 1984, "Complex Variables and Applications", (McGraw-Hill).

[92] Dwight, H.B., 1961, "Tables of Integrals and Other Mathematical Data", (Macmillan) (a) p79, #401.01, 401.02; (b) p153, #654.6, 654.7; (c)p135, #576.1.

[93] $\beta_r/|C(N)|$ is equal tne x in equation #700.1 on page 165 of reference [92].

[94] Avouris, Ph., and Demuth, J.E., 1983, "Surface Studies with Lasers", edited by F.R. Ausenegg, A. Leitner, and M.E. Lippitsch (Springer-Ver'ag) 24.

[95] Chance, R.R., Prock, A., and Silbey, K., 1978, Adv. Chem. Phys., 37, 1.

[96] Metiu, H., 1984, Prog. Surf. Sci., 17, 153; Metiu, H., and Das, P., 1984, Ann. Rev. Chem., 35, 507.

[97] Berlman, B., 1971, "Handbook of Fluorescence Spectra of Aromatic Molecules", (Academic Press).

[98] Kobayashi, T., Degenkolb, E.O., and Rentzepis, P.M., 1979, J. Appl. Phys., 50, 3118; Kobayashi, T., Terauchi, M., Uchiki, H., 1986, Chem. Phys. Lett., 126, 143.

[99] $\exp[\underline{A}]\exp[\underline{B}] = \sum_{j,k} \underline{A}^j\underline{B}^k/j!k! \neq \sum_{j,k} \underline{B}^k\underline{A}^j/j!k! = \exp[\underline{B}]\exp[\underline{A}]$, unless $\underline{A}\,\underline{B} = \underline{B}\,\underline{A}$.

[100] The "positive", rather than the "negative", half of the pulse is used for ease of application of the IMSL subroutine CERFZ, which calculates the complex error functions associated with the evolution operators, as formulated by the Riemann product integral method, for Gaussian pulsed laser-molecule interactions, see Sec. 2.2.1.

[101] Salzman, W.R., 1971, Phys. Rev. Lett., 26, 220.

[102] Askar, A., 1974, Phys. Rev. A, 10, 2395.

[103] Moloney, J.V., Ali, M.K., and Meath, W.J., 1974, Physics Lett. A, 49, 207.

[104] Ho, T-S., Chu, S-I., Tietz, J.V., 1983, Chem. Phys. Lett., 96, 464.

[105] Moloney, J.V., and Meath, W.J., 1978, Phys. Rev. A, 17, 1550; Thomas, G.F., and Meath, W.J., 1979, Phys. Lett. A, 70. 396.

[106] Goreslavskii, S.P., and Krainov, V.P., 1979, Sov. Phys. JETP, 49, 13.

[107] Guccione-Gush, R., and Gush, H.P., 1974, Phys. Rev. A, 10, 1474.

[108] Ho, T-S., and Chu, S-I., 1984, J. Phys. B: At. Mol. Phys., 17, 2101.

[109] Pain, H.J., 1983, "The Physics of Vibrations and Waves", (Wiley).

[110] Hutchinson, J.S., 1986, J. Chem. Phys., 85, 7087.

[111] Fleming, G.R., 1986, "Chemical Applications of Ultrafast Spectroscopy", (Oxford University Press), Chapter 4.

[112] Andrews, D.L., 1990, "Lasers in Chemistry", (Springer-Verlag); Ben-Shaul, A., Haas, Y., Kompa, K.L., Levine, R.D., 1981, "Lasers and Chemical Change", (Springer-Verlag).

[113] Graham, E M., Miskowski, V.M., Perry, J.W., Coulter, D.R., Stiegman, A.E., Schaefer, W.P., and Marsh, R.E., 1989, J. Am. Chem. Soc., 111, 8771.

[114] Thakkar, A.J., and Nilar, S., private communication.

[115] The initial conditions for states one through seven are:

$[\underline{b}(t = +4\tau_p)]^T = [(-0.01871389419 + i0.00115026410),$
$(-0.11726771051 - i0.99278335057), (-0.00000669914 - i0.00000194639),$
$(-0.00000000075 - i0.00000000241), (-0.00000000017 + i0.00000000264),$
$(0.00000000000 + i0.00000000000), (0.00000000000 + i0.00000000000)]$.